R-08-92

Bedrock hydrogeology Laxemar

Site descriptive modelling SDM-Site Laxemar

Ingvar Rhén, SWECO Environment AB

Lee Hartley, Serco Technical and Assurance Services

December 2009

Svensk Kärnbränslehantering AB
Swedish Nuclear Fuel
and Waste Management Co

Box 250, SE-101 24 Stockholm
Phone +46 8 459 84 00

ISSN 1402-3091
SKB R-08-92

Bedrock hydrogeology Laxemar

Site descriptive modelling
SDM-Site Laxemar

Ingvar Rhén, SWECO Environment AB

Lee Hartley, Serco Technical and Assurance Services

December 2009

Keywords: Laxemar, Hydrogeology, Hydrochemistry, Hydrogeological DFN, Modelling, Calibration.

Preface

The site descriptive modelling work at Laxemar was conducted by the Laxemar-Simpevarp multidisciplinary project group (POM) in close collaboration with various discipline-specific working groups. All members of the hydrogeological modelling expert group (HydroNet) are gratefully acknowledged for excellent teamwork and contributions to the development of the bedrock hydrogeological model of Laxemar.

The present report is intended to summarise the hydrogeological conditions and the hydraulic properties of the bedrock in Laxemar and to give the information essential for demonstrating understanding. It relies heavily on numerous background reports concerning details in data analyses and modelling. The selection of material from these reports is the responsibility of the authors.

Summary

The Swedish Nuclear Fuel and Waste Management Company (SKB) has conducted site investigations at two different locations, the Forsmark and Laxemar-Simpevarp areas, with the objective of siting a final repository for spent nuclear fuel according to the KBS-3 concept. Site characterisation should provide all data required for an integrated evaluation of the suitability of the investigated site. An important component in the characterisation work is the development of a hydrogeological site-descriptive model. The hydrogeological model is used by repository engineering to design the underground facility and to develop a repository layout adapted to site conditions. It also provides input to the safety assessment and the environmental impact assessment.

The current report (SKB R-08-92) is the main hydrogeology reference in connection to the development of the Site Descriptive Model (SDM) of Laxemar, providing a comprehensive summary of primary data, the hydrogeological conceptual model and the regional scale numerical groundwater flow modelling, based on the results presented in two supporting reports. The first supporting report (SKB R-08-78) describes the analysis of the primary data and the parameterisation of the bedrock, within two main domains; hydraulic conductor domains (HCD) representing the deterministic deformation zones and the hydraulic rock domains (HRD), representing the rock between the HCDs. The parameterisation of HRDs is associated with the development of hydrogeological DFN models. The second supporting report (SKB R-08-91) presents the hydrogeological conceptual model, the regional scale numerical groundwater flow modelling, confirmatory testing and associated sensitivity analyses.

The bedrock of the SDM-Site Laxemar regional model area, with main efforts made within the focused area, has been investigated with several hydrogeological investigation methods; e.g. single-hole tests and interference (or cross-hole) tests to characterise the hydraulic properties of the HCD and the HRD, monitoring of groundwater pressure in boreholes, monitoring of flow rates in water courses and sampling of water for chemical analysis.

The main hydrogeological characteristics of the investigated area are featured by a fairly flat topography (regional topographic gradient in the order of 4% towards the coast) but with relatively distinct valleys. The investigation area is located within a crystalline basement, mostly covered by a rather thin till in the elevated areas and with glaciofluvial sediments in the larger valleys.

The site-average annual precipitation and specific discharge are estimated to be in the order of 600 mm and 160-170 mm, respectively. The natural (undisturbed) groundwater level follows the topography of the ground surface, where depth to the water table is expected to be up to a few metres, with maximum depths at topographic heights and minimum depths in the valleys.

The hilly areas are dominated by exposed rock outcrops or shallow depth Quaternary deposits (i.e. a depth less than c. 0.5 m), where groundwater recharge occur. Groundwater discharge is conceptualised to take place in the low-altitude “valley” type areas, with sediments possibly as thick as 50 m and in some areas also close to the Baltic shoreline. A dominant part of the recharged groundwater flows in the Quaternary deposits and in the upper 100 m of the bedrock before it discharges to a stream or a lake. Below 100 m depth, the groundwater flow decreases due to a reduced permeability of the rock and the modelling shows that even at greater depth within the Laxemar local model area, the origin of the recharged groundwater is predominantly localised within or in the immediate vicinity of the Laxemar local model area.

The key interpreted HCD characteristics are:

- A clear trend of decreasing transmissivity with depth.
- A positive correlation between interpreted deformation zone “size” and transmissivity (size here corresponding to interpreted trace length on the surface).
- Indications that the transmissivity of HCDs is dependent on the orientation of deformation zones, E-W zones appearing more conductive than zones of other orientations.
- Significant lateral heterogeneity with an estimated standard deviation of Log10(transmissivity) of 1.4 (standard deviation of data within individual zones being in the range 0.5 to 2).

The key interpreted HRD characteristics are:

- The flowing features (fractures and minor deformation zones) can be grouped in four orientation sets; steep ENE, WNW, N-S and a subhorizontal set.
- The intensity of flowing features is generally highest for the WNW set (aligned with the principal horizontal stress) with the subhorizontal set also being important in the upper bedrock.
- A clear decreasing intensity of flowing features with depth, but generally with a similar transmissivity distribution of the flowing features for the specific depth interval studied (as measured by difference flow logging; PFL-f).
- As a consequence – a resulting clear trend of decreasing hydraulic conductivity with depth may be observed (as seen e.g. in injection tests, test scale 100 m).
- The hydraulic conductivity is c. 10 times lower in HRDs than that of the HCDs (injection tests, test scale 100 m).

There are some remaining uncertainties:

- Given that a large volume of rock has been investigated with a limited number of boreholes, and given that the spatial variation of hydraulic properties is large within the HCDs and the HRDs, the uncertainties associated with the hydraulic properties of an individual HCD and the spatial variation of hydraulic properties within individual HRDs are high.
- Below a depth of 650 m the rock is considered low-conductive. However, data are sparse and the assessment of properties is inherently uncertain.
- Some of the HCDs are associated with dolerite dykes that act as hydraulic barriers, as evidenced by *in situ* measurements, but it is unclear if these dykes act as barriers along their entire HCD extents.
- Some HCD, lacking surface outcrop (lineament), being only intercepted by one borehole, are modelled deterministically with an assumed radius of 564 m. The size and character of these HCD are considered highly uncertain. These HCDs are of similar size as the largest MDZ modelled stochastically.
- It is also recognised that the minor deformation zones (MDZ) are likely to be hydraulically heterogeneous. Of the geologically defined MDZs, c. 60% have a conductive feature (with transmissivity larger than c. 10^{-9} m^2/s). However, so far these MDZs are included as homogenous features in the hydrogeological DFN model.
- The developed hydrogeological DFN has been calibrated using different transmissivity models, but only the conceptually most reasonable model, the semi-correlated transmissivity-size model, has been tested in the context of regional scale flow modelling. The hydraulic anisotropy evidenced by the developed hydrogeological DFN model is also considered uncertain; it may in fact be larger than what the current model shows, as observed at the Äspö Hard Rock Laboratory immediately east of the focused area.

In summary, the general situation of the groundwater flow conditions in the Laxemar model area is well established after several stages of investigations followed by updated hydrogeological models. The aspects of the spatial variation of the hydraulic properties within the Laxemar focused area are well understood, with a clear depth dependency and the deterministic deformation zones (HCD) in general being c. one order of magnitude more conductive than the average rock. Numerical groundwater flow modelling has been used both to test the parameterisation of the hydraulic domains as well as for furnishing confirmatory tests of the understanding and interpretations developed. In particular, hydrogeological DFN models of the HRD and parameterisations of the HCD have been defined for end-users such as Repository Design and Safety Assessment. A demonstration of the consistency between these model parameterisations and hydraulic tests and head measurements performed at the site has been made. Further, the integrated understanding of the evolution of the hydrogeological and hydrochemical conditions in the Laxemar-Simpevarp area has been demonstrated by simulation of the palaeohydrogeological evolution during the Holocene period.

Contents

1 Introduction

1.1 Background

The Swedish Nuclear Fuel and Waste Management Company (SKB) has undertaken site investigations at two different locations, the Forsmark and Laxemar-Simpevarp areas, cf. Figure 1-1, with the objective of siting a geological repository for spent nuclear fuel. The investigations are conducted in campaigns punctuated by data freezes. After each data freeze, the site data are analysed and site descriptive modelling work is carried out. A site-descriptive model (SDM) is an integrated model for geology, rock mechanics, thermal properties, hydrogeology, hydrogeochemistry and transport properties, and a description of the surface system.

1.1.1 Scope and Objectives

The primary objectives of the work reported here are to:

- provide a hydrogeological 3D description and associated model parameterisation of Laxemar needed for the end users Repository Engineering, Safety Assessment and Environmental Impact Assessment;
- implement this description in a 3D regional groundwater flow model of Laxemar and its surrounding area to allow quantitative assessment and illustration of the conceptual understanding of the site;
- build confidence in the flow modelling work by testing the 3D model against a variety of field data, such as water levels/hydraulic pressure, interference tests, palaeohydrogeology (hydrogeochemistry) and near-surface hydrogeology.

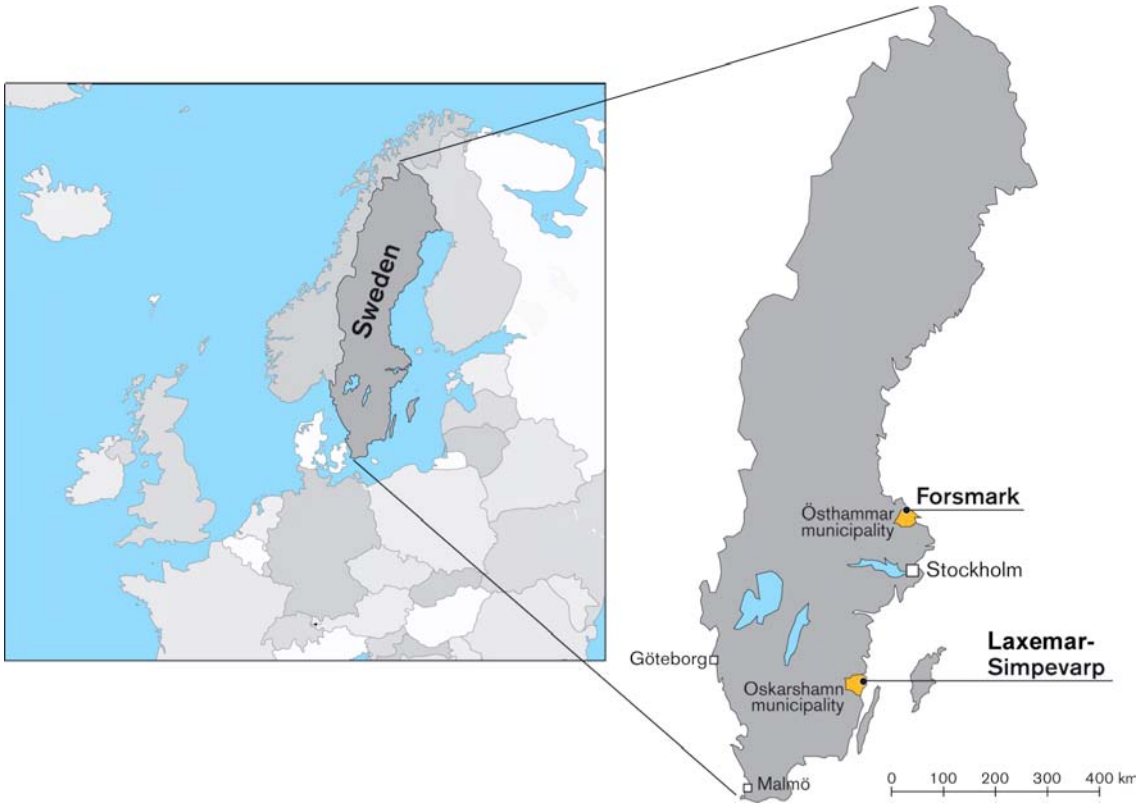

Figure 1-1. *Map of Sweden showing the location of the Forsmark and Laxemar-Simpevarp sites.*

The descriptions should focus principally on the hydraulic properties of deformation zones (HCDs) and the naturally fractured rock between the deformation zones (HRDs) in the potential repository volumes. This requires consideration of how to construct and parameterise the models of HCDs and the hydrogeological DFN models representative of the HRDs and parameterisation of the entire regional scale 3D groundwater flow domain, a volume of c. 600 km^3 (The corresponding local model volume is c. 20 km^3), cf. Section 1.3. Part of this is achieved by deriving specific:

- HCD models for deformation zones that cover the regional model domain /Rhen et al. 2008/ based on geological models presented by /Wahlgren et al. 2008/.
- Hydrogeological DFN models for the hydraulic domains /Rhén et al. 2008/ defined on the basis of defined fracture domains, covering the local model volume and where the defined rock domains account for the remaining part of the regional model. The geological fracture domain model is presented by /LaPointe et al. 2008/ and the rock domains in /Wahlgren et al. 2008/, as summarised briefly in Chapter 3.

The present report constitutes the main (level II) reference for the hydrogeological site-descriptive model of the Laxemar-Simpevarp area (as part of SDM-Site Laxemar). The hierarchy of various reports comprising SDM-Site Laxemar is shown in Figure 1-2. The report is based on two supporting comprehensive level III reports; /Rhén et al. 2008/ and /Rhén et al. 2009/.

1.1.2 Disposition of the report

The report is organised as follows:

- Chapter 1 provides background, objectives and disposition of the report. Furthermore, the geographical setting, model areas, documentation and previous knowledge (as reported) is reviewed.
- Chapter 2 presents SKB's systems approach to groundwater flow and solute transport in fractured crystalline rock as applied in SDM-Site. This chapter constitutes an important premise for Chapters 4 through 10.
- Chapter 3 presents an overview of the modelled deterministic deformation zones and the fracture domains derived for SDM-Site Laxemar. This chapter is important for the work presented in Chapters 4 through 10.
- Chapter 4 presents an overview of the hydraulic testing carried out up until data freeze Laxemar 2.3 for SDM-Site Laxemar, and a review of the data selected for hydrogeological analysis and modelling in the work reported here.
- Chapter 5 presents the hydrogeological conceptual model development and its integral parts.
- Chapter 6 describes the implementation of the conceptual model in the regional numerical groundwater flow model.
- Chapter 7 presents the calibration of the numerical groundwater flow model against natural groundwater level data, drawdown induced by the near-by Äspö laboratory, interference tests conducted in Laxemar, and hydrochemical data based on simulation of the period since the latest glaciation (the latter process is denoted Palaeohydrogeology throughout this report).
- Chapter 8 presents some exploratory simulations focused mainly on flow paths to and from the tentative repository layout.
- Chapter 9 presents the conceptual and parameter uncertainty analysis.
- Chapter 10 summarises the bedrock hydrogeological model, the confirmatory testing and the confidence and remaining uncertainties.

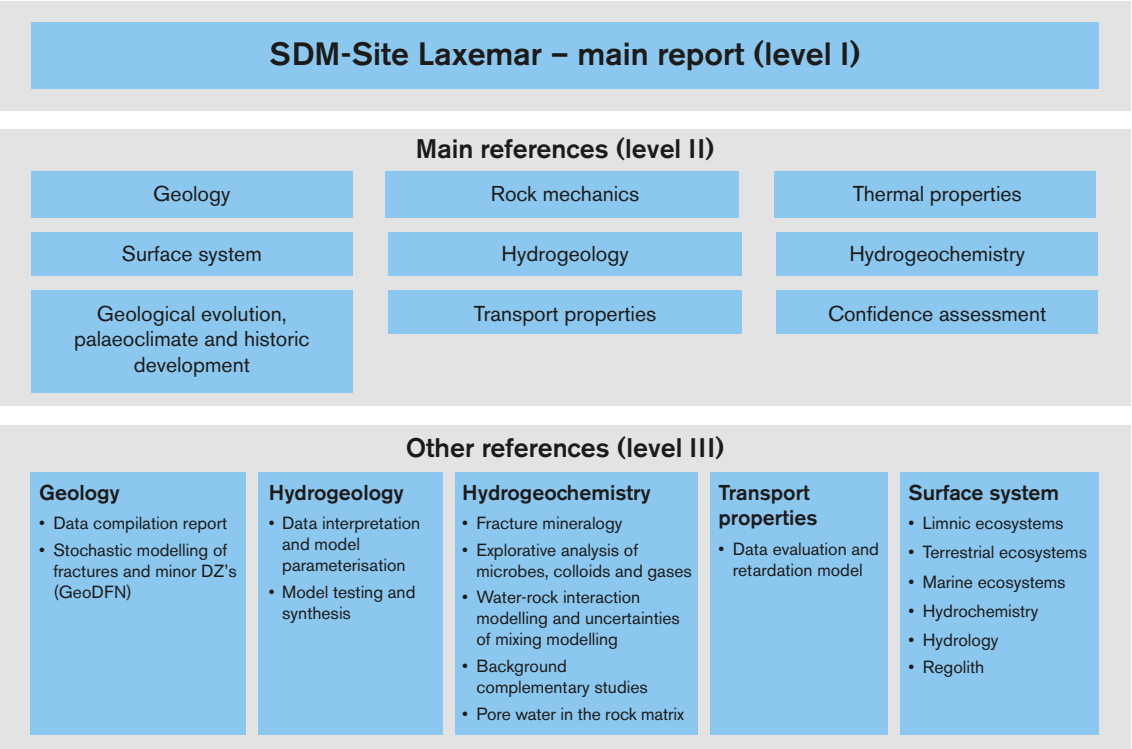

Figure 1-2. *SDM-Site Laxemar main report and background reports on different levels produced during model version SDM-Site Laxemar.*

1.2 Setting

The investigated area is close to the coast, cf. Figure 1-3. The topography is fairly flat (regional topographic gradient in the order of 4%; the topography corresponds to the Sub-Cambrian Peneplain /Fredén 2002/) but with relatively distinct valleys, cf. Figure 1-4 and Figure 1-5. The investigation area is located within a crystalline basement, mostly covered by a rather thin till in the elevated areas and with glaciofluvial sediments in the larger valleys. The site-average annual precipitation and specific discharge are estimated to be on the order of 600 mm and 160–170 mm, respectively /Werner et al. 2008, Larsson-McCann et al. 2002/ and the area is covered with a fairly large number of small streams indicating small local drainage basins within the regional model area, cf. Figure 1-3. The Äspö Hard Rock laboratory is an underground research facility that is located below the Äspö Island, cf. Figure 1-3, and the facility affects the groundwater flow locally in the area. The Simpevarp peninsula hosts the Clab interim facility and the nuclear power plants O1, O2 and O3. At Clab inflows are observed to the rock caverns near the surface and the shallow shafts surrounding the foundations of the power plants, but it has a very local effect on the groundwater flow. The geology of the area is described in more detail in Chapter 3.

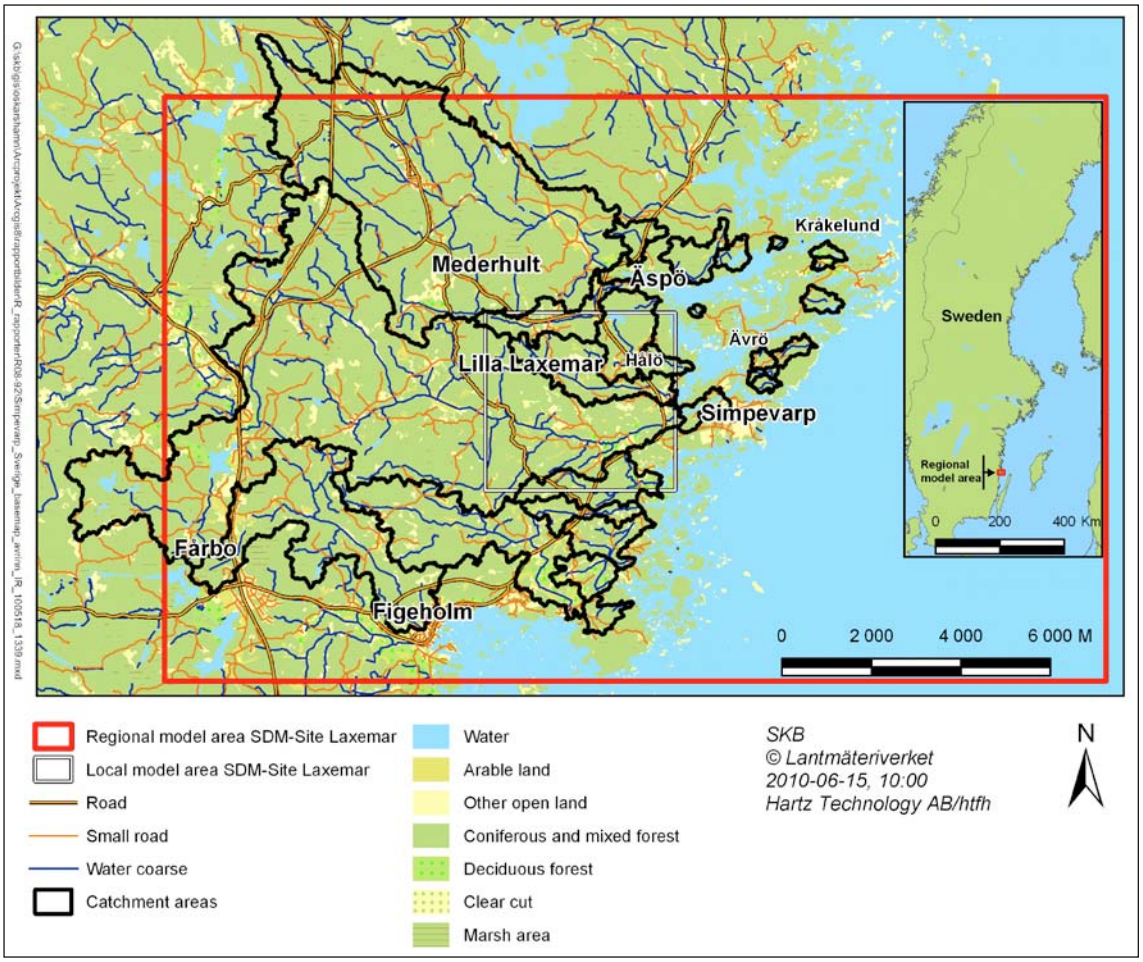

Figure 1-3. *Overview map of the Laxemar-Simpevarp regional model area with the SDM-Site Laxemar local model area indicated. The large number of small streams indicates small local drainage basins within the regional model area.*

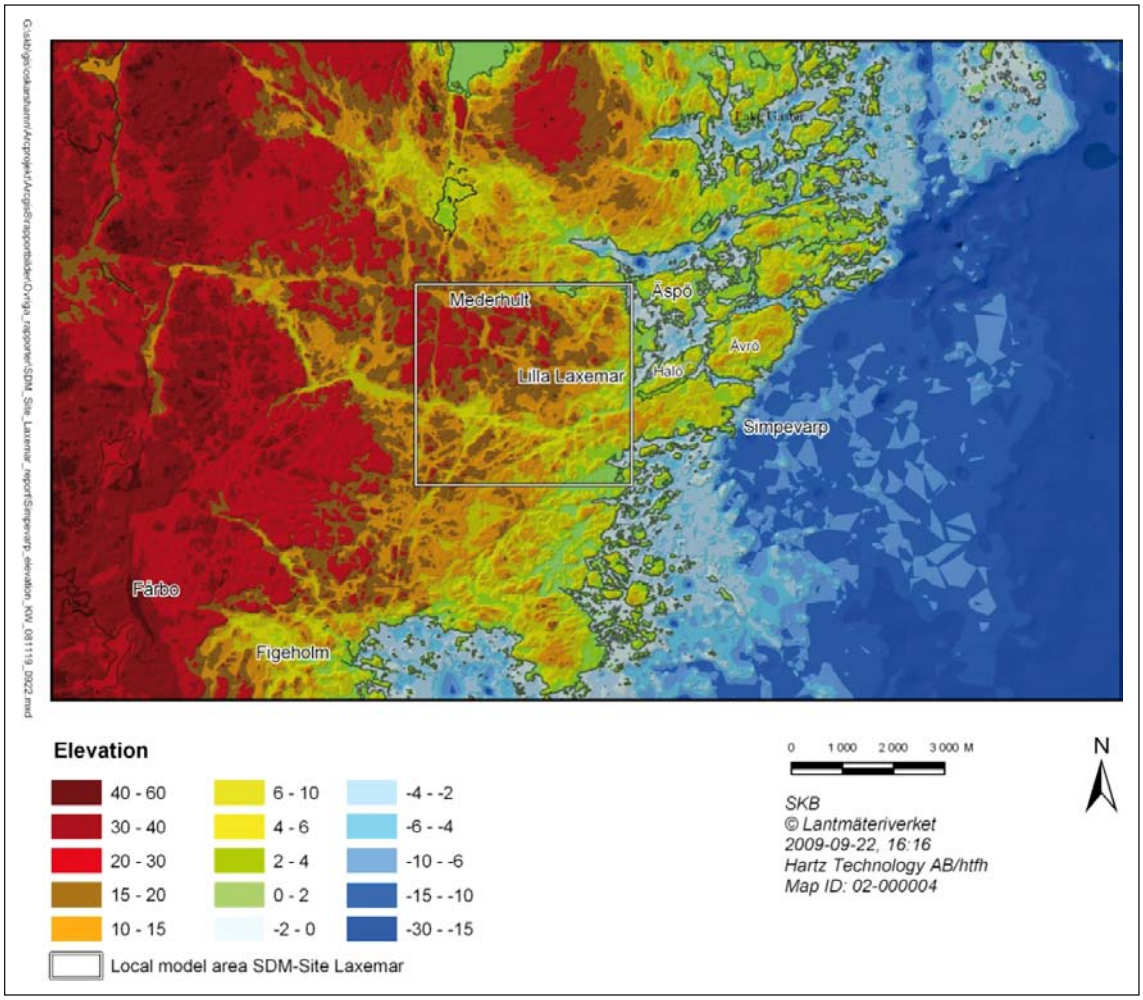

Figure 1-4. *Overview map illustrating the elevation of the ground-surface topography (m.a.s.l.) in an area corresponding to the Laxemar-Simpevarp regional model area, including the bathymetry of lakes and the sea.*

Figure 1-5. *Air photographs showing the flat topography, low gradient near shore situation in the Laxemar-Simpevarp area with shallow bays, a) view from the southeast, Clab facility in the foreground, b) view from the west, drill site KLX05/KLX12A in the centre of the photograph. Both photographs show the outline of the focused area in Laxemar in red, cf. Figure 1-6.*

1.3 Regional and local model areas

The regional and local model areas employed for model version SDM-Site Laxemar are shown in Figure 1-6. The *Laxemar-Simpevarp regional (scale) model area/volume* (Later in the report referenced as *Regional model area/volume*) for SDM-Site Laxemar is the same as the one used in model version Laxemar 1.2.

The coordinates outlining the surface area of the Regional model volume, cf. Figure 1-6, are (in metres):

RT90 (RAK) system: (Easting, Northing):
(1539000, 6373000), (1560000, 6373000), (1539000, 6360000), (1560000, 6360000).

RHB 70; elevation: +100 masl, –2,100 masl. (Observe that the maximum altitude within the regional area is c. +50 m but modelling volume is formally set to +100 m)

Volume: $21\times13\times2.2$ km^3=600.6 km^3.

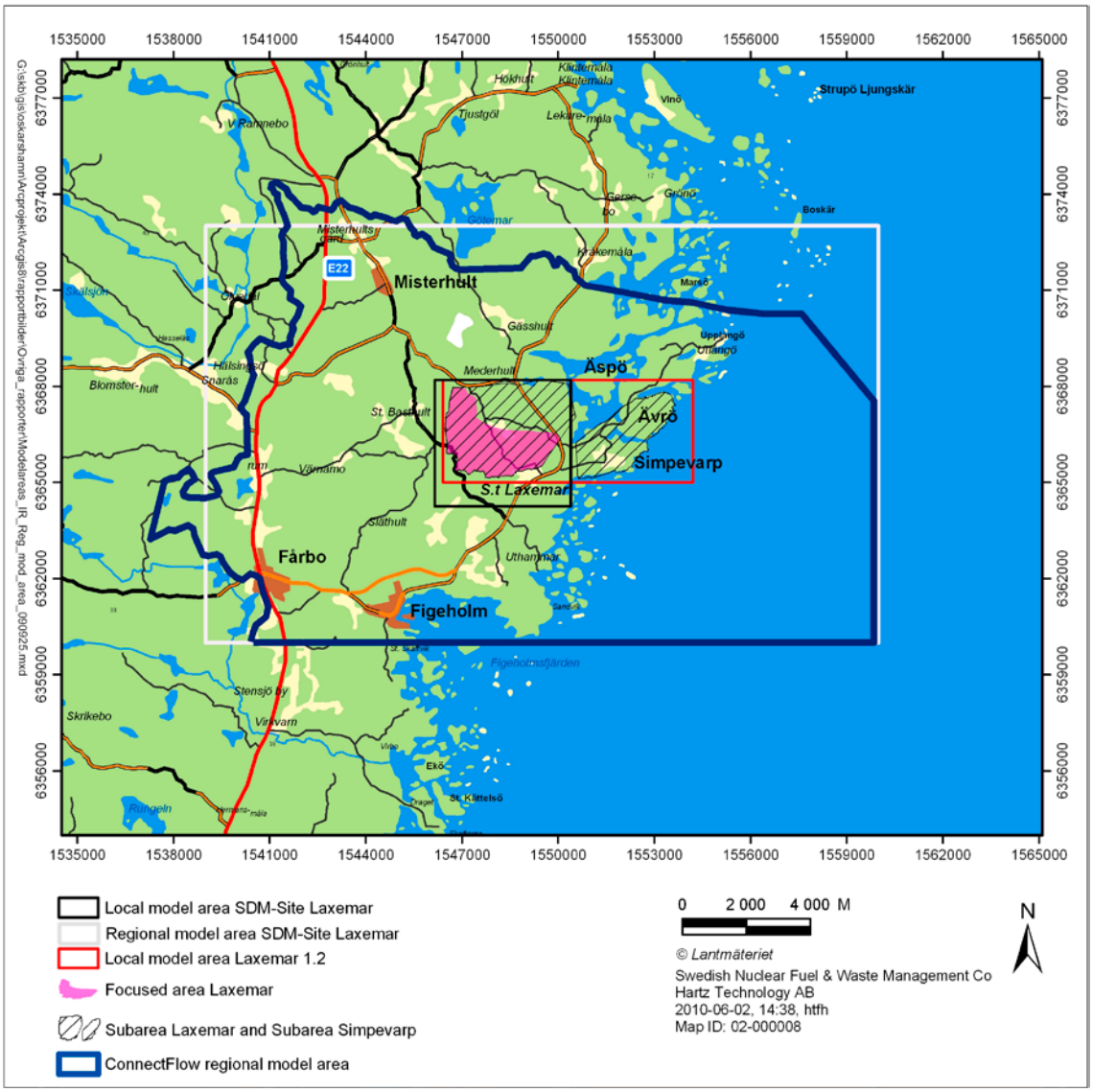

Figure 1-6. *Regional and local model areas used for model version SDM-Site Laxemar. The area coverage of the regional model is the same as that employed in previous model versions, whereas the local model area is significantly reduced compared to that employed in model version Laxemar 1.2. Laxemar subarea and Simpevarp subarea defined the investigation areas during the initial stage of the site investigations. The choice of boundaries used for the regional groundwater flow simulations (Using ConnectFlow) based on surface water catchments is also shown.*

The coordinates defining the *Laxemar local (scale) model area/volume* (Later in the report referenced as *Local model area/volume*) for model version SDM-Site Laxemar are (in metres):

RT90 (RAK system: (Easting, Northing): (1546150, 6368200), (1550390, 6368200), (1550390, 6364250), (1546150, 6364250).

RHB 70: elevation: +100 masl. –1,100 masl.

Volume: $4.24 \times 3.95 \times 1.2$ km^3=20.1 km^3.

Focused area/volume is the central, southern and western parts of the local model area, cf. Figure 1-6.

1.4 Review of documentation

The modelling work summarised in this report is based on the data available as of data freeze Laxemar 2.3, and is referred to as model version SDM-Site Laxemar. The detailed SDM-Site Laxemar hydrogeological reporting is provided in /Rhén et al. 2008/ and in /Rhén et al. 2009/. The complete SDM-Site Laxemar site-descriptive modelling work is reported in /SKB 2009a/ and the overall confidence assessment associated with the modelling work is detailed in /SKB 2009b/.

Table 1-1 shows the cumulative number of boreholes providing hydraulic information about the bedrock in the Laxemar-Simpevarp area. The number of boreholes is shown in relation to the two investigation stages; Initial Site Investigations and Complete Site Investigations (ISI and CSI), the five model versions (Version 0, Simpevarp 1.1, Simpevarp 1.2 and Laxemar 1.2, and model version SDM-Site Laxemar) carried out during the period 2002–2008. Model version Laxemar 1.2 represents the culmination of the ISI. The current hydrogeological modelling based on data freeze Laxemar 2.3 constitutes the principal contribution to SDM-Site Laxemar, corresponding to the CSI from a hydrogeological point of view. Investigations in ca 4,000 m of deep cored boreholes (KLX01–04) provided old and new (from ISI) hydraulic data within the Laxemar local model area for model version Laxemar 1.2. After Laxemar Stage 2.3 (CSI) hydraulic data from 16 additional deep cored boreholes within the Laxemar local model area with an approximate total length of 12,800 m were available (KLX05, KLX06, KLX07A, KLX08, KLX09, KLX10, KLX11A, KLX12A, KLX13A, KLX15A, KLX16A, KLX17A, KLX18A, KLX19A, KLX20A, KLX21B).

Table 1-1. The cumulative new (drilled during site investigation) number of boreholes providing hydraulic information about the bedrock in the Laxemar-Simpevarp area at the end of the five model versions carried out during the period 2002 through 2008. Kxx = core-drilled boreholes, Hxx = percussion-drilled boreholes (KLX and HLX: core-drilled boreholes percussion-drilled boreholes within Laxemar local model area). The reports listed in italics describe the hydraulic data collected and/or the hydrogeological modelling undertaken. The reports with underlined reference numbers summarise the development of the hydrogeological modelling along with the developments achieved within the other disciplines.

	Initial site investigation (ISI)			Complete site investigation (CSI)	
Desk top exercise	**Training exercise**	**Preliminary SDM**	**Preliminary SDM**	**Feedback and strategy**	**Model verification and uncertainty assessment**
Version 0	**Version 1.1**	**Simpevarp Version 1.2**	**Laxemar Version 1.2**	**Laxemar Stage 2.1**	**Laxemar Stage 2.3 (version SDM-Site)**
0 Kxx 0 Hxx	0 Kxx [(1)] 0 Hxx	4 Kxx [(2)] 3 Hxx	9 Kxx [(3)] 14 Hxx 3 KLX (7%)[(3)] 9 HLX(26%)	11 KLX (25%)[(4)] 9 HLX (26%)[(4)]	44 KLX (100%)[(5)] 34 HLX (100%)
R-02-35 *TR-97-06*	R-04-25 *TR-97-06* *R-04-63* *R-04-65*	R-05-08 *R-06-20* *R-05-11* *R-05-12*	R-06-10 *R-06-21* *R-06-22* *R-06-23* *R-06-24*	R-06-110 *R-07-57* *R-08-60*	TR-09-01 *R-08-78* *R-08-91* *R-08-92*

[(1)] Some old data from KLX01 and KLX02 were used besides earlier interpretations from the area.

[(2)] Old data from KLX01, KLX02, KAV01, KAV02 and KAV03 also used besides the indicated three KSH holes and KAV01 with some new data.

[(3)] KLX02–04. KLX02 included as some new tests were performed in that borehole. A few data from KLX05 and KLX06 were also available but these boreholes are not included here as the large amount of data became available later. Kxx also includes three KSH holes, KAV01, KAV04A, and KAV04B. Old data from KLX01 also used but not included in the numbers in the table.

[(4)] KLX02–12 included but data not complete for all these boreholes at this stage. Old data from KLX01 also used. New HLX boreholes were not considered.

[(5)] 19 core holes longer than 300 m and 25 shorter than 300 m. KLX01 and KLX27A not included.

Table 1-1 also shows references to the major background reports in relation to each model version/stage /Follin et al. 2004, 2005, 2006, Hartley et al. 2004, 2005, 2006, 2007, Holmén 2008, Rhén et al. 1997, 2006a, b, c, 2008, 2009, SKB 2002, 2004, 2005, 2006a, b/. The present report (R-08-92) provides a detailed summary of the work described in these reports, i.e. the field investigations, the data analyses, the conceptual model development and the numerical modelling of groundwater flow and solute transport. This summary report constitutes the main hydrogeological reference for the SDM. However, sometimes a reference is given in this report to the specific background reports for the sake of clarity.

1.5 Nomenclature and conventions

The basic nomenclature used for the Site Investigations is shown in Table 1-2 and are detailed in /SKB 2009a, Section 1.6.5 and Appendix 2 therein/. In this report some additional hydrogeological definitions are provided in the text with abbreviations. Decimal point "." is used and as 1,000-delimiter comma "," is used.

Table 1-2. Basic definitions applicable to the Laxemar site descriptive modelling and description /SKB 2009a/.

Laxemar-Simpevarp area	A general term for the Laxemar/Simpevarp region without a specified outer boundary. Essentially equating to the regional model area (see below) but also allowing for diffuse boundaries applied by the ecosystems modelling by SurfaceNET (partially adapting to groundwater divides). Note that for e.g. hydrogeochemistry purposes the entities "Oskarshamn" and KOV01 may be incorporated in the realm of this definition. The term "Laxemar-Simpevarp area" substitutes the previously used "Simpevarp area", with the same meaning/definition.
Candidate area	The candidate area refers to the area at the ground surface that was recognised as suitable for a site investigation, following the feasibility study work /SKB 2000/. Its extension at depth is referred to as the candidate volume.
Focused area/volume	The focused area in Laxemar refers to a part of the Laxemar subarea, primarily located in the southern part of the subarea, which was selected during the site investigation process as most suitable for hosting a final repository for spent nuclear fuel. Its extension at depth is referred to as the focused volume.
Rock unit	A rock unit is defined in the single-hole geological interpenetration on the basis of the composition, grain size and inferred relative age of the dominant rock type. Other geological features including the degree of bedrock homogeneity, and the degree and style of ductile deformation also help to define and distinguish some rock units. N.B. Defined rock units differ between boreholes.
Rock domain	A rock domain refers to a rock volume in which rock units that show specifically similar composition, grain size, degree of bedrock homogeneity, and degree and style of ductile deformation have been combined and distinguished from each other. The term rock domain is used in the 3D geometric modelling work and different rock domains in Laxemar are referred to as RSMxxx.
Deformation zone	Employed as a general notation of an essentially 2D structure characterised by ductile or brittle deformation, or a combination of the two. Those deformation zones which are possible to correlate between the surface (lineament with a length > 1,000 m) and an interpreted borehole intercept, or alternatively between one or more borehole intercepts, or exhibit an interpreted true thickness > 10 m are modelled deterministically, and are thus explicitly accounted for in the 3D RVS model. Deformation zones in Laxemar are denoted ZSM followed by two to eight letters or digits. An indication of the orientation of the zone is included in the identification code.
Fracture domain	A fracture domain is a rock volume outside deformation zones in which rock units show similar fracture intensity characteristics. Fracture domains in Laxemar are denoted FSMxx.
Repository depth	Normative depth and depth interval employed to sort and subdivide data in the analysis and modelling. Repository depth at Laxemar is tentatively set to –500 m, with an interval of –400 to –700 m. The designated repository depth for Laxemar is subsequently set by Repository Engineering as part of their design D2.

2 SKB's systems approach to hydrogeological modelling in the SDM

2.1 Overview of the SKB's system approach

The hydrogeological SDM modelling is conducted on different scales, regional scale as well as local scale. In model version SDM-Site Laxemar, particular attention is paid to the local model volume, see Section 1.3. In order to meet the objectives listed in Section 1.1, the groundwater system is divided into different hydraulic domains. Figure 2-1 illustrates schematically SKB's systems approach as employed in the hydrogeological SDM for Laxemar. The groundwater system consists of three basic hydraulic domain types, namely HSD, HCD and HRD, where:

- HSD represents the Quaternary deposits,
- HCD represents deformation zones (or "hydraulic conductors"), and
- HRD represents the fractured bedrock between the deformation zones.

The systems approach constitutes the basis for the conceptual modelling, the site investigations and the numerical simulations carried out in support of the hydrogeological SDM /Rhén et al. 2003/.

Besides the three hydraulic domains shown in Figure 2-1, the groundwater flow (saturated flow) and solute transport modelling with the ConnectFlow code consists of three additional elements:

- A solute (salt) transport model for the modelling of advective transport and matrix diffusion.
- Initial conditions for groundwater flow and hydrochemistry.
- Boundary conditions for groundwater flow and hydrochemistry.

The hydrogeological description of the site involves the integration of these six submodels with seven additional submodels provided by other disciplines to give an evaluation of thirteen different submodels in total, see Table 2-1.

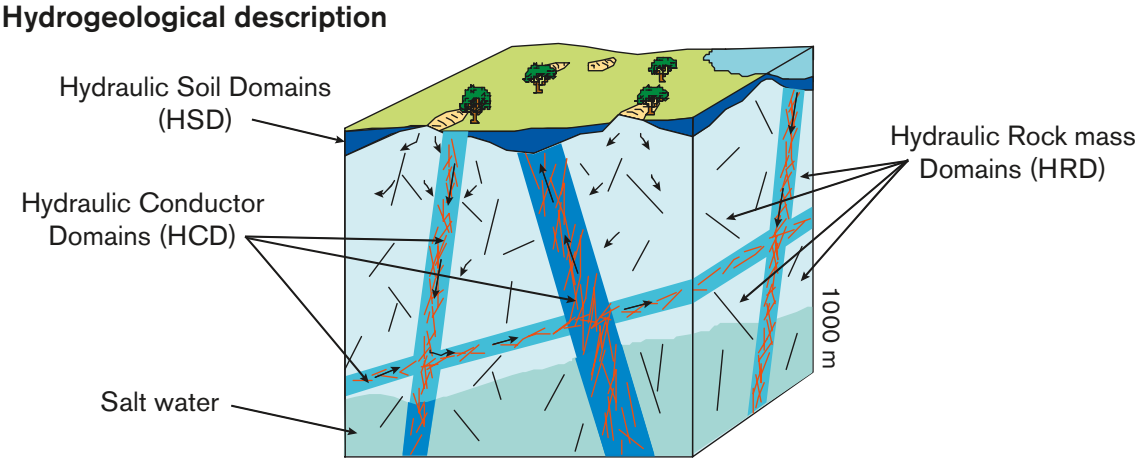

Figure 2-1. *Cartoon showing the division of the crystalline bedrock and the overburden (Quaternary deposits) into hydraulic domains. Within each domain, the hydraulic properties are represented by equivalent values, or by spatially distributed statistical distributions /Rhén et al. 2003/.*

Table 2-1. The groundwater flow and solute transport modelling with the ConnectFlow code is based on altogether 13 different submodels. The shaded fields show the key field/laboratory data used to conceptualise and parameterise the six elements listed in the top row. (Modified after /Follin 2008/.)

HCD, Hydraulic conductor domain model	HRD, Hydraulic rock mass domain model	HSD, Hydraulic soil domain model	Solute (salt) transport model	Initial conditions	Boundary conditions
2. Deformation zone (DZ) model	1. Rock domain model	3. Digital elevation model	7. Hydrogeological DFN model	10. Palaeo-hydrological model	3. Digital elevation model
5. Bedrock hydrogeological description of DZ	4. Fracture domain model	8. Quaternary deposits model	13. Bedrock transport properties model		11. Shoreline displacement model
	5. Bedrock hydrogeological description of rock between DZ	9. Quaternary deposits hydro-geological model			12. Baltic Sea salinity model
	6. Geological DFN model				
	7. Hydro geological DFN model				
Single-hole hydraulic tests (PSS, HTHB and PFL), Interference tests	Single-hole hydraulic tests (PSS, HTHB and PFL)	Slug-tests, Interference tests	Single-hole hydraulic tests (PFL)	Hydrochemical database	Hydrochemical database
Borehole core description	Borehole fracture data		Dilution tests, SWIW tests, In situ tracer tests, Laboratory tests (sorption/diffusion)		Hydrological monitoring data

The hydrogeological investigations/site-descriptive modelling of the groundwater system is divided up between the *surface systems* and *bedrock hydrogeology*, where the former treat the near-surface system (surface hydrology and the hydrogeology of surface rock and HSD), and the latter analyses the deeper (bedrock hydrogeology and hydraulic properties of the HCD and HRD), cf. Section 2.3. However, the bedrock hydrogeology modelling group also uses hydraulic properties of HSDs and interacts with the surface systems modelling group in the assessment of the hydraulic properties of HSDs. This division is purely pragmatic and the interface between the different descriptions is seamless from a conceptual modelling point of view. For instance, the hydraulic properties of the bedrock and the head distribution at the bottom boundary of the near-surface hydrogeological system are provided by the numerical flow modelling undertaken for the entire bedrock. A description of the approach taken by SKB for the near-surface hydrogeological modelling for Laxemar model version 1.2 is found in /Bosson 2006/ and for SDM-Site Laxemar in /Bosson et al. 2008/. The modelling focus is the shallow groundwater system but to obtain reasonable bottom boundary conditions the model extends down to c. 600 m depth with flow conditions that are consistent with the bedrock hydrogeological model that extends below c. 2,000 m depth, see Figure 2-2. A general description of the surface hydrology is presented in /Werner 2008/.

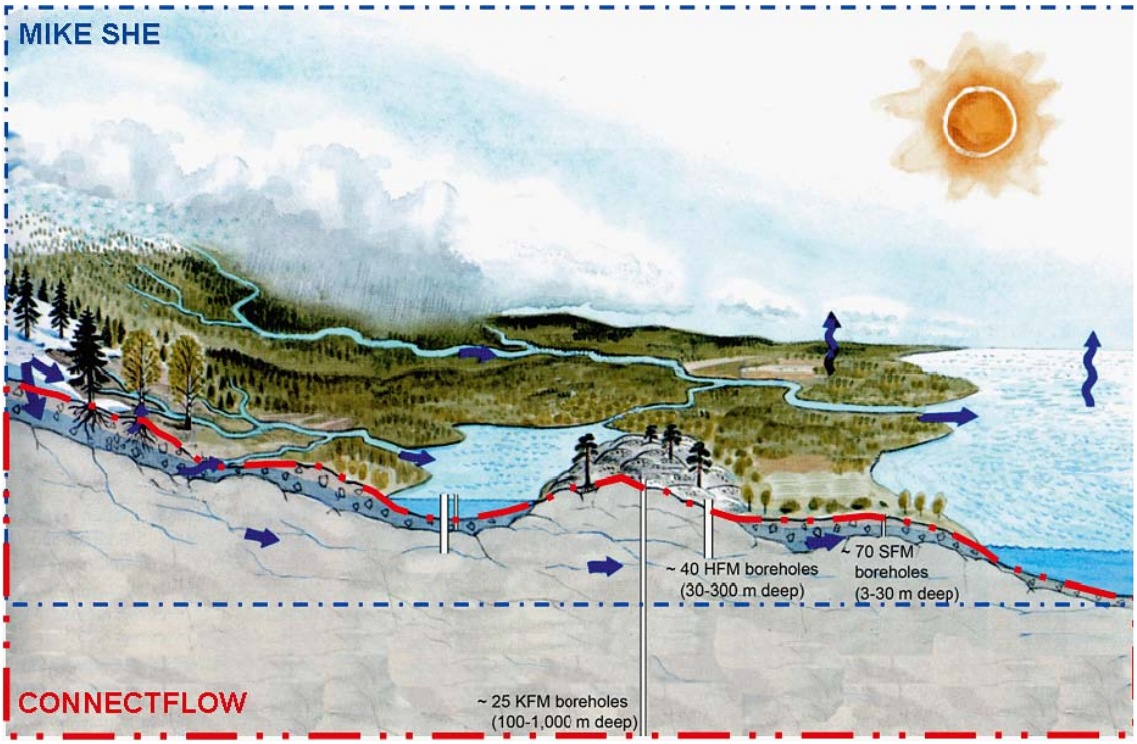

Figure 2-2. *Schematic illustration of how the modelling of the hydrologic cycle is divided into a surface-based system and a bedrock-based system. The former is modelled with the MIKE SHE code and the latter with the ConnectFlow code. Reproduced from /Follin et al. 2007c/.*

2.2 Methodology overview

As part of the preliminary Site Descriptive Modelling (SDM) for the Initial Site Investigation (ISI) phases at Forsmark, Simpevarp and Laxemar, a methodology was developed for constructing hydrogeological models of the crystalline bedrock at the studied sites. The methodology combined a deterministic representation of major deformation zones with a stochastic representation of the less fractured bedrock between these zones using a Discrete Fracture Network (DFN) concept. In order to perform regional scale groundwater flow and solute transport modelling, the hydrogeological description was generally implemented as an equivalent continuum porous medium (ECPM) concept by a process of upscaling the underlying DFN model.

The deterministic deformation zones and fracture network (between the deterministic deformation zones) are parameterised hydraulically with data from single-hole Posiva Flow Log (PFL) pumping tests, single-hole Pipe String System (PSS) injection tests and single-hole pump tests with Hydraulic Test System for Percussion Boreholes (HTHB), cf. Chapter 4 and also /Rhén et al. 2008/ for a detailed review of test methods.

The hydraulic properties of the HCD and DFN models form the basis constructing regional-scale ECPM flow models, cf. Chapter 6, which are used for example to simulate the palaeohydrogeological evolution over the last 10,000 years (Holocene), cf. Chapter 5 and 7. This modelling is conducted as a coupled process between variable density groundwater flow and the hydrodynamic transport of several reference waters, taking into account the process of rock-matrix diffusion. Results obtained from these simulations include prediction of hydrochemical constituents (e.g. major ions and environmental isotopes) for the present-day situation along boreholes, which is subsequently compared with results of groundwater samples acquired from the corresponding boreholes/borehole sections. By comparing the model predictions with measurements, the models developed can be partially calibrated to improve model parameterisation, thus improving our understanding of principal controls of the hydrogeological system, thereby building confidence in the conceptual models developed for the studied site, cf. Chapters 7 through 9.

For the complete site investigation (CSI) phase, the process of integrating geological, hydrogeological, hydrogeochemical and transport models has identified the need for more robust, discipline-consistent models to be produced by the final stage of the site descriptive modelling. As part of the solution for obtaining more robust models, a more coherent strategy has been formulated, see Figure 2-3. This "updated strategy" is not an entirely new direction in methodology, but rather a refocusing on and clarification of the key aspects of the hydrogeological SDM, i.e. assessing the current understanding of the hydrogeology at the analysed site, and provision of the hydrogeological input descriptions needed for the end users; design, safety assessment and environmental impact assessment. These input descriptions should focus especially on the hydraulic properties in the potential repository volumes of the explored sites and assessment of the distribution of flow paths at potential repository depth.

/Follin et al. 2007a/ introduced an updated procedure for integrating four kinds of data in the groundwater flow (GWF) modelling of the final SDM, see Figure 2-4, as a means of approaching the issue of confirmatory testing of the developed models (Step 4 in Figure 2-3).

At Laxemar the hydrogeological HCD and DFN-based models for the HRDs derived as part of model version Laxemar 1.2 and the hydrogeological and hydrochemical information from data freeze Laxemar 2.1 were used to explore some specific hydrogeological issues raised in the reviews of Laxemar version 1.2. The aim was not a full SDM update, but rather to provide preparatory modelling studies of regional boundary conditions, cf. /Holmén 2008/ that was based on /Ericsson et al. 2006/, as well as modelling studies intended to provide insight into new aspects of the suggested procedure and the use of field data (e.g. interference tests) and the possible effects in Laxemar of the nearby underground laboratory Äspö Hard Rock Laboratory (Äspö HRL) /Hartley et al. 2007/, thereby providing premises and support for the subsequent work reported here.

It is noted that an underlying idea behind Figure 2-4 is that the same GWF model is used for each type of simulation to make it transparent that a single implementation of the conceptual model can be calibrated against all four types of field observation (although A is used for conditioning the borehole near-field while B–D are the basis for confirmatory testing), although it might have been possible to improve the model performance further in relation to a particular data type by refining, e.g. the geometry or material property distribution around a particular observation borehole.

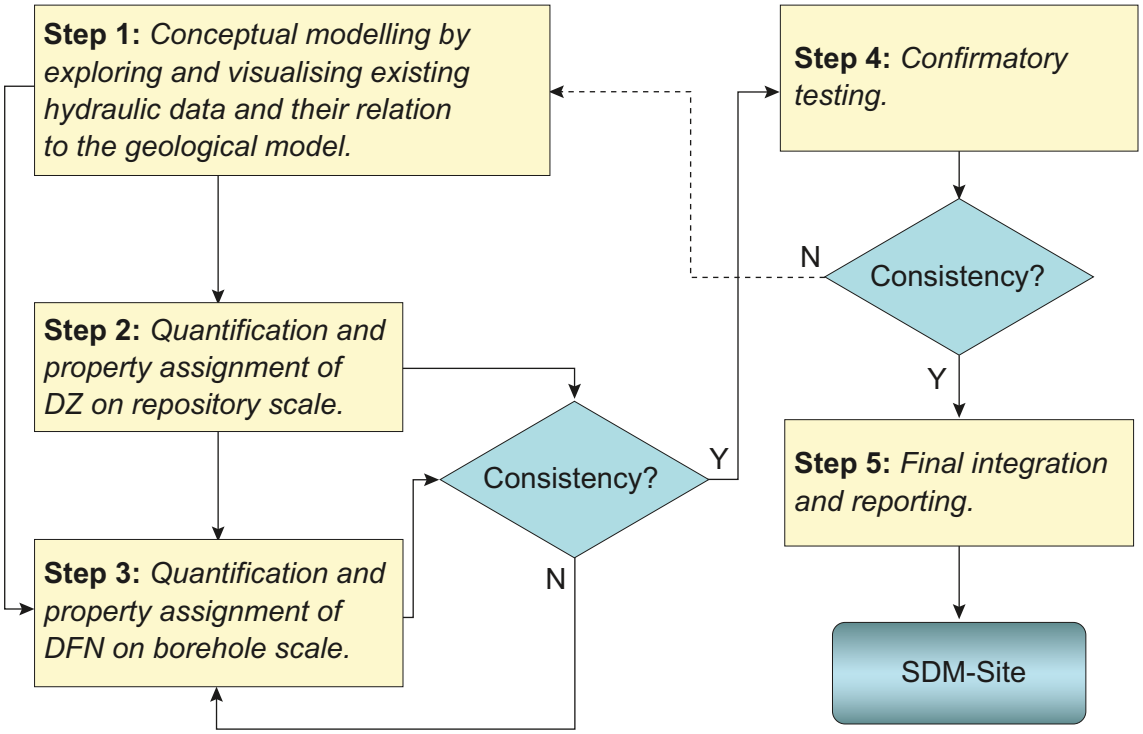

Figure 2-3. *Flow chart of the five steps suggested for the hydrogeological modelling of the complete site investigation (CSI) phase.*

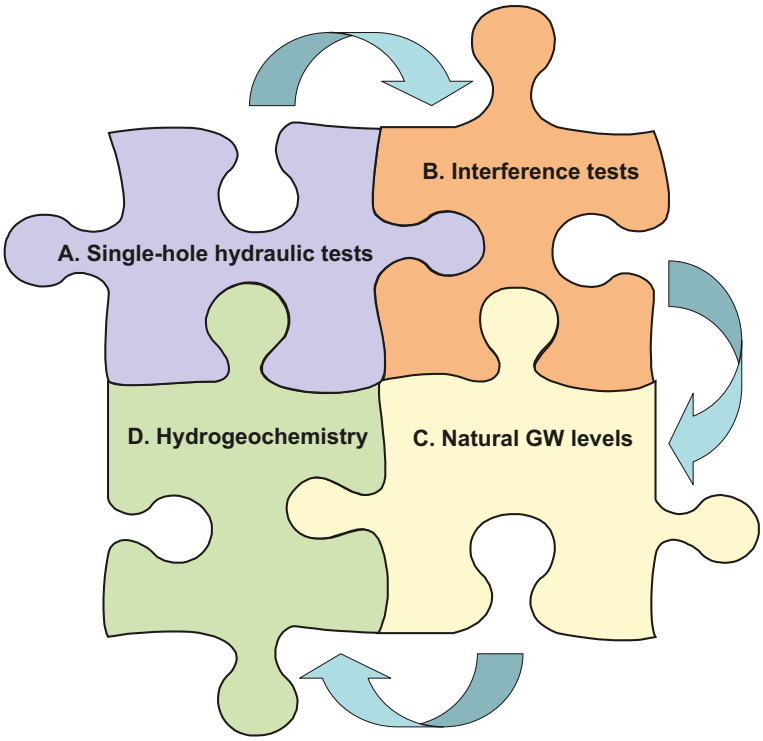

Figure 2-4. *Four kinds of data are used in the numerical groundwater flow modelling of the final SDM as a means of approaching the issue of confirmatory testing, cf Step 4 in Figure 2-3: A) Hydraulic properties of deformation zones and discrete fracture networks as deduced from single-hole hydraulic tests; B) Interference tests; C) Natural groundwater levels; D) Hydrogeochemistry /Follin et al. 2007b/.*

2.3 Primary concepts and assumptions

The evaluation of data and building of hydrogeological models are based on several conceptual ideas and assumptions that are outlined in this section.

2.3.1 Deterministic and stochastic features

A cornerstone of the bedrock hydrogeological description concerns the hydraulic characterisation of the deterministic deformation zones (HCD) and the fractured bedrock between these zones (HRD). The approach taken by SKB combines a deterministic representation of the major deformation zones with a stochastic representation of the fractured bedrock between these zones using a DFN concept. The hydraulic characterisation of the fractured bedrock between the deterministic deformation zones at repository depth is a vital, yet complex task given the relatively limited number of data available at this depth. The hydrogeological SDM is based on data from investigations in vertical to steeply inclined cored boreholes drilled from the surface, typically extending to depths between 300 to 1,000 m. The current understanding of the groundwater system at depth is constrained by this fact, where the subvertical boreholes also tend to favour sampling of subhorizontal structures.

The principal structural-hydraulic approach taken by SKB in the hydrogeological modelling within SDM-Site Laxemar, i.e. modelling large deformation zones deterministically and identifying the maximum size for 2D hydraulic features modelled stochastically ($L \leq 1{,}000$ m) is illustrated in Figure 2-5.

The figure indicates that features larger than c. 10 m can be considered as deformation zones and if they are in the range 10–1,000 m they are minor deformation zones, cf. also Table 2-2. However, there is no strict length limit between single fractures and minor deformation zones. Single fractures tens of meters long can be found. Deformation zones are discussed in more detail in Sections 2.3.3 and 3.2.

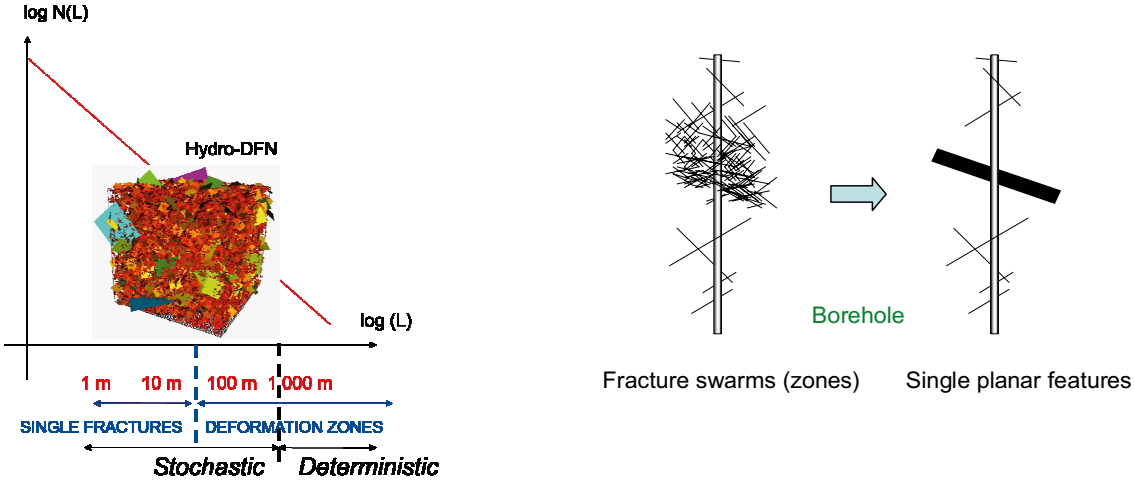

Figure 2-5. *Schematic illustrations showing the structural-hydraulic approach in the hydrogeological SDM used for the treatment of the deterministic deformation zones and minor deformation zones, the latter modelled stochastically in the hydrogeological SDM and considered to be in the size range 10 to 1,000 m, cf Table 2-2. Right: The hydraulic data collected between the upper and lower bounds of an interpreted deformation zone interval in a borehole are lumped together to form one single integrated transmissivity value for the zone in that interval. In the same fashion all fractures in the deformation zone interval are also lumped together, to form one single planar feature with an integrated transmissivity made up of the sum of individual fracture transmissivities. Left: A tectonic continuum is envisaged where the number of features/fractures of different sizes follows a power law relationship. Features up to size L = 1, 000 m. (Features up to r = 564 m in size (corresponding to a 1,000×1,000 m square) are regarded as uncertain and are consequentially treated stochastically using the Hydrogeological DFN concept) Reproduced from /Follin et al. 2007c/.*

The tectonic continuum hypothesis implies that the size and intensity of fractures on multiple scales can be approximated by a *single* power-law relationship, indicated by the red line in Figure 2-5, which by definition requires global fracture orientation sets. However, the density functions may vary between the sets. The orientations of the global fracture sets used in the hydrogeological DFN modelling within the Laxemar-Simpevarp regional model volume are assumed to be Fisher distributed.

Fracture intensity is intimately connected to the spatial arrangement of the fractures. The hydrogeological DFN modelling is based on the assumption that the spatial distribution of fracture centres of each fracture set within each fracture domain follows a Poisson process and a Euclidean size-intensity scaling[1] /La Pointe et al. 2008/.

The assumption of a Euclidean scaling was tested in the geological DFN modelling in parallel with other assumptions. Fracture intensity scaling was found to be Euclidian to weakly fractal and the recommended base model assumes Euclidian intensity scaling, cf. /Wahlgren et al. 2008/. It was also concluded that a three-dimensional Poisson process is adequate to describe the locations of fracture centres in space. The conclusion that fracture locations follow a Poisson process is equivalent to fracture centres having a uniform probability of being located anywhere in space. In /Wahlgren et al. 2008/ it is also stated that fracture volumetric intensity model (P_{32}) for *all fractures* generally can be described by a Weibull or Gamma probability distribution, comparing with borehole data down to a minimum scale of approximately 9–15 m (bin size along the borehole) in most of the geological fracture domains (FSM) modelled and may be appropriate for smaller scales. Details of the geological DFN modelling is presented in /La Pointe et al. 2008/.

[1] Euclidean scaling is a particular kind of a tectonic continuum where the number of fractures is linearly proportional to the dimensionality of observation (length, area or volume). Thus, Euclidean scaling implies that doubling of the scale (size) of observation, effectively doubles the number of fractures, i.e. constant fracture intensity.

In effect, the primary geometrical concepts and statistical distributions of the global fracture sets defined in the geological DFN modelling are the same as those used in the hydrogeological DFN modelling. That is:

- Fisher distributed fracture orientations.
- Set-specific power-law intensity (size) density functions.
- Poissonian fracture locations.

A key difference between the two DFN descriptions is in the data; the geological DFN modelling considers primarily the geometrical properties of *surface data* (outcrop data and lineament data) and borehole data representing *all fractures (open and sealed)*, whereas the hydrogeological DFN modelling focuses solely on the geometrical properties of *borehole data* representing two different sets of fracture data: (*i*) *potentially flowing features* (*open and partly open fractures*), and (*ii*) *continuously flowing features* detected by the Posiva Flow Log method (so-called *PFL-f* features)[2].

The differences between the databases used by geology and hydrogeology impacted on how the DFN modelling was carried out. However, since the intensity of *potentially flowing features* constitutes a fraction of *all fractures*, the envisaged relationship between the associated power-law density functions can be illustrated as in Figure 2-6. Figure 2-6 implies that completely sealed features exist only among the small fractures (small features), whereas large features, i.e. deformation zones, are all heterogeneous with regard to fractures within the deformation zones , i.e. there are generally a number of more or less open fractures that are connected that makes these large structures almost always flowing. Figure 2-6 shows also the conceived behaviour of the *continuously flowing features,* i.e. the *connected open fractures*. The *PFL-f features* are envisaged as a subset of the latter category, see Chapter 6. A demonstration of the relevance of the notion illustrated in Figure 2-6 is shown for HRD_C in Figure 6-7.

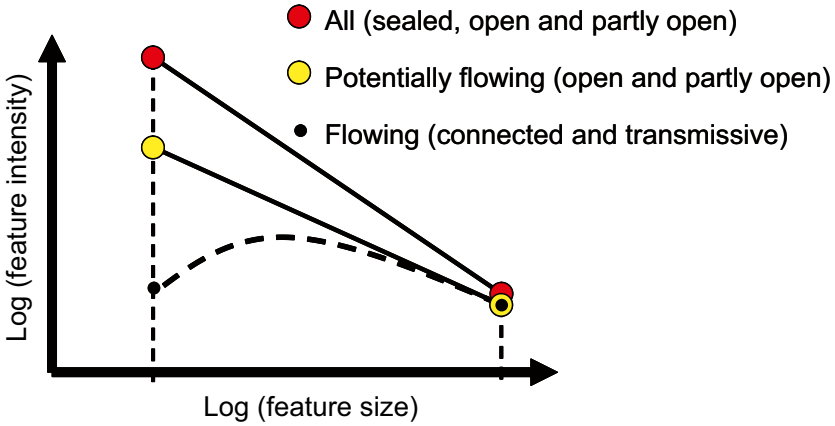

Figure 2-6. *Cartoon showing the envisaged relationship between the pdf intensity functions of all, potentially flowing and flowing features as a function of feature size. The flowing features detected with the PFL-f method are envisaged to be a subset of the flowing features in the hydrogeological DFN modelling work /modified after Follin 2008/.*

[2] In the context of the SDM, '*all fractures*' means that no distinction was made between fractures with regard to fracture aperture. Hence, *sealed* fractures were pooled with *partly open* and *open* fractures in the geological DFN modelling. In contrast, the hydrogeological DFN modelling focused, to begin with, on the properties of the '*potentially flowing features*', which implies that the analysed fractures must be at least partly open. In order for a partly open or open fracture to be detected as a flowing fracture it must be (*i*) connected to a positive hydraulic boundary (either directly or indirectly via a network of other flowing features) and (*ii*) have a sufficient transmissivity relative to the measurement threshold of the test equipment used, cf. Section 2.3.2.

2.3.2 Evaluation of single-hole hydraulic tests

The geological deterministic deformation zones (DZ) and the DFN models are parameterised hydraulically using data from single-hole *Posiva Flow Log* (PFL) pumping tests and single-hole *Pipe String System* (PSS) injection tests in cored boreholes as well as the HTHB method in percussion boreholes (Swedish abbreviation for *Hydraulic Test System for Percussion Boreholes* (*Hydro Testutrustning i Hammar-Borrhål)*, cf. Chapter 4 and /Rhén et al. 2008/.

In relation to the three methods used for hydraulic borehole investigations, PFL, PSS and HTHB, the hydraulic characterisation of fractured bedrock between deterministic deformation zones may be envisaged as illustrated in Figure 2-7. The constituent parameters measured, where the fractures intersects the borehole, are the flow rate Q and the pressure p. Since the two entities are coupled the material property studied is really the specific discharge, $Q/\Delta p$. The specific discharge is dependent on several important aspects, among which are particularly noted:

- Q_{limit}; the lower measurement limit of the flow rate for the test method.
- T_{bh}; the transmissivity of the tested fracture intersecting the borehole. Evaluation of transmissivities (T_{bh}) can be affected by the hydraulic resistance close to the borehole (positive or negative skin factor), with either reduced or enhanced hydraulic communication between the borehole and the rock, respectively.
- C; the connectivity of the tested fracture to other fractures away from the borehole. Some fractures are isolated, or are a part of an isolated cluster of fractures. Others are well connected and a part of the overall connected hydrological system.
- T/S; the hydraulic diffusivity of the fracture system within the radius of influence.
- t; the duration of the hydraulic testing, i.e. the test time.
- ΔL; the length of the test interval (test section) in the borehole.

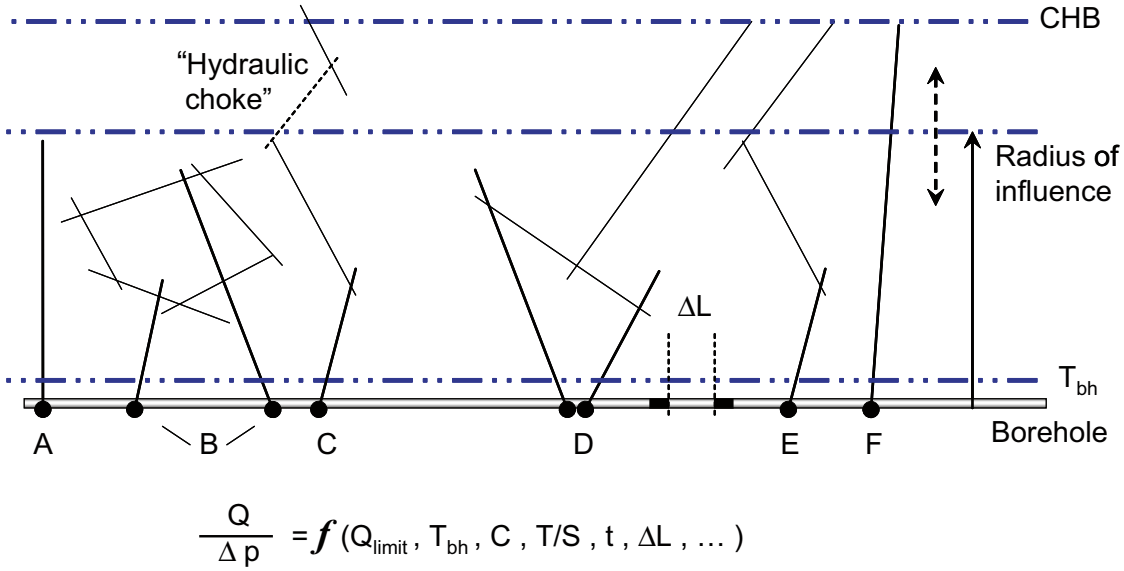

Figure 2-7. *Cartoon showing a borehole with six different symbolic fracture network situations, cases A–F. The specific capacity, $Q/\Delta p$, measured along the borehole is dependent on several factors, e.g. the measurement limit, Q_{limit}, of the test method, the transmissivity of the fracture intersecting the borehole, T_{bh}, the fracture connectivity, C, the hydraulic diffusivity, T/S, of the fracture network, the test time, t, the length of the test section, ΔL, etc. The hydraulic characterisation of the fracture system varies depending on the method used as well as on the in situ conditions, e.g. the occurrence of "hydraulic chokes". Cases A–C represent isolated fracture networks and cases D–F represent fracture networks connected to the overall hydrogeological system. The overall hydrogeological system for the latter is here indicated by a constant head boundary (CHB) suggesting a pseudo steady-state flow regime at long test times. The cartoon is rotated 90° to improve the readability. Reproduced from /Follin et al. 2007c/.*

The differences between the two test main methods used in Laxemar, PFL and PSS, are described in detail in Chapter 4 and in /Rhén et al. 2008/. From a site descriptive modelling point of view it is noted that the modelling approach taken by SKB focuses on the conductive fracture frequency (CFF) measured by the so called PFL-f method. This emphasis on the PFL-f method means, among other things, that fracture network situations such as A and B in Figure 2-7 are not honoured in the SDM-Site modelling, neither in the hydrogeological DFN modelling nor in the subsequent ECPM groundwater flow modelling[3].

Neglecting situations like A and B does not mean that they are unimportant. On the contrary, the relevance of compartmentalised fracture systems is well recognised by the hydrogeological modelling group and a procedure has been suggested for its handling in the repository modelling carried out in the forthcoming safety assessment project SR-Site. However, situations such as C–E, cf. Figure 2-7, with larger systems of connected fractures that connect to a positive boundary, are regarded as more important for the groundwater flow modelling addressed in the hydrogeological SDM modelling (PSS tests may indicate compartmentalised fracture systems where PFL-f indicates low-permeable rock, or rather no connected fractures with transmissivities above the measurement limit of the PFL-method).

A pertinent question to be answered in due time, is the role of the presumably connected fractures of transmissivity less than the practical lower measurement limit of the PFL-f method, which is c. $1 \cdot 10^{-9}$ m^2/s. This matter is discussed further in /Rhén et al. 2008/. Another circumstance to consider is that not all boreholes in the potential deposition volumes in Laxemar have been hydraulically tested with both test methods, cf. Appendix 1. It also differs slightly between Site investigations in Forsmark and Laxemar in that PSS with 5 m test sections were only performed at Laxemar in the elevation interval –300 to –700 m, whereas in Forsmark generally these tests were made in the entire borehole below casing.

2.3.3 Hydraulic conductor domain (HCD) model

The term deformation zone is used in all phases of the geological work, bedrock surface mapping, surface based interpretations, single-hole geological and hydrogeological interpretations and 3D modelling. Hence, a deformation zone is a general term referring to an essentially planar structure along which there is a concentration of brittle, ductile or combined brittle and ductile deformation. Table 2-2 presents the terminology for brittle structures based on trace length and thickness as presented in /Andersson et al. 2000/. The geometric borderlines between the different structures are highly approximate. Deformation zones are considered to have a variable thickness and a spatial variability of the properties that is important when evaluating the data /Wahlgren et al. 2008/, cf. Figure 2-8.

SKB's geologists interpret zones within the local model area with associated surface lineaments longer than 1,000 m (1,600 m within regional model area but outside the local model area) as being deterministic (major local or regional) deformation zones, whereas those with length less than 1,000 m are referred to as minor local deformation zones (MDZ) and are consequently modelled stochastically using DFN models. Deformation zones with inferred true thickness of 10 m or more in boreholes that are not possible to relate to a structure (lineament) on ground surface, are modelled deterministically as circular discs with a size equivalent to a 1,000×1,000 m^2 square /Wahlgren et al. 2008/. The size of these discs, with a judged thickness of 10 m or more based on borehole data, is highly uncertain and is in fact similar in size (i.e. radius) to the larger MDZs modelled stochastically.

Deformation zones are important hydrogeological objects as they generally are more conductive than the surrounding rock but may also occasionally act as hydraulic barriers. All deformation zones modelled deterministically in the geological model are also defined as HCDs in the hydrogeological model. Based on hydrogeological evaluation of important hydrogeological features, some HCDs may also be defined as deterministic hydraulic features that do not correspond to the deterministically modelled deformation zones by geology, but still firmly link to hydraulic and geological observations in boreholes, cf. Section 3.2.

[3] The reason why the PFL method cannot address situations like A and B in Figure 2-8, in contrast to the PSS method, is explained in Section 4.1. It is also explained in Section 4.1 why the PSS method has problems in distinguishing situations A and B from situations C–E.

Table 2-2. Terminology and general description (length and width are approximate) of brittle structures (modified after /Andersson et al. 2000/).

Terminology	Length	Width	Geometrical description
Regional deformation zone	> 10 km	> 100 m	Deterministic
Local major deformation zone	1 km–10 km	5 m–100 m	Deterministic (with scale-dependent description of uncertainty)
Local minor deformation zone	10 m–1 km	0.1–5 m	Stochastic (if possible, deterministic)
Fracture	< 10 m	< 0.1 m	Stochastic

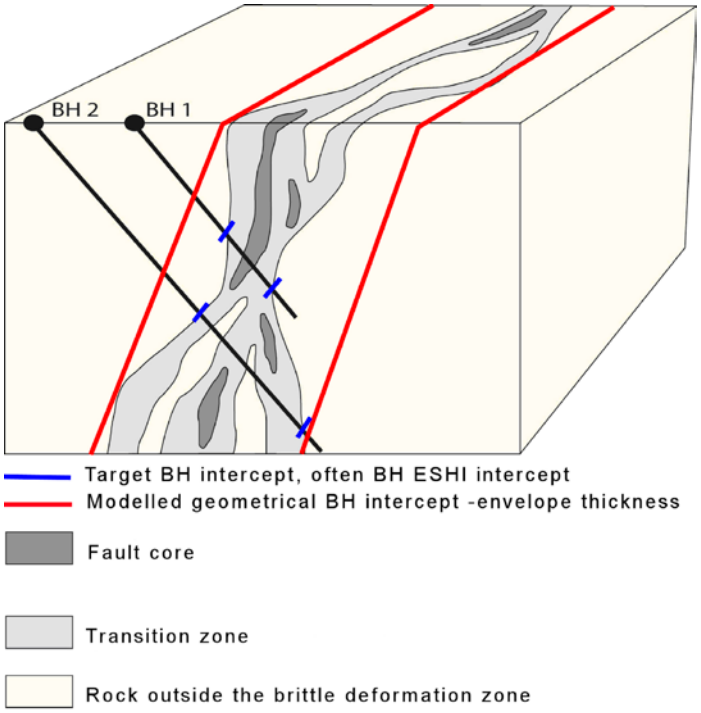

(redrawn after Caine et al. 1996)

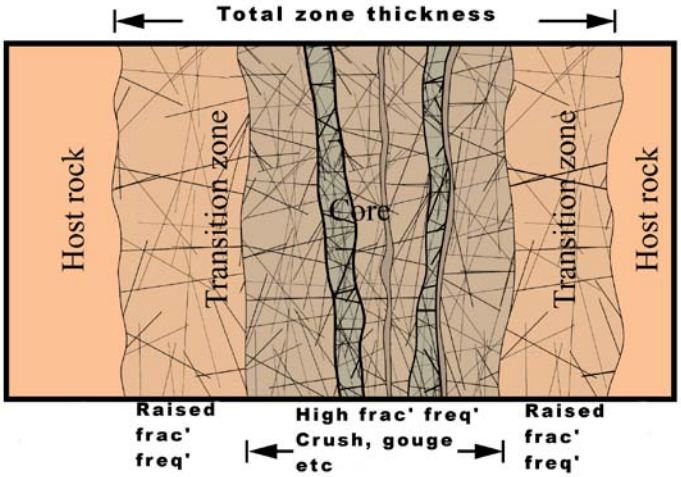

Figure 2-8. *Top: Three-dimensional schematic conceptual geometric model for a brittle deformation zone in Laxemar along which shear displacement has occurred (redrawn after /Caine et al. 1996/). Note the variable character of the deformation zone along the two borehole intersections. Bottom: Schematic illustration of a brittle deformation zone. From /Wahlgren et al. 2008/.*

The hydraulic characterisation of the deformation zones is fairly straightforward. The hydraulic data between the upper and lower bounds of an interpreted deformation zone interval in a borehole, as described in the single-hole geological interpretation /Wahlgren et al. 2008/, are the base for the assignment, regardless of the hydraulic test method used. The hydraulic data collected are pooled, i.e. lumped together, to form an integrated single transmissivity value for the particular borehole interval for any given method and means of test evaluation employed, cf. Figure 2-5.

2.3.4 Hydraulic rock domain (HRD) model

The fracture domains and rock domains defined in the geological interpretation, cf. /Wahlgren et al. 2005, 2008/ have been the base geometrical models for the study of the spatial variation of hydraulic properties and for the subsequent definition of hydraulic rock domains (HRD), cf. Chapters 4 and 5 and /Rhen et al. 2008/. Fracture domains, cf. /Wahlgren et al. 2005/, potentially have significance for the hydraulic characteristics of the rock since fracture intensity and orientations vary between them, and these properties have a control on the permeability of the rock.

Hydraulic rock domains were defined based on the framework of fracture domains within the local model volume, but with some fracture domains being combined where the differences between adjacent fracture domains were not considered hydraulically significant. The resulting hydraulic rock domains are parameterised in terms of a stochastic DFN model, by calibration against available hydraulic data mainly from the PFL-tests. The hydrogeological DFN modelling is based on the assumption that:

$$P_{10,all} \geq P_{10,open} \geq P_{10,cof} \geq P_{10,PFL} \qquad (2\text{-}1)$$

where $P_{10,cof}$ denotes the linear intensity (1/m) of "connected open fractures", a key property of any hydrogeological DFN model. The meaning of the different suffixes (*all*, *open*, *cof* and *PFL*) in Equation 2-1 is explained in Figure 2-9.

To complete the parameterisation, the following quantities are required; they are either estimated directly from the data or derived from the calibration process.

- The fracture surface area per unit volume of *open* fractures ($P_{32,\ open}$, volumetric fracture intensity; m^2/m^3).
- The shape parameter k_r and the location parameter $r_{0,}$ assuming that the fracture size distribution follows a power-law distribution /Rhén et al. 2008/.
- The parameters relating transmissivity to fracture size. Three different kinds of correlations between fracture transmissivity and fracture size are considered as variants, as described in Table 2-3.

The hydrogeological DFN models allow the parameters described above to vary by fracture set, by depth zone and between different hydraulic rock domains.

The values of the power-law intensity distribution parameters (k_r and r_0) are not uniquely constrained by the methodology adopted and the data available. It is therefore necessary to consider several different combinations of parameters which allow the sensitivities to these parameters to be quantified in subsequent modelling. The combinations of the different parameters were based on the results reported in the preliminary SDM /SKB 2006a/. Details on the development of the hydrogeological DFN model are provided in Chapter 6.

Table 2-3. Transmissivity parameters used for all sets when matching measured PFL-f flow distributions. (Log base 10) /Rhén et al. 2008/.

Type	Description	Relationship	Parameters
Correlated	Power-law relationship	$\log(T) = \log(a\ r^{b})$	a , b
Semi-correlated	Log-normal distribution about a power-law correlated mean	$\log(T) = \log(a\ r^{b}) + \sigma_{log(T)}$ N[0.1]	a , b, $\sigma_{log(T)}$
Uncorrelated	Log-normal distribution about a specified mean	$\log(T) = \mu_{log(T)} + \sigma_{log(T)}$ N[0.1]	$\mu_{log(T)}$, $\sigma_{log(T)}$

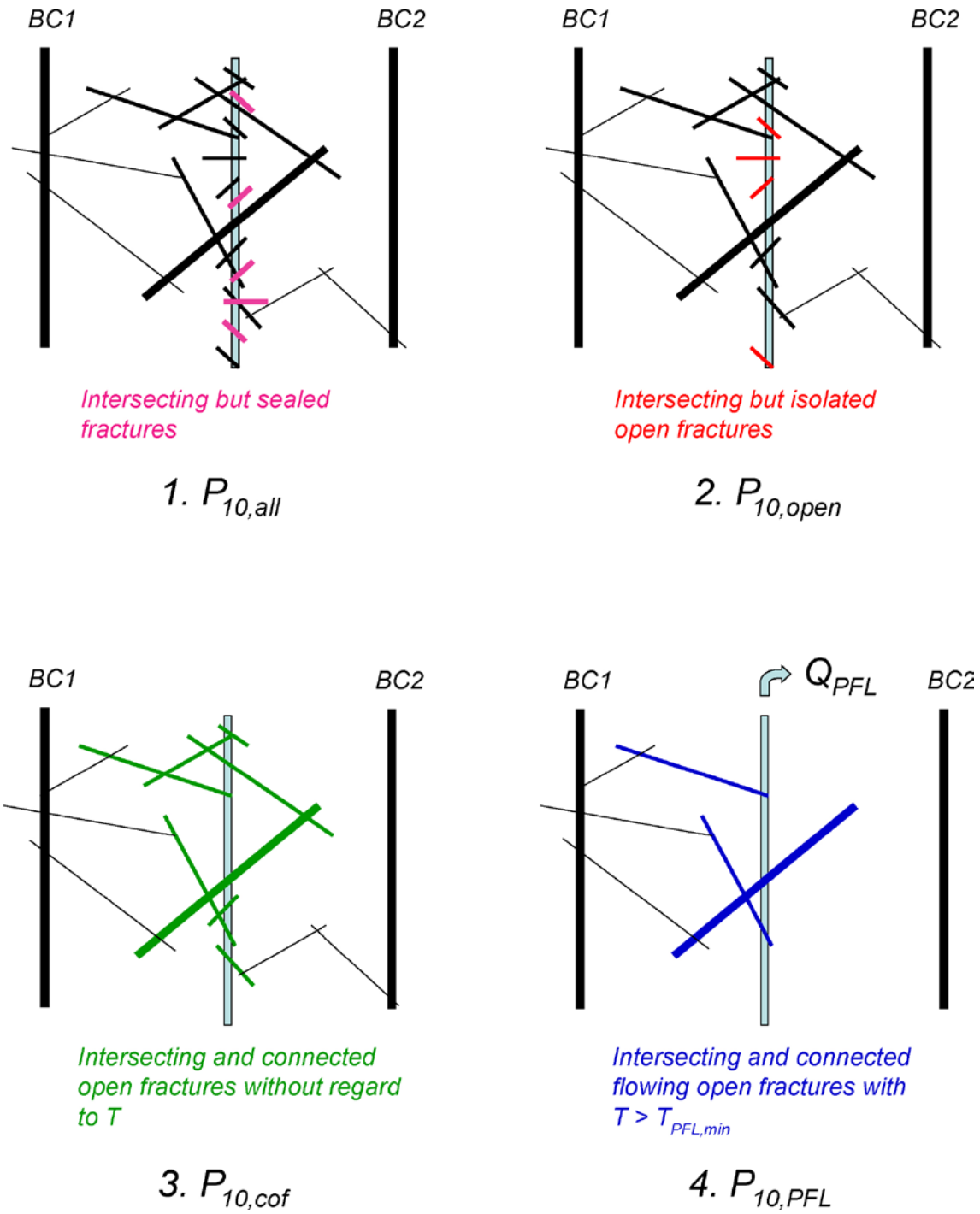

Figure 2-9. *$P_{10,all}$ is the linear intensity of "all fractures"(sealed and open fractures) intersecting the borehole, $P_{10,open}$ is the intensity of "open fractures", $P_{10,cof}$ is the intensity of "connected open fractures" and $P_{10,PFL}$ is the intensity of "flowing connected open fractures" identified with the PFL-f method. BC1 and BC2 represent hydraulic boundary conditions, e.g. the surface and/or nearby deformation zone which is connected to the surface. $P_{10,cof}$ cannot be measured but simulated values can be compared with the measured value of $P_{10,PFL}$ /Rhén et al. 2008/.*

2.3.5 Hydraulic soil domain (HSD) model

The Quaternary deposits are generally much more permeable than the average crystalline rock and a large part, roughly 70% in the model presented in this report, cf. Table 7-1, of the groundwater infiltration will flow through the Quaternary deposits to its discharge point. The hydraulic importance of the Quaternary deposits varies greatly depending on the type of hydrogeological problem studied, being most important when considering the hydraulic contact between the bedrock and surface water bodies such as the sea and lakes.

The Quaternary deposits model consisting of 6 layers (Z1–Z6), cf. Section 3.5 and /Sohlenius and Hedenström 2008, Nyman et al. 2008, overburden model, or as expressed in the report; Regolith depth and stratigraphy model (RDM) therein/, was provided as a soil type indicator, a horizon depth for the bottom of each layer, and the total Quaternary deposits thickness on a grid resolution for the data of 20×20 m. This detailed model was simplified in the regional groundwater flow modelling representing it by four finite-element layers vertically, each with a constant 1 m thickness, with the horizontal extent of the hydrogeological grid elements (40–120 m), to represent the HSD. The same hydraulic conductivity tensor was specified for each element in the vertical stack of 4 grid elements, but varied horizontally from element-to-element, and was anisotropic with regard to horizontal and vertical components in order to represent the effective hydraulic properties of the Quaternary deposit layers, cf. Chapters 3, 5 and 6 and /Rhén et al. 2009/ for details of the implementation.

2.3.6 The ECPM approach

Any numerical groundwater model is a simplified representation of geometry, material properties parameterisation and boundary and initial conditions of a real physical groundwater system. The Equivalent Continuum Porous Medium (ECPM) approach is used in the current hydrogeological SDM for the transformation of geometrical and hydraulic properties of a modelled system consisting of planar discrete flow conduits (HCD and hydrogeological DFN features) into a 3D continuum porous medium, see Figure 2-10.

In the regional scale modelling presented in this report, different hydrogeological DFN models are defined for all defined HRDs and the ECPM element-properties are calculated from the hydraulic properties of the flowing features defined by the respective hydrogeological DFN models and the properties of the HCDs. Since each ECPM model studied is based on a particular underlying stochastic DFN realisation, the ECPM models are inherently also stochastic. It should be mentioned that within the subsequent Safety Assessment, the flow pattern within the repository volume is assessed using the hydrogeological DFN model directly, rather than the regional scale ECPM used extensively in the SDM work. The ECPM model is well suited for the palaeohydrogeological regional simulations, as described in this report, cf. Chapter 7, but also for hydrochemical simulations within the Safety Assessment.

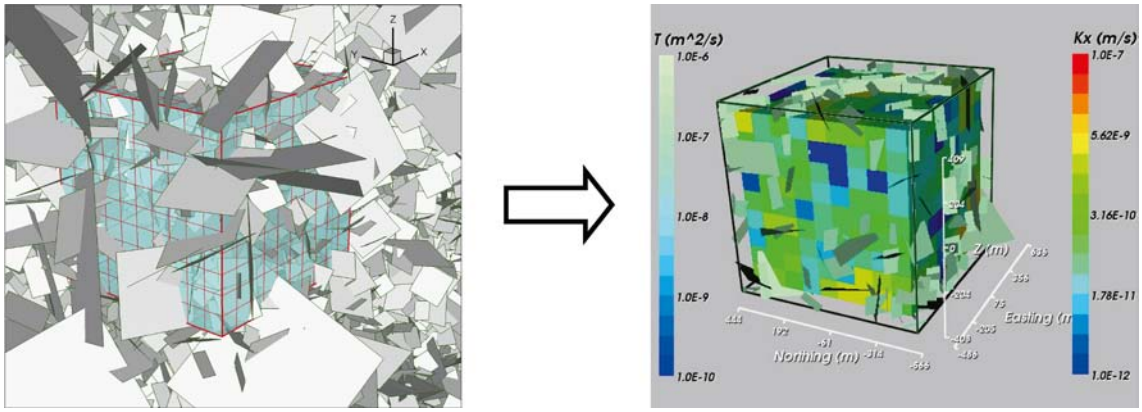

Figure 2-10. *Illustrations of the ECPM concept. Geometrical and hydraulic properties of modelled 2D discrete features (deformation zones and DFN) are transformed into a 3D equivalent continuous porous medium. Reproduced from /Follin et al. 2007c/.*

2.3.7 Solute transport model

The solute transport model applied in the hydrogeological modelling is based on the ECPM approach. In the ECPM approach, the total connected pore space available to solutes is divided between a pore space containing mobile water, known as the *kinematic porosity*, in which both groundwater flow and solute transport takes place, and a pore space containing immobile water referred to as *diffusion accessible porosity*, in which only solute transport through diffusive exchange with the mobile pore space is considered. For the sparsely fractured bedrock, the mobile pore space may be interpreted as the open fracture channels that are connected and responsible for the circulation of groundwater, and the immobile pore space is the rest of the total connected pore space including inter-granular pore space and micro-fractures with stagnant water. The immobile pore space may also include contributions from fractures in which there is negligible flow and from regions of nearly immobile water in the larger fractures (resulting from constrictions in fracture aperture or the presence of gouge material). In practice, it may be difficult to estimate either type of pore space accurately by direct measurement, and hence one purpose of the solute transport modelling of natural tracers in the SDM is to confirm the interpretation of transport properties.

Details of how the solute transport parameters were applied in the modelling is presented in /Rhén et al. 2009/.

2.3.8 Boundary and initial conditions

Boundary and initial conditions are needed for the cases B–D indicated in Figure 2-4 and are fairly straight forward for cases B and C but more complicated for case D, the palaeohydrogeological modelling, due to uncertainties about conditions in the past.

The essential components of the palaeohydrogeological development presented in this section are the shoreline displacement and the different stages of the Baltic Sea. The geological evolution, palaeoclimate and historical development of the Laxemar-Simpevarp area are described in /Söderbäck 2008/. The groundwater evolution in Laxemar is expected to have been influenced by these climate changes and historical development of the Baltic Sea. In this section, the parts essential to hydrogeology and palaeohydrogeology are summarised and a few more details are provided in Chapter 5.

The ice retreated more or less continuously during the early part of the Holocene. As soon as the vertical stress started to decrease, due to a thinner ice cover, the crust started to rise (isostatic land uplift). The net effect of the interplay between isostatic recovery on the one hand and eustatic sea-level variations on the other results in shoreline displacement, a process modelled by e.g. /Påsse 1996, 1997, 2001, Morén and Påsse 2001/.

The shoreline displacement started before the final deglaciation and is still an active process throughout Sweden. For instance, the displacement rate in the Laxemar-Simpevarp area, around 11,500 years ago, was very rapid at about 50–60 mm per annum, but has now reduced to about 1 mm per annum. Figure 2-11 shows the shoreline displacement specified for SDM-Site Laxemar. In comparison with the curve used previously for version Laxemar 1.2, the displacement rate for SDM-Site Laxemar is slightly reduced at later times, but shows a sharp peak between 8700 and 7200 BC. The data points for the interpreted shoreline curve shown in /Söderbäck 2008/ indicate that there are uncertainties in the actual position of the curve and it is also pointed out in this reference that there are uncertainties in the shoreline curve, especially for the last 9,500 years. This uncertainty justifies tests with alternatives of the shoreline displacement, cf. Figure 2-11, and Chapter 7. The simulation results presented in Chapter 7 indicate that the *SDM-Site Laxemar, Alt.1* works better than the curve *SDM-Site Laxemar* shown in Figure 2-11 since it allows for some infiltration of Littorina sea water over a larger area of the site (The modelling suggesting this is necessary to reproduce the traces of Littorina water interpreted in the hydrochemical analysis, e.g. KLX01, KLX15A, KLX19A). For the *SDM-Site Laxemar* shore line curve, only very limited areas of the Laxemar-Simpevarp area are below sea level during the Littorina maximum 4500 to 3000 BC, cf. Figure 5-18 and Figure 5-19.

The changes in the salinity of the aquatic systems in the Baltic basin during the Holocene are closely coupled to the shoreline displacement. The changes are divided into four main stages /Björck 1995, Fredén 2002/, cf. /Rhén et al. 2009/. The most saline period during the Holocene occurred c. 4500–3000 BC, when the superficial water salinity of the Littorina Sea south of Åland was 10–15‰

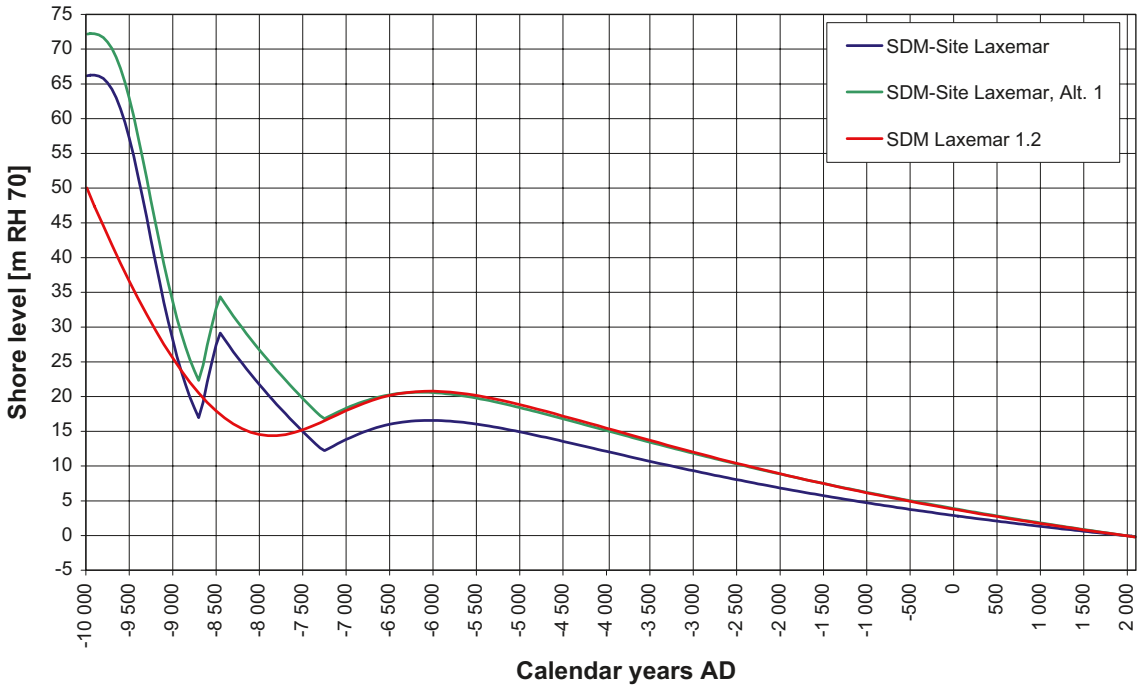

Figure 2-11. *Shoreline displacement specified for SDM-Site Laxemar and compared with the evolution used in model version Laxemar 1.2. Based on /Påsse 1997, 2001/. In addition, an alternative model is presented.*

compared with approximately 7‰ in the current Baltic Sea /Westman et al. 1999/, see Figure 2-12. The period of the brackish Yoldia Sea was probably short, 100–150 years, which suggests that the intrusion of denser saline water into the bedrock was limited compared to the effect during the Littorina Sea period. Accordingly, the effect of the Yoldia Sea has not been simulated in the current modelling, cf. Chapter 7.

The range of salinity in the Baltic Sea, excluding the Yoldia Sea, in the vicinity of Laxemar is shown in Figure 2-12. It is suggested that the curve appropriate to the palaeohydrogeological simulations should be contained in the indicated interval between SDM-min and SDM-max in the figure. The influence of salinity has been investigated in the palaeohydrogeology simulations (see Chapter 9) by considering SDM-site Alt1 in the *base case*, and Alt.2 as a variant.

Coupled groundwater flow and solute transport is modelled in terms of mass fractions of five reference waters (see Section 4.5). The chemical composition at any point and time is then described in terms of the mass fractions of these five reference waters. Using mass fractions as the transported entities makes the definition of boundary and initial conditions intuitive since they relate directly to the hydrogeochemical conceptual model of water origin. Likewise, it is useful to interpret the results in terms of the dilution or penetration of waters of different origin. The reference waters contain both conservative and non-conservative species, but the flow modelling assumes a conservative behaviour of these species, i.e. no chemical reactions are involved in the modelling. However, it is the conservative species that are considered important in the flow calibration and the non-conservative species are simply used as qualitative indicators of relative changes in groundwater signatures by depth. The assumption is that reference water mixing is the dominant process for the evolution of the groundwater compositions below the uppermost part of the bedrock /Laaksoharju et al. 2009/. The formulation of the solute transport equations in terms of mass fractions is described in more detail in /Rhén et al. 2009/.

The hydrochemical boundary conditions (BC) and initial conditions (IC) are based on the five reference waters and are further described in Sections 5.2 and 6.6. An added comment is that the BC and IC used in the super-regional model, cf. /Ericsson et al. 2006/ are consistent (although more simplified) with the ones presented here.

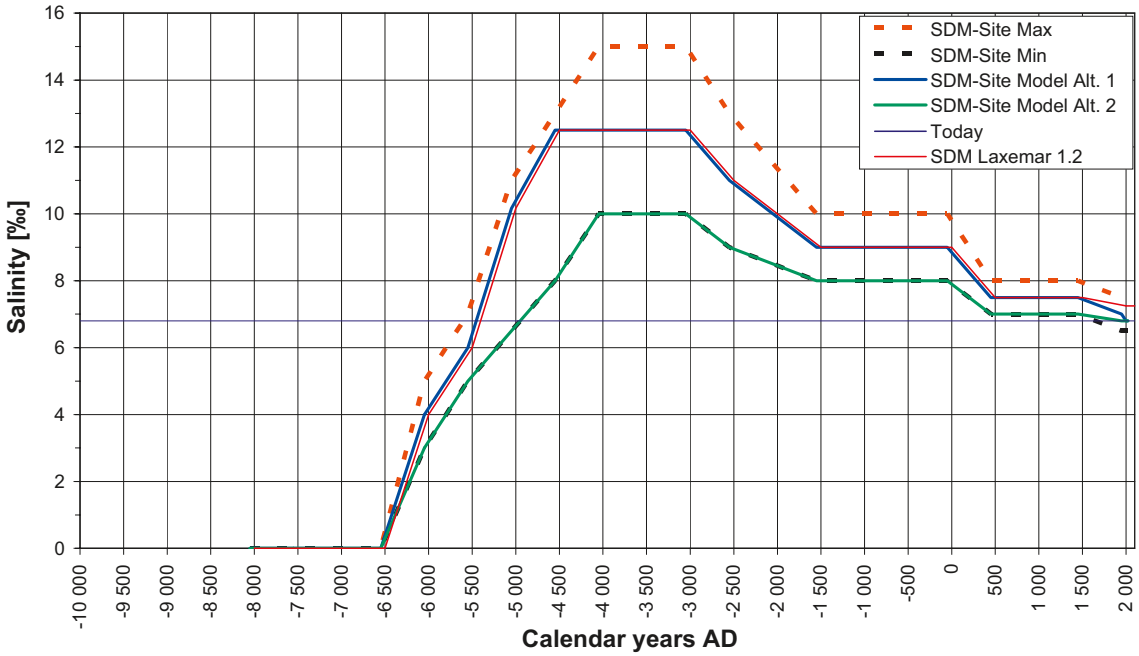

Figure 2-12. *The range in the salinity of the aquatic systems in the Baltic basin specified for SDM-Site Laxemar and version 1.2. (SDM-Site Laxemar 1.2 is equal to SDM-Site Alt. 1 and SDM-Site Min is equal to SDM-Site Model Alt. 2.) Based on /Westman et al. 1999/, cf /Söderbäck 2008/.*

3 Geological setting

This chapter provides a brief outline of the geological setting, mainly based on /Wahlgren et al. 2008/. Maps of drilled boreholes are provided in Appendix 1, but the core and percussion drilled boreholes within the Laxemar local model area can also be seen in Figure 3-2.

3.1 Bedrock geology

The Laxemar-Simpevarp regional model area is dominated by a geological unit referred to as the Transscandinavian Igneous Belt (TIB). The bedrock is dominated by well preserved c. 1.8 Ga intrusive rocks varying in composition between granite-syenitoid-dioritoid-gabbroid. Although a non-uniformly distributed faint to weak foliation, is present, the most prominent ductile structures at Laxemar are discrete, low-temperature, brittle-ductile to ductile shear zones of mesoscopic to regional character, which are related to the waning stages of the Svecokarelian Orogeny. Subsequently, the rock mass has been subjected to repeated phases of brittle deformation, under varying regional stress regimes, involving reactivation along earlier formed structures. There are indications that the ductile anisotropy, including both larger ductile shear zones as well as the weak to faint foliation, minor shear zones and mylonites, has had an influence on the later brittle deformation. With a few exceptions, the deterministically modelled deformation zones at Laxemar are characterised by brittle deformation although virtually all the zones have their origin in an earlier ductile regime. The brittle history of the Laxemar-Simpevarp area is complex and involves a series of reactivation events that have prevented the construction of a consistent simplistic model covering their development. /Wahlgren et al. 2008/. /Söderbäck 2008/ provides a detailed description of the geological evolution of the Fennoscanian Shield in south-eastern Sweden from c. 1.91 Ga and to the Quaternary period.

3.2 Deformation zone model

3.2.1 General

Within the local model volume, see Figure 3-2 , the deterministically modelled deformation zones are of modelled size (trace length at surface) of 1 km or longer whereas within the regional model volume, see Figure 3-1, but outside the local model volume, deterministic zones are modelled with a size of 1.6 km or longer /Wahlgren et al. 2005, 2008/.

The true thicknesses of the deformation zones, including the transition zone and core, inside the focused volume are up to a few tens of meters, cf. Figure 2-8. It is judged that the presence of undetected deformation zones inside the focused volume, which are significantly longer than 3 km, is highly unlikely /Wahlgren et al. 2008/.

Hydraulically, deformation zones are conceptualised as near planar conductive features with generally higher permeability than the surrounding rock, and hence are of importance. However, some deformation zones may in fact act as partial hydraulic barriers by geological inference, e.g. through association to dolerite dykes or existence of fault gouge, both of low hydraulic conductivity, cf. Chapter 5 and /Rhén et al. 2008/.

The essential basis for the 3D model of deterministically modelled deformation zones and the statistics of the minor deformation zones (MDZ) is the “extended single-hole interpretation” (ESHI), cf. /Wahlgren et al. 2008/. The regional scale 3D deformation zone model for SDM-Site Laxemar /Wahlgren et al. 2008/ contains 189 deterministically modelled deformation zones (if deformation zone elements with the same name but with extension A, B etc are counted as one deformation zone, e.g. ZSMNS001A, ZSMNS001B etc.) within the regional model volume. The local model volume contains 64 deformation zones (or 70 deformation zone elements deformation zone elements with the same name and extension A, B are counted as one deformation zone), see Figure 3-1 to Figure 3-2. Most of these deterministic deformation zones in the 3D model are referred to as ZSMxxx. However, a subset, 25 zones do not have linked lineament at ground surface. Two of these, ZSMEW946A and ZSMNW928A

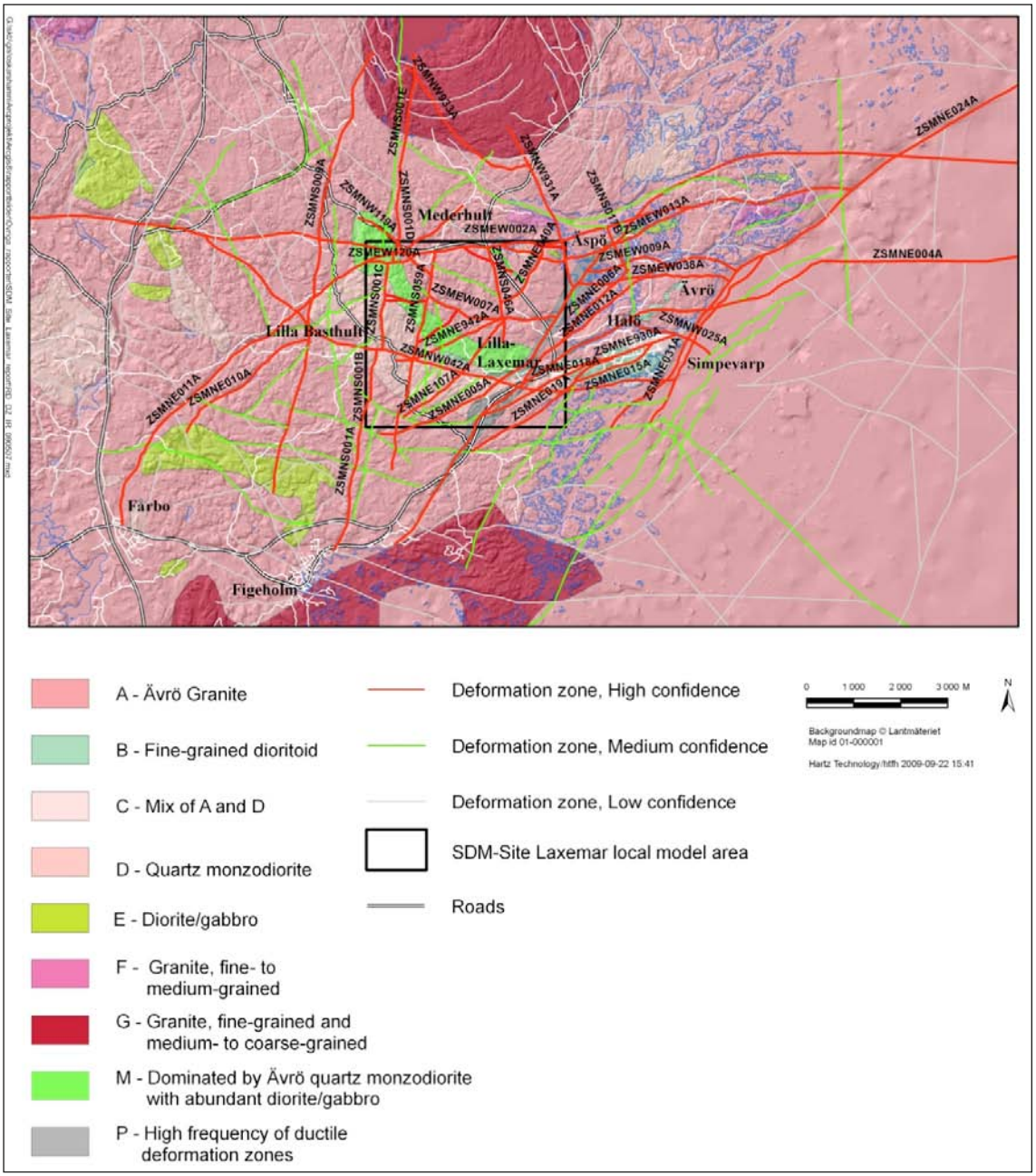

Figure 3-1. *Deformation zones and rock domains in the regional model area. Modified after /Wahlgren et al. 2008/.*

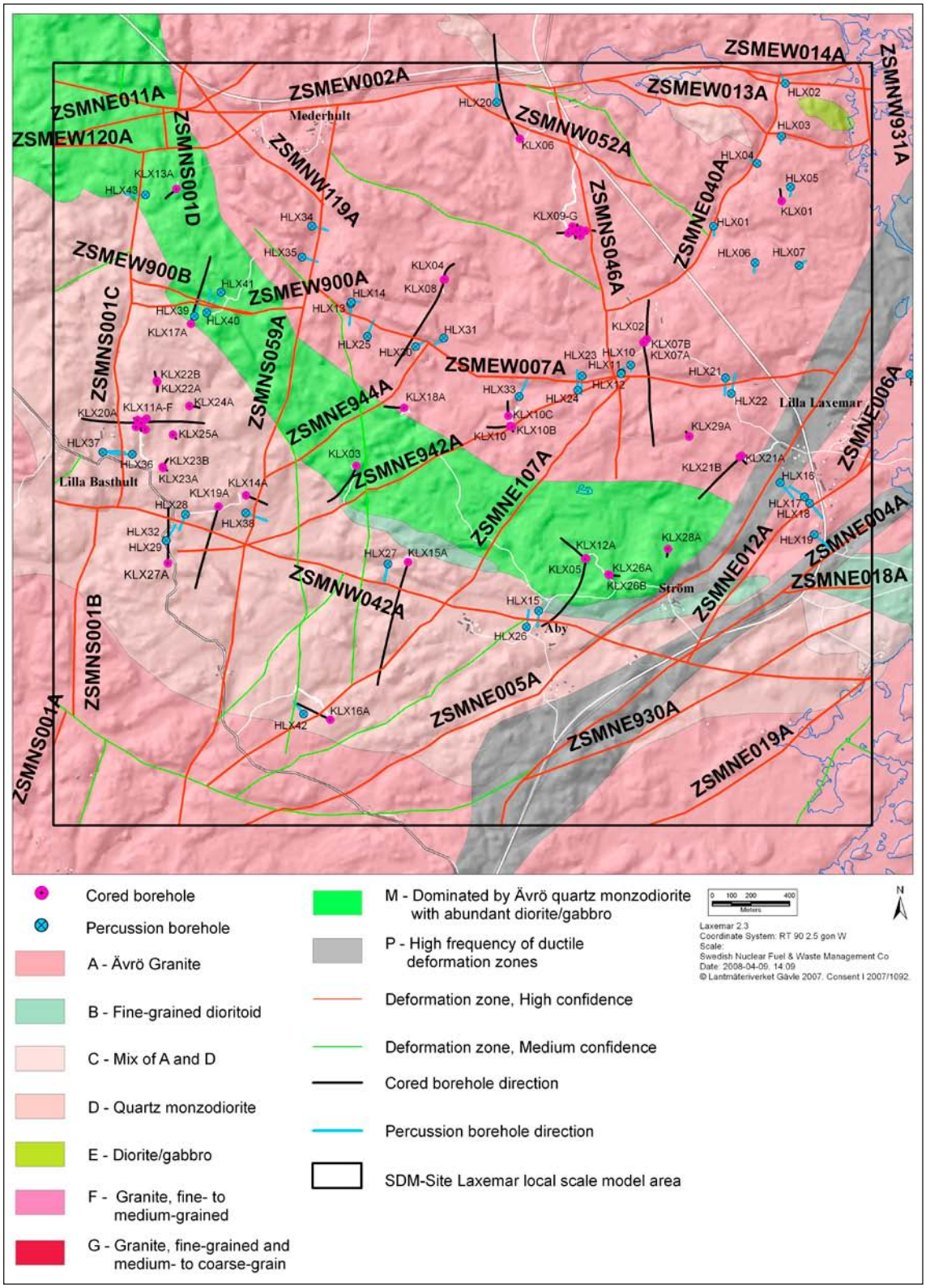

Figure 3-2. *Interpreted deterministic deformation zones and rock domains within the local model area, cf /Wahlgren et al. 2008/.*

are supported by seismic reflector geometries. The other 23 of the deterministic zones are interpreted on the basis of one single borehole intercept. In doing so, only those zones with an interpreted true thickness of 10 m or more in a borehole are interpreted to have a size (length) in excess of 1,000 m. These deformation zones are named *Borehole-ID_DZ-unit*, where the DZ-unit is defined in the geological single-hole interpretation (e.g. KLX07_DZ9). The 23 deformation zones modelled as discs are modelled deterministically as discs with radius 564.2 m (based on an equal area of 1×1 km^2). The true size and properties of these modelled discs is considered very uncertain. These 23 deformation zones are not considered to be minor deformation zones (MDZ) but their size correspond to the assessed maximum size of MDZs, cf. Section 2.3.

The minor deformation zones (MDZ) are not modelled deterministically in space by Geology, but are part of the geological DFN. According to /Wahlgren et al. 2008/ and /Hermanson et al. 2008/ there are 211 MDZs with estimated orientations based on ESHI within the Laxemar local model volume. The true thickness is less than 1 m for 51% of the MDZs, while the intensity of MDZs is P_{10}(MDZ) c. 0.01 to 0.02 1/m and P_{32}(MDZ) c. 0.02 to 0.06 m^2/m^3 for different fracture domains /Wahlgren et al. 2008, Table 6-7 therein/. The minimum radius of MDZ is estimated to be in the range of 50–200 m for several cases, combining two methods for estimation /La Pointe et al. 2008, cf. Section 5.5 therein/. These MDZs were analysed hydraulically and incorporated in the hydrogeological DFN model if found to be permeable from hydraulic tests/Rhén et al. 2008/. However, a few MDZ defined in ESHI, treated stochastically by Geology in the geological DFN, were modelled deterministically as five additional HCDs by Hydrogeology. Their identification and the rationale for their special treatise by Hydrogeology is provided by /Rhen et al. 2008, cf. Chapter 7 and Appendix 3 therein/, but are briefly also commented in Section 5.1.2.

3.2.2 SDM-Site Laxemar deformation zone model

The regional scale ductile deformation zones according to the SDM-Site Laxemar deformation zone model strike NNE-SSW and NE-SW, are subvertical and are characterised by sinistral (left-lateral) strike-slip displacements, while E-W oriented zones, although more strongly overprinted by brittle deformation, display moderate to steep dips to the south or north, cf. Figure 3-1. The kinematics of the latter are not resolved at Laxemar, but E-W ductile shear zones in the Simpevarp subarea show complex kinematics, including both reverse and normal dip-slip as well as sinistral and dextral (right-lateral) strike-slip displacements. It should be noted that the regional and local major deformation zones, although the majority have a ductile precursor, are mainly brittle in character /Wahlgren et al. 2008/.

The focused volume is bounded in the west by the N-S oriented, steeply dipping deformation zone ZSMNS001C, in the south by the WNW-ESE oriented, moderately south-dipping ZSMNW042A, in the north by the E-W oriented, moderately north-dipping ZSMEW007A and in the east by the NE-SW oriented, steeply to subvertically dipping ZSMNE005A, the latter of which corresponds to the rock domain RSMP01. All these zones, with the exception of ZSMNE005A, are mainly brittle in character and ZSMNS001C (and possibly the entire ZSMNS001 zone) in the west is associated with a dolerite dyke. The focused volume is intersected by a series of smaller deformation zones with a variety of orientations and with dips varying from subvertical to subhorizontal. Apart from a characteristic increase in fracture intensity, most of the deformation zones in Laxemar commonly contain associated fault rocks, such as different types of cataclasites, breccias and fault gouge. All available evidence indicates that multiple episodes of deformation took place within a broadly-defined brittle regime under different physical conditions /Wahlgren et al. 2008/.

3.2.3 Deformation zones associated with dolerite dykes

Dolerite has not been observed in outcrop within Laxemar, but has been observed on the Äspö Island and north of the area, in conjunction with the Götemar Granite, cf. Figure 3-1 (Rock domain G in the northern part). Only a few of the interpretations of possible dolerite dykes based on geophysics have been confirmed by borehole observations. Two of these three dolerite dykes, with approximately N-S strike, have been modelled by Geology and treated deterministic features / Wahlgren et al. 2008/, see also Figure 3-1:

- ZSMNS001 (KLX20A, HLX36, HLX37 and HLX43)

- ZSMNS059A (KLX14A, HLX38)
- klx19_dz5-8_dolerite (KLX19A, devoid of associated surface expression, assumed to me 1,000 m in size, with strike/dip: 185/81. This feature is only defined as a HCD and is not included as a deterministic deformation zone in the geological model.

Thicker dolerite dykes, associated with ZSMNS001C and ZSMNS059A, are of hydraulic importance as they, at least locally, act as predominant anisotropic features, due to the low-permeable characteristics of the core of the dolerite and have quite permeable rock flanking parts. The hydraulic implications of these dolerite dykes are discussed further in Chapter 5 and in detail by /Rhén et al. 2008/.

3.3 Rock domain model

The rock domains are defined on the basis of a combination of composition, grain size, texture, homogeneity and ductile structural overprinting. The rock domain model is discussed in /Wahlgren et al. 2008/ and shown here in Figure 3-1, Figure 3-2 and Figure 3-3. The Ävrö granite (Domain A) is dominant in the regional model area, whereas Domain M (dominated by Ävrö quartz monzodiorite with abundant diorite/gabbro) and Domain D (Quartz monzodiorite) make up large parts of the local model volume.

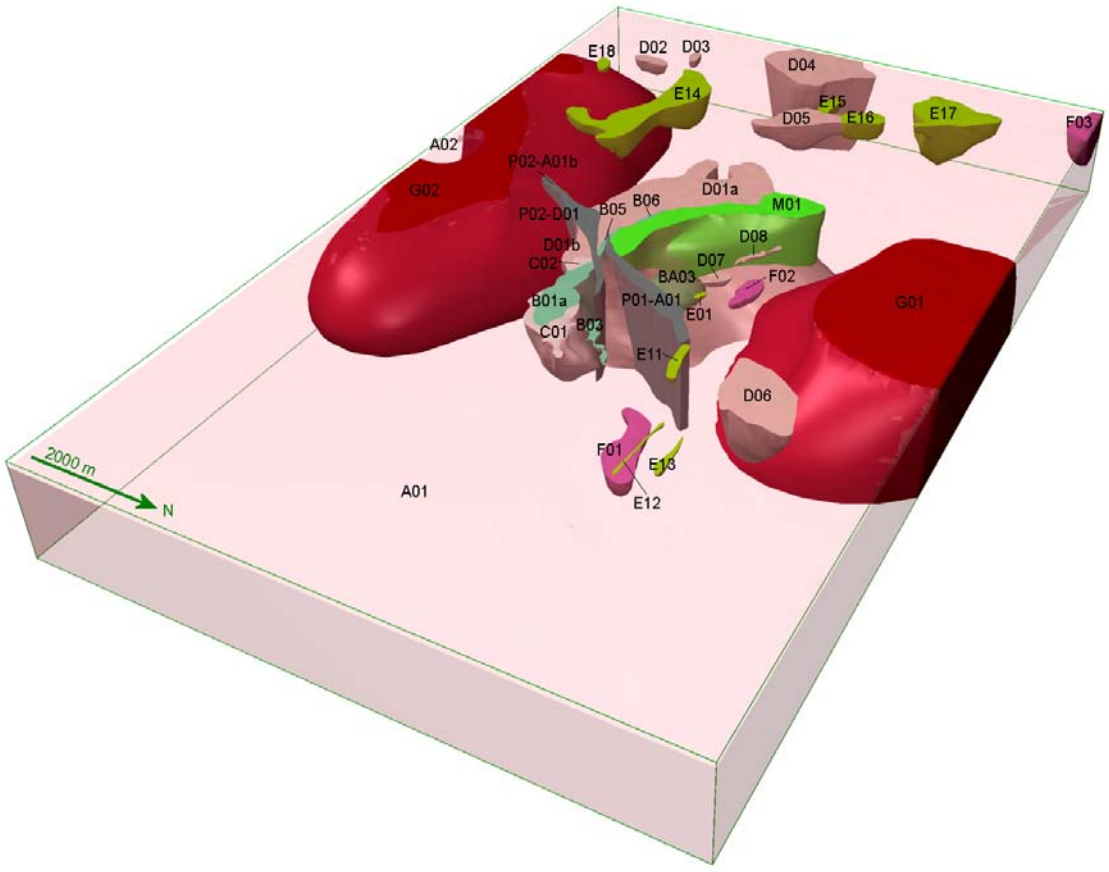

Figure 3-3. *Rock domains visualized in 3D, bounded by the regional model area. Ävrö granite shown transparent. From /Wahlgren et al. 2008/.*

The rock domains have been given different codes where domains denominated with the same capital letter are dominated by the same characteristics as displayed below:

- RSMA-domain: dominated by Ävrö granite;
- RSMB-domain: dominated by fine-grained dioritoid;
- RSMBA-domain: characterised by a mixture of Ävrö granite and fine-grained dioritoid (e.g. RSMBA03 only seen as an interpreted small body at depth in borehole KLX02);
- RSMC-domain: characterised by a mixture of Ävrö granite and quartz monzodiorite;
- RSMD-domain: dominated by quartz monzodiorite;
- RSME-domain: dominated by diorite/gabbro;
- RSMG-domain: dominated by the Götemar type granite;
- RSMM-domain: characterised by a high frequency of minor bodies to small enclaves of diorite/gabbro in particularly Ävrö quartz monzodiorite;
- RSMP-domain: characterised by a high frequency of low-grade ductile shear zones in the above mentioned rock types.

3.4 Fracture domain model

Detailed analysis of the spatial distribution of fractures and other geological characteristics motivated the definition of fracture domains /La Pointe et al. 2008/. The fracturing of the near surface rock is also discussed in /Söderbäck and Lindborg 2009/.

Fracture domains provide a local scale conceptual framework for describing spatial variability in rock fracturing in SDM-Site Laxemar. The six identified fracture domains in Laxemar (FSM_C, FSM_EW007, FSM_N, FSM_NE005, FSM_S, and FSM_W) are for the most part bounded by deformation zones, and are defined based on identified contrasts in relative fracture frequencies between orientation sets and between open and sealed fractures, cf. Figure 3-4 through Figure 3-6. The fracture domains exist inside a volume (the 'fracture domain envelope') which is smaller than the local model volume. Patterns of relative fracture intensity inside each domain appear to correspond well to the tectonic history interpreted as part of the deformation zone modelling, cf. /Wahlgren et al. 2008/.

Bedrock fracturing between deterministic deformation zones in Laxemar can be described in terms of four distinct orientation sets: A subvertically-dipping, N-S striking set that appears to be the oldest; an ENE-WSW striking, subvertically-dipping set; a WNW-ESE striking, subvertically-dipping set; and a subhorizontally- to moderately-dipping fracture set that generally strikes N-S to NNW (SH set). Fracture sizes are described according to a power-law (Pareto) distribution of equivalent radii, with parameters dependent on modelling assumptions employed. The majority of the fractures in the Laxemar cored boreholes are sealed, whereas open and partly open fractures make up between 15–45% of the fracture population in most cored boreholes, cf. /Wahlgren et al. 2008/.

The intensity of fracturing within a given fracture domain is described in terms of the average volumetric intensity P_{32} of a given orientation set. The spatial variability of the fracture intensity between deterministic deformation zones follows either a Gamma or a Weibull distribution at scales greater than 9 m for the N-S, SH, and WNW sets, and at scales greater than 15 m for the ENE set. The intensity of all fractures (Sealed +open + partly open fractures) was not found to be a function of depth or rock domain at a given statistical significance level, although weak to moderate correlations between fracture intensity and specific lithologies were noted. Fracture locations can be approximated using a Poisson point process, and fracture sizes appear to scale in an Euclidean fashion, cf. /Wahlgren et al. 2008/.

HRDs, later presented in Section 5.1.3, are within the local model volume based on fracture domains and are outside the local model volume based on the rock domains.

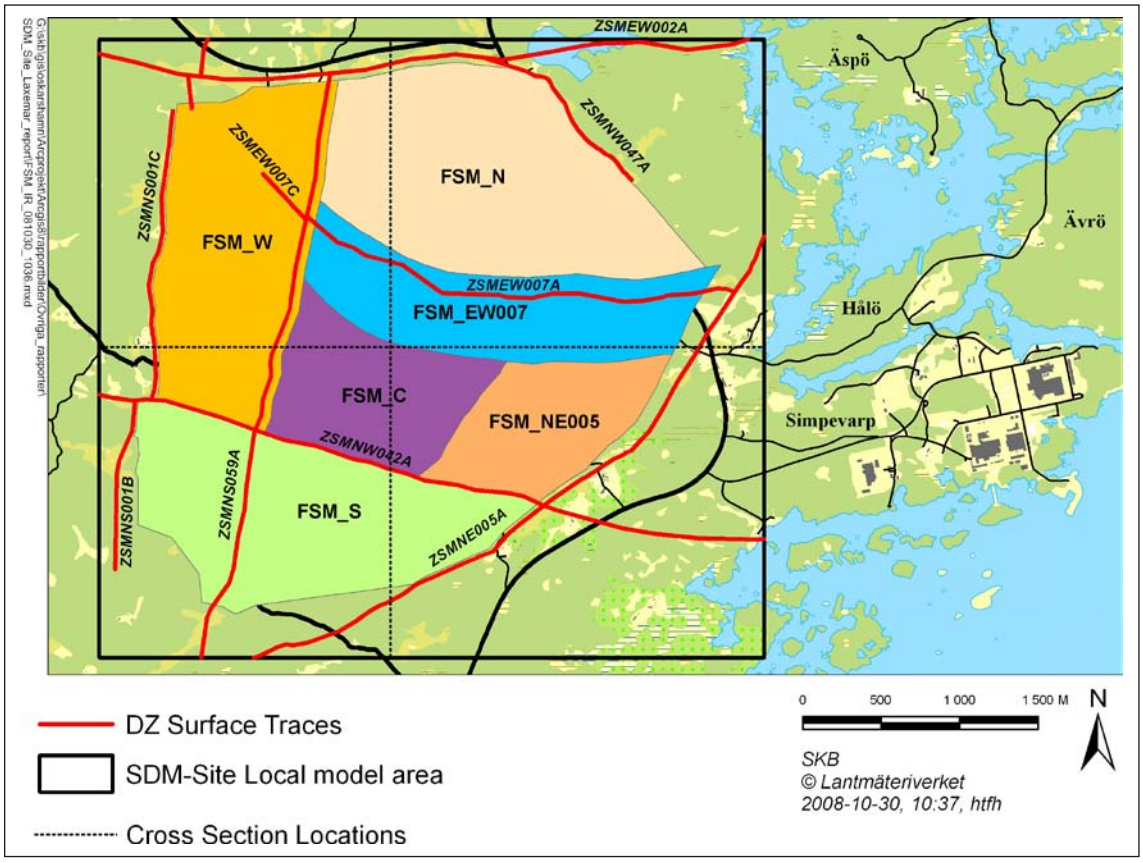

Figure 3-4. *Illustration of the SDM-Site Laxemar Fracture Domain Model, based on /La Pointe et al. 2008/.*

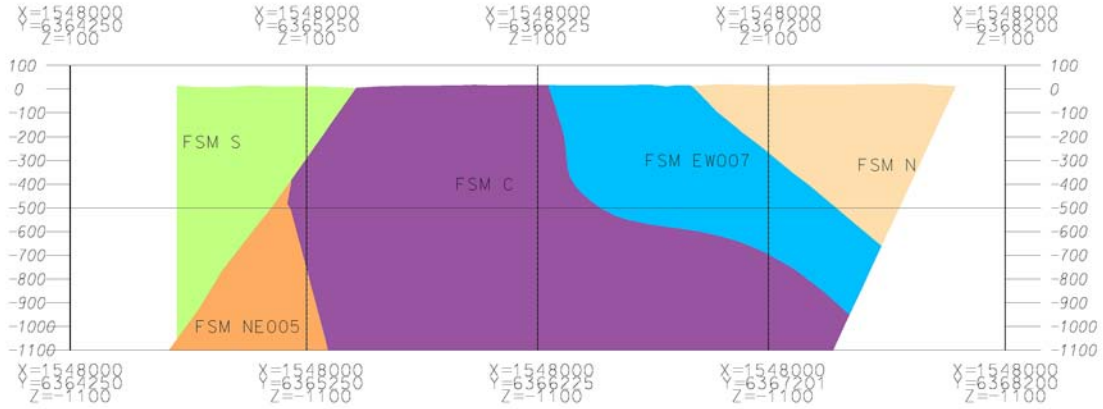

Figure 3-5. *RVS cross-section, oriented north-south through the middle of the Laxemar local model volume, of identified fracture domains. Vertical section from south (left) to north at Easting's X=154,800 m, cf /La Pointe et al. 2008/.*

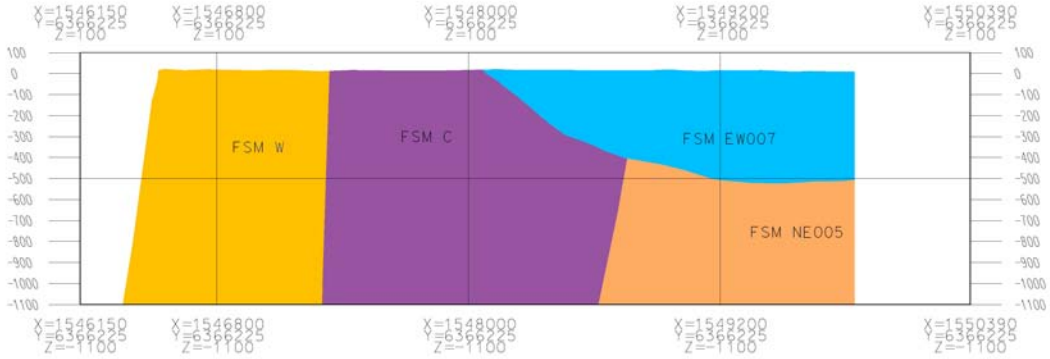

Figure 3-6. *RVS cross-section, oriented east-west through the centre of the Laxemar local model volume, of identified fracture domains. Vertical section from west (left) to east at Northing's Y=6366,225 m, cf /La Pointe et al. 2008/.*

3.5 Model of Quaternary deposits

The data and concepts for description of the Quaternary deposits in the Laxemar-Simpevarp regional model area are given in /Sohlenius and Hedenström 2008/ and a more detailed description of the 3D-modelling of the Quaternary deposits is reported by /Nyman et al. 2008/. The hydraulic properties of the Quaternary deposit types are discussed in /Werner et al. 2008/. In this section the description of the Quaternary deposits is summarised.

All Quaternary deposits in the Laxemar area have most probably been deposited during or after the latest deglaciation during which the ice sheet in the area advanced from the north-west. The Baltic Sea completely covered the investigated area after the latest deglaciation c. 12,000 BC. Land uplift was fastest during the first couple of thousand years following the deglaciation and has subsequently decreased to the present rates of 1 mm/year. Older Quaternary deposits have been eroded in areas exposed to waves and currents and the material has later been re-deposited. Fine-grained sediments have been deposited on the floor of bays and in other sheltered positions. Peat has accumulated in many of the wetlands situated in topographically low positions. The groundwater table in many of the former wetlands has been artificially lowered to reclaim land for forestry and agriculture, which has caused the peat to partly or completely oxidise. As land uplift proceeds, some new areas are being subjected to erosion at the same time as other new areas are becoming lakes and sheltered bays where fine-grained sediments can accumulate.

The geographical distribution and depth of the Quaternary deposits is largely determined by the topography of the underlying bedrock. Areas with outcrop bedrock and a thin till cover dominate the whole regional model area, including the sea floor. These areas are intersected by a number of fissure valleys where the cover of Quaternary deposits is considerably thicker. Glacial clay with a thin cover of sand is the dominating surface deposit in the valleys on the sea floor. In the bays and land areas, the valleys are dominated by clay gyttja, which at many locations in the terrestrial areas is covered by a thin layer of peat. There are several glaciofluvial deposits, with a northerly strike, in the investigated area. The Tuna esker in the western part of the regional model area is the largest of these deposits. In a morphological sense, this esker is the most significant Quaternary deposit in the model area. In certain areas the till has a more coherent distribution than in the area in general. These areas are characterised by hummocks, which are probably not due to the morphology of the underlying bedrock.

The properties of Quaternary constituents have been classified at sites representing ten land classes. These are not discussed further here. The reader is referred to /Sohlenius and Hedenström 2008/ for a detailed discussion.

Most data on the total depth of the Quaternary deposits cover were obtained from geophysical investigations. The stratigraphical distribution of Quaternary deposits was obtained from drilling and excavations. The results show that the stratigraphical distribution of Quaternary deposits in the

investigated area is rather uniform. Till is the oldest Quaternary deposit in the area, and is consequently resting directly upon the bedrock surface. The till in the valleys is often overlain by glacial clay, which in many valleys is overlain by a thin layer of sand followed by clay gyttja and peat.

The chemical compositions of the Quaternary deposits in the Laxemar-Simpevarp area are close to the Swedish averages. The petrographical and mineralogical composition of the till reflects that of the local bedrock even though the till has been transported from the north. Since the till has been subjected to chemical weathering, the chemical composition of the till differs slightly from that of the bedrock. The mineralogy of the clay is different from that of the bedrock since the clays have a high content of clay minerals, which were formed by chemical weathering of primary rock-forming minerals. The chemical composition of the clay is also affected by the environmental conditions prevailing during deposition.

/Nyman et al. 2008/ present a depth and stratigraphic model of the Quaternary deposits (/Nyman et al. 2008/) of the Laxemar-Simpevarp area. These models are based on the detailed digital elevation model of the area (with a horizontal resolution of 20 m by 20 m), the detailed map of the Quaternary deposits, and a large amount of geological and geophysical data. The RDM takes into account site investigation data available in the Laxemar 2.2 data freeze (Dec. 31, 2006). The RDM developed by /Nyman et al. 2008/ contains six layers of Quaternary deposits, denoted Z1–Z6; Z1 represents the upper layer of the Quaternary deposits. These layers, illustrated in the cross section in Figure 3-7, are defined and described briefly in /Rhén et al. 2009/ and in /Nyman et al. 2008, Sohlenius and Hedenström 2008/.

With the exception of layer Z1, the lower boundary of all layers is produced by kriging. The lower boundary of layer Z1 is calculated based on the DEM, the elevation of the rock surface and assigned rules for the layer thickness. In order to enable the construction of the RDM, /Nyman et al. 2008/ divided the area into 3 type areas (denoted I–III) and 9 domains, see Figure 3-8. Figure 3-9 shows the modelled distribution of total overburden depth in the Laxemar-Simpevarp regional model area. As can be seen the depth of the overburden is in general just 0–3 m. Below the sea, in the eastern part of the regional model area, there seem to be linear features but they are only artefacts from the interpolation of data from the survey lines of the marine geological survey /Nyman et al. 2008/. Figure 3-10 illustrates the variable depth of the Quaternary deposits along a vertical north-south section across the Mederhult zone (ZSMEW002A). /Rhén et al. 2009, Appendix 5 therein/ summarises the Quaternary deposits RDM layer definitions, including notations on which layers that are present "locally" and average thicknesses of the individual layers, given different types of deposits on the map of Quaternary deposits.

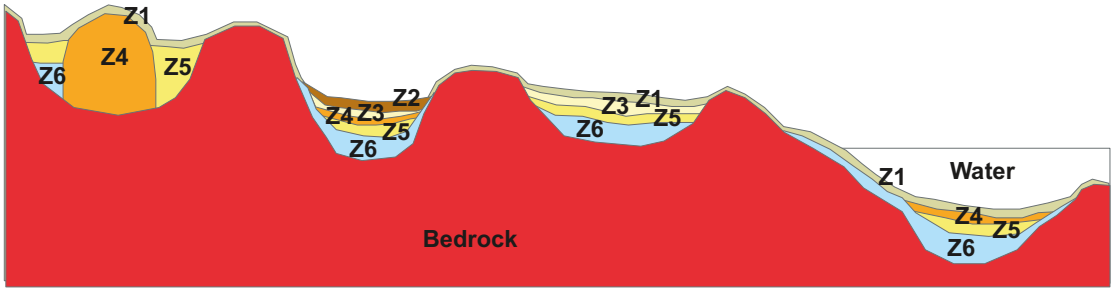

Figure 3-7. *The stratigraphical model which was used for modelling stratigraphy and total depth of Quaternary deposits in the Laxemar-Simpevarp regional model area. /Sohlenius and Hedenström 2008/. Layer Z1–6:*

- *Layer Z1 represents a thinv surface(-affected) layer.*
- *Layer Z2 represents (fen or bog) peat.*
- *Layer Z3 represents postglacial clay, clay gyttja/gyttja clay, gyttja or recent fluvial sediments.*
- *Layer Z4 represents postglacial sand/gravel, glaciofluvial sediments or artificial fill.*
- *Layer Z5 represents glacial clay.*
- *Layer Z6 represents (glacial) till.*

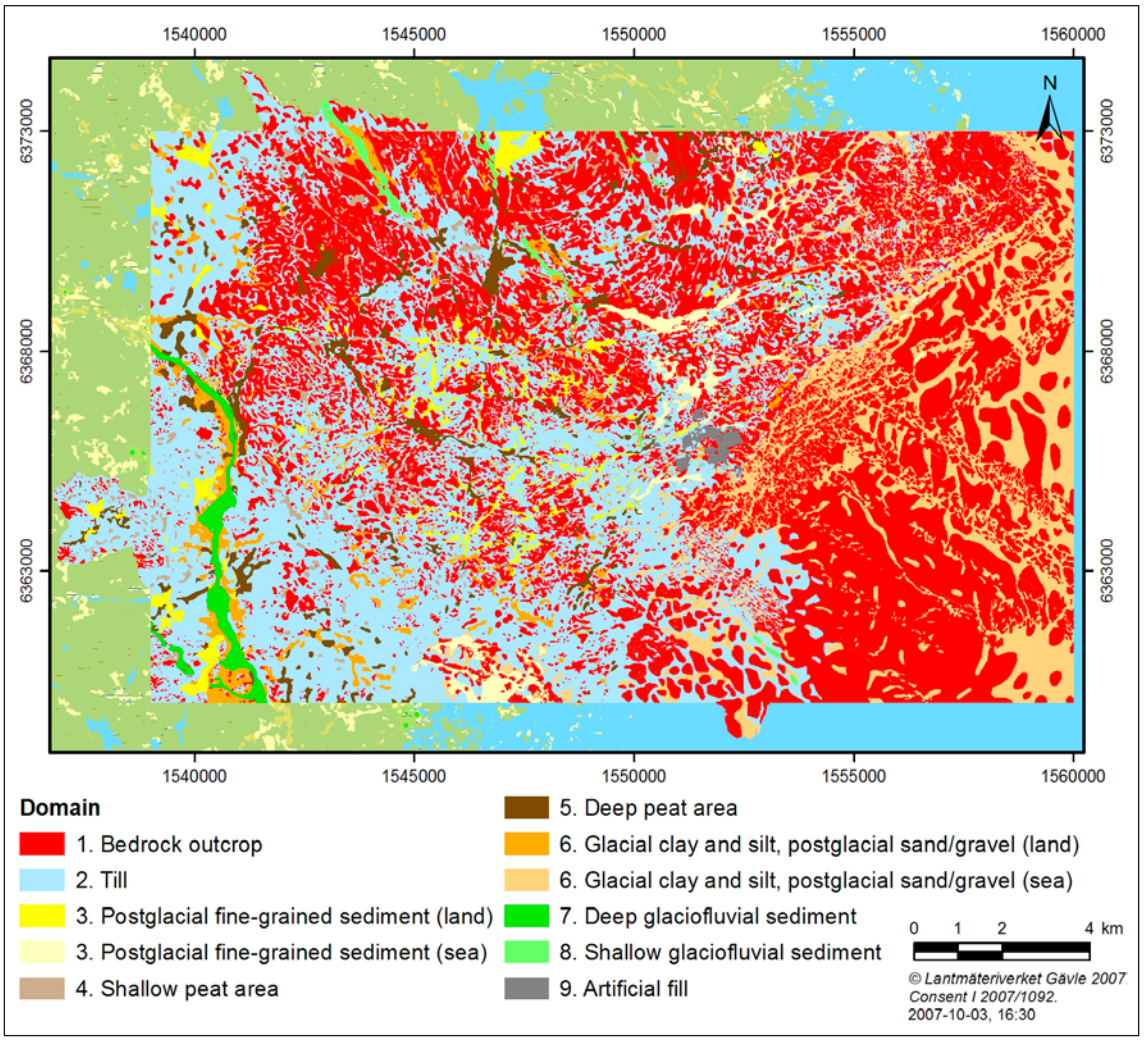

Figure 3-8. *The model area classified in nine types of domains, which were used in the depth and stratigraphy models of the Quaternary deposits /Sohlenius and Hedenström 2008/.*

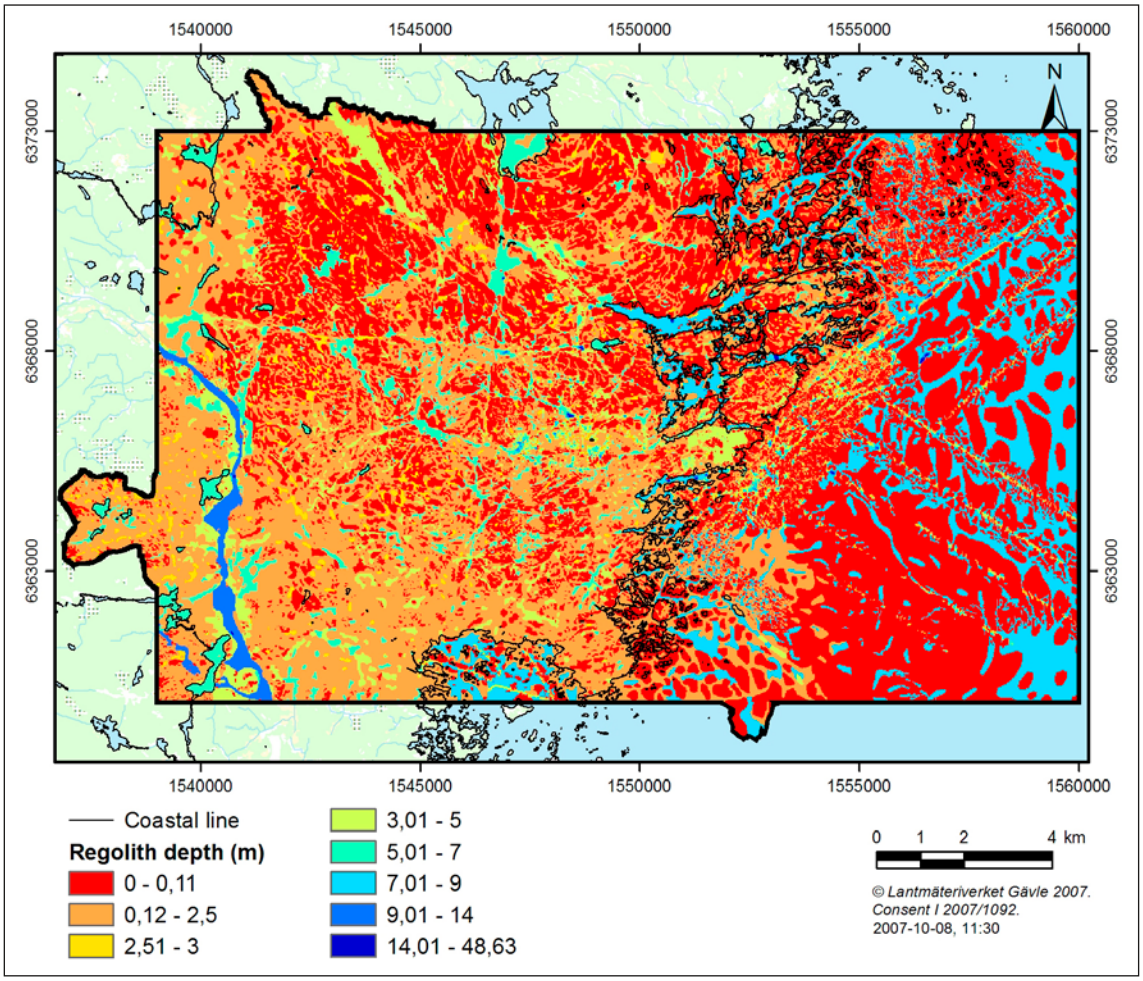

Figure 3-9. *The modelled distribution of total depths of the Quaternary deposits in the Laxemar-Simpevarp area. /Sohlenius and Hedenström 2008/.*

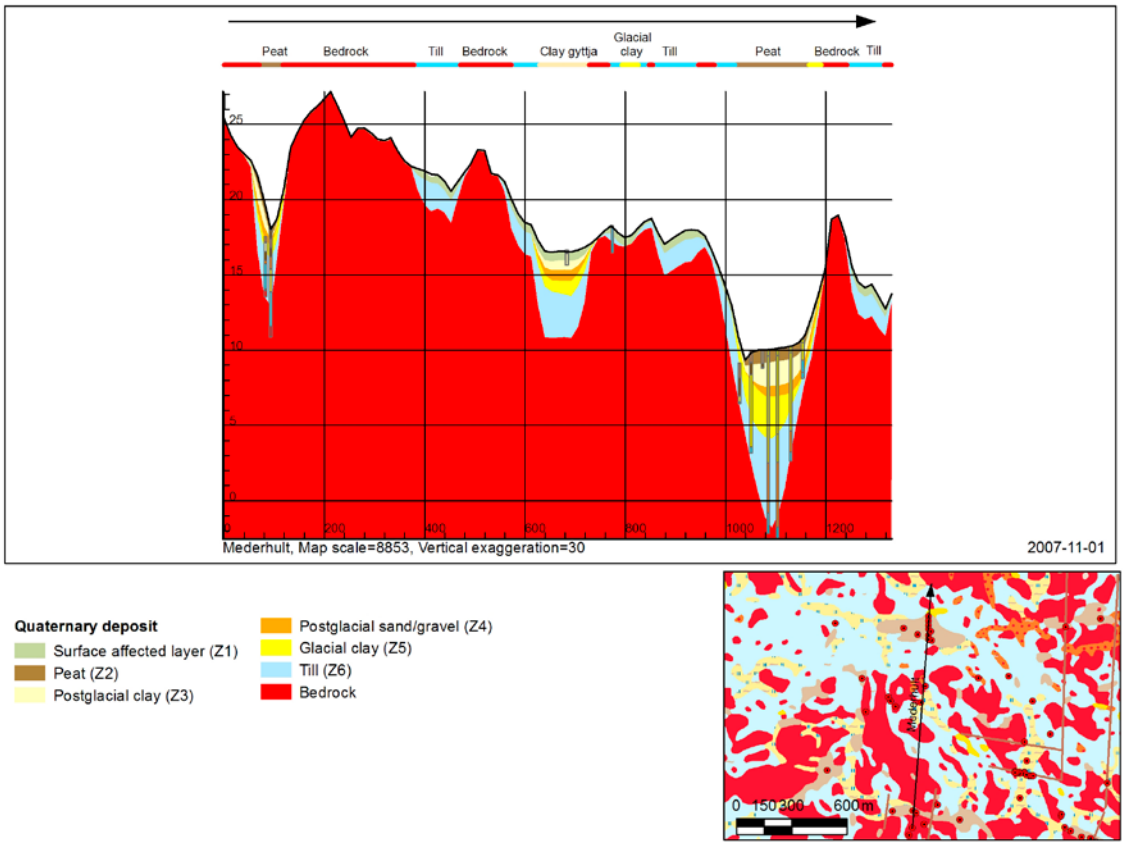

Figure 3-10. *The profile shows the total depth and stratigraphy of the Quaternary deposits in a north-south profile close to Mederhult. The valley in the right part of the profile (between 1,000 and 1,200 on the horizontal scale) is one of the largest lineaments in the model area (ZSMEW002A in Figure 3-1), /Sohlenius and Hedenström 2008/.*

4 Evaluation of primary data

Single-hole hydraulic tests, interference tests, groundwater levels and hydrochemical data are summarised in this chapter, based on /Rhén et al. 2008, Rhén et al. 2009/. Field and laboratory data of matrix properties that is of importance for the large-scale groundwater flow modelling is mainly discussed in /Crawford and Sidborn 2009/ but are also briefly commented in /Rhén et al. 2008/.

4.1 Evaluation of single-hole hydraulic tests

In this section a brief summary is presented of test methods and primary test results. Hydraulic results in relation to geology and the definition of hydraulic domains are shown in subsequent chapters. The description of test methods in this section and Section 2.3 is important for understanding the hydraulic test results limitations, but also for assessing the advantage of one method compared to another, concerning different hydrogeological modelling issues discussed in Chapters 6 through 10.

4.1.1 Available data

The logging and test methods as well as the core mapping procedures applied to the drill cores employed by SKB have developed significantly over the years and consequently the borehole data from the current site investigation period (2002–2007) are more comprehensive and also based on new methodologies. These data therefore constitute the cornerstone of the results reported in this report. Some of the older data have been used for assessing properties of deformation zones (in some instances denoted DZ) and for assessing probable ranges of hydraulic properties for some rock domains (Götemar granite), properties of deformation zones, and in some cases properties of rock between deformation zones (using the 100 m test scale).

The boreholes available within the regional model area are listed in Appendix 1. Appendix 1 also lists the cored boreholes investigated with the *Posiva Flow Log* (PFL) method and the *Pipe String System* (PSS) method, respectively.

Tests with PSS have been performed using 3 different test scales: 5, 20 and 100 m with 5 m tests only being performed in the depth interval –300 m to –700 m, covering the foreseen repository depth. PSS provides transient hydraulic tests as a basis for evaluation of hydraulic properties. See /Rhén et al. 2008/ for a detailed discussion of performance, evaluation and a complete set of references. Notably, test results from KLX27A and transient evaluation of the PFL-pumping tests /Enachescu et al. 2008c, d/ were not available for the evaluation for the SDM.

A large number of boreholes have been tested with the PFL method. The PFL-s provides an estimate of the transmissivity within a certain test section length, 5 m at Laxemar, that is moved stepwise 0.5 m. PFL-s (s stands for section) also provides the undisturbed flow rate distribution with indicated flow direction (in or out of the borehole) along the borehole. The PFL-f (f stands for fracture or feature) method is a geophysical logging device developed to detect continuously flowing features in sparsely fractured crystalline bedrock by means of difference flow logging, using a 1 m test section that is moved stepwise 0.1 m. The PFL method essentially provides an estimate of the specific capacity (Q/s), which is used as an estimation of the transmissivity. See /Rhén et al. 2008/ for details on performance, evaluation and a complete set of references.

The PFL-f method uses a short test interval in the borehole and a long test time, whereas the PSS method employs the opposite test conditions, i.e. a long test interval and a short test time. Thus, the resolution of the PFL-f method is sufficient to study the transmissivity of individual fractures and the method can be used to evaluate the conductive fracture frequency (CFF) of continuously flowing networks, e.g. situations like cases D–F in Figure 2-7. However, the PFL-f method cannot identify situations with isolated fractures/clusters or “hydraulic chokes” such as in cases A–C. The PSS method, on the other hand, has great problems in distinguishing closed network situations like cases A–C from connected network situations like cases D–F, which means that using data from the PSS method alone for the hydrogeological DFN modelling could easily result in an over-prediction

of fracture connectivity in the sparsely fractured bedrock in between the deformation zones. The PSS methods provide a more local estimate of the transmissivity but no indication of the hydraulic connectivity on a larger scale. Due to this difference, the hydrogeological DFN modelling is based on the information acquired by the PFL-f method. This modelling is thoroughly explained in /Rhén et al. 2008/.

Pumping tests, and on a few occasions flow logging, have been performed with the Hydraulic Test System for Percussion Boreholes (HTHB) (Swedish abbreviation for *Hydro Testutrustning i Hammar-Borrhål)*, for details on performance and relevant references, cf. /Rhén et al. 2008/. In some cases the borehole was judged to be so low-conductive, after examining data from drilling, that a pumping test was found infeasible. Instead, data from airlift pumping during drilling could sometimes be used, either to estimate a transmissivity or set a measurement limit value to the borehole (if flow rate was estimated as zero).

All new percussion-drilled boreholes in the Laxemar-Simpevarp area have been investigated with the HTHB method (combined pumping and impeller flow logging) in conjunction with drilling, except those showing a very poor total yield. Only a few percussion boreholes have been investigated with impeller flow logging or injection/pumping tests within limited test sections in boreholes using a dual-packer system. Therefore, observations during drilling (bit penetration rate, core losses and loss of drilling fluid circulation) are generally the only indications as to where there are possible conductive fractures and zones along percussion drilled boreholes.

4.1.2 Results

Correlation between PSS and PFL

The transmissivities of the hydraulic features identified with PFL-f were summed up to correspond to 5 and 20 m PSS-sections, to explore the difference between the methods. Figure 4-1 shows an overview of all data using the notation:

–Tsum (xm-ΣPFL-f): x indicating the section length 5 or 20 m that the PFL-f features are summed over;

–T-BC(xm-PSS): x indicating PSS-test scales 5 or 20 m and BC is the “best choice” of the transmissivities evaluated from the transient data (if available, otherwise in some cases steady state values), then considered to be most relevant for the test section. Transmissivity data from PSS test sections without PFL-f anomalies are plotted to the left at an arbitrary low value on the abscissa. One reason for the presence of these values is that these test sections probably partly represents compartmentalised parts of the fracture network that carry no continuous flow during tests with PFL. However, some of these test sections may also be related to the uncertainties of the positioning of PFL-f and PSS test sections in the borehole; occasionally a PFL-f feature may be wrongly connected to a certain PSS section. A third reason is that the lower measurement limit is slightly lower for PSS compared with PFL, which indicates that possibly some of the sections with no PFL-f features may in fact still have connected fractures with very low transmissivities. These sections with possibly compartmentalised parts of the fracture network generally have transmissivities lower than 10^{-8} m^2/s, but occasionally up to c. 10^{-7} m^2/s, as can be seen.

As can be seen in Figure 4-1 there is a tendency that (T-BC(xm-PSS)) is slightly higher than (Tsum (xm-ΣPFL-f)), but overall the values for corresponding sections are within a factor of 10 in difference. The deviation for 20 m sections seems a bit larger with high T-values; (T-BC(xm-PSS)) is higher than (Tsum (xm-ΣPFL-f)). It may be because the PFL technique has an upper measurement limit that possibly has been reached and that no repeated measurements were made with a lower drawdown for these test sections to avoid reaching the upper measurement limit, although some tests were re-made with a lower head in 22 of the tested core holes.

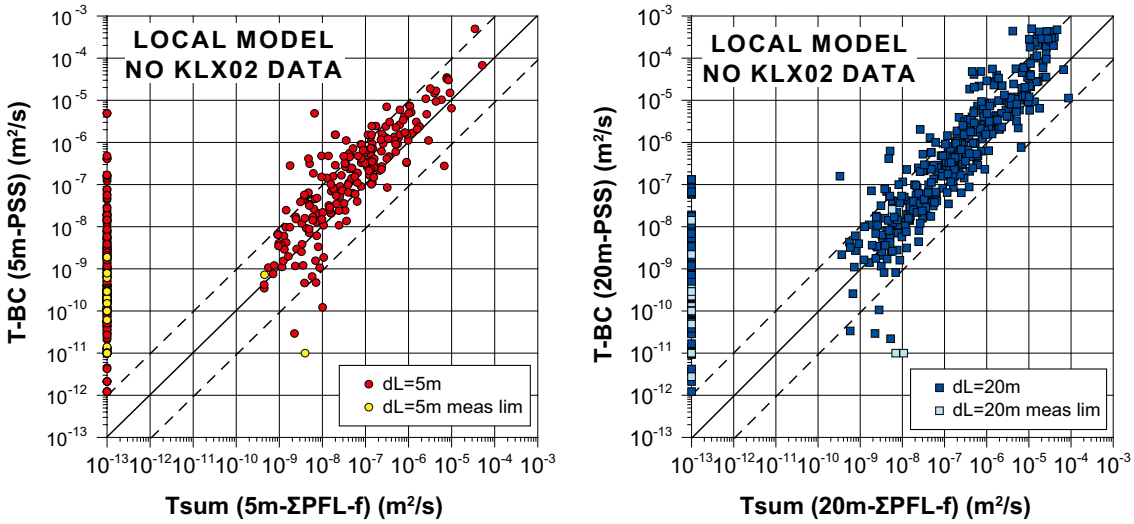

Figure 4-1. *Cross-plot of PSS BC- transmissivity (T) data vs. Σ PFL-f T data. The solid line indicates a 1:1 slope and the dotted lines a spread of ± 1 order of magnitude. Data are shown for two test section lengths dL between the PSS packers, i.e. 5 m and 20 m. Transmissivity data from PSS test sections without PFL-f anomalies are plotted to the left at an arbitrary low value on the abscissa /Rhén et al. 2008/.*

Correlation between geological interpretation and PFL

As PFL-f data have been correlated with the core log (Boremap), orientations of PFL-f features have been possible to assess. The correlation between the core log and the PFL-f data is reported in detail by /Forsmark et al. 2008, Forssman et al. 2005a, b, Teurneau et al. 2008, Wikström et al. 2008a, b, c. / and is briefly discussed in /Hermanson et al. 2008/. The uncertainties involved in the structural interpretations of PFL-f transmissivity data are explained in /Rhén et al. 2008/. Figure 4-2 through Figure 4-4 show examples of PFL-f transmissivity data and interpreted orientations from the core-drilled boreholes within the focused area, cf. /Rhén et al. 2008/ for a complete account of all coreholes tested. The geological fracture domain (FSMxxxx) is shown by name and colour code. The deterministically modelled deformation zones (DZ) are indicated by name: NNxxxx (leaving out the prefix ZSM-) and possible deformation zones by the names (DZx) given by the geological extended single-hole interpretation (ESHI).

As can be seen in the figures, some of the possible deformation zones according to ESHI are modelled as deterministic and the rest are consequently considered to be minor deformation zones (MDZ) and part of the hydrogeological DFN model as discussed in Section 2.3, cf. Figure 4-2. Figure 4-5 summarises the mean PFL-f intensities and how these features are coupled to the geological mapping categories; certain, probable and possible, for open and partly open fractures, respectively, and for each cored borehole within the Laxemar local model area. Table 4-1 summarises fracture and PFL-f mapping of the cored boreholes.

Summary

The PSS, HTHB and PFL tests, have provided data for assessment of the HCD properties /Rhén et al. 2008/. The PSS data have also been compared with PFL data for the same borehole sections and the results indicate similar estimates of transmissivity for the same test sections, although the test and evaluation methods differ. However, the comparison also indicates the presence of clusters of hydraulically locally connected fractures that are not seen in long term tests, such as PFL tests, cf. Section 2.3.3 and /Rhén et al. 2008/. This may have an effect on groundwater flow modelling including underground tunnels, but not on regional scale modelling of natural undisturbed conditions as discussed in Chapters 7 through 9. Also, the flow dimension was evaluated for tests in borehole KLX11A and nearly all tests have a flow dimension between 1.5 to 2.3, indicating that these tests are rather close to radial flow (flow dimension = 2), which is assumed by the evaluation methods employed for PSS and PFL /Rhén et al. 2008/.

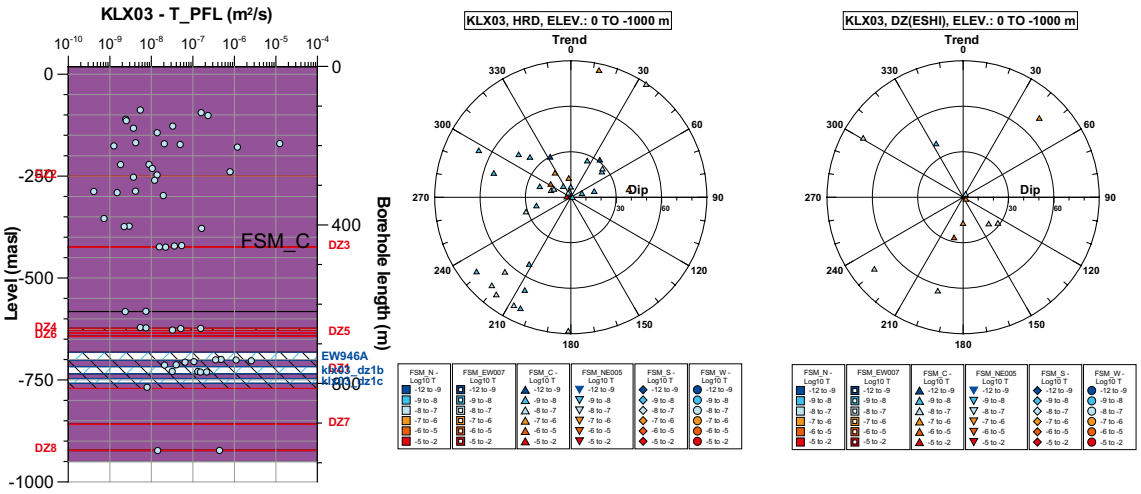

Transmissivities of PFL-f features plotted versus elevation (left side of the figure) and the borehole length (right side of the figure).

Poles for PFL-f feature planes in rock between the possible deformation zones defined by ESHI.

Poles for PFL-f feature planes within minor deformation zones (MDZ).

Figure 4-2. *KLX03. PFL-f transmissivities vs. elevation, stereo net PFL-f features in rock between possible deformation zones (as interpreted from ESHI) and stereo net PFL-f features in MDZ (part of "possible deformation zones")/Rhén et al. 2008/.*

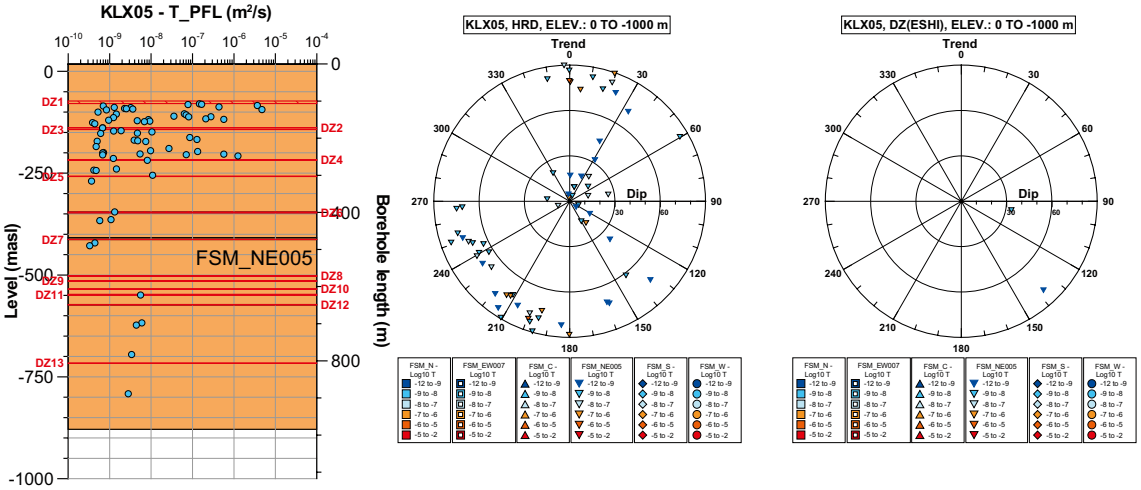

Transmissivities of PFL-f features plotted versus elevation (left side of the figure) and the borehole length (right side of the figure).

Poles for PFL-f feature planes in rock between the possible deformation zones defined by ESHI.

Poles for PFL-f feature planes within minor deformation zones (MDZ).

Figure 4-3. *KLX05. PFL-f transmissivities vs. elevation, stereo net PFL-f features in rock between possible deformation zones (as interpreted from ESHI) and stereo net of PFL-f features in MDZ (part of "possible deformation zones"). No PFL-f in MDZ or deterministically defined deformation zones exists in the hole /Rhén et al. 2008/.*

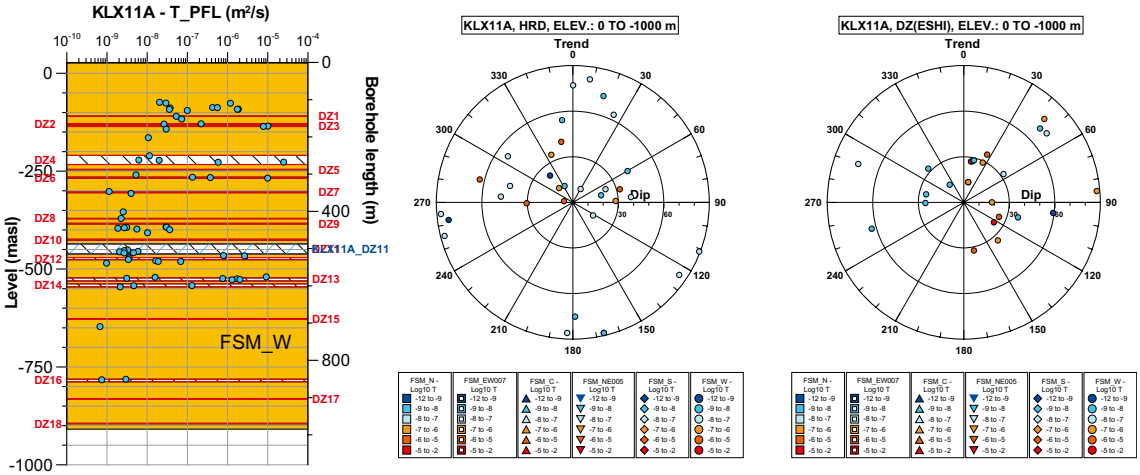

Transmissivities of PFL-f features plotted versus elevation (left side of the figure) and the borehole length (right side of the figure).

Poles for PFL-f feature planes in rock between the possible deformation zones defined by ESHI.

Poles for PFL-f feature planes within minor deformation zones (MDZ).

Figure 4-4. KLX11A. PFL-f transmissivities vs. elevation, stereo net PFL-f features in rock between possible deformation zones (as interpreted from ESHI) and stereo net of PFL-f features in MDZ (part of "possible deformation zones")/Rhén et al. 2008/.

4.1.3 Comparison of Laxemar and Äspö hydraulic properties

Extensive investigations have been performed during the site investigation programme for the Äspö HRL, sited immediately east of the Laxemar local model area, cf. Figure 1-3. The investigations conducted during the site investigation for a deep repository differs to some extent from those for the Äspö HRL but some comparison can be made to indicate differences which can later provide guidance when using experiences from the tunnel excavations at Äspö HRL. It should be remembered that the siting of Äspö HRL was chosen to provide variable conditions suitable for an underground research laboratory and not to find suitable rock for a repository.

PSS tests were performed at tests scales 3, 30 and 100 m during the site investigation programme for the Äspö HRL. During the site investigations at Laxemar, the test scales were 5, 20 and 100 m, respectively. In /Rhén et al. 2008/ test results from surface-drilled cored boreholes at Äspö of test scales 3 and 30 m are compared with tests in HRD_C, HRD_W and HRD_EW007 south of deformation zone ZSM_EW007, employing test scales of 5, 20 m. The data compared does not differentiate between tests in HRD or HCD.

The conclusion drawn is that the hydraulic conductivity within the elevation interval –150 to –400 m is slightly lower in Laxemar compared with that of the Äspö data and lower within elevation interval –400 to –650 m in Laxemar compared with Äspö. Below –650 m the hydraulic conductivity in Laxemar is possibly lower than in Äspö, but the number of data points is limited at both sites. Above elevation –150 m the data are also too limited to draw any firm conclusion. However, HRD_EW007 is more conductive than HRD_C and HRD_W according to /Rhén et al. 2008/, which indicates that the hydraulic conductivity in HRD_EW007 may be similar to Äspö conditions.

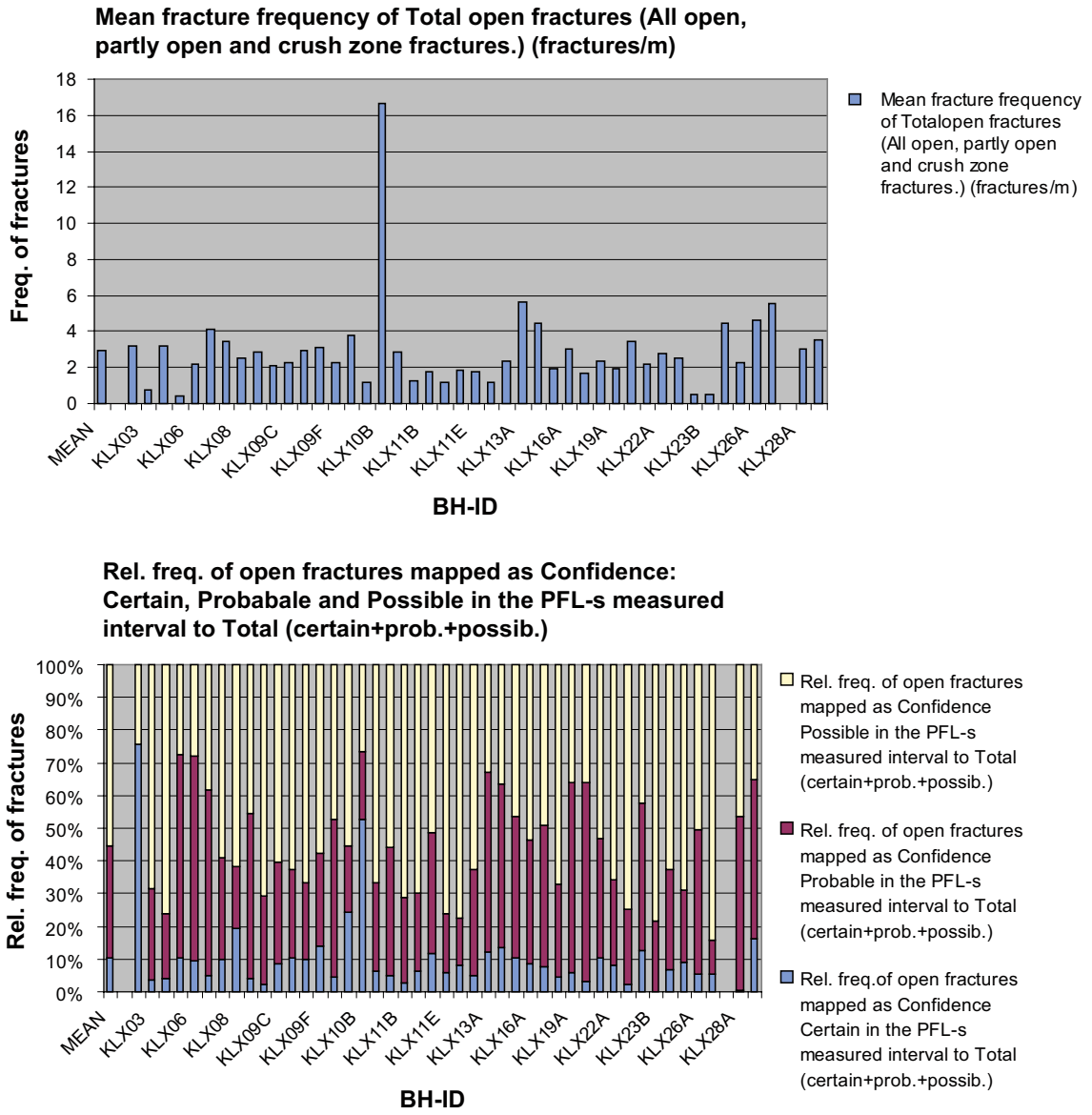

Figure 4-5. *Top: Mean fracture intensity of total open fractures (All open, partly open and crush zone fractures (40 fractures/m assumed for crush zones)). Boreholes KLX02 through KLX29A (KLX27A data not included). KLX10B is a short borehole. Bottom: Relative intensity of mapped open fractures attributed confidence levels "certain, probable and possible". Boreholes KLX02 through KLX29A (KLX27A data excluded) /Hermanson et al. 2008/.*

Table 4-1. Summary of sampled borehole lengths and numbers of fractures within Laxemar local model area at the time of data freeze Laxemar 2.3 according to different categories and the conductive PFL-f features in each of the boreholes measured with the PFL-f method.

Borehole	Top (m)	Bottom (m)	Length (m)	Total number of sealed	Number of all open [1]	Open[1] and certain	Open[1] and prob.	Open[1] and poss.	Number of PFL-f
KLX02	205.82	1,005.83	800	853	2,208	1,608	3	597	87
KLX03	101.4	992.42	891	3,694	683	29	188	466	55
KLX04	101.43	986.22	885	3,458	2,019	85	402	1,532	129
KLX05	108.01	987.43	879	3,172	320	34	199	87	71
KLX06	101.79	987.52	886	4,184	1,048	108	649	291	186
KLX07A	101.98	827.56	726	4,131	2,388	135	1,349	904	240
KLX07B	19.8	192.75	173	658	522	55	161	306	80
KLX08	100.88	987.0	886	3,291	1,974	392	371	1,211	138
KLX09	102.00	871.45	769	2,699	1,959	84	984	891	68
KLX09B	12.6	97.6	85	381	172	5	46	121	44
KLX09C	15.5	117.0	102	457	226	19	71	136	36
KLX09D	12.91	117.91	105	493	310	38	82	190	41
KLX09E	13.87	114.4	101	654	280	27	68	185	34
KLX09F	9.9	146.53	137	683	316	47	89	180	43
KLX09G	22.3	92.58	70	449	266	13	128	125	42
KLX10A	102.13	993.21	891	3,239	594	149	120	325	191
KLX10B	10.73	43.5	33	229	506	270	103	133	24
KLX10C	9.75	139.75	130	1,101	375	25	101	249	25
KLX11A	101.53	985.12	884	4,278	1,074	54	420	600	66
KLX11B	4.18	94.26	90	249	156	4	41	111	37
KLX11C	5.66	115.73	110	308	125	8	30	87	41
KLX11D	12.55	112.54	100	445	187	22	69	96	49
KLX11E	2.00	115.28	113	453	202	12	36	154	37
KLX11F	3.37	113.38	110	293	120	10	17	93	24
KLX12A	102.13	597.25	495	1,814	1,154	55	378	721	77
KLX13A	101.22	589.58	488	1,650	2,047	247	1,127	673	155
KLX14A	17.14	167.5	150	675	613	88	302	223	72
KLX15A	77.58	971.02	893	3,471	1,686	181	727	778	78
KLX16A	20.39	420.63	400	2,489	1,191	107	446	638	78
KLX17A	68.45	693.85	625	3,320	1,049	81	455	513	47
KLX18A	101.35	604.79	503	1,954	1,104	57	309	738	151
KLX19A	100.73	794.3	694	1,510	1,200	72	695	433	60
KLX20A	100.9	448.09	347	1,376	920	27	562	331	55
KLX21B	100.85	850.68	750	4,187	1,654	177	601	876	59
KLX22A	13.53	94.9	81	371	223	18	58	147	43
KLX22B	13.4	93.37	80	346	195	4	45	146	28
KLX23A	19.28	94.28	75	135	40	5	18	17	17
KLX23B	14.88	44.88	30	19	14	0	3	11	4
KLX24A	18.36	93.46	75	400	307	23	93	191	41
KLX25A	13.82	43.82	30	165	68	6	15	47	8
KLX26A	15	94	79	311	307	18	134	155	25
KLX26B	15	43	28	50	155	9	16	130	17
KLX27A	70.38	640.61	570	2,048	863	137	405	321	50
KLX28A	16.97	75.4	58	241	164	1	87	76	36
KLX29A	7.1	54.42	47	230	163	27	79	57	27
Sum BH			16,456	66,614	33,147	4,573	12,282	16,292	2,916

[1]: “Open” includes fractures mapped as open and partly open. Fractures that are judged to be open are assigned a confidence: certain, probable or possible.

4.2 Interference test caused by the underground facility of the Äspö Hard Rock Laboratory

The Äspö Hard Rock Laboratory (Äspö HRL) is situated below the Äspö island north-east of the Laxemar local model area, cf. Figure 3-1. The recorded drawdown and tunnel inflow data have been used to test and calibrate numerical groundwater flow models as part of the construction phase of the Äspö HRL /Rhen et al. 1997/ and as part of the SKB organised "Task Force on modelling of groundwater flow and transport of solutes" modelling /Rhén and Smellie 2003/. More recently, drawdown and inflow data has been used as part of on-going modelling work at Äspö HRL /Vidstrand 2003/ and as part of model testing for the site investigation in conjunction with model version Laxemar 1.2 /Hartley et al. 2007/.

In the current SDM-Site Laxemar work the influence of the Äspö HRL is tested in the flow modelling using updated geometric models and parameterisations in a manner similar to that employed by /Hartley et al. 2007/, cf. Section 7.2.

4.3 Evaluation of hydraulic interference tests

Interference tests during the site investigations in the Laxemar-Simpevarp area have been performed in a number of boreholes. A full account and detailing of performance, evaluation and relevant references related to the interference tests is given in /Rhén et al. 2009/.

Some of the interference tests have been of fairly short duration (a day up to a few days) and involving only a few observation sections in boreholes. However, some tests have employed both a long duration and involved several observation (monitoring) sections, thus being of interest for the SDM-Site Laxemar flow modelling.

Two interference tests were chosen for model testing and calibration as the number of observation sections is fairly large, the pumping durations relatively long and the tests being situated in two areas of interest for a possible deep repository. The two interference tests are in the following referred to as the HLX28 and the HLX33 interference test, respectively.

4.3.1 Results

Interference test HLX33

The HLX33 interference test focuses on testing the character of the deformation zone ZSMEW007A, cf. Figure 4-6.

The test in HLX33 provides verification that the hydraulic features along ZSMEW007A should be steep or dipping to the north, striking approximately E-W. The reason for this conclusion is the distribution of responses along borehole KLX07A when borehole HLX33 was pumped. As there were no responses in the deeper part of KLX07A, there exist no indications of splays to ZSMEW007A dipping to the south (or other conductive zones dipping south being in hydraulic contact with ZSMEW007A). Later, pumping tests along KLX07A confirmed this picture because pumping the deeper sections in KLX07A did not seem to generate hydraulic responses towards the north.

A few prior single-hole and cross-hole (interference) tests performed along the interpreted surface outcrop of deformation zone ZSMEW007A, cf. Figure 4-6, provide additional insight in the geometry and hydraulic character of the zone. These tests supported the geological interpretation of the structure dipping towards the north. For instance, an earlier pumping test in HLX10, cf. /Rhén et al. 2009 and Appendix A.1.7 therein/, shows a very clear response in one of the monitoring sections in KLX02 (borehole length c. 200–300 m). This fits well with the geologically interpreted geometry of the zone ZSMEW007A /Wahlgren et al. 2008/, as the zone ZSMEW007A is interpreted to be a feature more conductive than the surrounding rock.

The early interference tests using KLX02 as the abstraction hole provides further insight in the geometry of deformation zone ZSMEW007A, in particular its moderate dip towards north, roughly 45°. Interference tests performed in 1992–1995 involving pumping of the entire length of KLX02 (201–1,700 m) indicated hydraulic responses in KLX01 (mainly below 700 m borehole length) /Ekman 2001/. A closer look at KLX02 /Andersson et al. 2002/ indicated that in KLX02 borehole section 200–400 m the flowing features were oriented WNW-NW and that the transmissivity in the

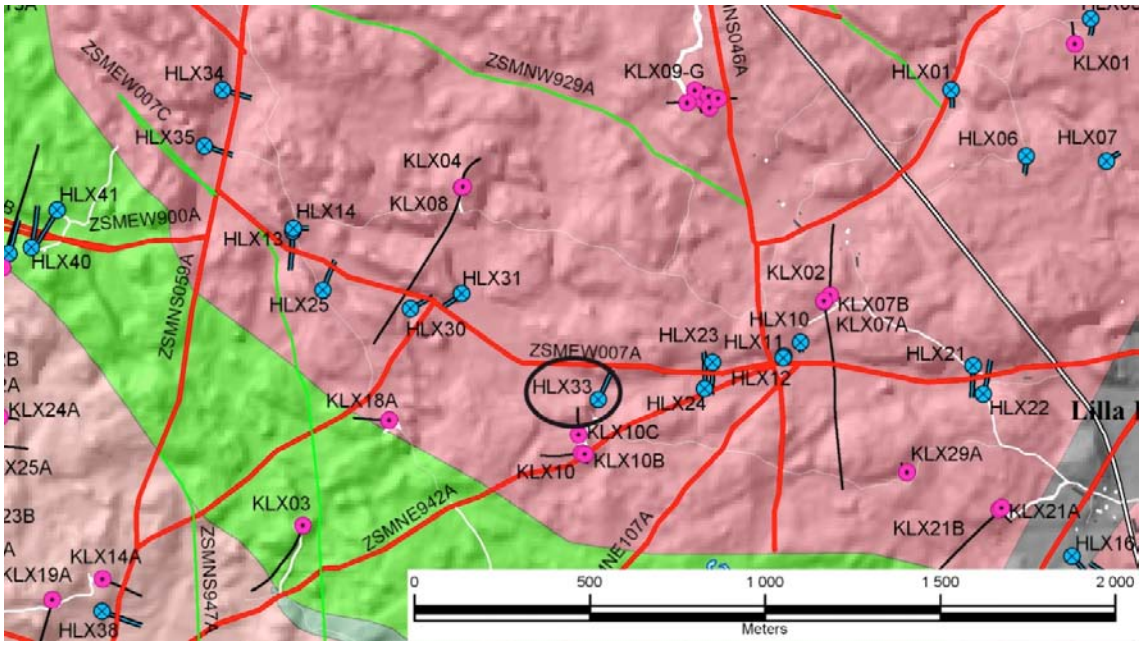

Figure 4-6. *Overview of boreholes involved in the interference test run in June–August 2006 using HLX33 as pumping borehole. The projected trajectories of the cored boreholes are shown as black lines. Only the surface expression of the HCD is indicated. Rock domains shown in background, cf. Figure 3-2.*

upper 500 m of KLX02 was considerably higher than below 500 m. Furthermore, the deformation zone model /Wahlgren et al. 2008/ projects that ZSMEW007A should intersect KLX02 between 180–200 m borehole length and then dip northwards to intersect KLX01 between 1,000–1,020 m borehole length. These observations indicate that ZSMEW007A may be one of the important structures providing hydraulic connection between KLX02 and the lower part of KLX01.

Interference test HLX28

The HLX28 interference test focuses on testing the character of the HCDs near HLX28; (ZSMEW42A, ZSMNS001C, ZSMNS059A, KLX19_DZ5-8_dolerite and HLX28_DZ1 cf. Figure 4-7). The latter two HCDs cannot be seen in the figure as they are modelled as subsurface discs without surface outcrops.

Deformation zone ZSMNS001C is of particular interest since it is associated with a dolerite dyke, and as such, a potential hydraulic barrier as thicker dolerite dykes are expected to be low-conductive, cf. Chapter 5. As reported in /Rhén et al. 2009, Appendix 1 therein/, two earlier pumping tests were conducted in KLX20A verifying the expected character and behaviour of the dolerite dyke. Due to some practical considerations; KLX19A was also pumped during the same period as the tests in KLX20A, cf. Figure 4-7 for location of boreholes, which however also confirms the barrier character of ZSMNS001C, cf. /Rhén et al. 2009, Appendix 1 therein/. During these tests, observations were made in two packed-off percussion boreholes; HLX37 and HLX43, cf. Figure 4-7. It is concluded from the responses that ZSMNS001C must have a tight core but permeable flanking wall rock on either side, at least in the southern part of ZSMNS001C near KLX20A, see Appendix 1 for further details.

The test demonstrates that ZSMNS001C acts as a hydraulic barrier (due to the lack of response in the uppermost section in HLX37, situated west of the dolerite dyke). These responses also indicate that the deformation zone HLX28_DZ1, intersecting HLX28 (cannot be seen in the Figure 4-7 as it is modelled as a disc without surface outcrop), is probably not intersecting ZSMNS001C for the same reason. It also appears that ZSMNS059A acts as a hydraulic barrier due to the poor response in KLX14A east of the zone and that the lower dolerite dyke in KLX19A (Part of HCD KLX19_DZ5-8, cf. Section 4.1.2) also acts as a barrier as no response is seen in observation boreholes east of this dyke. The small responses south of ZSMNW042A in HLX32 also indicated that ZSMNW042A acts as a barrier to some extent, at least in its western part. Possibly both HLX28_DZ1 and ZSMNW042 are responsible for transmitting hydraulic responses laterally, at least on the eastern side of ZSMNS001C. More details on the HLX28 interference test are reported in /Rhén et al. 2009, Appendix 1 therein/.

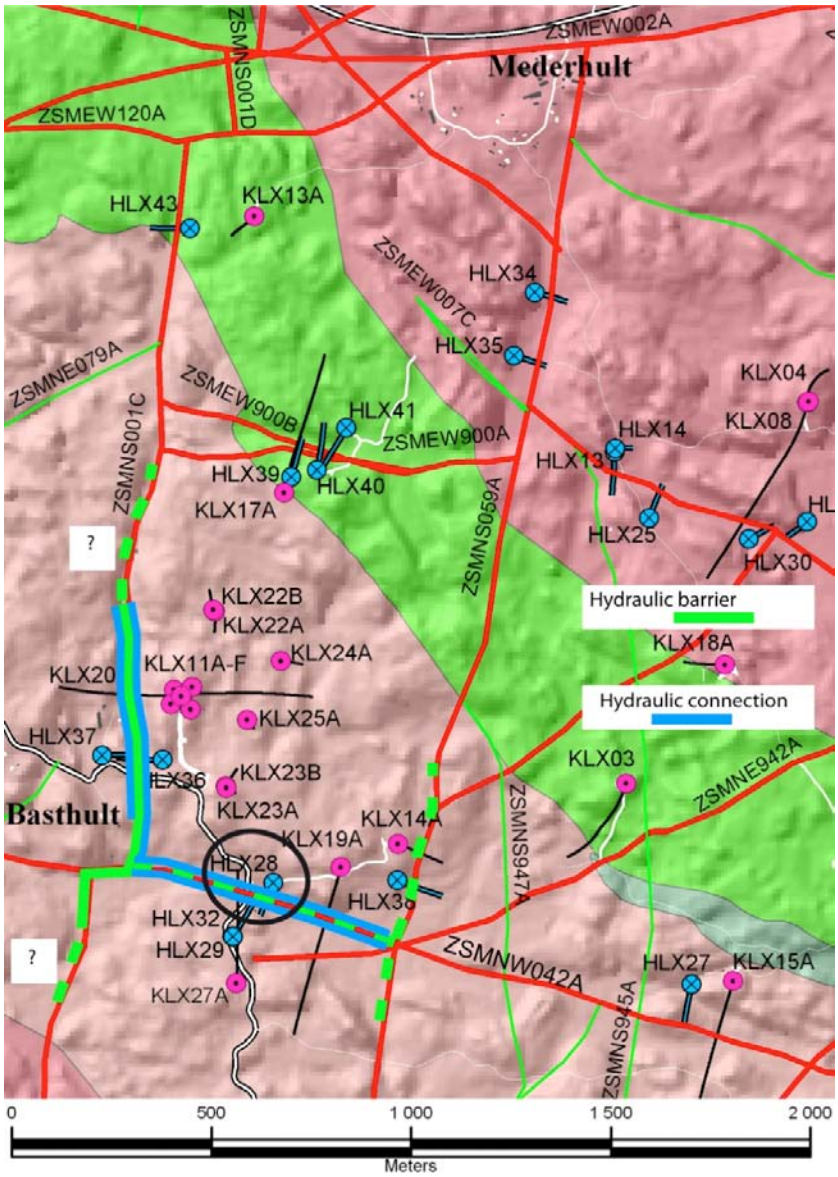

Figure 4-7. *Overview of boreholes involved in the interference test run in April 2007 using HLX28 as pumping borehole. KLX20A intersects ZSMNS01, KLX14A intersects ZSM059A and KLX19A, HLX27A and others intersects ZSMNW042A. The borehole trajectories of the cored boreholes are shown as black lines. Rock domains shown in background, cf Figure 3-2.*

4.4 Evaluation of groundwater levels

The monitoring of the variation in groundwater levels is carried out within the groundwater monitoring programme, which is one of the activities performed within the site investigation in the Laxemar-Simpevarp area. The overall objective of the groundwater monitoring programme is to further support the hydrogeological characterisation of the area and to document base-line groundwater conditions before the possible excavation of a final repository. The monitoring data are stored in the Sicada data base and are reported regularly in progress reports, see e.g. /Nyberg and Wass 2008/.

The groundwater monitoring programme related to the current site investigation programme started in December 2002 and the number of boreholes monitored has continuously increased during the course of the site investigations. Monitoring takes place in the cored boreholes, percussion boreholes and groundwater monitoring wells (the SSM boreholes in Quaternary deposits). Note: Boreholes located on the Äspö Island are not part of the site investigation programme. For details on the monitoring programme cf. /Rhén et al. 2009/ and Werner et al. 2008/. The locations of the boreholes are shown in Appendix 1.

4.4.1 Available data

Monitoring data from groundwater monitoring wells completed in Quaternary deposits and monitoring in percussion and core holes are presented in /Werner et al. 2008/, which also covers meteorological, hydrological and hydrogeological monitoring as well as near-surface hydrogeological properties. The data set for groundwater levels spans the period December 4th 2002 to December 31st 2007 for groundwater monitoring wells in Quaternary deposits and January 1st 2004 to December 31st 2007 for cored and percussion-drilled boreholes, i.e. three months after Laxemar data freeze 2.3. In order to estimate natural (undisturbed) groundwater levels, data were screened to remove periods with hydraulic disturbances due to e.g. drilling or hydraulic testing, for details on the screening see /Werner et al. 2008/. Some of the screened time series are rather short, which may imply that the min, max, and average values of groundwater levels are uncertain (ideally at least one annual cycle should be available). Therefore, borehole sections with 150 days of data or more (i.e. more than c. five data months) have generally been used for calibration of the current flow model. The measured head data are considered representing the section mid-elevations, which are calculated simply as the average of the upper and lower section elevations.

4.4.2 Results

In Figure 4-8 and Figure 5-14 the groundwater levels in rock in the percussion drilled boreholes and cored boreholes in Laxemar are shown (cf. /Werner et al. 2008/ for groundwater monitoring in wells and boreholes on Ävrö and Simpevarp peninsula). In total, data from 44 percussion boreholes and 37 cored boreholes were available. The number of monitored observation sections has varied; at the time of data freeze Laxemar 2.3 in August 31st 2007 some 37 percussion borehole sections and 132 sections in cored boreholes were being monitored and on December 31st the corresponding numbers were 35 and 120, respectively.

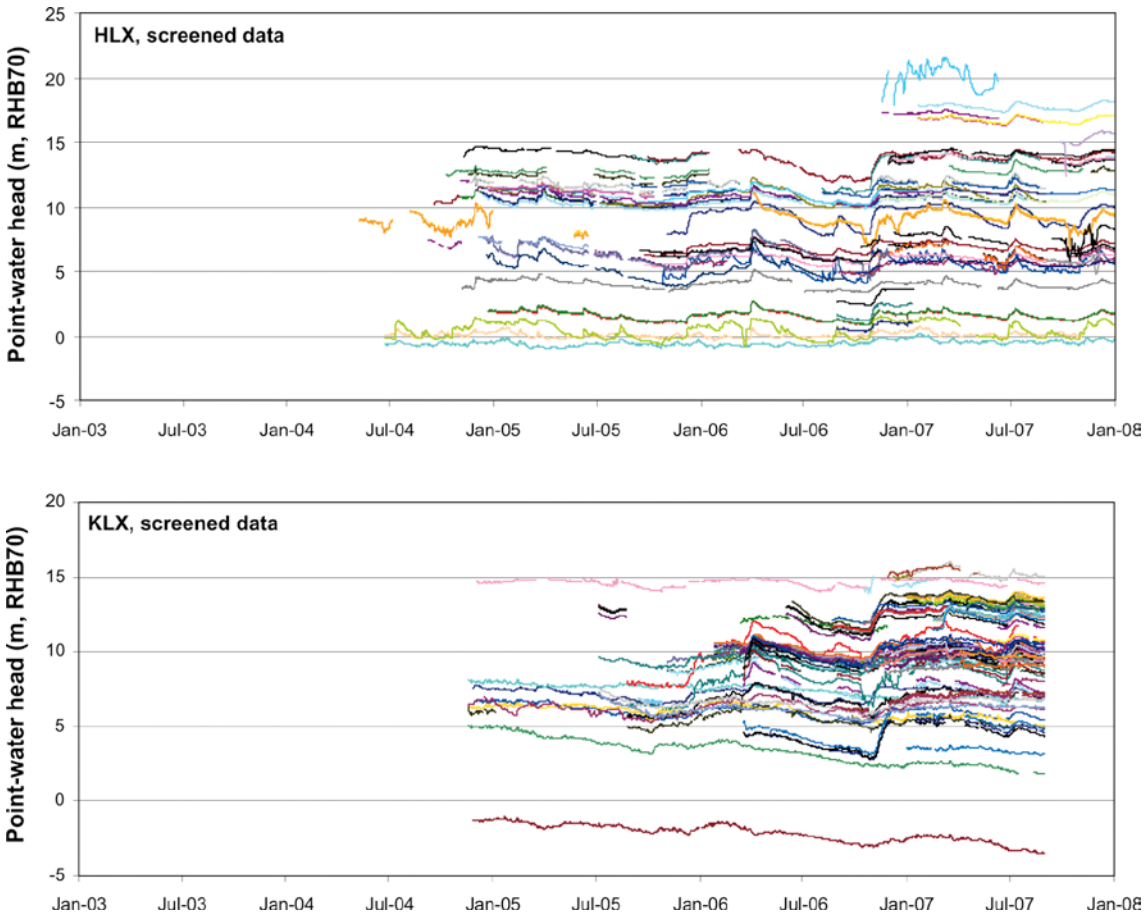

Figure 4-8. *Range for groundwater levels (daily mean) in monitored borehole sections in Laxemar local model area (screened data). Monitored boreholes shown are in bedrock. /Werner et al. 2008/.*

For the SDM-Site Laxemar regional scale modelling, data from 31 cored boreholes distributed between different areas have been obtained:

- 27 boreholes in Laxemar (KLX02–06, 07A–B, 08–10, 11A18A, 11E, 20A, 21B, 23A, 24A and 26A28A)
- 2 boreholes at Simpevarp (KSH01A and KSH02)
- 2 boreholes at Ävrö (KAV01 and KSH04A)

These boreholes are equipped with multiple-packer systems, dividing them into sections (borehole section numbering starting from the bottom). Groundwater densities have been measured on water sampled from the borehole sections. For some boreholes or borehole sections, there are no density data available. However, in a few of these boreholes electrical conductivity (EC) data are available, and the density was estimated using an empirical relationship /Werner et al. 2008/. The temperature of the bedrock is of hydrogeological interest as viscosity and density of water are temperature dependent. However, the temperature increase with depth is fairly modest and has only limited effect on the hydraulic properties; mean temperature near surface being c. +7ºC and the average temperature gradient is generally between 12 to 15°C/1,000 m, cf. /Rhén et al. 2009, Sundberg et al. 2008/

As described in /Rhén et al. 2009/ the measured, and stored data value, is the water level in the standpipes, and it represents a *point-water head (PWH)* (cf. /Rhén et al. 2009/ and Appendix 3 therein) assuming that the density is constant in the standpipe and tubes down to the observation section. Assuming that the density in the standpipes represents the density of the formation water at the level of the observation section, it is possible to calculate the *environmental-water head (EWH),* or for short, *environmental head* (cf. /Rhén et al. 2009/ and Appendix 3 therein) for the section, using the density profile for all sections above the measurement up to the surface. The usefulness of EWH is that along the borehole, the vertical hydraulic gradient can be judged in a medium that is hydraulically well-connected vertically and horizontally. It turns out that generally the difference between EWH and PWH is small but at very deep levels the difference can be significant due to increasing salinity of the groundwater, which renders lower PWH than EWH. As stated in /Rhén et al. 2009/ the pumping of the water in the standpipes may not always provide a density that can be expected to be similar to the formation water at the level of the observation section. This means that densities appropriate for calculation of EWH must be carefully examined and generally estimated from different sources, e.g. chemical sampling and geophysical logging of fluid electrical conductivity. This has not been possible to achieve during the site investigations and as a consequence EWH below elevation c. –800 m should not be used for calibration purposes. Consequently, these data are not included in the figures used to present the comparison of the modelled results to measured and calculated heads.

In this report the *groundwater level* is generally used for the measured value in a borehole, that may represent the water table in an upmost section of a borehole or another potentiometric surface deeper down in the rock /Wilson and Moore 1998/. In some cases *point-water head (PWH)* and *environmental-water head (EWH)* are used to explain what is plotted in the figures.

The yearly amplitude in groundwater level is c. 1.9 m in the percussion boreholes and c. 1.5 m in the cored boreholes, based on data with at least a series of 150 days /Werner et al. 2008/. As can be seen in Figure 5-14 there is a tendency that also the groundwater levels in the percussion boreholes follow the ground surface elevation. One can also see that there are two wells indicating artesian conditions (HLX15 and HLX28).

Figure 4-8 shows the time series data and reveals that some groundwater levels are negative. The reason is that the density in the standpipes generally becomes higher than the average formation density in the deep observation sections, as each standpipe from an observation section is pumped and filled with water from that observation section. These cases with higher density in the standpipes compared to average (in a vertical column) formation density, are generally borehole sections below elevation c. –400 m, and high salinity values in the standpipes are generally found below c. –800 m.

The basis for the calibration of the regional groundwater flow model is the mean point-water head (or environmental head) and in Section 7.1.2 the min, mean and max point-water head are presented for the monitored groundwater monitoring wells and percussion boreholes for the time period available. The corresponding data from cored boreholes are exemplified for a few boreholes only in Section 7.1.2.

4.5 Evaluation of hydrogeochemistry data

The spatial distribution of some of the hydrogeochemical components can be expected to be strongly linked to the evolution of the groundwater flow system and therefore the hydrogeochemical data can provide insights on the flow system, and in turn the groundwater flow modelling may mutually provide essential inputs for the discussion of hydrogeochemical processes.

In this section essential data are presented that have been used for the palaeohydrogeological conceptualisation and simulations presented in Sections 5.2, 6.6 and 7.4, respectively. The bedrock hydrogeochemistry of the Laxemar-Simpevarp area is described in detail in /Laaksoharju et al. 2009/ and hydrochemistry of surface water and shallow groundwater is discussed in more detail in /Tröjbom et al. 2008/.

4.5.1 Hydrochemical data available

The hydrochemistry data delivery consists of measurements of major ions, isotopes, porewater data and calculated M3 mixing fractions (M3: a model for multivariate analyses of hydrochemical data, cf. /Gimeno et al. 2009, Laaksoharju et al. 2009/). The major ions considered in the groundwater flow model calibration are Br, Ca, Cl, HCO_3, Mg, Na, K and SO_4. The two isotopes of interest to hydrogeology are δ^2H and $\delta^{18}O$. /Rhén et al. 2009/ provides a summary of the constituents and boreholes (core-drilled and percussion-drilled boreholes) considered in the model calibration for SDM-Site Laxemar. It should be mentioned that porewater data were collected in only three boreholes; KLX03, KLX08 and KLX17A. A full list of the constituents encompassed by the hydrochemical programme providing data for SDM-Site Laxemar is given in /Laaksoharju et al. 2009/. The uncertainty in the hydrochemical analysis, shown in figures in Section 7.4, of the water samples is discussed in more detail in /Nilsson 2009/.

The hydrochemistry data delivery has been sorted into five major categories, where Categories 1 and 2 represent high quality samples, Category 3 intermediate quality samples and Categories 4 and 5 intermediate to low quality samples. In Table 4-2, the number of samples and the location of sampled data in each category are shown. As can be seen from the table, categories 3 and 4 are important to get some spatial resolution of the hydrochemical data. Category 5 data were not used for comparison of the hydrogeological modelling results presented in Section 7.4.

Limiting the selection of data used in the modelling to only those that fulfil criteria such as a low level of drilling water residue and full coverage of major ions and isotopes would leave a large number of samples not used. Some of these samples are found at elevations where data of higher quality are missing. It was therefore decided to use some of the Category 4 samples as supplementary data in the SDM-Site Laxemar groundwater flow modelling in order to provide more data for the comparison. The category 4 data are discussed in /Rhén et al. 2009/.

Table 4-2. Number of samples and location of sampled data in each category in the extended hydrochemistry data freeze Laxemar 2.3.

Category	Number of samples and position
Category 1	3 samples (2 in KLX03, 1 in KSH02)
Category 2	4 samples (1 in KLX05, 1 in KLX08, 1 in KLX15A, 1 in KSH01A)
Category 3	58 samples (11 in percussion-drilled boreholes, 47 in core-drilled boreholes)
Category 4	48 samples (17 in percussion-drilled boreholes, 31 in core-drilled boreholes)
Category 5	322 samples (9 in percussion-drilled boreholes, 313 in core-drilled boreholes)

Salinity

In the present study, the focus is on the results for salinity (expressed as TDS), Cl, Br/Cl-ratio, Na, Ca, Mg and HCO_3. Salinity is a very important natural tracer because variations in salinity lead to one of the driving forces for groundwater flow, and density-dependent flow is also used in the regional scale numerical groundwater flow modelling, cf. Section 2.2 and Chapter 6. The salinity for a given water composition in the groundwater flow model is calculated as the sum of the products of each reference water fraction and the salinity of that reference water (i.e. Br, Ca, Cl, HCO_3, K, Mg, Na and SO_4). The modelled salinities were compared with those observed through a visual comparison of the profiles along the boreholes, comparing the trends and major features in the boreholes. Details of the use of the salinity data are found in /Rhén et al. 2009/.

See Figure 4-9 for a summary plot of all available salinity data for the cored boreholes in Laxemar.

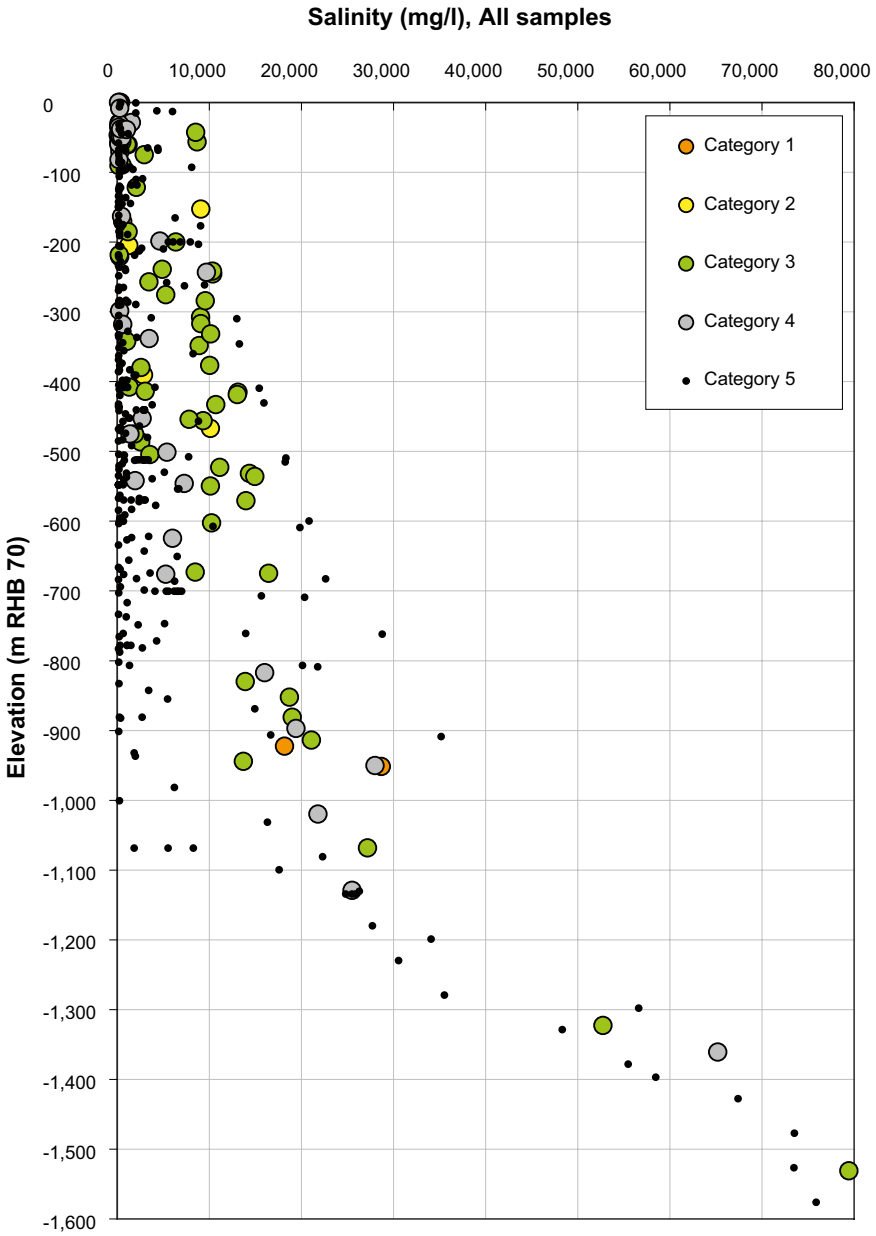

Figure 4-9. *Plot of all available salinity data from the core-drilled boreholes and percussion-drilled boreholes in Laxemar sorted according to quality category. For the sake of comparison, the reference water salinities (TDS)(mg/L) are: Deep Saline Water = 76,291; Inter-glacial Porewater = 280; Glacial Melt Water = 2; Littorina Sea Water = 11,912; Altered Meteoric Water = 452.*

4.5.2 Major ions and isotope data

The water samples collected in boreholes represent water from hydraulically connected fractures that that had a transmissivity enough to enable sampling of water within reasonable time. These samples are assumed mainly representative of water found in the fracture system with medium to high transmissivities. The porewater from fresh core samples is here referred to as matrix porewater, i.e. water in the connected pore space of the rock matrix that is accessible for diffusion-dominated interaction with groundwater circulating in nearby (micro) fractures /Waber and Smellie 2008/. In the numerical groundwater flow modelling it is assumed that matrix water is immobile; matrix water is only transported by diffusion, cf. Chapter 7.

Fracture groundwater and porewater

Data indicate fresh recharge groundwaters (< 200 mg/L Cl) down to a depth of c. –250 m. Within the depth interval –250 to –600 m, the Laxemar groundwaters are characterised mainly by brackish glacial types with some examples of brackish non-marine and transition types. The depth interval –600 to –1,200 m marks the transition from brackish non-marine to saline groundwater type, characterised by a steady increase in chloride to about 16,000 mg/L /Laaksoharju et al. 2009/.

The compiled $\delta^{18}O$ data for the Laxemar local model volume shows a wide spread, indicating a significant heterogeneity, but also clear indications of groundwater with a glacial component recognised by their low $\delta^{18}O$ (< –13.0‰ V-SMOW) /Laaksoharju et al. 2009/ around –300 to –600 m depth.

Porewater data

The hydrochemistry delivery for SDM-Site Laxemar model contained matrix porewater data for the components Cl, $\delta^{2}H$ and $\delta^{18}O$ extracted from matrix core samples collected in KLX03, KLX08 and KLX17A. /Waber et al. 2009/ provides an extensive summary of the porewater analysis. An interpretation of the palaeohydrogeological aspects of the matrix porewater data is provided by /Laaksoharju et al. 2009/, cf. Section 4.9 therein/, and summarised in /Rhén et al. 2009/.

The porewater data indicates a distinction between bedrock characterised by high transmissivity and a high intensity of water-conducting fractures at shallow to intermediate depth, and bedrock characterised by low transmissivity and a low intensity of water-conducting fractures at greater depth, cf. /Rhén et al. 2009/. In several cases when the rock sample for porewater has a long distance to the nearest conductive fracture (as defined by PFL method), there is an indication of a difference between porewater and fracture groundwater and thus the system is in a transient state, cf. /Rhén et al. 2009/ and /Laaksoharju et al. 2009/.

4.5.3 Mixing fractions

In addition to measurements of major ions, isotopes and porewater data, the hydrochemistry data delivery for SDM-Site Laxemar includes calculated M3 mixing fractions /Laaksoharju et al. 2009/ for the four reference waters: *Deep Saline Water*, *Littorina Sea Water*, *Glacial Melt Water* and *Altered Meteoric Water*, cf. Table 4-3. The calculated mixing fractions are available for all Category 1 and 2 data. The calculation of M3 mixing fractions did not consider the Inter-glacial Porewater used in the hydrogeological modelling. Any component of such a water present in groundwater samples would most probably be interpreted as being part of the *Altered Meteoric Water* fraction by the M3 analysis.

For the delivered M3 mixing fractions, a general uncertainty of ±10% was used /Laaksoharju et al. 1999/.

The transport of reference waters is simulated as chemically conservative (non-reactive) solutes in the groundwater flow model, cf. Sections 6.6 and 7.4. The reference water compositions in the fracture system are given in Table 4-3. Four main hydrochemical indicators were used in the palaeohydrogeological calibration:

- Cl – since it is conservative and indicates the locations of *Littorina Sea Water* and *Deep Saline Water*;
- Br/Cl ratio – since both are conservative and their ratio can be used to determine where the origin of saline water changes from a *Littorina Sea Water* to *Deep Saline Water* when the ratio increases from around 0.004 to 0.007, or more;
- $\delta^{18}O$ – since this is conservative over the timescales considered in the simulations and indicates any remnants of *Glacial Melt Water* when $\delta^{18}O < -13$ /Laaksoharju et al. 2009/;

- HCO_3 – because we model the infiltration of an *Altered Meteoric Water* into the bedrock. The HCO_3 is used as a signature for infiltrating post-glacial meteoric water (although it is a non-conservative species), this signature can also be traced by the low Cl content. The reference water composition of *Altered Meteoric Water* takes into account the major changes that meteoric water has undergone in the Quaternary deposits and the uppermost part of the bedrock such as organic decomposition and calcite dissolution. Mixing is important for the groundwater components in *Altered Meteoric Water* but still the HCO_3 content can also be dependent on reactions.

The concentrations of the major ions and the isotope ratios (and the salinity) can be readily determined from the fractions of the reference waters. In this study, these concentrations are compared with those observed, which represent in a sense measured data. In addition to this, the modelled mixing fractions of the reference waters are compared with the M3 mixing fractions inferred from the data (using a principal component analysis).

It is perhaps worth noting that ConnectFlow could have directly simulated the transport of the major ions and isotopes. However, it is more convenient (computationally effective) to specify the boundary and initial conditions in terms of the reference waters, cf. Section 7.4 and /Rhén et al. 2009/ for more details. Furthermore, although some chemical constituents, such as Cl, Br and $\delta^{18}O$, are transported conservatively (i.e. no chemical reaction takes place during transport), others are likely to be non-conservative, such as HCO_3 and SO_4, which can be affected by chemical and microbial processes. The effects of non-conservative processes that take place in the soil and top few tens of metres of bedrock are accounted for implicitly by using an *Altered Meteoric Water* reference water derived from groundwater samples in the uppermost bedrock to represent the composition of infiltrating water on the top surface above the shoreline. Mg is not a conservative tracer either, but it is a useful indicator when differentiating between *Deep Saline Water* at depth and shallower *Littorina Sea Water* near the top surface of the model domain. However, because of the ion exchange mechanisms involving Mg, great caution should be taken when using these non-conservative tracers for model calibration purposes. In fact, even a qualitative evaluation might be misleading. The Br/Cl ratio should be considered as a better alternative to indicate the transition zone from *Littorina Water* to *Deep Saline Water*. The environmental isotopes δ^2H and $\delta^{18}O$ provide guidance to differentiate between *Glacial Melt Water* and meteoric reference waters such as *Old Meteoric Waters* (from periods before the last glaciation) and *Inter-glacial Porewater.* Cl, Br/Cl and $\delta^{18}O$ are used quantitatively in the calibration of the regional flow model and the others ions are only used as indicators that are discussed, cf. Chapter 7.

Reactive solute transport is further discussed in /Laaksoharju et al. 2009/, cf. Section 5.3 therein, and in /Molinero et al. 2009/.

Table 4-3. Composition of the reference waters selected for the mixing calculations in the Laxemar-Simpevarp area. Data provided for hydrochemistry data delivery for SDM-Site Laxemar. All concentrations are in mg/L , except for pH (units) and δ^2H (‰ VSMOV) and $\delta^{18}O$ (‰ VSMOV).

	Deep Saline water	Littorina sea water	Altered Meteoric water	Glacial melt water	Inter-glacial Porewater	
					Case 1	Case 2
pH	8	7.6	8.17			8
HCO_3	14.1	92.5	265.0	0.12	265.0	10
Cl	47,200	6,500	23.0	0.5	23.0	5,000
SO_4^{2-}	906.0	890	35.8	0.5	35.8	375
Br	323.66	22.2	0		0	34
Ca	19,300	151	11.2	0.18	11.2	1,585
Mg	2.12	448	3.6	0.1	3.6	2
Na	8,500	3,674	110.0	0.17	110.0	1,440
K	45.5	134	3.0	0.4	3.0	4
Si	2.9	3.94	7.0	–	–	–
Fe^{2+}	–	0.002 (Fe tot)	0.08		–	–
S^{2-}	–	–	–		–	–
δ^2H (‰)	–44.9	–37.8	–76.5	–158.0	–50	–50
$\delta^{18}O$ (‰)	–8.9	–4.7	–10.9	–21.0	–5	–5

5 Conceptual model development

This chapter presents the hydrogeological conceptual models in terms of basic geometry of the underlying deformation zone model (HCD), the hydraulic rock domains (HRD), Quaternary deposits (HSD) and their hydraulic parameterisation, cf. Section 5.1. This is followed by descriptions of basic data important for the formulation of hydraulic boundary conditions, cf. Section 5.2. An effort is furthermore placed on the description of the palaeohydrogeological development as a basis for formulating hydrogeochemical boundary and initial conditions, cf. Section 5.2.

5.1 Hydrogeological description and conceptual model

In this section the components of hydrogeological conceptual models, as introduced in Table 2-1, are presented including some of the data that constitute the basis for these models. The component conceptual models constitute the integral parts for the construction of the numerical groundwater flow models and modelling as reported in Chapters 6 through 9.

5.1.1 General

The Laxemar-Simpevarp regional model area is in general characterised by an undulating bedrock surface with a thin cover of Quaternary deposits, mainly till on the top of the hills and thicker Quaternary deposits in the valleys made up of till overlain by postglacial deposits. The crystalline bedrock is intersected by a number of deformation zones, denoted Hydraulic Conductor Domains (HCD) in the hydrogeological model, which are mainly steeply dipping, with less fractured bedrock between these zones. The bedrock in between the HCDs is in the hydrogeological model called Hydraulic Rock Domains (HRD). Hydraulically, the deformation zones are generally more conductive than the bedrock in between. The general tendency within the Laxemar-Simpevarp regional model volume is that the hydraulic conductivity decreases with depth in both HCDs and HRDs. The Quaternary deposits, called Hydraulic Soil Domains (HSD) in the hydrogeological model are generally more conductive than the bedrock. Figure 5-1 shows a generalised vertical section illustrating the overall hydrological and hydrogeological conceptual model of the Laxemar-Simpevarp area. The hydrogeological characteristics of the HCDs, HRDs and HSDs are further described in Sections 5.1.2 through 5.1.4 and details are found in /Rhén et al. 2008/.

5.1.2 Hydraulic conductor domains (HCD) within regional model area

In the preliminary SDM /SKB 2006a/, 90 deformation zone intercepts representing 25 different deformation zones in the regional model area were investigated hydraulically. The deformation zone model developed for the preliminary SDM (model version Laxemar 1.2) /SKB 2006a/ was further elaborated and consolidated during the CSI stage, a work that is concluded as part of the SDM-Site Laxemar modelling based on data freeze Laxemar 2.3. In SDM-Site Laxemar, the corresponding numbers of zones are 158 and 57, respectively, which imply a more or less doubled information density. The deformation zone model, as implemented in the regional scale flow model, is shown in Figure 5-2.

As stated in Section 3.2, 23 of the HCDs are modelled as discs based solely on borehole information and the size as assessed by Geology is uncertain. Based on the hydrogeological evaluation it was decided to add five more HCDs, modelled as discs with radius 564 m; KLX19_DZ5-8_dolerite as hydraulic tests indicated effects of this dolerite dyke; klx09_dz9, klx09_dz14, klx16_dz6 and klx19_dz2 which are linked to MDZs in the borehole and considered important to include deterministically. These are modelled as discs with, on average, similar transmissivities as all other HCDs.

The transmissivity data acquired from the single-hole tests constitute the basis for assigning hydraulic properties to the deformation zones in the SDM.

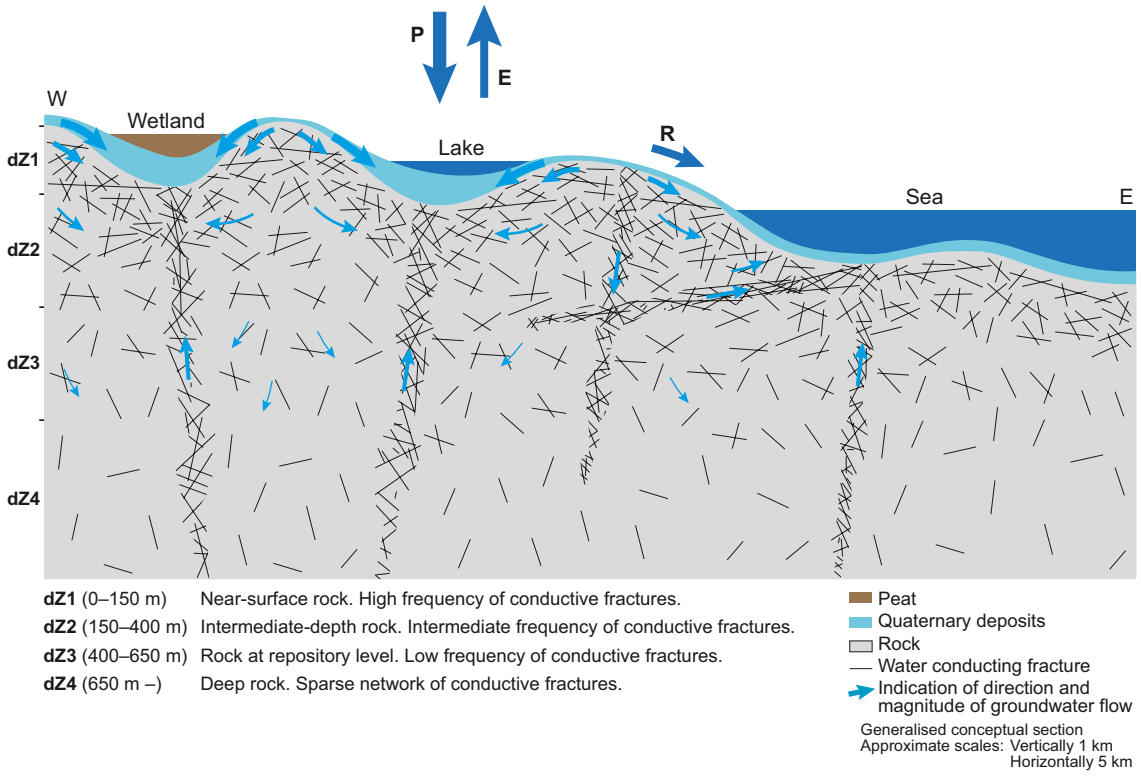

Figure 5-1. *Generalised section illustrating the conceptual model of hydrology and hydrogeology in Laxemar. Note the different horizontal (5 km) and vertical (1 km) scales. Furthermore, the thickness of the Quaternary deposits is exaggerated in the figure.*

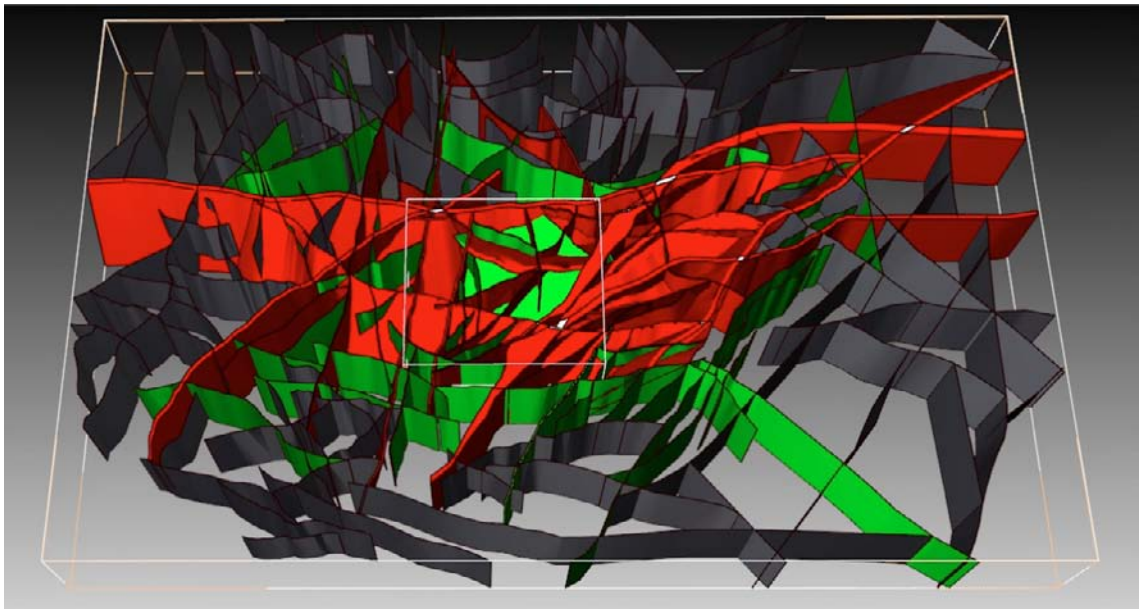

Figure 5-2. *3D visualisation of the regional model domain (large box with white lines) and local model area (small box with white lines) and the 184[(1)] deformation zones included in the SDM-Laxemar deterministic deformation zone model. Colouring of zones according to judged confidence. Red: high confidence, green: medium confidence, grey: low confidence. ([(1)]: Some of these 184 deformation zones are modelled as multiple segments (A, B etc) of a given numbered zone (e.g. ZSMxxxxxxA, ZSMxxxxxxB, etc.).*

Supporting data for geometries of the HCDs

The geometries of the HCDs are based on the geological deformation zone model, but in some cases interference tests have provided support for the suggested geometries. The best example is the geometry of the deformation zone ZSMEW007A, where interference tests indicated that it should dip to the north and probably not have any vertical or south dipping splays, cf. Figure 3-2 and Section 4.3.2. The interpretation of the geometry and hydraulic properties of zone ZSMNS001C was also sustained by interference tests, cf. Figure 3-2 and Section 4.3.2.

Trend models for transmissivity in HCDs

The data and the general models suggested for the initial assignment of hydraulic properties to HCDs in the groundwater flow modelling are presented in Figure 5-3, cf. a detailed account in /Rhén et al. 2008/. The variability in transmissivity is large but considering mean values for depth zones employed in the HRD modelling, see Section 5.1.3, the transmissivity decreases with depth, cf. /Rhén et al. 2008/. There is also a tendency that the transmissivity is positively correlated to the interpreted lineament length of the HCD and also that HCDs with E-W orientations are slightly more transmissive than HCDs of other orientations, cf. Figure 5-3 and /Rhén et al. 2008/.

However, some of the HCDs are intersected by several boreholes a range of depths and it was judged that there were enough data for assessment of zone-specific trend functions for seven of the HCDs, cf. /Rhén et al. 2008/.

Supporting data for anisotropic properties in HCDs

Several interference tests have shown that dolerite dykes may act as hydraulic barriers, at least locally. The best example relates to the HCD ZSMNS001C, associated with a core of dolerite, cf. Section 4.3. Both interference tests and monitoring data show fairly large differences in hydraulic head on either side of two other HCDs associated with dolerite dykes, ZSMNS059A and the KLX19_DZ5-8_dolerite, are also acting as hydraulic barriers, but probably to a lesser degree where the dykes become thinner. The dolerite dykes in Laxemar, cf. /Rhén et al. 2008/, seem to be steep and be mainly oriented N-S and are also expected to have a low hydraulic conductivity at their core, but are still heavily fractured and the rock at the margins of dolerite dykes is fairly transmissive. The hydraulic conductivity of the dolerite core is expected to be less than 10^{-9} m/s, cf. /Rhén et al. 2008/, whereas the transmissivity of the flanking contacts or the dolerite-associated deformation zones is significantly higher, varying between $1.2 \cdot 10^{-5}$ m^2/s and $4.8 \cdot 10^{-4}$ m^2/s, suggesting significant anisotropy.

Mapping of the cored boreholes and outcropping deformation zones has shown that fault gouge is present in at least ZSMEW002A (KLX06), ZSMEW007A (observation in trench) and ZSMNW042A (KLX27A) /Wahlgren et al. 2008/. This implies that these HCDs can exert some hydraulic barrier effect, most likely highly localised. The evaluation of monitoring data and the simulations shown in Chapter 7 indicates that both ZSMEW002A and ZSMNW042A western part (i.e. west of ZSMNS059A) need to be modelled with a lower permeability across the HCD compared to the permeability along their planes. Difference in heads along KLX06 cannot be reproduced in the simulations unless parts of ZSMEW002A act as a barrier, cf. Chapter 7. Beside the observation of fault gauge in KLX27A, the lack of hydraulic responses south of ZSMNW042A during pumping in HLX28 indicates that there is a barrier effect in ZSMNW042A, cf. Section 4.3.2 and Chapter 7. It is not known if the eastern part of ZSMNW042A exhibits any barrier effect. Anisotropic conditions for specific zones as implemented in the numerical groundwater flow model are discussed in /Rhén et al. 2009/.

Internal variability in HCD properties

The variability of transmissivity of HCDs is readily apparent by studying the entire sample of HCD transmissivities. The standard deviation of log10(T) of the corresponding transmissivity data is c. 1.4 /Rhén et al. 2008/. However, as there are a number of HCDs which individually have been subjected to several hydraulic tests at multiple locations, the standard deviation related to individual HCDs is of interest in comparison with that of all data shown in /Rhén et al. 2009, Figure 4-4 therein/. The standard deviation versus elevation is shown for the HCDs included in the regional model volume

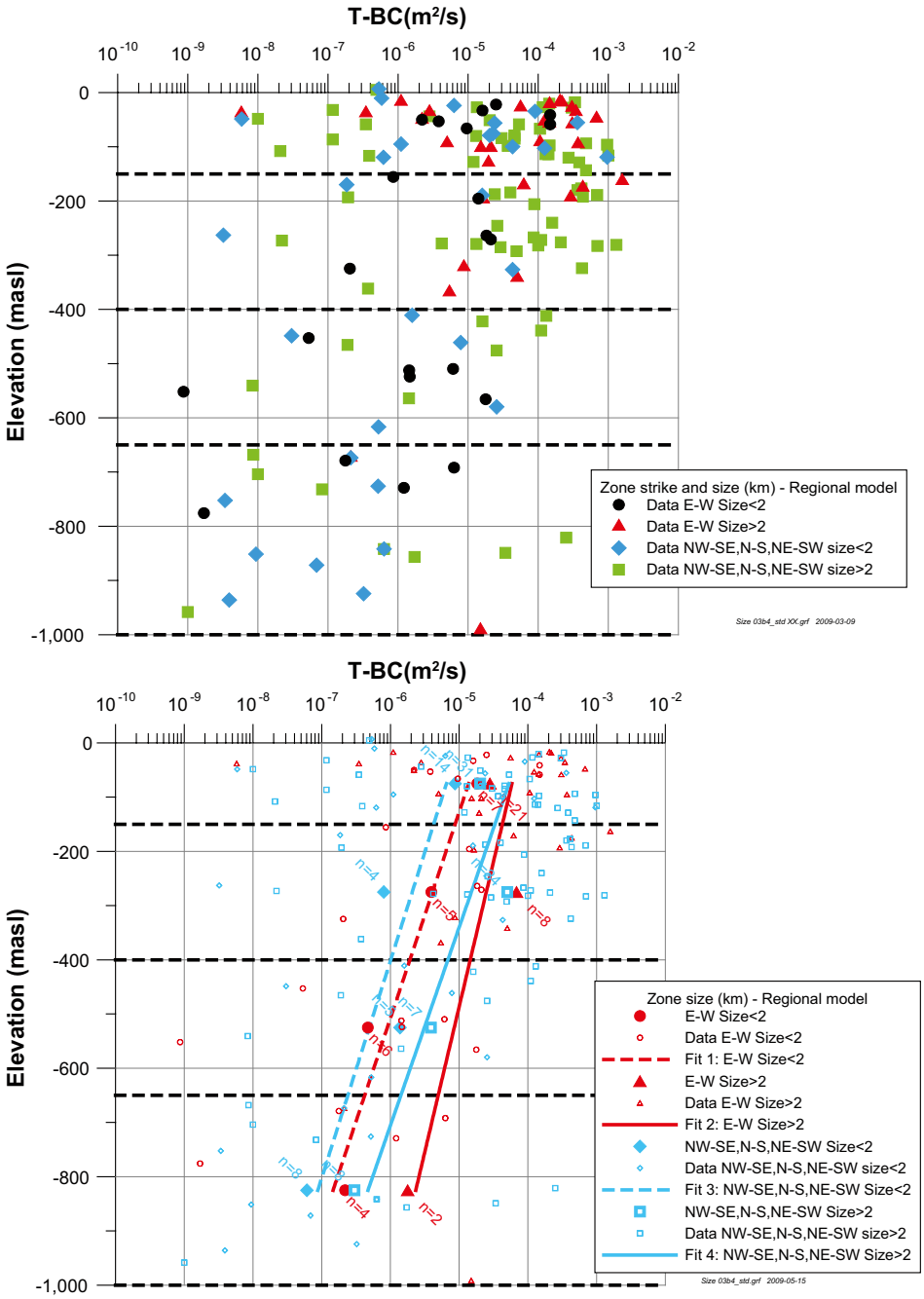

Figure 5-3. *Deformation zone transmissivity (T) related to deformation zone orientations in the horizontal plane and size, versus elevation. Mean of log10(T), plotted as well as the number of observations (n). (Top: Data in regional model. Bottom: Regression line and data, regional model.*

that are subjected to several hydraulic tests. /Rhén et al. 2009/ indicate that the standard deviation of log10(T) is in the range 0.5 to 2 for an individual zone. The estimated standard deviations are based on generally small samples and the highest standard deviations are based on very small samples and are not considered good measures for the range of standard deviations of HCD transmissivity.

The range for the PFL-f features in terms of P_{10} and $P_{10\text{–corr}}$ (Terzaghi corrected frequency) within a HCD is c. 0.05–1 m^{-1} and 0.05–2 m^{-1} respectively, with a mean around 0.2–0.5 m^{-1} and 0.3–1 m^{-1}, respectively, and a standard deviation of c. 0.15–0.25 m^{-1} and 0.2–0.6, m^{-1}, respectively, /Rhén et al. 2008/.

5.1.3 Hydraulic rock domains (HRD) within regional model area

Overview

Hydraulic rock domains are defined based on the spatial distribution of hydraulic properties in space, and analysis has shown that some of the fracture domains can be used directly as hydraulic domains, whereas some fracture domains can be merged in the definition of hydraulic rock domains, cf. /Rhén et al. 2008/. Figure 5-4 through Figure 5-6 show the HRDs (HRD_N, HRD_EW_007, HRD_C, HRD_W) corresponding to hydraulic rock domains and the detailed motivation for their individual formation is provided in /Rhén et al. 2008/. Some essential data and considerations that formed the basis for defining the HRDs are discussed below.

Given that fracture domains are not defined outside the bounds of the envelope as defined in Figure 3-4, the regional hydraulic rock domains outside this envelope, cf. Figure 3-3, are motivated and based on the hydraulic properties of geological rock domains as outlined in /Rhén et al. 2006c/, but is also briefly discussed below.

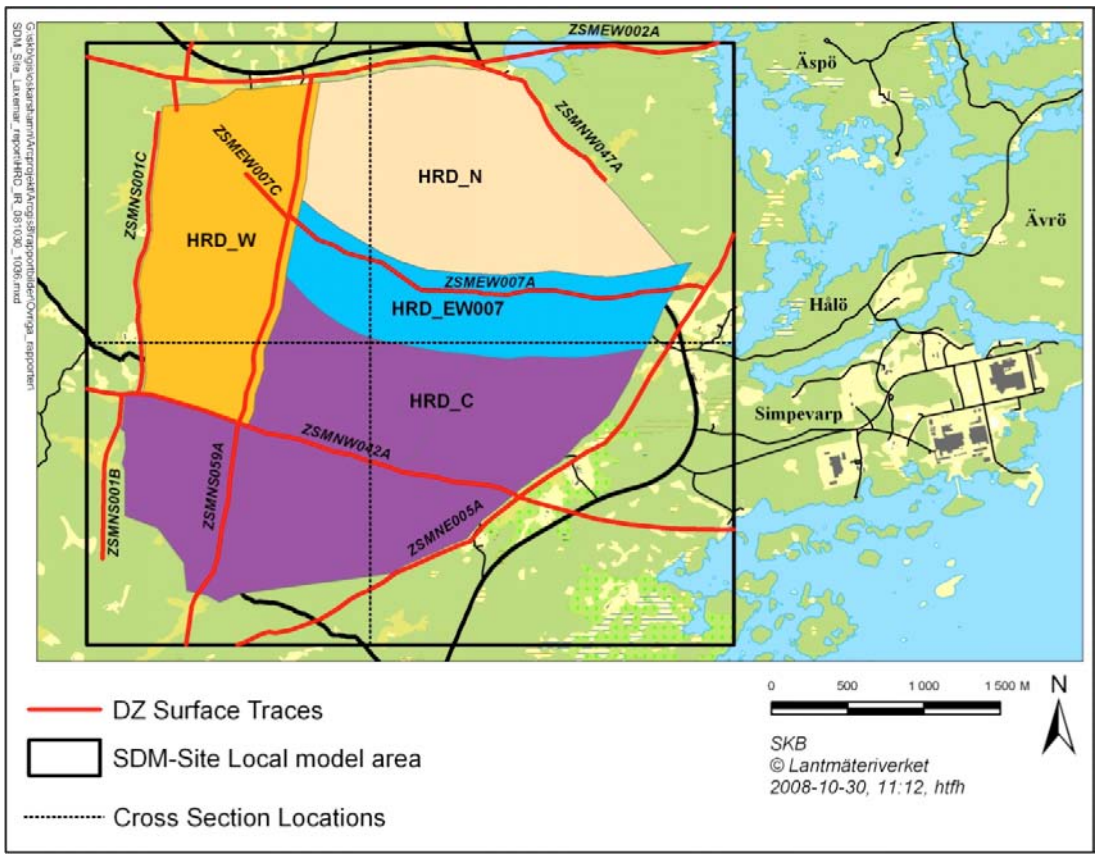

Figure 5-4. *Illustration of the SDM-Site Laxemar Hydraulic Rock Domain Model.*

Figure 5-5. *Illustration of the SDM-Site Laxemar Hydraulic Rock Domain Model, vertical section from south (left) to north at Easting's X=154,800 m, cf Figure 5-4.*

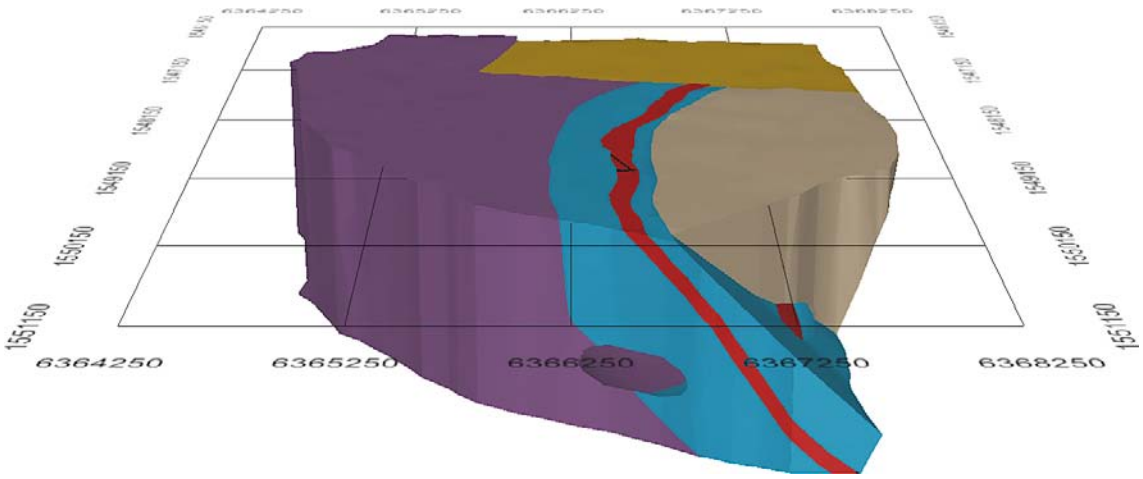

Figure 5-6. *Illustration of the SDM-Site Laxemar Hydraulic Rock Domain Model, 3D perspective view looking westward.*

Basis for assignment of HRD properties

The geological description of the bedrock between deformation zones is reported in /Wahlgren et al. 2008/ and /La Pointe et al. 2008/. The evaluation of the HRD properties in terms of general characteristics and developed hydrogeological DFN models is reported in /Rhén et al. 2008/. Below some principal geological and hydrogeological characteristics of the HRDs are outlined:

- The flowing features can be grouped in four orientation sets; steep ENE, WNW, N-S and a subhorizontal set, cf. Figure 5-7 and Figure 5-8.
- The intensity of flowing features is generally highest for the WNW set (aligned with the principal horizontal stress) with the subhorizontal set also being important in the upper bedrock.
- There is a clear decreasing intensity of flowing features with depth but generally with a similar transmissivity distribution of the flowing features for the specific depth interval studied as measured by PFL-f, cf. Figure 5-9 and Figure 5-10, with Terzaghi correction of the intensity (the bias of the orientation of the fractures relative to the boreholes is compensated for /Terzaghi 1965/).
- As a consequence – a resulting clear trend of decreasing hydraulic conductivity with depth, cf. Figure 5-11 (test scale 100 m) is obtained.
- The hydraulic conductivity is generally c. 10 times lower in HRDs than that of the HCDs (test scale 100 m), cf. Figure 5-12.

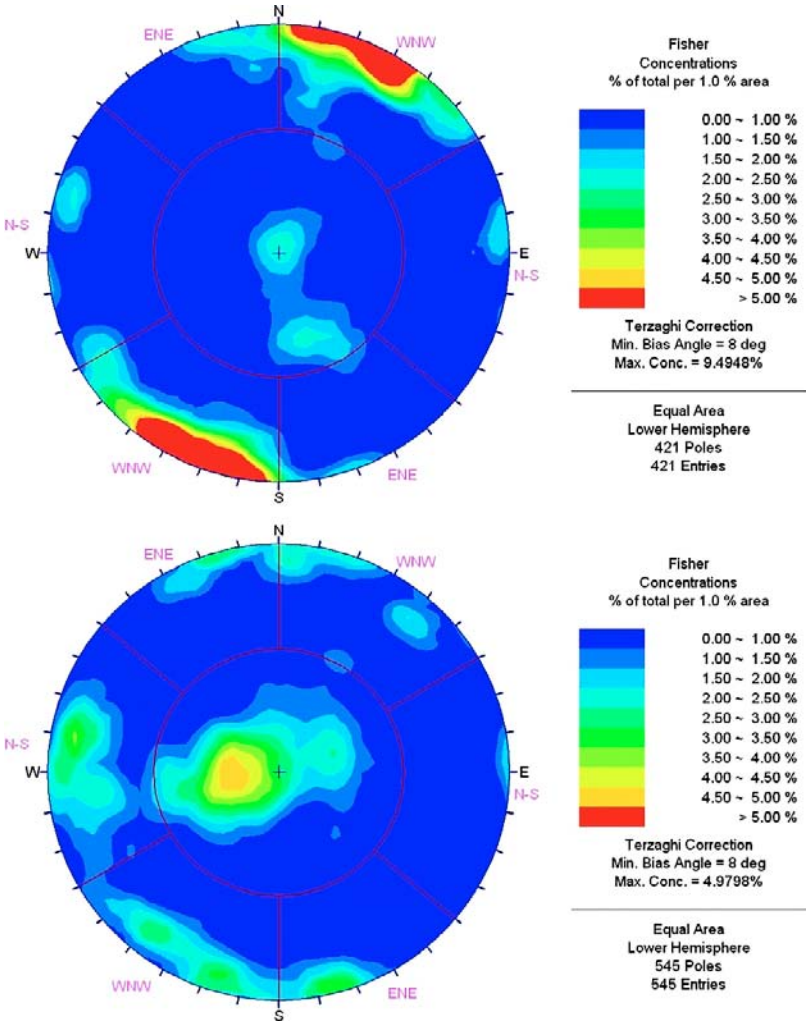

Figure 5-7. *Stereonets for FSM_EW007 (top) and FSM_W (bottom): Terzaghi-corrected intensity for PFL-f features /Rhén et al. 2008/, which corresponds to HRD_EW007 and HRD_W.*

The orientations of the sets of flowing features roughly correspond to the main orientation groupings of the deterministic deformation zones, see /Wahlgren et al. 2008, cf. Chapter 5 therein/. /Stigsson 2008/ investigated the orientation uncertainty of flowing features identified by the Posiva Flow Log in 43 cored boreholes in the Laxemar subarea, and concluded that the uncertainty in orientations of fractures is not a major problem for the confidence in the data used in the SDM-Site Laxemar hydrogeological DFN modelling. For more details, see /Stigsson 2008/.

Figure 5-11 shows the hydraulic conductivity of all HRDs pooled into one single population, based on transient tests performed in Laxemar with test scale 100 m and Figure 5-12 illustrates the depth trend and difference in hydraulic conductivity between HCDs and HRDs. The fracture orientations are not uniformly distributed, but clustered around particular orientations. It was argued in /Rhén et al. 2008/ that the fractures of every HRD could be divided in four fracture sets:

- a set striking roughly N-S;
- a set striking roughly ENE;
- a set striking roughly WNW;
- a subhorizontal (SH) set.

The exact boundaries between the different fracture sets are not precise and vary slightly between different HRDs.

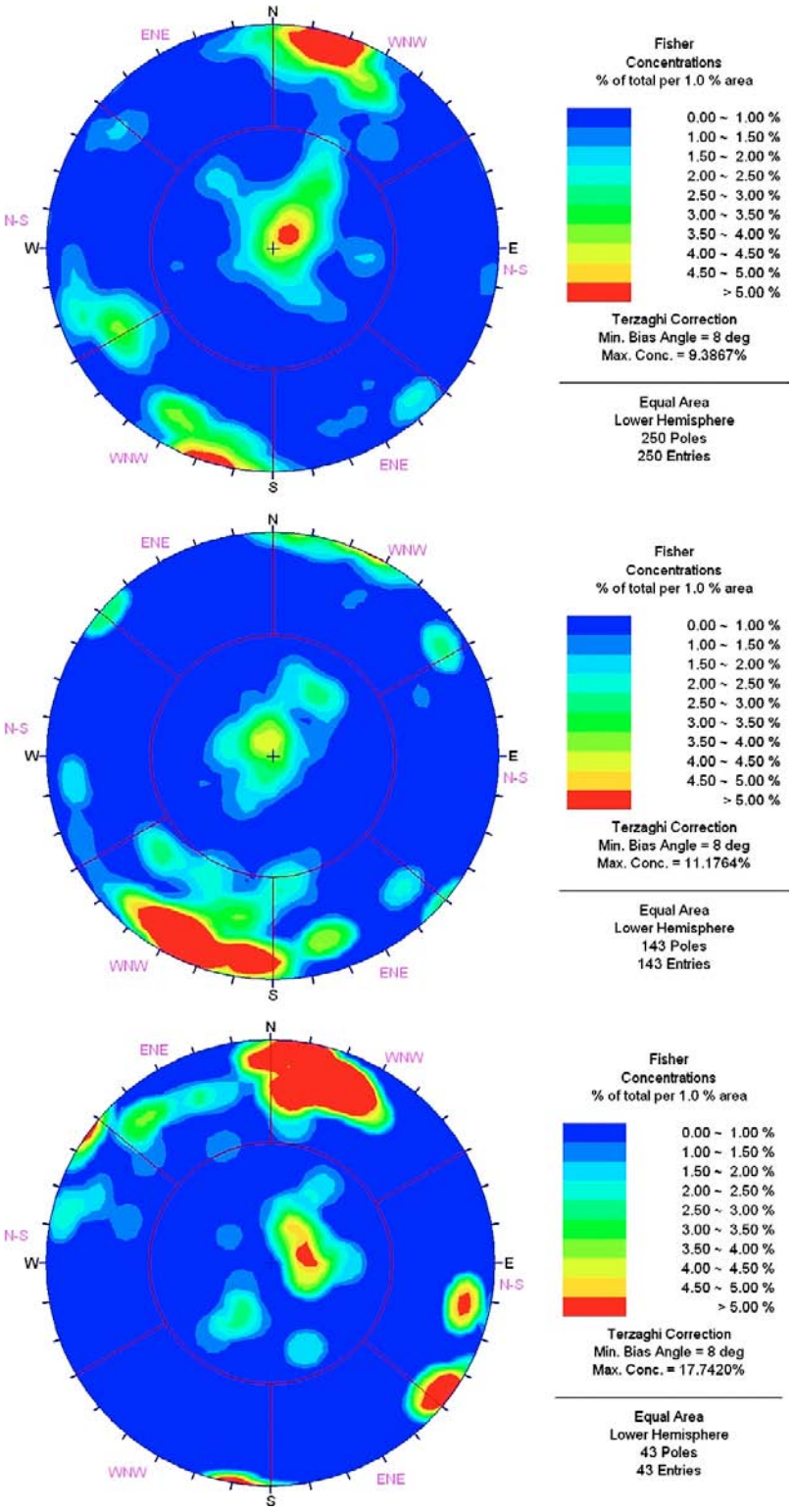

Figure 5-8. *Stereonets for FSM_NE005 (top), FSM_C (bottom) and FSM_S (bottom), and: Terzaghi-corrected intensity for PFL-f features /Rhén et al. 2008/, FSM_C and FSM_S in combination correspond to HRD_C.*

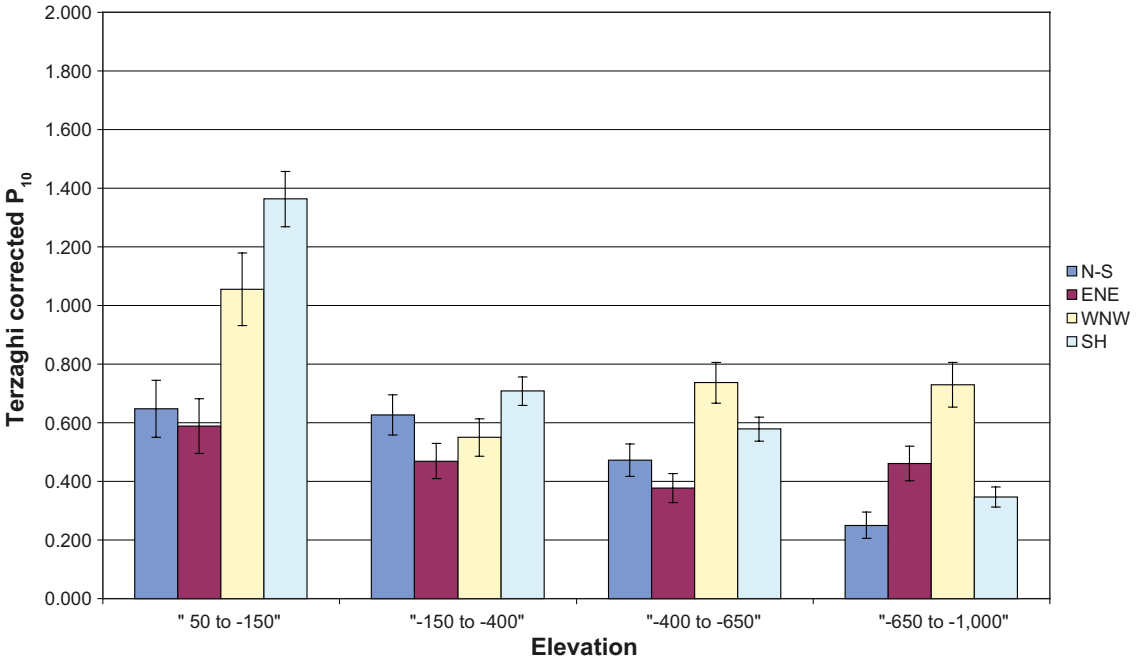

Figure 5-9. *Variation with depth of the Terzaghi-corrected fracture intensity for open and partly-open fractures for the fully characterised sections of boreholes penetrating Hydraulic Rock Domain HRD_C. /Rhén et al. 2008/.*

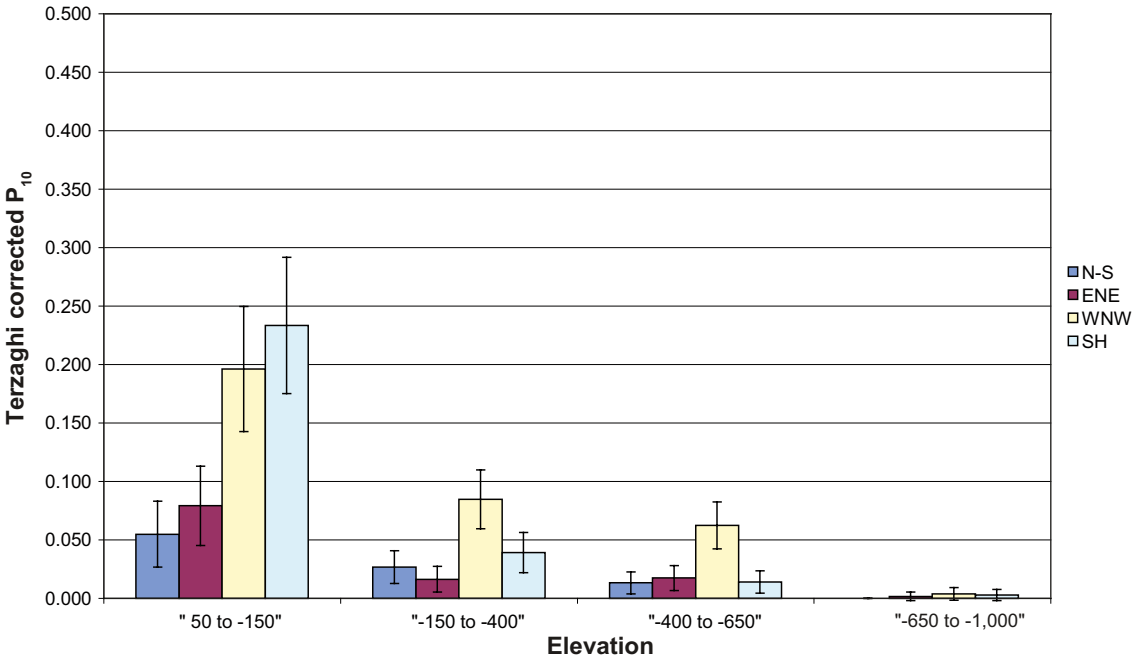

Figure 5-10. *Variation with depth of the Terzaghi-corrected fracture intensity for PFL-f features for the fully characterised sections of boreholes penetrating Hydraulic Rock Domain HRD_C./Rhén et al. 2008/.*

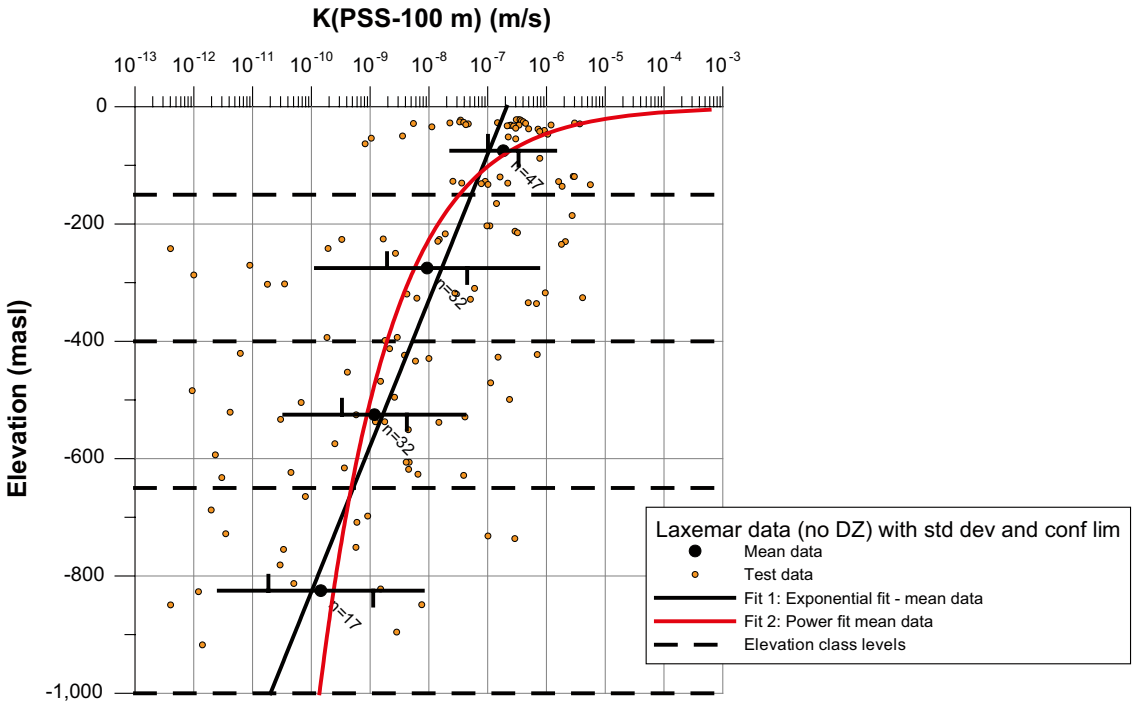

Figure 5-11. *Hydraulic conductivity (K) versus elevation (test scale 100 m). Data from test sections between deterministic deformation zones. Data from local model area. For the defined depth zones; geometric mean K, 95% confidence limits for mean log10(K)(vertical bars on horizontal line through mean data point) and ±1 standard deviation log10(K)(entire horizontal line through mean data point) are plotted. Curves are fitted to the calculated four geometric mean values (black).*

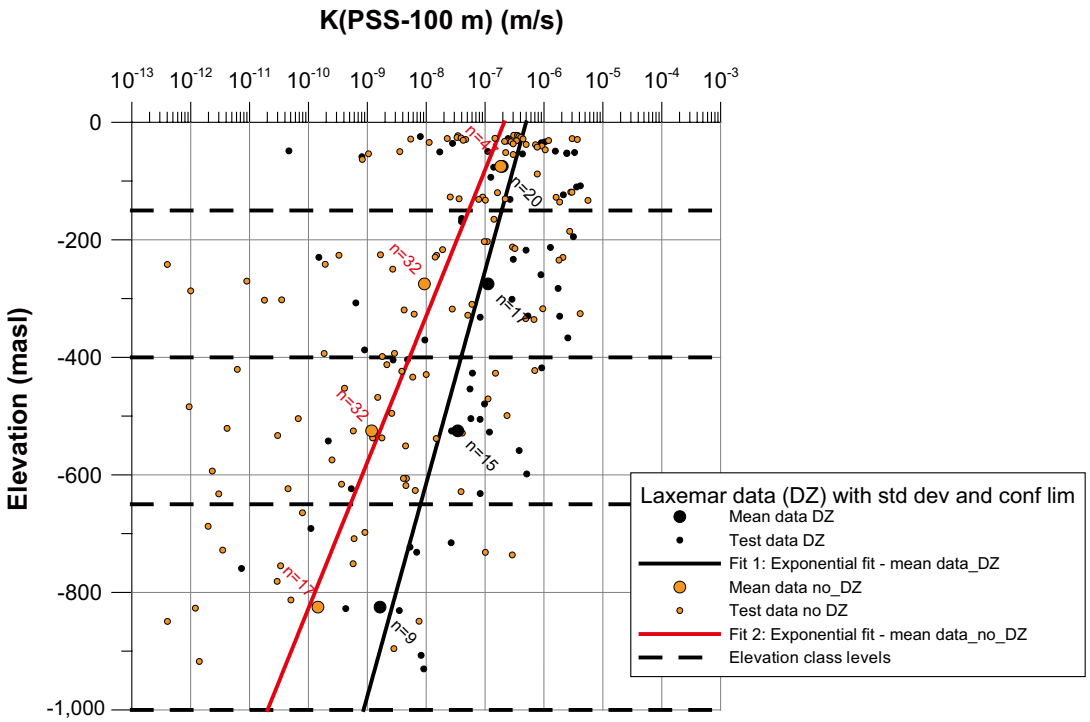

Figure 5-12. *Hydraulic conductivity (K) versus elevation (test scale 100 m). K shown for test sections between HCDs (DZ in figure) and test sections intersected by a HCD. Data from local model area. For depth zones lines are fitted to the four geometric mean values.*

A careful inspection of the results of the analyses of intensities of fracture types (open, partly open, PFL features) was made, individual fracture sets and all fracture sets combined, as subdivided in 50 m depth intervals, cf. /Rhén et al. 2008/. As a result it was decided that a reasonable choice of defined depth zones applicable to all HRDs should be: ground surface down to –150 m, –150 to –400 m, –400 to –650 m and below –650 m.

The depth intervals, here denoted dZ1–dZ4 (cf. Figure 5-1), can be described as follows:

- dZ1 (0 to –150 m): Near-surface rock, characterised by a high intensity of conductive fractures. Subhorizontal and steeply dipping fractures striking WNW dominate.
- dZ2 (–150 to –400 m): Intermediate-depth rock, characterised by an intermediate intensity of conductive fractures. Steeply dipping fractures striking WNW dominate except for in HRD_W where no set is clearly dominant, while in HRD_N and HRD_C the subhorizontal set is also important besides the WNW set.
- dZ3 (–400 to –650 m): Rock at repository level, characterised by a low intensity of conductive fractures. Steeply dipping fractures striking WNW dominate except for HRD_W where no set is clearly dominant.
- dZ4 (< –650 m): Deep rock, characterised by a sparse network of conductive fractures. Steeply dipping fractures striking WNW dominate except for HRD_W where no set is clearly dominant (however rather few data within dZ4).

There is no unique best choice for the defined depth zones. The above choice, however, enables a good representation of the main features of the distribution of fracture intensity. The top zone allows the higher fracture intensity and specifically the higher intensity for the SH fracture set in the near-surface rocks to be represented. The deepest zone allows the much lower intensity of PFL-f features below about –650 m to be represented. The division of the intervening bedrock into two depth zones allows the noted weak trend with elevation over this range to be represented. Furthermore, depth zone dZ3 effectively straddles the typical repository elevation at –500 m.

The change in intensity with depth and fracture set is illustrated by an example for HRD_C, a domain corresponding to the main part of a potential deposition volume, in Figure 5-9 and Figure 5-10.

For a more detailed account of the key findings of the analysis of basic statistical measures of flowing fracture intensity and transmissivity as detected by the PFL method, and their relation to definition of HRDs and depth zones, the reader is referred to /Rhén et al. 2008, cf. Sections 9.3 through 9.5 therein/.

Near surface rock

As pointed out above, there is a clear decrease in the intensity of flowing features and a smaller decrease of open fractures with depth. Some near-surface data were explored more comprehensively in /Söderbäck and Lindborg 2009, Olsson et al. 2006/. These data also show a depth trend but also indicate that there is a significant decrease of open fractures from the top surface down to c. 100 m depth. This suggests the possibility that the uppermost 10–20 m of the bedrock, where hardly any hydraulic tests have been performed, may be more conductive than suggested by the hydraulic tests above –150 m that constitute the basis for the calibration of the Hydrogeological DFN models. For an account of results see /Rhén et al. 2009, cf. Section 4.2.3 therein/ and for key detailed results cf. /Söderbäck and Lindborg 2009/.

Hydraulic properties of HRD domains

According to /Rhén et al. 2008/, four separate hydraulic rock domains (HRD) should be modelled in the local model area:

- **HRD_C**: Corresponding to FSM_C, FSM_NE005 and FSM_S in combination.
- **HRD_EW007**: Corresponding to FSM_EW007.
- **HRD_N**: Corresponding to FSM_N
- **HRD_W**: Corresponding to FSM_W with reasoned exclusion of data from KLX13A, cf. /Rhén et al. 2008/.

The relatively small lens-shaped rock domain RSMBA03 (RSMBA03 is surrounded by FSM_C and FSM_EW007, cf. Figure 3-3) has not been modelled as a defined fracture domain by Geology due to the small size and few data /La Pointe et al. 2008/. However, RSMBA03 is hydraulically modelled as part of HRD_C as the few data for RSMBA03 indicate that it is fairly low-conductive, it is reasonable to incorporate it in HRD_C.

The rock mass in the regional model, outside the defined FSMs, is based on the material property assignments made in model version Laxemar 1.2 /SKB 2006a, Rhén et al. 2006c/ (summarised in /Rhen et al. 2009/) and assessments of similarities between regional HRDs and the newly developed HRDs inside the Laxemar local model volume.

The subdivision in hydraulic rock domains and the superimposed additional division in depth zones within the local model volume have also been employed for presentation of statistics of basic hydraulic test data, cf. Table 5-1 and Table 5-2. In the depth zone –400 to –650 m, the true average spacing between conductive fractures in HRD_C is c. 9 m, which is nearly half of the corresponding average spacing in HRD_W. The lower conductive fracture intensity in the rock mass of HRD_W is more than compensated by an average hydraulic conductivity (ΣT/L) of $2.8 \cdot 10^{-8}$ m/s in the same depth interval, which is close to a factor 8 higher hydraulic conductivity (ΣT/L) than in the corresponding depth interval in HRD_C.

Table 5-1. Summary of intensity statistics of flowing features detected by PFL for the borehole intervals outside of interpreted deterministic deformation zones. MDZ are included in these statistics, but the numbers of individual PFL-f features are summed up within an MDZ such that each zone is treated as one single feature. (Length corresponds to mapped borehole length minus length of deterministic deformation zone, where borehole length is approximated with a straight line for each domain in the calculations). Modified after /Rhén et al. 2008/.

Domain	Depth zone (m)	Length	Count	PFL $P_{10,corr}$ (m^{-1})	PFLP_{10} (m^{-1})
FSM_EW007/	50 to –150	279	107	0.816	0.384
HRD_EW007	–150 to –400	1,001	241	0.550	0.241
	–400 to –650	843	72	0.225	0.085
	–650 to –1,000	213	0	0.000	0.000
FSM_NE005	50 to –150	371	167	0.820	0.451
	–150 to –400	806	62	0.169	0.077
	–400 to –650	615	17	0.071	0.028
	–650 to –1,000	434	4	0.013	0.009
FSM_N/	50 to –150	933	331	0.773	0.355
HRD_N	–150 to –400	608	115	0.339	0.189
	–400 to –650	441	20	0.115	0.0385
	–650 to –1,000	177	9	0.082	0.051
FSM_C	50 to –150	204	48	0.350	0.235
	–150 to –400	579	40	0.103	0.069
	–400 to –650	1,040	51	0.129	0.0389
	–650 to –1,000	950	4	0.006	0.004
FSM_W/	50 to –150	1,282	379	0.499	0.296
HRD_W	–150 to –400	904	33	0.078	0.037
	–400 to –650	677	23	0.060	0.034
	–650 to –1,000	272	1	0.005	0.004
FSM_S	50 to –150	166	21	0.254	0.126
	–150 to –400	65	20	0.655	0.308
	–400 to –650	N/A	N/A	N/A	N/A
	–650 to –1,000	N/A	N/A	N/A	N/A
HRD_C	50 to –150	741	236	0.564	0.319
	–150 to –400	1,451	122	0.164	0.084
	–400 to –650	1,655	68	0.107	0.0381
	–650 to –1,000	1,384	8	0.008	0.006

Table 5-2. Selected statistics of flowing features detected by PFL for the borehole intervals outside of interpreted deterministic deformation zones. Lengths and statistics are based on several boreholes within each domain. (Note that each MDZ is considered to be a single feature, even if it corresponds to several PFL within a borehole. Length corresponds to mapped borehole length minus length of deterministic deformation zone, where borehole length is approximated with a straight line for each domain in the calculations). Modified after /Rhén et al. 2008/.

Domain	Depth zone (m)	Length	PFL $P_{10,corr}$ (m^{-1})	Sum *T* / L	Min T (m^2/s)	Max *T* (m^2/s)
FSM_EW007/	50 to –150	279	0.816	3.1E–07	4.4E–10	3.2E–05
HRD_EW007	–150 to –400	1,001	0.550	1.2E–07	3.1E–10	3.7E–05
	–400 to –650	843	0.225	1.2E–08	7.9E–10	1.8E–06
	–650 to –1,000	213	0.000	0.0E+00	0.0E+00	0.0E+00
FSM_NE005	50 to –150	371	0.820	2.4E–07	3.9E–10	1.4E–05
	–150 to –400	806	0.169	4.0E–09	3.7E–10	1.2E–06
	–400 to –650	615	0.071	2.2E–09	3.3E–10	8.1E–07
	–650 to –1,000	434	0.013	1.6E–10	1.5E–09	6.1E–08
FSM_N/	50 to –150	933	0.773	6.7E–07	7.7E–10	6.5E–05
HRD_N	–150 to –400	608	0.339	2.1E–07	8.3E–10	3.6E–05
	–400 to –650	441	0.115	1.5E–08	1.1E–09	5.2E–06
	–650 to –1,000	177	0.082	4.1E–10	1.3E–09	2.6E–08
FSM_C	50 to –150	204	0.350	1.0E–07	2.4E–09	9.4E–06
	–150 to –400	579	0.103	3.4E–08	4.1E–10	1.2E–05
	–400 to –650	1,040	0.129	4.2E–09	3.9E–10	1.1E–06
	–650 to –1,000	950	0.006	7.3E–10	1.4E–08	4.4E–07
FSM_W/	50 to –150	1,282	0.499	2.8E–07	3.7E–10	4.6E–05
HRD_W	–150 to –400	904	0.078	2.9E–08	1.1E–09	1.0E–05
	–400 to –650	677	0.060	2.8E–08	6.7E–10	9.2E–06
	–650 to –1,000	272	0.005	1.4E–11	3.7E–09	3.7E–09
FSM_S	50 to –150	166	0.254	2.9E–07	1.3E–10	3.8E–05
	–150 to –400	65	0.655	1.9E–07	3.3E–11	6.7E–06
	–400 to –650	N/A	N/A	N/A	N/A	N/A
	–650 to –1,000	N/A	N/A	N/A	N/A	N/A
HRD_C	50 to –150	741	0.564	2.1E–07	3.9E–10	3.8E–05
	–150 to –400	1,451	0.164	2.4E–08	3.7E–10	1.2E–05
	–400 to –650	1,655	0.107	3.4E–09	3.3E–10	1.1E–06
	–650 to –1,000	1,384	0.008	5.5E–10	1.5E–09	4.4E–07

Minor deformation zones

Among the MDZs representing the rock between the HCDs, 58% have at least one PFL-f feature associated with the individual MDZ /Rhén et al. 2008/.That is, grossly about 60% of the MDZ-intercepts in boreholes can be expected to have a conductive feature with a transmissivity $T > 10^{-9}$ m^2/s (the measurement limit of the PFL-tool) /Rhén et al. 2008/. A large portion of the MDZs defined in ESHI are very thin, less than 1 m thick.

For HRD_C, the fraction of MDZs that have a PFL-f feature associated with them is about 39%, whereas the fraction of open fractures that have a PFL-f feature associated with them is about 7%. For HRD_W, the fraction of MDZs that have a PFL-f feature associated with them is about 69%, whereas the fraction of open fractures that have a PFL-f feature associated with them is about 17%. Hence, a MDZ is significantly more likely to have a PFL-f feature associated with it than an open fracture is. This strongly supports the view that, overall, MDZs have hydrogeological significance /Rhén et al. 2008/. It is found that in the HRDs the intensity of open fractures as well as the intensity of PFL-f is c. 4 times larger in MDZs compared to the equivalent intensities in the background rock.

The intensity of MDZ $P_{10-corr}$ (MDZ) decreases with depth with a more pronounced reduction for the subset of MDZs containing at least one PFL-f, as seen Table 5-3, cf. also Section 3.2.1.

Table 5-3. Terzaghi-corrected intensities (P10 corrected) of MDZs in various categories for HRD_C and HRD_W /Based on Tables 10-35 and 10-36 in Rhén et al. 2008/.

HRD	Depth zone (m.a.s.l.)	P10 corrected MDZ	P10 corrected MDZ with PFL-f
HRD_C	0 to –150	0.0396	0.0369
HRD_C	–150 to –400	0.0366	0.0114
HRD_C	–400 to –650	0.0279	0.0065
HRD_C	Below –650	0.0097	0.0007
HRD_W	0 to –150	0.0342	0.0271
HRD_W	–150 to –400	0.0221	0.0161
HRD_W	–400 to –650	0.0266	0.0143
HRD_W	Below –650	0.0195	0.0054

The range of sizes of the MDZs was estimated based on the intensities of MDZ as shown in Table 5-3 and the derived hydrogeological DFN models. It was found that the minimum radius of a MDZ for different fracture sets and depth zones are from a few metres up to several hundred metres. /Rhén et al. 2008/.

Internal variability in Minor deformation zones

The range of P_{10} and $P_{10\text{–corr}}$ of PFL-f features within a MDZ, with **at least one PFL-f feature** is c. 0.1–10 m^{-1} and 0.2–25 m^{-1} respectively, with mean around 1–1.5 m^{-1} and 1–2.5 m^{-1} respectively and a standard deviation of c. 1–1.5 m^{-1} and 2–3 m^{-1} respectively. One can observe that P_{10} and $P_{10\text{–corr}}$ is higher for MDZs compared to HCDs in Section 5.1.2. This is probably due to that most MDZ are rather narrow features with some relevant characteristics for MDZs, while a HCD (and the underlying deformation zone) generally are more complex, with several MDZs and less fractured parts of rock between the MDZs within the defined thickness of the HCD /Rhén et al. 2008/.

Hydraulic anisotropy

/Rhén et al. 2008/ presents results of block modelling made using the derived hydrogeological DFN models to study scaling issues and the anisotropy in the hydraulic properties of rock blocks of grid cells size of 5, 20 and 100 m, respectively. It was found that:

- Median values of the ratio K_{hmax}/K_{hmin} were in the range 5 to 9 for HRD_C and HRD_EW007 and c. 2–4 for HRD_W. The ratio K_{hmax}/K_z was 1–1.6 for HRD_C and HRD_EW007 and c. 1–2 for HRD_W, for all grid sizes tested. (K_h: Horizontal hydraulic conductivity, K_z: Vertical hydraulic conductivity).
- The estimated strike interval of K_{max} for HRD_C, HRD_W and HRD_EW007 were; c. 90–150, 100–180, 80–150 degrees, respectively, for all grid sizes tested.
- There seems to be a tendency that the anisotropy becomes more pronounced the larger the block is. The explanation is that the larger, but few, conductive fractures/features from a certain fracture set on average become more dominant for lager blocks, but are too few in the smaller blocks. Thus, the mean anisotropy may change with scale considered.

The magnitude of the anisotropy calculated above is lower than comparable inference made based on probe boreholes sampling subvertical fractures in the nearby Äspö HRL access tunnel. It was found that the highest conductivity in the horizontal direction is WNW-NW, but also N-S direction showed high conductivity /Rhén et al. 1997/. The ratio between the maximum and the minimum hydraulic conductivity in the horizontal plane was c. 100, which is considerably higher than the corresponding ratios estimated for the blocks of the Laxemar local model volume discussed above.

Evaluation of hydraulic data from the Prototype Repository at Äspö HRL shows similar results to those obtained in the Äspö access tunnel, but also indicates that the most conductive fracture set is subvertical, with an approximate WNW strike /Rhén and Forsmark 2001/. It was also shown that the hydraulic conductivity was c. 100 times less in vertical boreholes compared to horizontal boreholes, indicating that subvertical fractures are the dominant conductive fractures at Äspö.

Anisotropy in Laxemar may be even higher than indicated by the block modelling as the upscaling from the hydrogeological DFN models to ECPM has some tendency to average out heterogeneities, but possibly also due to the fact that it is difficult to fully capture the true nature of anisotropy from a limited set of single borehole tests using the above procedure. The possibility to evaluate hydraulic anisotropy from the site-investigation field data is possibly also restricted due to the fact that most boreholes are more or less vertical.

As a part of the multidisciplinary site descriptive model of Laxemar, the rock mechanics model for model version SDM-Site Laxemar is presented by /Hakami et al. 2008/. It can be concluded that the present orientation of the maximum principal stress in WNW-ESE corresponds well to the major set of conductive hydraulic features and that also the change in the minimum principal stress to be lower than the vertical stress below c. 200–400 m corresponds well to decrease by depth in the horizontal conductive feature intensity.

Numerical modelling performed by /Hakami et al. 2008/ analysed the potential influence of the interpreted major deformation zones in the area on the stress field. It was concluded that the rock above deformation zones ZSMEW007A and ZSM002A, cf. Figure 5-4, has a lower stress level compared to other rock blocks between major deformation zones. Other studied borehole sections seemed to show no major change in the stress field due to nearby or intersecting deformation zones in the Laxemar local model volume.

5.1.4 Hydraulic soil domains (HSD) within regional model area

Regional scale quantitative groundwater-flow modelling also requires a parameterisation of the hydraulic properties of the Quaternary deposits. Based on /Werner et al. 2008/, the assignment follows the geometrical representation of the Quaternary deposits according to the stratigraphic model of the Quaternary deposits /Nyman et al. 2008, overburden depth and stratigraphy model (RDM) therein./, cf. Section 3.5. The assignment of hydrogeological properties (hydraulic conductivity and storage parameters) to each layer defined in the stratified model of the Quaternary deposits (RDM) is found in /Rhén et al. 2009, cf. Appendix 5 therein/.

The interpreted thicknesses of the layers of the Quaternary deposits and the hydraulic conductivities of these layers are presented in Table 5-4, based on data from /Rhén et al. 2009, cf. Appendix 5 therein/ and illustrated in Figure 3-7. As can be seen in the table, the Quaternary deposit layers are relatively thin but the assigned hydraulic conductivities are generally much higher than the interpreted mean hydraulic conductivity of the superficial bedrock with the exception of Gyttja that has a hydraulic conductivity comparable to that of the superficial bedrock.

It should be noted that the hydrogeological properties assignment given in /Rhén et al. 2009, cf. Appendix 5 therein/ was the starting point for the quantitative groundwater-flow modelling. Parameter values in the numerical model were subjected to change as a result of the flow model calibration. E.g. the pre-modelling of effects of Äspö HRL drawdown indicated that the sea sediments should be less conductive compared to what was proposed on the basis of Laxemar model version 1.2 /Hartley et al. 2007/. The calibrated HSD model is commented in Section 6.4.

Table 5-4. Description of the layers used in the model of Quaternary deposits and the interpreted hydraulic conductivities proposed to be used as initial assignments, cf. a detailed accounting in /Rhén et al. 2009, cf. Appendix 5 therein/. The stratigraphic distribution of the Z-layers is shown in Figure 3-7.

Layer	Description	Thickness (m)	Hydraulic conductivity (m/s)
Z1	This layer represents the uppermost Quaternary deposits and is present within the entire modelled area, except in areas covered by peat. On bedrock outcrops, the layer is set to 0.1 metre and in other areas to 0.6 metre. If the Quaternary depth is less than 0.6 m, Z1 will be the only layer. In the terrestrial areas, **this layer is supposed to be affected by soil forming processes.** (Mostly till but in minor areas also postglacial shingle, boulder deposits, peat, sand-gravel, artificial fill, cf. /Appendix 5 in Rhén et al. 2009/.)	0.1–0.6	Till: $K_h=4\cdot10^{-4}$ m/s $K_h/K_v=1$ Other: $K_h=3\cdot10^{-6}$–$1\cdot10^{-2}$ m/s $K_h/K_v=1$
Z2	This layer is present where ***peat*** is shown on the map of Quaternary deposits. The peat areas have been subdivided into deep and shallow peat lands (see Table 3-2).	0.85	$K_h=3\cdot10^{-6}$ m/s $K_h/K_v=1$
Z3	The layer represents ***postglacial clay gyttja, gyttja*** or ***recent fluvial sediments***.	1.6–1.7	Gyttja clay/clay gyttja: $K_h=1\cdot10^{-7}$ m/s $K_h/K_v=1$ Gyttja: $K_h=1\cdot10^{-8}$ m/s $K_h/K_v=1$
Z4	This layer represents ***postglacial coarse-grained sediments (mostly sand and gravel), artificial fill*** and ***glaciofluvial sediments***. Z4 is equivalent to artificial fill or glaciofluvial sediments in areas shown as these deposits on the map of Quaternary deposits. In all other areas, Z4 represents the postglacial sediments. Two different average depths were used for the glaciofluvial deposits. One value for the Tuna esker and another value for the other shallower deposits. The glaciofluvial sediment and artificial fill rest directly upon the bedrock. The postglacial sand and gravel are always underlain by glacial clay (Z5) and till (Z6). Post glacial sand/gravel is the most common deposit in this layer.	Postglacial sand/gravel: 0.7–0.8 Glaciofluvial sediments: 3.5–13.2 Artificial fill: 4.4	Postglacial gravel: $K_h=1\cdot10^{-2}$ m/s $K_h/K_v=1$ Postglacial sand: $K_h=1\cdot10^{-3}$ m/s $K_h/K_v=1$ Glaciofluvial sediments, **postglacial sand/gravel:** $K_h=5\cdot10^{-3}$ m/s $K_h/K_v=1$ Postglacial fine sand: $K_h=5\cdot10^{-4}$ m/s $K_h/K_v=1$ Artificial fill: $K_h=4\cdot10^{-5}$ m/s $K_h/K_v=1$
Z5	The layer represents ***glacial clay***. Z5 is always overlain by postglacial sand/gravel (Z4).	1.3–2.6	Glacial clay: $K_h=1\cdot10^{-8}$ m/s $K_h/K_v=1$
Z6	This layer represents ***glacial till***, which is the most common Quaternary deposits in the model area. Z6 is 0 if the total Quaternary depth is < 0.6 metre (e.g. at bedrock outcrops) or if Z4 (see above) rests directly on the bedrock surface. The lower limit of Z6 represents the bedrock surface, i.e. Z6 represents the DEM for the bedrock surface.	2.0–3.6	Glacial till: $K_h=4\cdot10^{-5}$ m/s $K_h/K_v=1$ Where Quaternary deposits depth > 10 m: $K_h=4\cdot10^{-4}$ m/s $K_h/K_v=1$

5.1.5 Hydraulic boundary conditions

Groundwater table and natural point-water heads

The natural (undisturbed) groundwater level follows the topography of the ground surface, as shown in Figure 5-13 and /Werner et al. 2008/. In the Quaternary deposits the depth to the water table is expected to be up to a few metres, with maximum depths at topographic heights and minimum depths in the valleys. The natural (undisturbed) groundwater level in the upper bedrock is also expected to follow the topography as shown in Figure 5-14, but artesian conditions can be expected occasionally in valleys (e.g. HLX15 and HLX28 indicate artesian conditions, cf. Figure 5-14). The implication of these observations is that topography should be a good indicator for defining the groundwater table and also for defining groundwater divides. However, in the numerical groundwater flow modelling a head dependent flux boundary condition is used, cf. Section 6.5.

Generally, boreholes at lower ground elevations show groundwater levels close to the ground surface while boreholes at higher elevations indicate lower groundwater levels at elevations c. 5 m below the bedrock surface, cf. Figure 5-14.

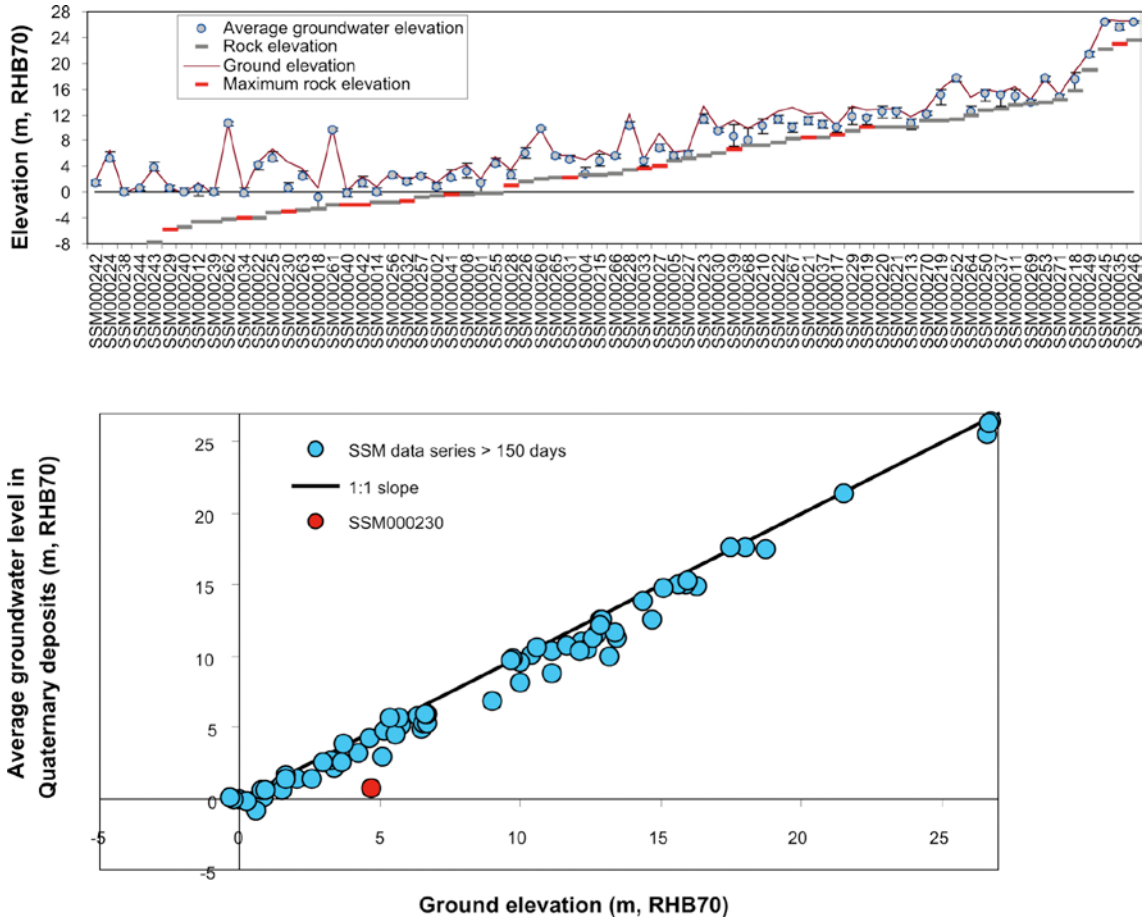

Figure 5-13. *Top: Plots of averages, minimum and maximum groundwater levels in monitoring wells, ground-surface elevations, and rock-surface elevations. Bottom: Mean groundwater levels (of daily mean) in Laxemar local model area. Monitoring wells in Quaternary deposits with data period longer than 150 days. /Werner et al. 2008/.*

Recharge, discharge and water balance components

Sandy-gravely till is overlying the bedrock in almost the whole area. The hilly areas are dominated by exposed rock outcrops or shallow depth Quaternary deposits (i.e. a depth less than c. 0.5 m), where groundwater recharge occurs. The infiltration capacity of the Quaternary deposits in Laxemar is generally considered to exceed the rainfall intensity and the snowmelt intensity /Werner et al. 2008/.Groundwater discharge is conceptualised to take place in the low-altitude "valley" type areas. The latter are characterised by thicker overburden, possibly as thick as 50 m, including, from bedrock surface; till, glacial clay, postglacial sand/gravel and postglacial clay. Besides valleys, groundwater discharge occurs near the coast.

Except for a few wetlands, the surface waters (lakes, streams and wetlands) are located to low-altitude areas /Werner et al. 2008/. The interaction between the lakes and the groundwater is expected to be in the near-shore area /Werner et al. 2008/.

Joint evaluations of groundwater levels in the Quaternary deposits and point-water heads in boreholes in the bedrock indicate that groundwater discharge from the superficial rock/Quaternary deposits part of the system to the surface (surface waters) is strongly influenced by the geometry and the hydrogeological properties of the Quaternary deposits overlying the till. Moreover, there is also an influence on this process by the hydrogeological properties of the superficial rock (including the deformation zones). Locally, there is a fractionation into groundwater that discharges to the surface and groundwater that flows horizontally along the valley in the upper rock/Quaternary deposits system; groundwater discharge to the surface is facilitated in areas where there are no layers of glacial clay and postglacial sediments above the till. The varying discharge conditions are illustrated in

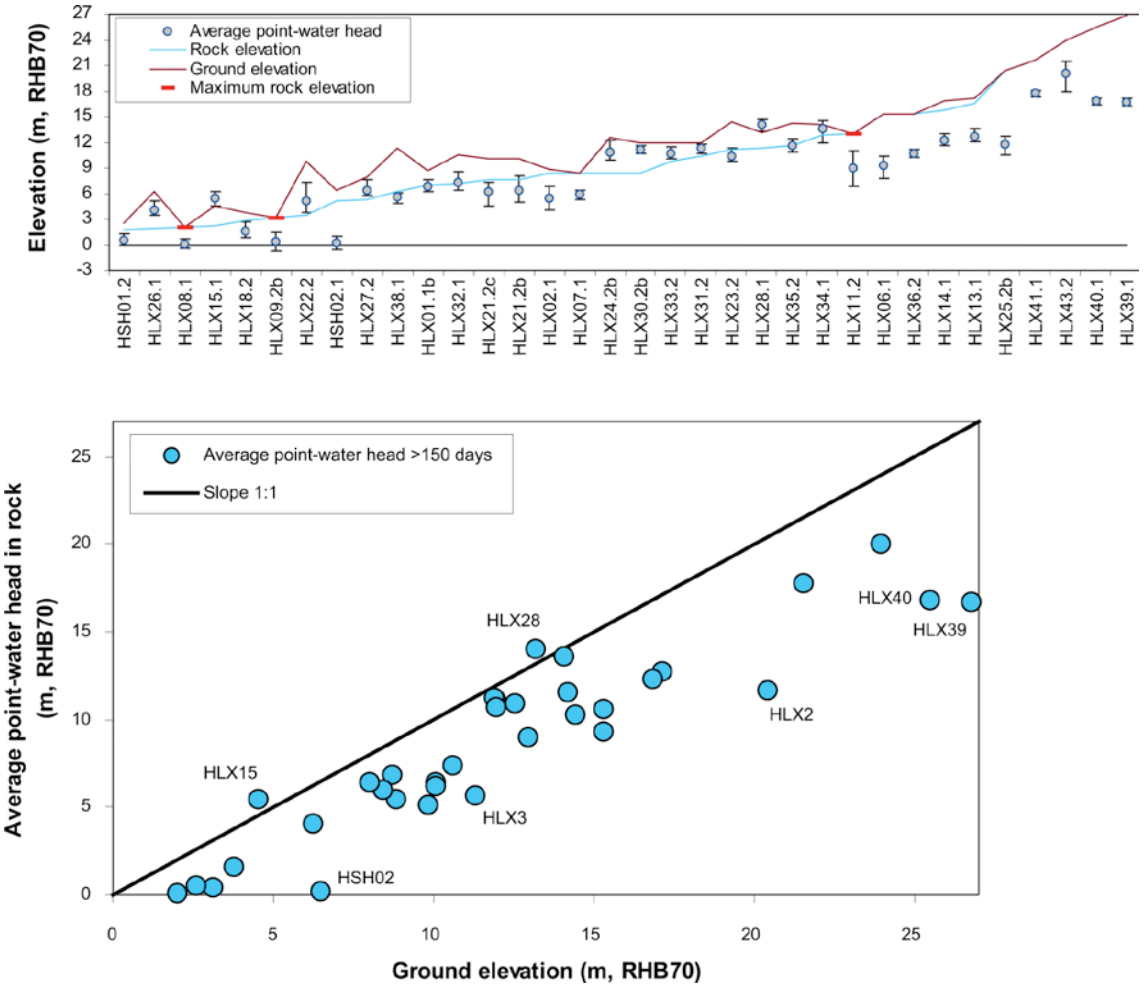

Figure 5-14. *Top: Plots of averages, minimum and maximum groundwater levels in percussion boreholes, ground-surface elevations, and rock-surface elevations. Bottom: Plot of average groundwater levels (of daily mean) in percussion boreholes versus ground elevation. Note that for boreholes with packers, data are used for the upper borehole section. Also note that only borehole sections with more than 150 days of data collection are shown, /Werner et al. 2008/.*

Figure 5-15 through Figure 5-17. For a detailed discussion of the presented conceptual sections, cf. /Söderbäck and Lindborg 2009/.

The site-average long-term annual precipitation in the Laxemar-Simpevarp area can be approximated at c. 600 mm/yr and the precipitation is somewhat higher inland compared to coastal areas /Werner et al. 2008/. The specific-discharge is estimated to be in the order of 160–170 mm/year (5.3–5.6 L/(s·km^2)), cf. /Werner et al. 2008/. The regional estimate is 150–180 mm/year (4.9–5.9 L/(s·km^2)), cf. /Larsson-McCann et al. 2002/. The evapotranspiration is thus estimated to be slightly higher than 400 mm/yr.

Baltic sea level and salinity

The present Baltic sea level varies with time but generally is not more than c. ±0.5 m from mean sea level /Wijnbladh et al. 2008, cf. Section 3.2.5 therein/ and /Werner et al. 2008, cf. Section 2.3.1 therein/ and the present salinity in the Baltic varies with time and depth in the range 6–8‰ near Oskarshamn, /Wijnbladh et al. 2008, cf. Section 3.1.2 therein/ and /Tröjbom et al. 2008, cf. Appendix E therein/. Data compilations of similar character from the period prior to the site investigations started can be found in /Larsson-McCann et al. 2002/.

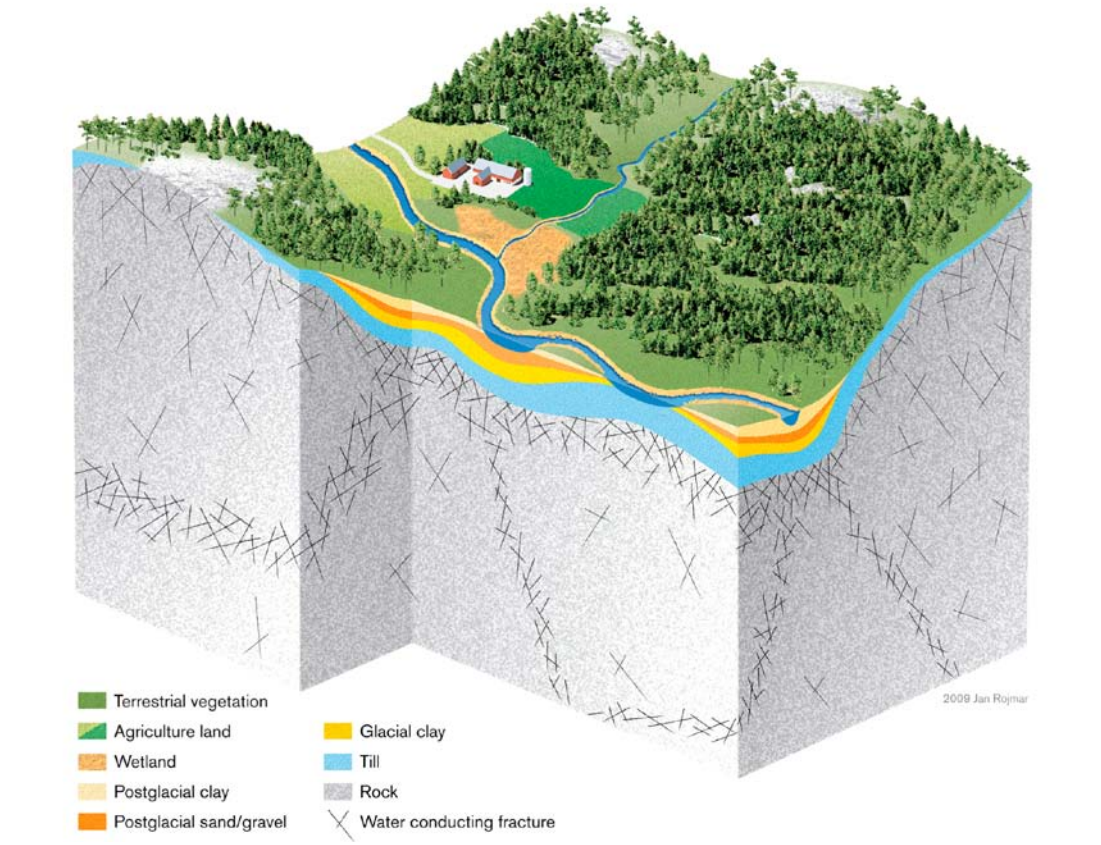

Figure 5-15. *Conceptual view of a typical large east-west valley in Laxemar, cf cross-sections in Figure 5-16 and Figure 5-17.*

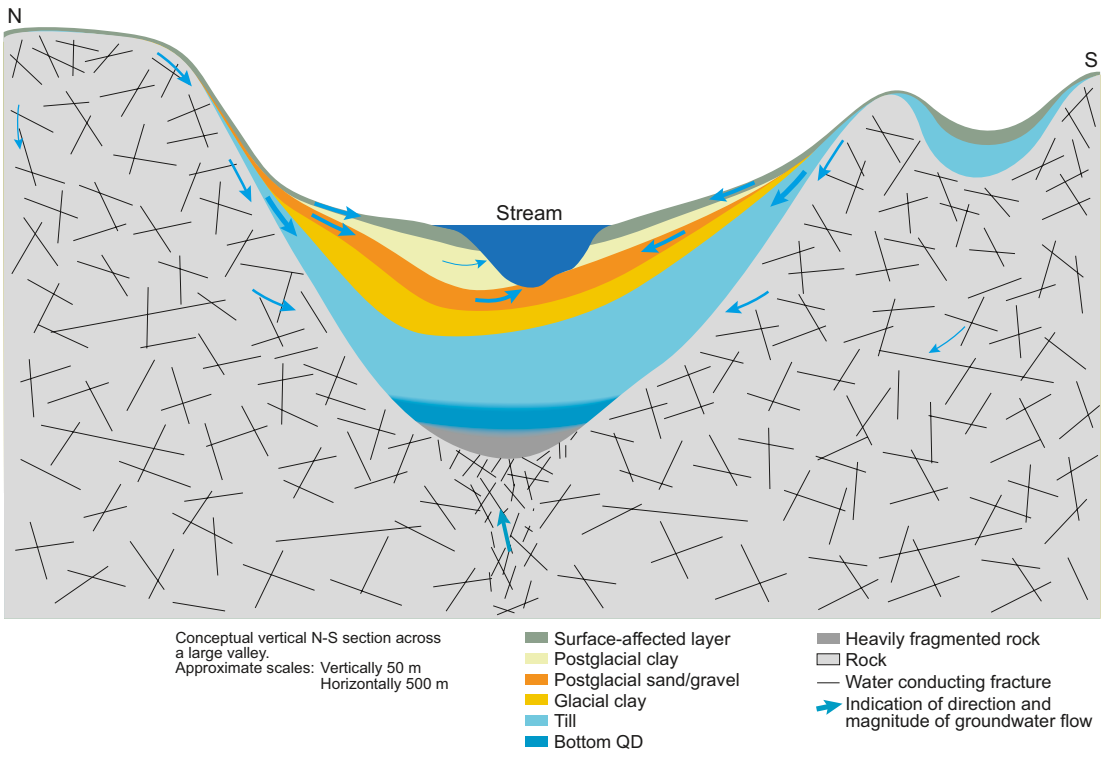

Figure 5-16. *Conceptual vertical N-S section across a typical large valley in Laxemar. Note the different horizontal (1 km) and vertical (50 m) scales in the figure.*

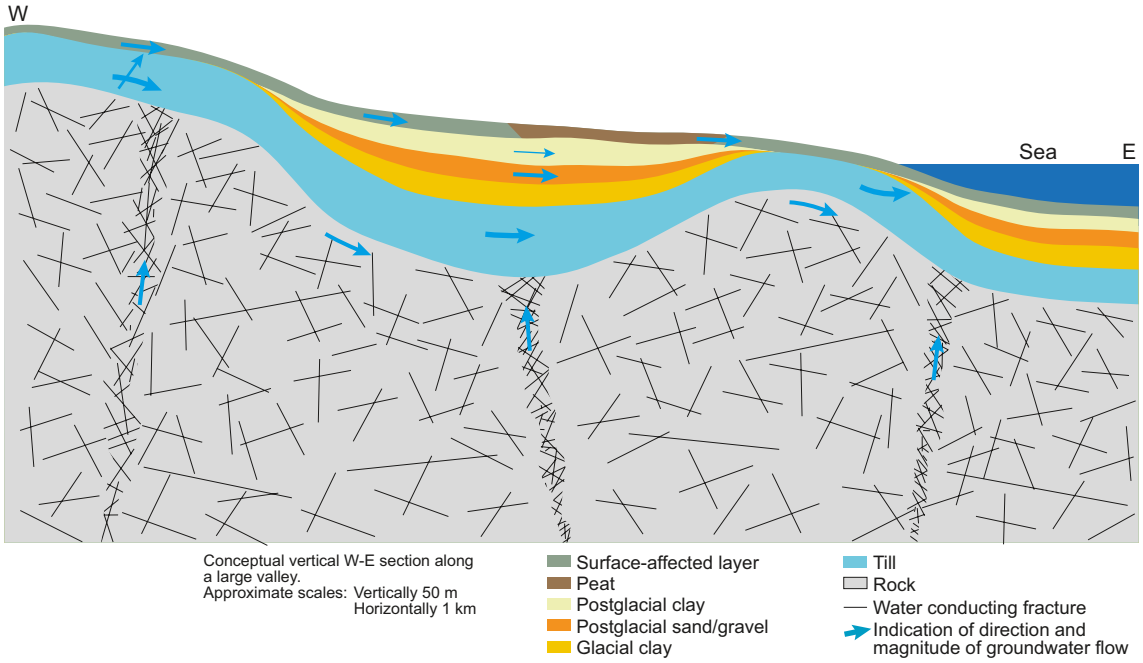

Figure 5-17. *Conceptual vertical W-E section along a typical large valley in Laxemar. Note the different horizontal (1 km) and vertical (50 m) scales in the figure. (The deep recharge is assumed to be mainly perpendicular to the plane shown and originating mainly from the nearby hills, cf Figure 5-15 and Figure 5-16.).*

5.2 Palaeohydrogeological conceptual model

The essential components of the palaeohydrogeological development presented in this section are the shoreline displacement and the different stages of the Baltic Sea. The geological evolution, palaeoclimate and historical development of the Laxemar-Simpevarp area are described in /Söderbäck 2008/. The groundwater evolution in Laxemar is expected to have been influenced by these old climate changes and the development of the Baltic Sea. The parts essential to hydrogeology and palaeohydrogeology are summarised in /Rhén et al. 2009/ and are briefly discussed in this section and in Section 2.3.8.

Solute transport and reference waters

Coupled groundwater flow and solute transport is conceptualised in terms of the evolution of a number of groundwater constituents in order to understand the hydrochemical evolution in terms of the mixing of groundwaters of different origin. In the fracture, water mixing takes place through the processes of advection, dispersion, diffusion (including rock matrix diffusion), while porewater composition is assumed to evolve only as a result of rock matrix diffusion. Groundwater composition is described in terms of mixtures of references waters, consistent with the concepts used for interpretation of hydrogeochemistry as described in Section 4.5, and based on the SDM-Site Laxemar hydrochemistry description /Laaksoharju et al. 2009/. Fracture water is assumed to be a mixture of the following four reference waters whose composition characteristics can be described in terms of chloride, magnesium bicarbonate and $\delta^{18}O$ as:

- Deep Saline Water;
- Glacial Melt Water;
- Littorina Sea Water;
- Altered Meteoric Water.

An additional fifth reference water is introduced in the palaeohydrogeological modelling to illustrate some conceptual ideas on how the composition of the porewater may evolve in areas of the rock matrix away from the connected flowing fracture system:

- Inter-glacial Porewater.

The latter reference water is considered likely to be very old water residing primarily in the matrix composed of meteoric and brackish waters from periods before the Weichselian glaciation. For details about the reference waters, cf. /Rhén et al. 2009/ and Section 4.5.3.

5.2.1 Boundary conditions for palaeohydrogeological modelling

The *SDM-Site Laxemar* shoreline curve, cf. Figure 2-11, was used to map out in detail how the shoreline changes with time within the Laxemar-Simpevarp area. Figure 5-18 shows an illustration of where the denser saline Littorina water intruded along larger valleys, mixing with older glacial and brackish groundwater. According to the modelling results, the Littorina Sea covered possibly a slightly larger area than shown in Figure 5-18 as shoreline curve *SDM-Site Laxemar, Alt 1* was used as *base case model*, cf. Section 7.4. Figure 5-18 also illustrates that the larger parts of Laxemar-Simpevarp area (central and western part at higher elevations) have been exposed to Meteoric water since the last glaciation. It can be stated that the Meteoric water has since the last glaciation been infiltrating successively larger areas and has mixed and flushed out older waters in the upper part of the bedrock. The western part of the regional model area has, however, never been exposed to Littorina sea water when it rose early above the sea, cf. Figure 5-19. However, some of the valleys in the west have an elevation indicating that Littorina could have been present, but possibly the Littorina seawater in such long bays would be diluted by freshwater streams from the west.

The changes in salinity of the aquatic systems in the Baltic basin during the Holocene are closely coupled to the shoreline displacement, cf. Figure 2-12 and /Rhén et al. 2009/.

The assignment of boundary conditions in the groundwater flow model is discussed in Sections 6.6 and 7.4.

5.2.2 Initial conditions for palaeohydrogeological modelling

The assessed initial conditions are based on the five reference waters, cf. 4.5.3, and are discussed in Sections 6.6 and 7.4.

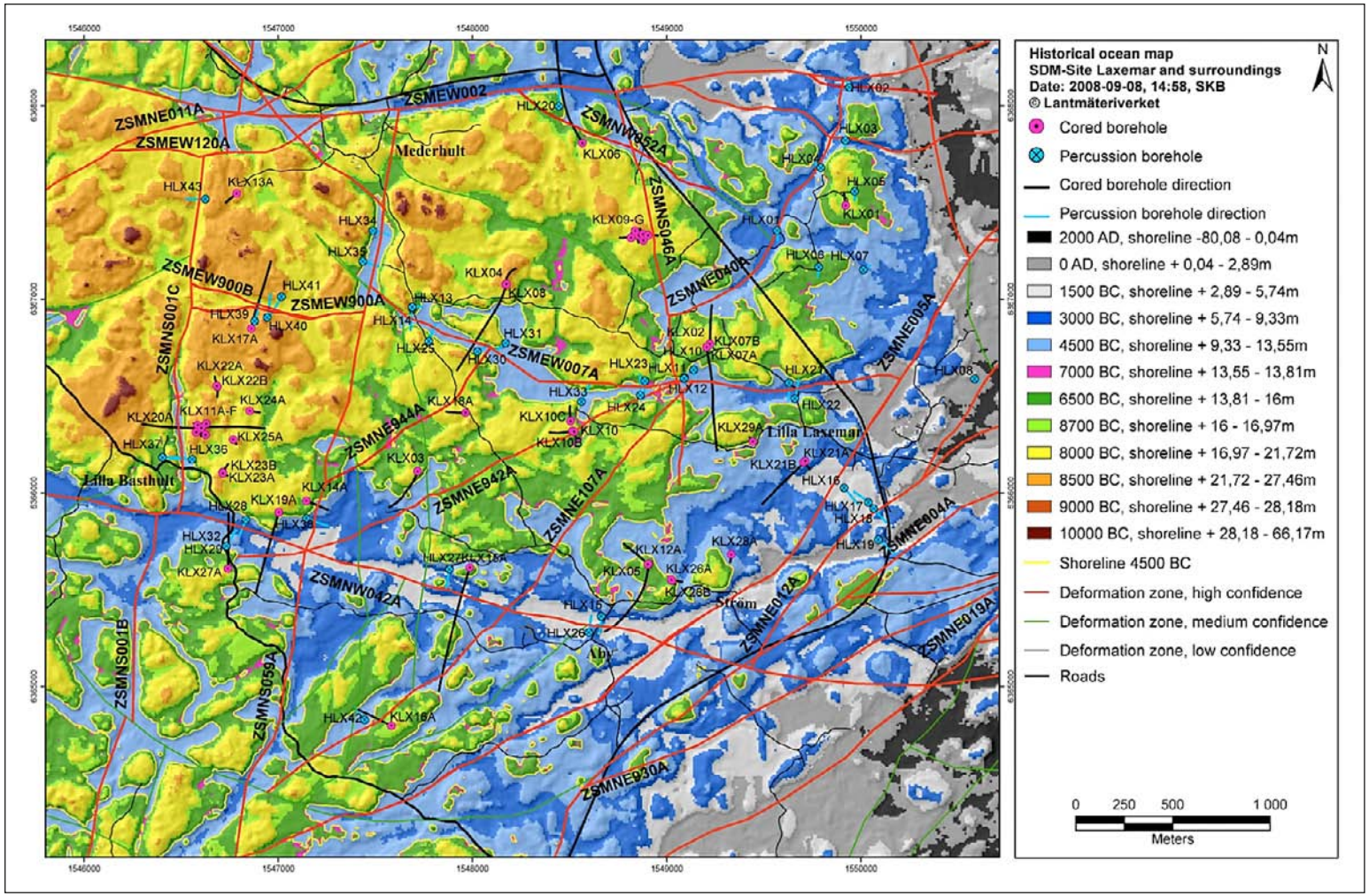

Figure 5-18. *Shoreline changes in the Laxemar-Simpevarp area during the Littorina period (based on the SDM-Site Laxemar curve, cf Figure 2-11, applicable to the Laxemar local model area. The maximum salinity in the Baltic during the Littorina period occurred between 4500 BC and 3000 BC (Blue and grey areas indicate the coverage of the Littorina sea 4500–1500 BC).*

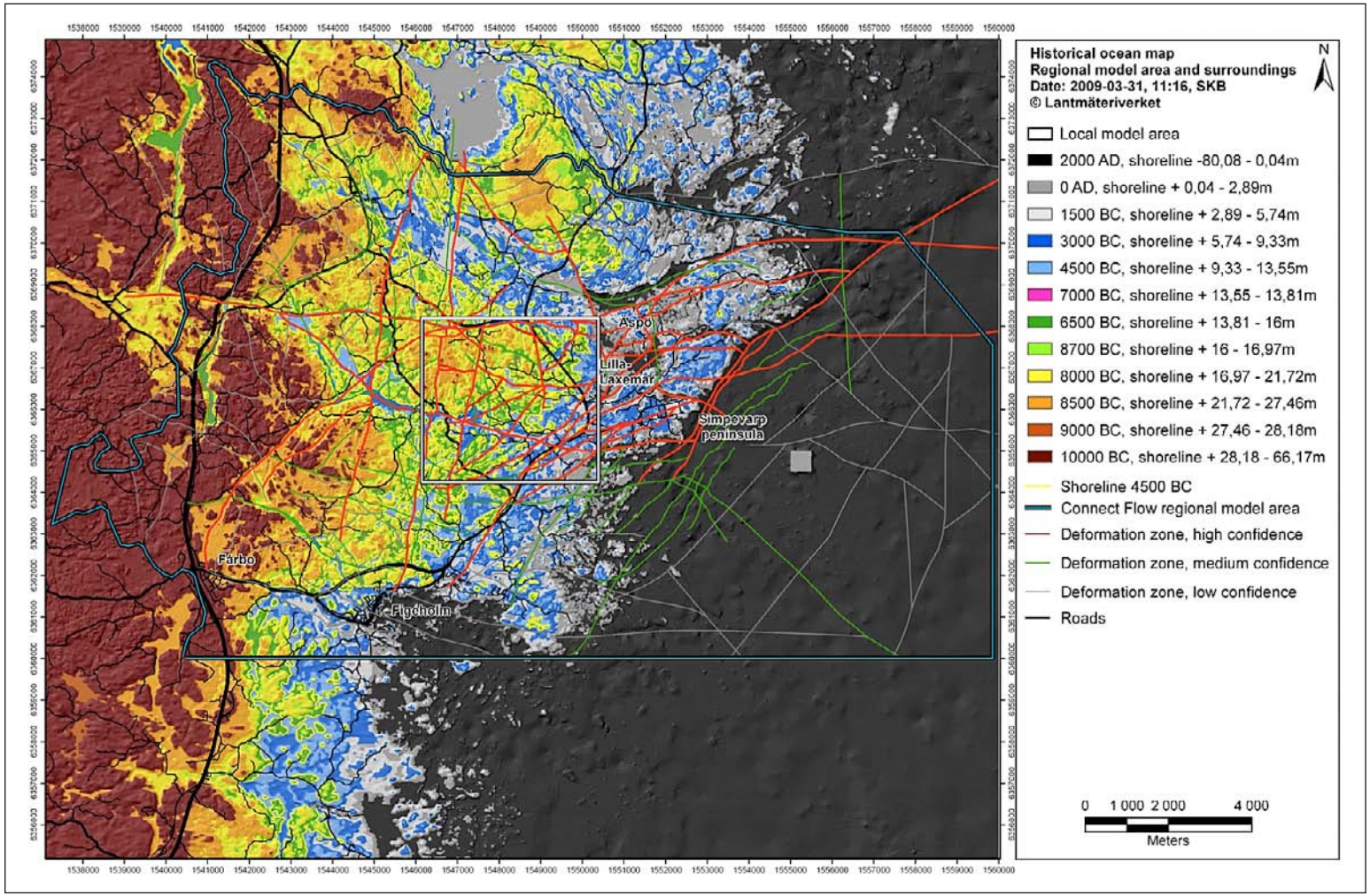

Figure 5-19. *Shoreline changes in the Laxemar-Simpevarp area during the Littorina period (based on the SDM-Site Laxemar curve, cf Figure 2-11), covering an area larger than the regional model area. The maximum salinity in the Baltic during the Littorina period occurred between 4500 BC and 3000 BC (Blue and grey areas indicate the coverage of the Littorina sea 4500–1500 BC).*

6 Parameterisation of hydraulic domains

This chapter describes the numerical implementation of the conceptual model described in Chapter 5. The initial parameterisation of the model was based on the data interpretation given in /Rhén et al. 2008/. Some changes to the parameterisation and other modelling settings were made as part of a calibration process against the calibration targets described in /Rhén et al. 2009, Chapter 6 therein/. In order to keep the description of the flow modelling brief, the approach used in this report is to describe some (more complete in /Rhén et al. 2009/) of the hydrogeological parameters and settings for the calibrated *base case* flow model in this chapter. In Chapters 7 through 9 where the matching to data is demonstrated, additional results for sensitivity variants on the calibrated model are presented to illustrate why key steps in the calibration process were made[4]. That is, rather than presenting all the trials and sensitivities considered in the evolution of the model from initial parameter settings to the calibrated model, the parameterisation of the calibrated model is presented here, and then sensitivity cases are constructed *a posterior* to demonstrate why the more important changes to the model were made. Additional variant simulations were made as sensitivity studies to scope some of the remaining uncertainties, such as spatial variability, and are described in Chapter 9.

6.1 Topography, model domain geometry and grid resolution

The full Laxemar-Simpevarp regional model area used in the site descriptive geological modelling is about 21 km by 13 km and 2.2 km deep. The lateral boundaries of the flow model domain were based on identified surface water divides. As shown in Figure 6-1, this required extension of the model domain outside the Laxemar-Simpevarp regional model area in some parts and limiting the extent slightly in others. The bottom elevation of the model was set at –2,160 m, which is far below the top demarcation of the lowest hydraulic depth zone interpreted at –650 m in the hydrogeological DFN modelling. Flowing features below –650 m are generally rare and HCD have a maximum transmissivity of less than around $4 \cdot 10^{-6}$ m^2/s at elevation –1,000 m. For the HRD, the intensity of PFL-f features is less than 1 per 100 m and the mean hydraulic conductivity for borehole sections outside of deformation zones below –650 m is less than 10^{-9} m/s, apart from possibly in HRD_EW007. Taking this into account together with the high salinities in excess of about 20 g/L TDS seen below about –1,000 m, little flow of any significance is expected to circulate below –1,000 m, and hence the vertical and horizontal extent of the regional model domain is expected to be entirely adequate for describing groundwater flow within the Laxemar local model area.

In a study comparing effects of model domain size /Holmén 2008/ considered a similar and much larger regional model domain based on model version Laxemar 1.2, and demonstrated that the weakly developed surface water divide employed for delimiting the western regional model boundary is in fact not a groundwater divide for the groundwater flow at greater depth. Hence, the effects of the deep groundwater flow that passes below the weakly developed surface water divide predicted by the larger model will not be included in the current model. Given that the deep groundwater flow across the western boundary is not included in the current model, this model may underestimate groundwater flow at repository depth, and overestimate both lengths of flow paths as well as the breakthrough times of flow paths from the repository area. However, the comparison by /Holmén 2008/ estimated these differences as being small (within a factor of c. 1.5), since the component of deep groundwater flow missing in the current model is not large. Given the strong depth trends in hydraulic properties interpreted in SDM-Site Laxemar, it is expected that the results presented here will be even less sensitive to deep groundwater flow across the western boundary of the model.

[4] *"Base case"* in this report accounting for the SDM-Site Laxemar modelling corresponds to "*Deterministic base model simulation"* in the SDM-Site Forsmark modelling /Follin 2008/.

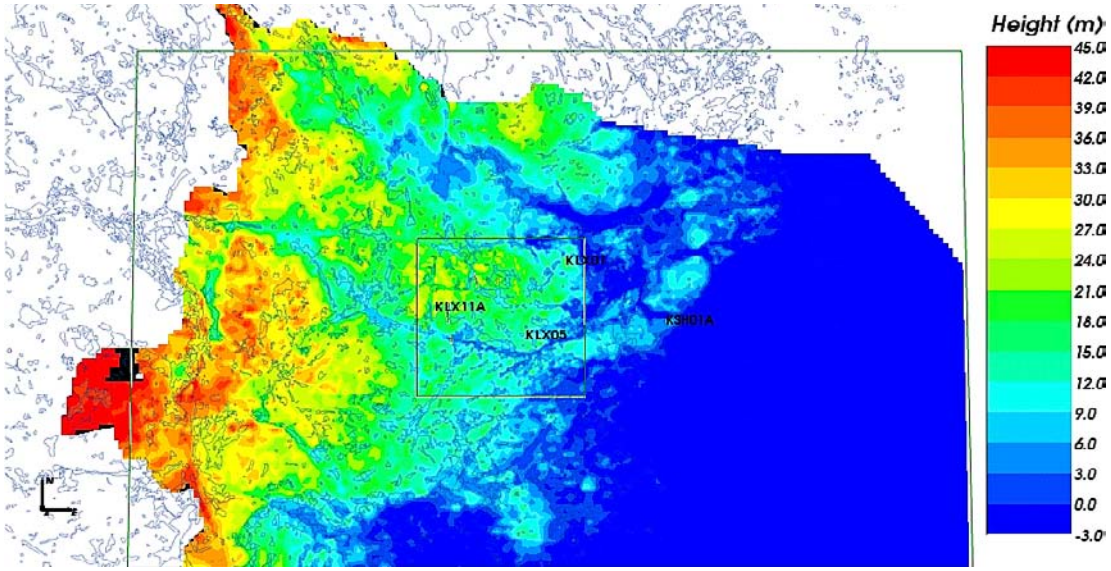

Figure 6-1. *Representation of topography on the regional scale hydrogeological model (top), and around the Laxemar local scale model area (bottom). The extent of the regional scale model area is shown by the outer green line. For topography outside the ConnectFlow model area cf. Figure 1-4. © Lantmäteriverket Gävle 2007, Consent I 2007/1092.*

Selection of grid resolution

Since data on the topography, fracture domains and Quaternary deposits data were supplied on a 20 m scale, the appropriate finite-element sizes were chosen as multiples of 20 m. Due to the volume of the local-scale model, c. 16 km^3, a computational grid of 40 m was used to make the palaeohydrogeological simulations tractable, since these require around 500 time-steps (i.e. 20 yr/step for a 10,000 year simulation period) of coupled flow and transport of several reference waters. As mentioned above, the facility in ConnectFlow to embed sub-domains of higher spatial resolution within a coarser grid was used, with appropriate conditions applied at the interface between sub-domains to ensure conservation of fluxes and continuity of variables. A horizontal slice through the embedded grid around the Laxemar local model area and an area around Äspö, is shown in Figure 6-2, cf. /Rhén et al. 2009/ for more details.

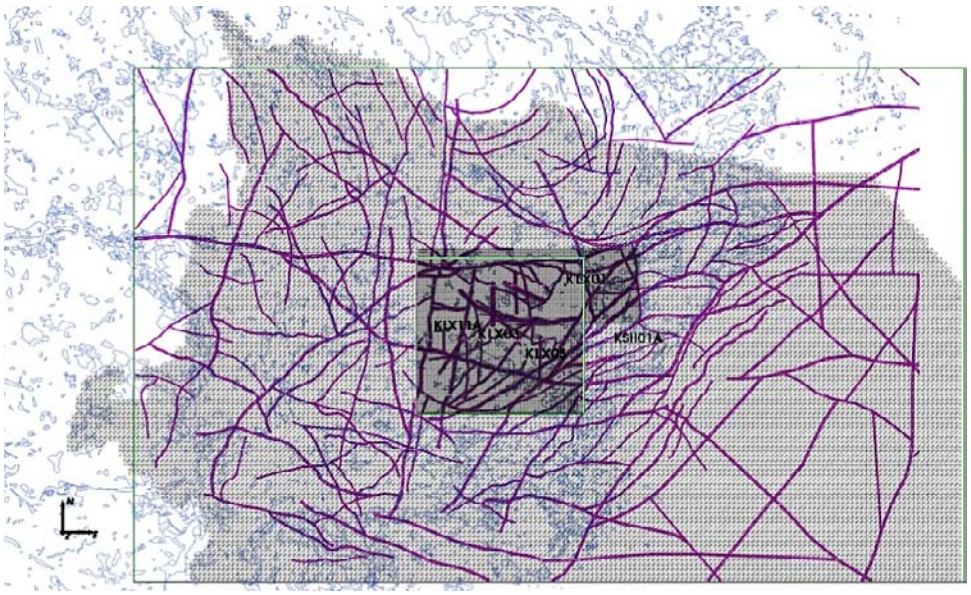

Figure 6-2. *Embedded refined finite-element grid around the Laxemar local model area and an area around Äspö, with size 40 m square. A 120 m grid was used on the regional-scale outside the local scale model area. The elements have a square horizontal cross-section, but are visualised here as artificially split into two triangles. The positions of the core-drilled boreholes are shown, and a horizontal slice at elevation 0 m through the deformation zone model is superimposed (purple) to show the grid resolution of volumes between HCD.*

6.2 Hydraulic conductor domains (HCD)

The HCD are included in the flow model using their geometrical description provided by the Geology team and the hydraulic property assignment suggested in /Rhén et al. 2008/. An exponential depth trend model is used for the transmissivity:

$$T=10^{(a+B\cdot Z)} \qquad (6\text{-}1)$$

Z: Elevation in m (m.a.s.l.) (Z defined positive up). The coefficients *a* and *B* in the exponential trend model are based on a linear regression of Log10(T_i). See /Rhén et al. 2008/ for details.

There are rather few HCDs with well characterised hydraulic properties (only seven, cf. /Rhén et al. 2008/) such that they have individual *T* versus depth trend functions. Most of the HCD are described using generalised depth dependencies. The HCD are divided into four main categories based on orientation and size, cf. Figure 5-3. The four categories are denoted by: E-W orientation with size < 2 km; E-W orientation with size > 2 km; other orientations with size < 2 km; other orientations with size > 2 km, cf. /Rhén et al. 2008/). For the *base case model*, transmissivity was assigned according to a depth trend defined for each HCD with no lateral heterogeneity (apart from some localised conditioning to measurement values). For details regarding discretisation and material properties assignment in the numerical model, cf. /Rhén et al. 2009/.

The palaeohydrogeological simulations suggested that the HCD transmissivities should generally be reduced. Multiplication factors of 1.0, 0.3 and 0.1 of original values were assessed between ground surface down to –150 m, between –150 to –650 m and below –650 m, respectively. The factor interpreted below –650 m is uncertain given the limited hydrochemical and hydraulic data at such depths. Still, data suggests groundwater is a mix of *Deep Saline Water* and *Glacial Melt Water* with *Altered Meteoric Water* absent, which for modelling to reproduce requires reduction factors in the range 0.1 – 0.3. However, based on natural head measurements and interference tests it was found that for a few specific HCD other factors were needed. cf. /Rhén et al. 2009/.

The distribution of the mean transmissivity in the HCD for the *base case* is shown in Figure 6-3. For stochastic realisations with lateral heterogeneity, these values are used as the mean sampled value for a log-normal distribution with specified standard deviation, but truncated at ± 2 standard deviations. Equivalent plots for one example realisation of the HCD with spatial variability, standard deviation in Log(*T*)=1.4, is shown in Figure 6-4. In both cases, the heterogeneous transmissivity field is conditioned to measured values at the intercept with borehole intervals where measurements are available. In order to simulate the interference test in HLX33 and HLX28, a homogeneous specific storage coefficient around 10^{-7} m^{-1} was used throughout the bedrock.

Additional details of the HCD properties from different aspects are found in /Rhén et al. 2008/.

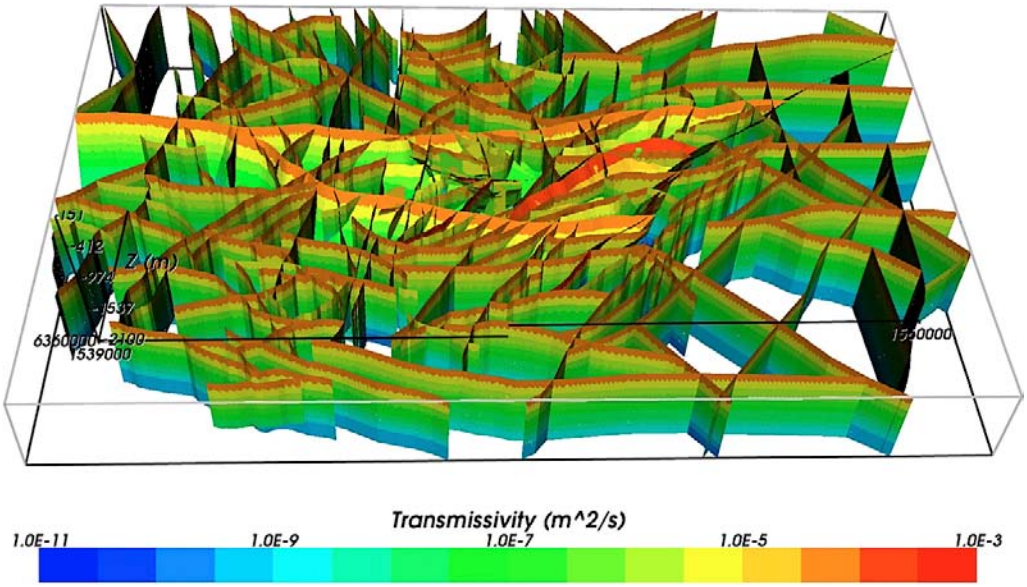

Figure 6-3. *All HCD and their inferred depth dependent transmissivity for the deterministic base case model (cf Figure 3-1 and Figure 3-2). Oblique view looking from the south.*

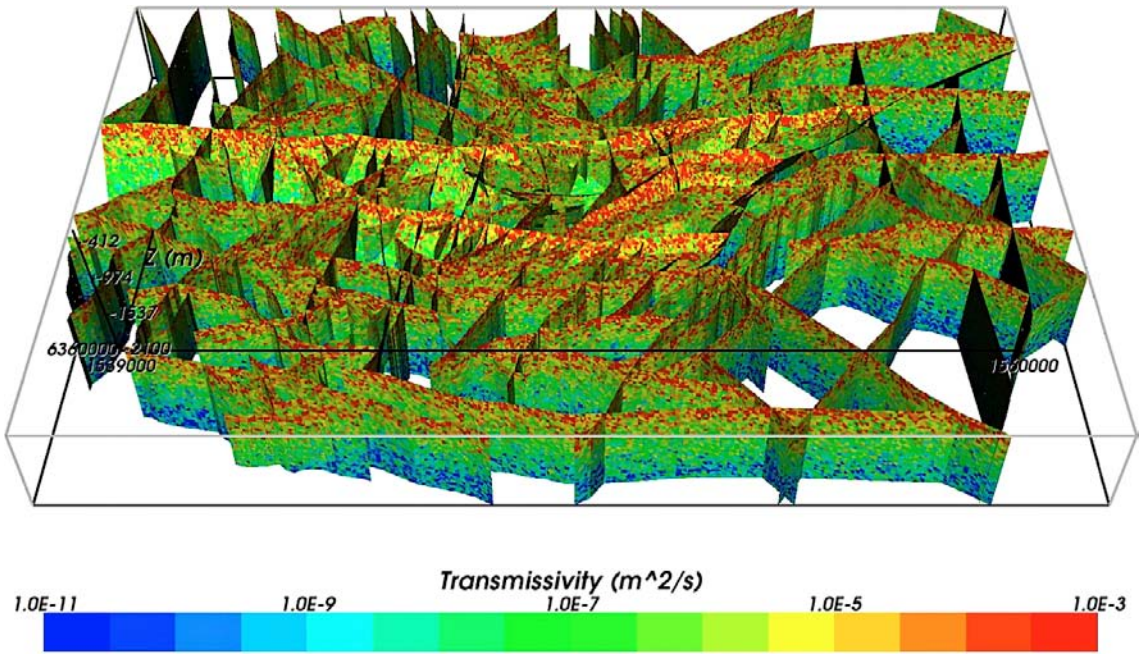

Figure 6-4. *All HCD and their inferred depth dependent transmissivity for a case with spatial variability and a standard deviation in Log(T) of 1.4. Oblique view looking from the south (cf Figure 3-1 and Figure 3-2).*

6.2.1 Transport properties

The transport properties of kinematic porosity (n_e) and flow wetted surface area (a_r) are also assigned to the deformation zones in the HCD model. These two entities have been inferred as depth-dependent properties and depend critically on the intensity of connected open fractures. Since the corrected P_{10} values within HCD are about 3 times larger than in HRD, the kinematic porosities for the HCD were based on typical kinematic porosities calculated for the HRD, multiplied by 3 giving a depth-dependent kinematic porosity. Hence, the transport parameters used for the HCD follow the same prescription as that for the HRD described in Section 6.3.1, but with kinematic porosity and flow-wetted surface area increased to account of the higher fracture intensity. The values of flow-wetted surface area were based on Terzaghi corrected P_{10} values obtained from PFL measurements within HCD /Rhén et al. 2008/. Hence, a_r is estimated by using the relationship $a_r = 2 \cdot P_{10,corr}$(PFL-f). For details concerning assignment of kinematic porosity and flow wetted surface area, cf. /Rhén et al. 2009/.

6.3 Hydraulic Rock Domains (HRD)

The hydraulic rock domains are parameterised in terms of a stochastic DFN model, by calibration against available hydraulic data mainly from the PFL-f-tests, cf. Figure 6-5. This parameterisation is briefly described below and details are found in /Rhén et al. 2008, cf. Chapter 10 therein/.

The hydrogeological DFN modelling is based on the assumption, discussed in Section 2.3.5, that:

$$P_{10,all} \geq P_{10,open} \geq P_{10,cof} \geq P_{10,PFL} \qquad (2\text{-}1)$$

where $P_{10,cof}$ denotes the intensity of "connected open fractures", a key property of any hydrogeological DFN model. The meaning of the different suffixes (*all*, *open*, *cof* and *PFL*) in Equation 2-1 is explained in Figure 2-9.

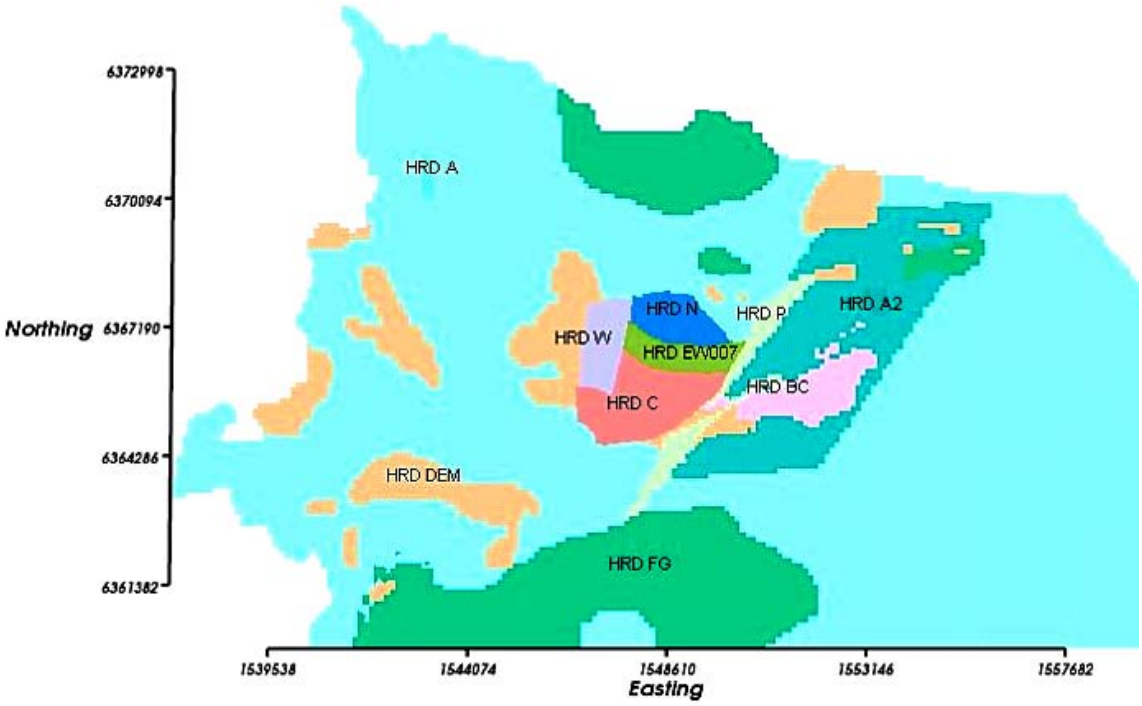

Figure 6-5. *Hydraulic rock domains on the top surface of the bedrock in the regional scale hydrogeological model (c.f. Figure 3-1).*

To complete the parameterisation the following quantities are required; they are either estimated directly from the data or derived through the calibration process.

- The fracture surface area per unit volume of *open* fractures ($P_{32,\ open}$).
- The shape parameter k_r and the location parameter $r_{0,}$ assuming that the fracture size distribution follows a power-law distribution /Rhén et al. 2008/.
- The parameters relating transmissivity to fracture size. Three different kinds of relationships between fracture transmissivity and fracture size are considered as variants, as described in Table 2-3.

The hydrogeological DFN models allow the parameters described above to vary by fracture set, by depth zone and between different hydraulic rock domains.

The values of the power-law intensity distribution parameters (k_r and r_0) are not uniquely constrained by the methodology adopted and the data available. It is therefore necessary to consider several different combinations of parameters which allow the sensitivities to these parameters to be quantified in subsequent modelling. The combinations of the different parameters were guided by the results reported in the preliminary SDM /SKB 2006a/.

A further uncertainty considered was how to identify the *open* (i.e. potentially flowing) fractures in the data. In the *base case*, open fractures were assumed to correspond to any fracture classified as either open or partly open in the boreholes, and hence denoted 'OPO' fractures. A variant with a different classification of *open* fractures was used to assess the sensitivity, based on the restricted set of OPO fractures with either certain or probable classification during core mapping, and hence denoted 'OPO-CP' fractures. In short, four different combinations of values of the power-law intensity distribution parameters and $P_{32,open}$ were tested, cf. Figure 6-6.

The hydrogeological DFN simulations were repeated ten times (producing ten realisations) using the Monte Carlo method. For each HRD, a simulation model was constructed as a representative volume surrounding a notional vertical borehole with the volume sub-divided in to 4 depth zones to represent the changes in fracture intensity and transmissivity with depth. For each of the variants considered, the hydrogeological DFN calibration was made in three steps:

- A check was made that the proposed DFN model could reproduce the measured intensity of *open* fractures in the boreholes. For each variant the fracture surface area per unit volume of rock, $P_{32,open}$ ($r \geq r_0$), was altered until a fair match between simulated and computed values of $P_{10,open,corr}$ was achieved, i.e.:
  $P_{32,open} \approx P_{10,open,\,corr}$ (6-1)
- A connectivity calibration was made where the aim was to adjust the fracture size distribution parameters to obtain a match to the observed intensity of PFL-f features. This is a 'fine-tuning' of the power-law size parameters for each fracture set i to produce an accurate match between $P_{10,cof,corr}$ and $P_{10,PFL,corr}$, i.e.:
  $P^{i}_{10,cof\,,corr} \approx P^{i}_{10,PFL,corr} \quad , \quad i \in (ENE, WNW, N-S, SubH)$ (6-2)
- Flow simulations were carried out using three different kinds of relationships between fracture transmissivity and fracture size (see Table 2-3). These simulations used the power-law size parameters derived previously in the connectivity calibration.

Figure 6-6 shows the results of the connectivity calibration. Below –650 m elevation, the models predict very low mean connected open fracture intensities, but most predict a small non-zero intensity for the N-S fracture set. Partly this is to be expected since a stochastic approach is being used and some realisations happen to have a small number of connected fractures intersecting the borehole. One way of reconciling the hydrogeological DFN model is to consider a depth variation in the hydraulic properties, such that fractures below –650 m elevation have a lower fracture transmissivity as well as intensity, chosen so that a number of the fractures simulated below –650 m elevation have transmissivities below the detection limit for the PFL-f method. This approach was adopted in the subsequent flow modelling.

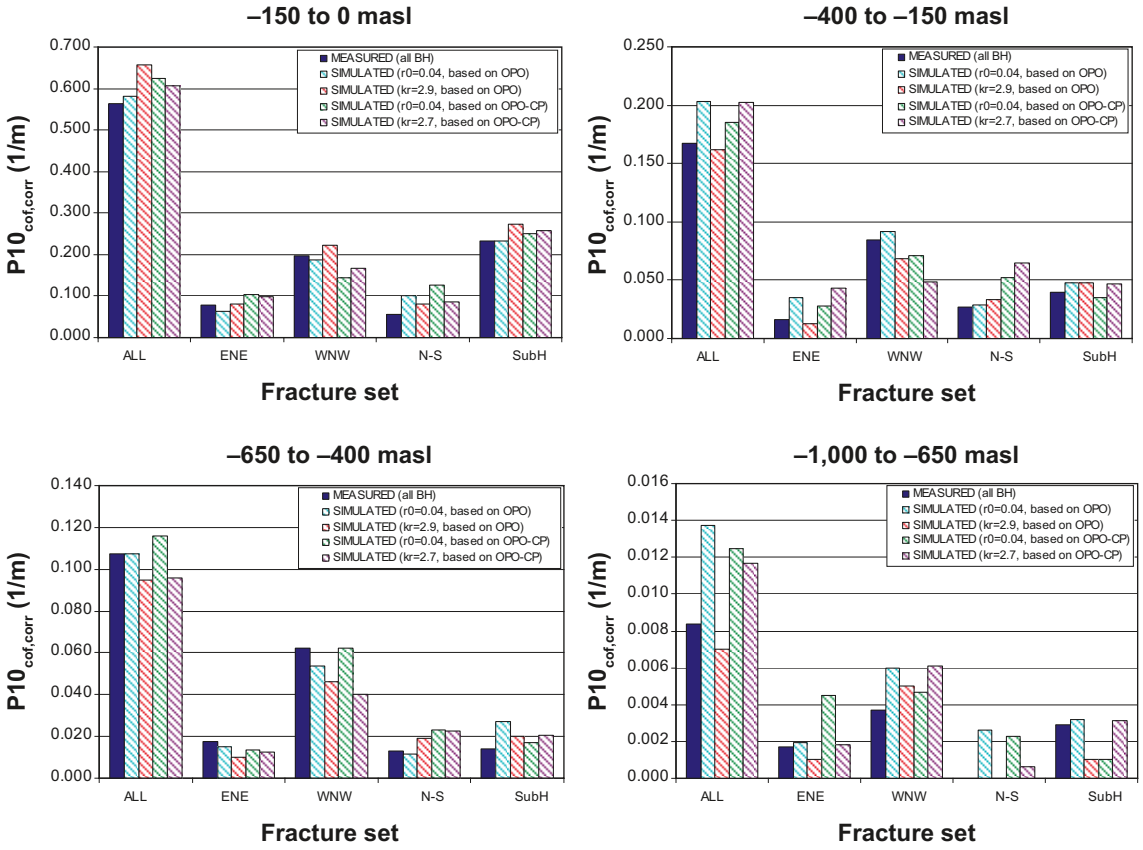

Figure 6-6. *Comparison of the Terzaghi corrected connected open fracture intensities, $P10_{,cof,corr}$ for the individual fracture sets with the measured fracture intensities for PFL-anomalies for HRD_C. Four alternative geometrical fracture models were considered: k_r fixed with r_0 varying or r_0 fixed with k_r varying, and fracture intensity based on all open fractures (OPO); r_0 fixed with k_r varying or r_0 fixed with k_r varying, and fracture intensity based only fractures characterised as open with high certainty (OPO-CP).*

Figure 6-7 shows plots of the fracture intensities of *all* fractures (taken from the geological DFN model), *open* fractures and *connected open fractures* as calculated in the connectivity analysis for HRD_C. The green lines represent the k_r-scaled (or r_0 fixed) model discussed in the geological DFN modelling and are based on the corrected linear borehole intensity of *all* fractures in the analysed boreholes $P_{10,all,corr}$. The red lines represent the k_r-scaled model used in the hydrogeological DFN modelling and are based on borehole intensity of *open* fractures $P_{10,open,corr}$. The blue lines represent the intensity of *connected open fractures* $P_{10,cof,corr}$ simulated in ten realisations of the hydrogeological DFN model. The parameter r_0 is set to the scale of observation, i.e. the borehole radius (0.038 m) and r_1 is set to 564.2 m (L = 1,000 m). Discrete features above this size are modelled deterministically in SKB's systems approach. Figure 6-7 confirms the expected consistency between the geological and hydrogeological k_r-scaled models, with a higher intensity of *all* fractures versus *open* fractures at all length scales, cf. Equation 2-1. The curves representing the hydrogeological DFN honour the observed variations with depth of the total intensity of *open* and *PFL* fractures. This depth variation is not so apparent in the intensity of *all* fractures, which is the reason why there is only a single fracture size model representing the geological DFN. Reassuringly, for the sparsely fractured rock at depths below about –150 m, such distributions of intensity versus size for connected open fractures tend to be similar for each of the calibrated parameter variants considered in Figure 6-6. This is significant since it indicates that, despite the uncertainty in basic input, such as open fracture intensity and size distributions, the possible distributions of connected open fractures are sufficiently constrained by the connectivity calibration, hence providing some robustness in the resulting hydrogeological DFN models.

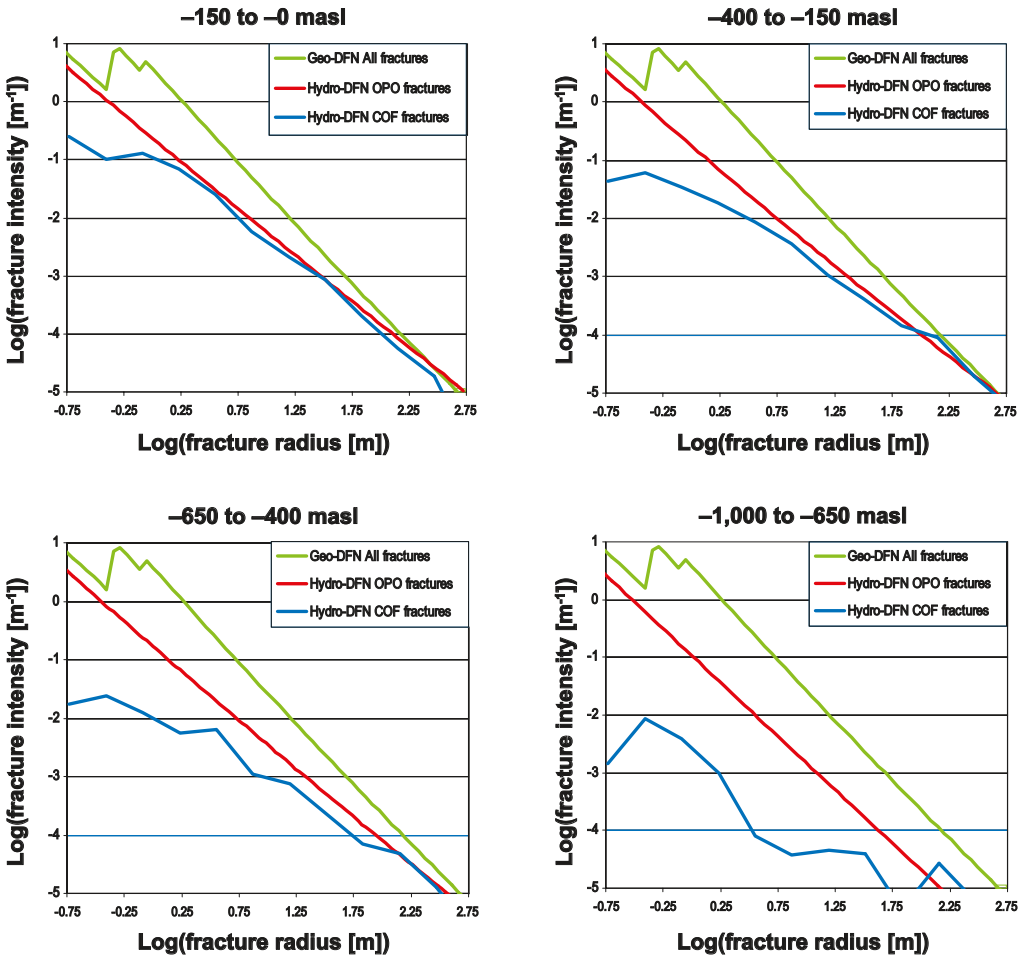

Figure 6-7. *Comparison of the distributions of fracture intensity, P_{32}, with fracture size for 'all' fractures (as predicted by the geological DFN in green), that for 'open' fractures (as predicted by the hydrogeological DFN, OPO case, shown in red), and that for simulated 'connected open fractures' using the hydrogeological DFN connectivity analysis (shown in blue). Note that the jagged part of the geological DFN size distribution reflects the use of different r_0 parameters for each set.*

To complete the hydrogeological DFN parameterisation, flow simulations were performed to calibrate a set of alternative relationships between fracture transmissivity and size that reproduced the numbers of inflows and the distribution of their magnitude as measured with the PFL-f tests. An example of a flow simulation is shown in Figure 6-8. The model configuration has zero head imposed on the vertical sides and top, a uniform 10 m drawdown in the vertical borehole, and hence there is an inflow at every connected open fracture intersection with the borehole. Only combinations of parameter values for open fracture intensity and power-law size distributions derived during the connectivity calibration step were considered in the flow modelling.

Three alternative relationships between fracture transmissivity and size were studied: direct correlation, semi-correlation and no correlation (see Table 2-3). By semi-correlation it was implied that the mean transmissivity of a fracture increases with its size, but there is a superimposed random component or spread of values for any given fracture size. This is perhaps the most realistic situation. Hence, in the flow calibration, the aim was to establish appropriate choices for the parameters for each relationship between fracture size and transmissivity that gives a match to the magnitude of the inflows. Five main calibration targets were used to quantify how well the model simulates the data (cf. Figure 6-9 through Figure 6-13):

- Target 1: A histogram of the distribution of PFL-f specific flow-rates, *Q/s*, was compared using a bin size of half an order of magnitude.
- Target 2: A histogram of the distribution of PSS (5 m scale) specific flow-rates, *Q/s*, within elevation –400 to –650 m, was compared using a bin size of half an order of magnitude.
- Target 3: The total specific flow to the borehole, sum of PFL-f specific flow-rates, *Q/s,* (calculated as an arithmetic average over the realisations).
- Target 4: The specific inflow to 100 m borehole intervals for PFL-f and PSS (100 m scale) (calculated as a geometric mean over the realisations).
- Target 5: The numbers of PFL features associated with each fracture set and the distribution of *Q/s*, for each set. This distribution is quantified in terms of the mean, plus/minus one standard deviation, minimum and maximum of Log(*Q/s*).

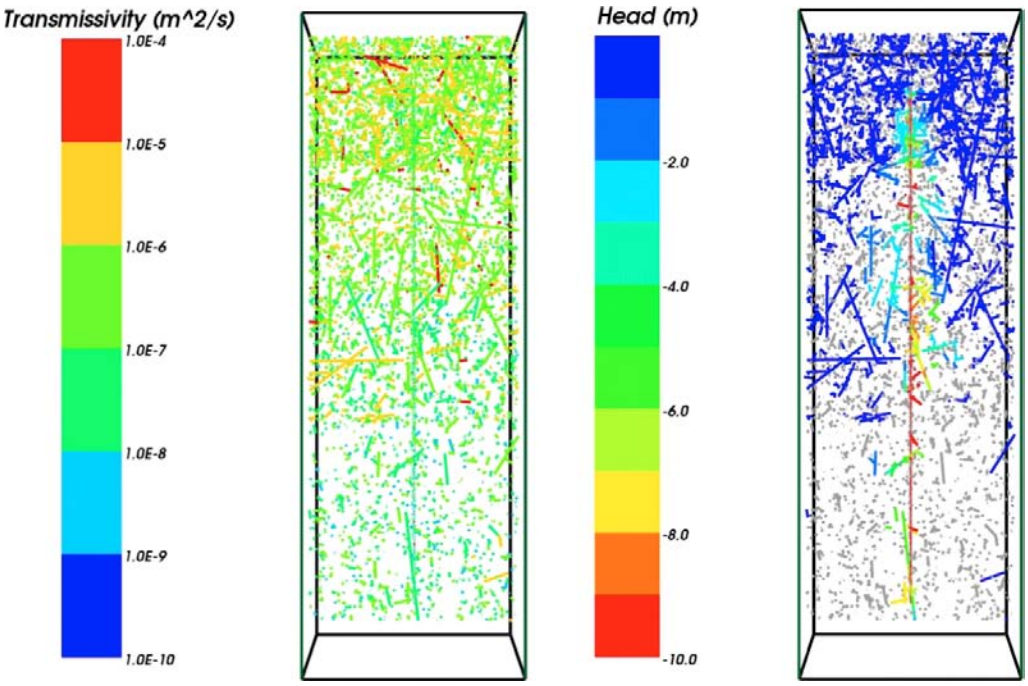

Figure 6-8. *Vertical cross-section through one realisation of the hydrogeological DFN model of HRD c (model volume including the four depth zones: 1,000×400×400 m³). Left: All open fractures coloured by transmissivity. The 1 km generic vertical borehole is in the middle of the figure. This figure indicates how the parameterisation changes the fracture intensity, fracture size, and fracture transmissivity with depth. Right: The connected open fractures coloured by drawdown with unconnected fractures coloured grey.*

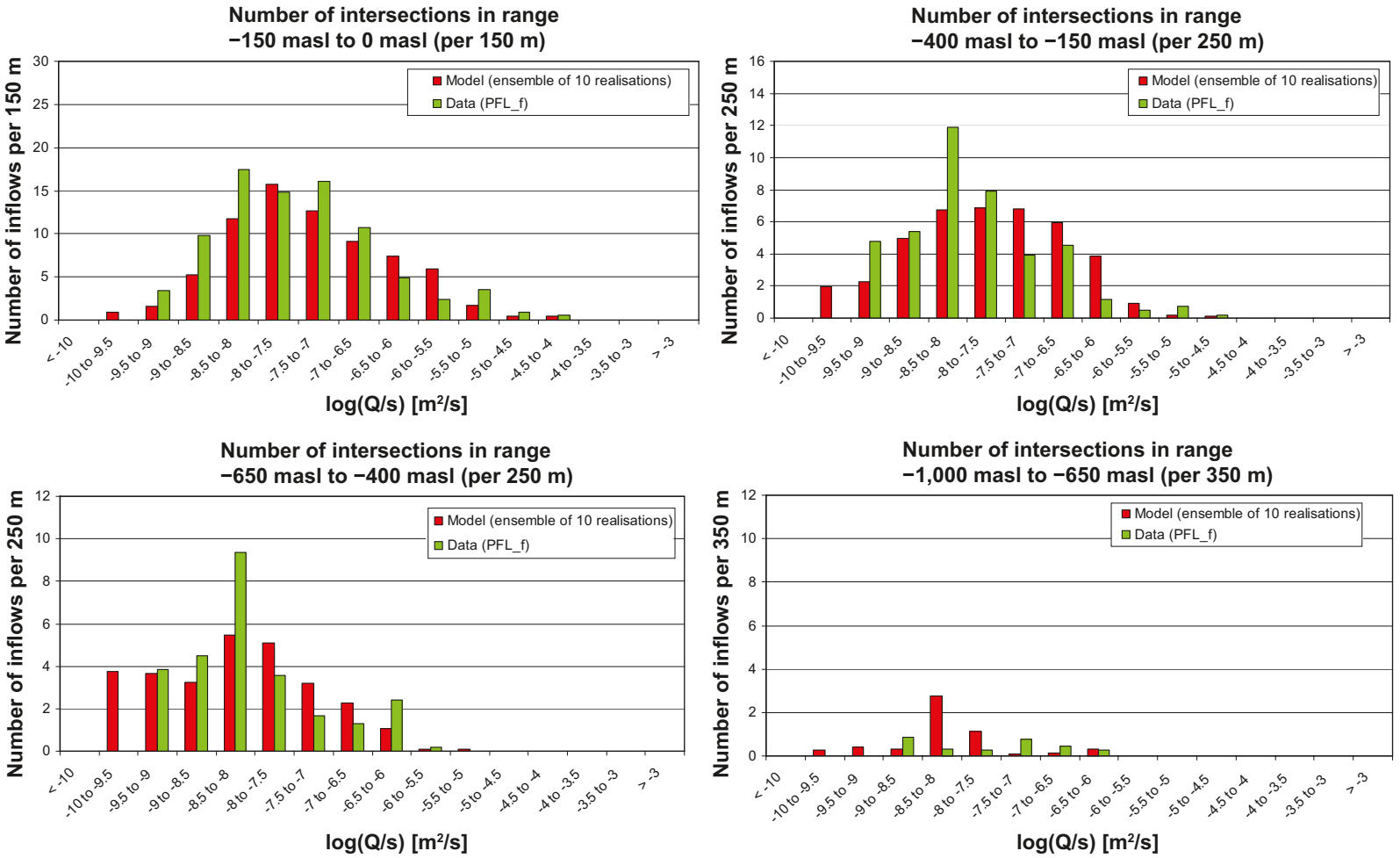

Figure 6-9. *Calibration Target 1: Histogram comparing the distribution of the magnitude of inflows divided by drawdown, Q/s, at abstraction boreholes in HRD_C. The model has a semi-correlated transmissivity, with r_0 fixed and open fracture intensity based on OPO fractures. The PFL-f measurements are treated as ensemble over all boreholes sections within HRD_C. The simulations represent the combined results of 10 realisations of the hydrogeological DFN model. The numbers of intersections are Terzaghi weighted and normalised to the length of borehole which is provided in the heading of each graph.*

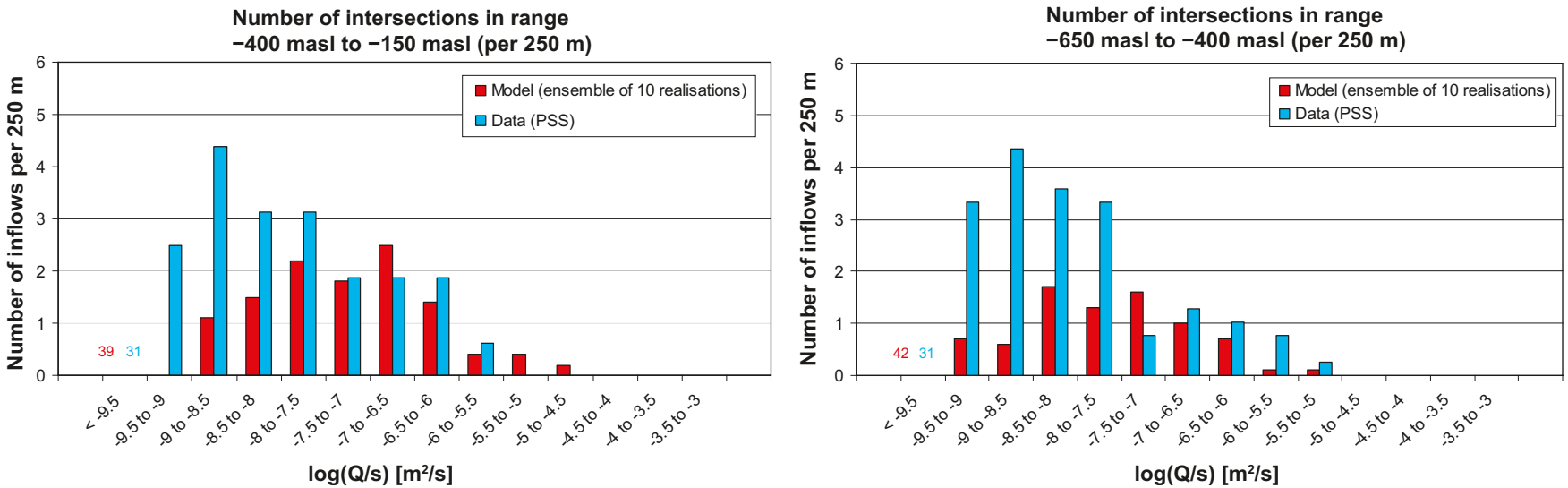

Figure 6-10. *Calibration Target 2: Histogram comparing the distribution of the magnitude of inflows divided by drawdown, Q/s, in 5 m sections at abstraction boreholes in HRD_C. The model has a semi-correlated transmissivity, with r_0 fixed and open fracture intensity based on OPO fractures. The PSS measurements are treated as ensemble over all boreholes sections within HRD_C. The simulations represent the combined results of 10 realisations of the hydrogeological DFN model. The numbers of intersections are normalised to the length of borehole which is provided in the heading of each graph.*

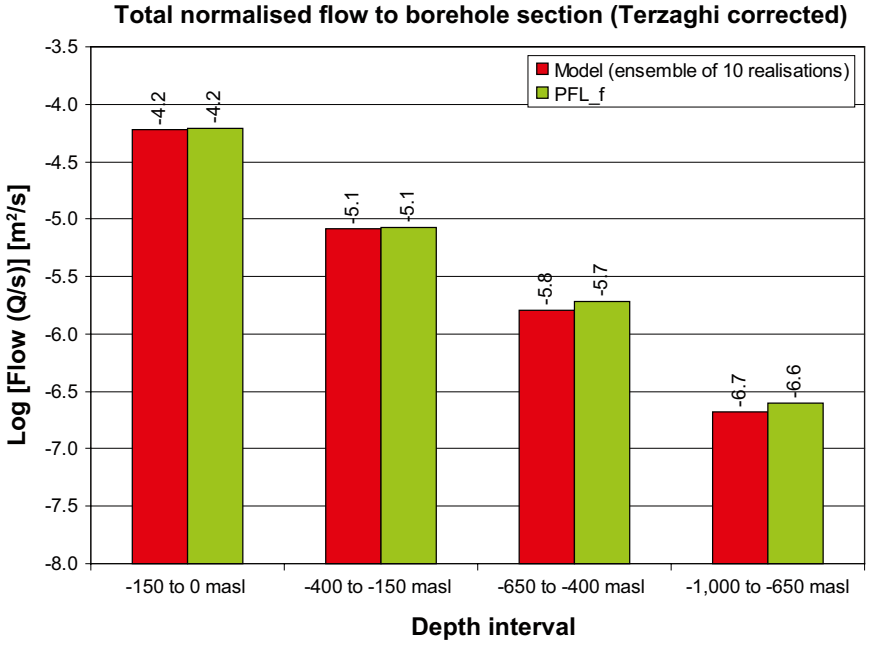

Figure 6-11. *Calibration Target 3: Comparison of the sum of individual flows, Q/s, for the PFL-f data from borehole sections within HRD_C against the hydrogeological DFN model. The model has a semi-correlated transmissivity, with r_0 fixed and open fracture intensity based on OPO fractures. For the model, the arithmetic mean is taken over 10 realisations. The flows are Terzaghi weighted and normalised to the borehole length indicated by the range on the horizontal axis.*

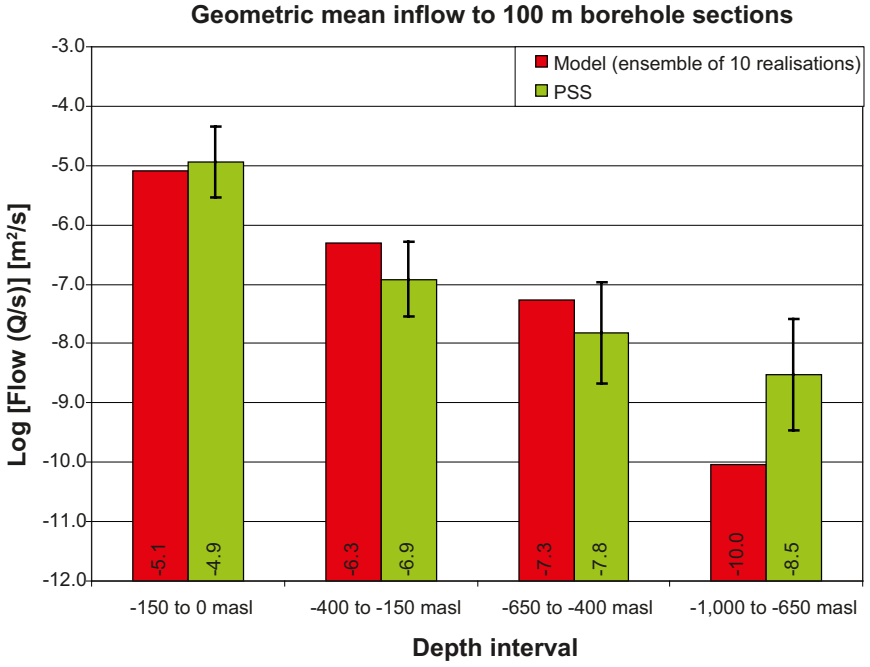

Figure 6-12. *Calibration Target 4: Comparison of the geometric mean of total flows, Q/s, to 100 m borehole intervals for the PSS data from borehole sections within HRD_C against the hydrogeological DFN model. The model has a semi-correlated transmissivity, with r_0 fixed and open fracture intensity based on OPO fractures. For the data, the geometric mean is shown as well as the 95% confidence interval in the mean. For the model, the mean value of total flow is taken over 10 realisations.*

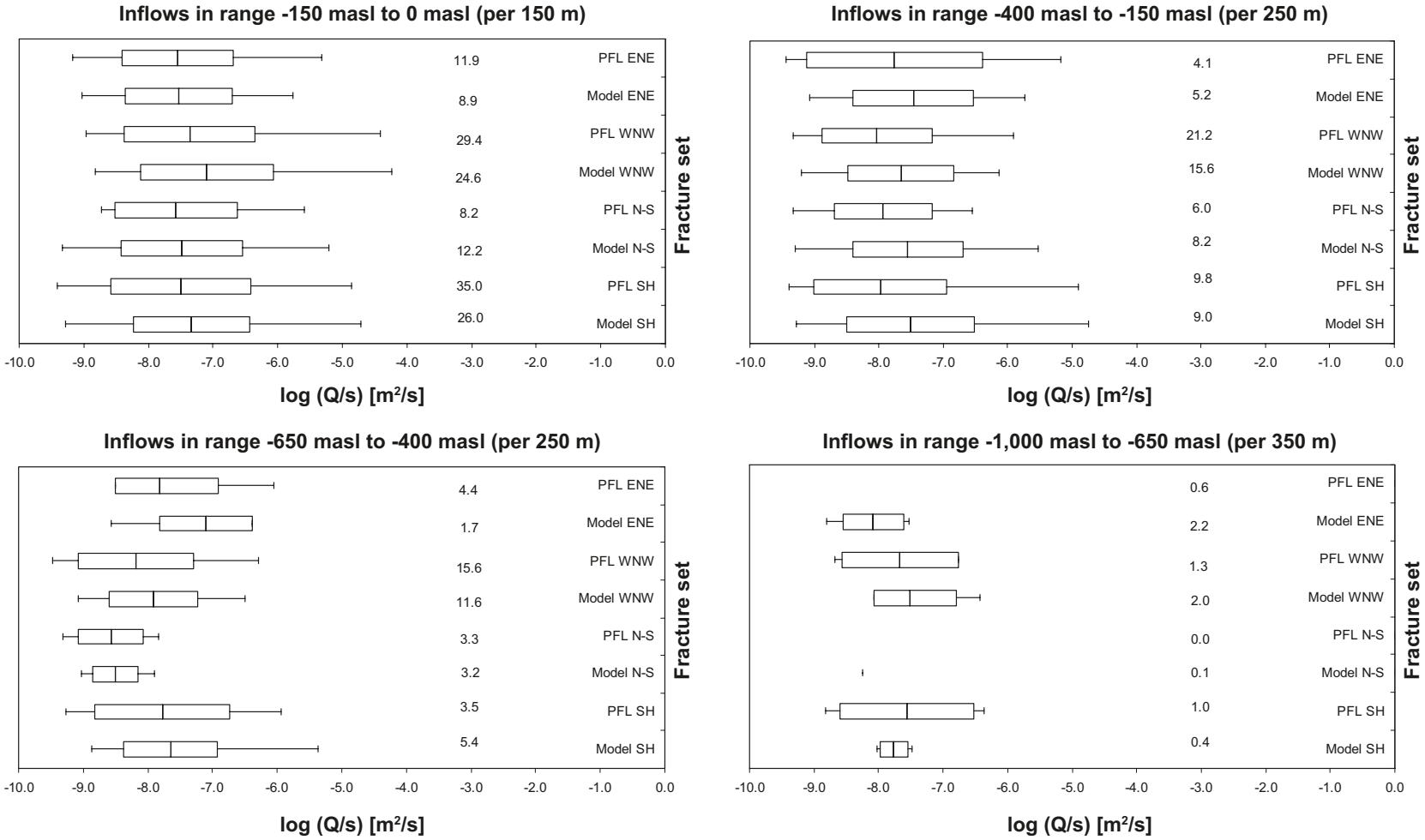

Figure 6-13. *Calibration Target 5: Bar and whisker plots comparing statistics taken over each fracture set for the individual inflows, Q/s, for the PFL-f data from borehole sections within HRD_C against statistics for an ensemble over 10 realisations of the hydrogeological DFN model. The model has a semi-correlated transmissivity, with r_0 fixed and P_{32} based on OPO fractures. The centre of the bar indicates the mean value, the ends of the bar indicate ±1 standard deviation, the error bars indicate the minimum and maximum values and the value is the number of flowing features above the PFL-f detection limit per borehole section. For the data statistics are taken over the identified flowing features within each set. For the model, statistics are taken over the fractures generated within each set and over 10 realisations. The numbers of fractures are Terzaghi weighted and normalised to the length which is provided in the respective graph heading.*

The resulting hydrogeological DFN parameterisations for HRDs are provided in /Rhén et al. 2008, cf. Section 10.5 therein/.

An example of the comparison of inflows between model and data for HRD_C is given for the model using a semi-correlation between fracture size and transmissivity (Figure 6-9 to Figure 6-13). The match to the observed flow is poorest for the deepest depth zone (below –650 m elevation). However, it should be noted that there are very few fractures carrying flow at this depth, so the distributions of PFL-f data or flows are not very well defined. Figure 6-13 shows bar and whisker plots that compare the measured and simulated inflows for the different fracture sets, normalised to appropriate borehole length sections. The numbers alongside the bars represent the Terzaghi weighted numbers of inflows above the detection limit per borehole section. Figure 6-13 shows that the inflows are dominated by the WNW and SubH fracture sets with a small contribution from the ENE set.

The matches for all three transmissivity models, cf. Table 2-3, were found reasonable above –650 m /Rhén et al. 2008/). The most significant difference in hydraulic characteristics between these 3 cases comes in the scale dependence of hydraulic conductivity, where the uncorrelated model has the least dependence. Considering the PSS measurement scale statistics (for 5, 20 and 100 m) (cf. /Rhén et al. 2008/), the uncorrelated model has less consistency with observations. It also predicts a factor 3 times higher kinematic porosity. An additional check on the plausibility of the chosen transmissivity parameters was to calculate the maximum transmissivity that could be generated for a stochastic fracture (< 564.2 m radius) and make sure this did not greatly exceed the maximum transmissivity measured in the deterministically interpreted deformation zones (HCD). This was satisfied for all HRD and variants and ensures that when the hydrogeological DFN model is applied on the regional scale then no anomalously high transmissivities are generated compared with field data.

To illustrate how the different transmissivity-size relationships compare they are plotted as log-log plots for the SubH set in HRD_C, cf. Figure 6-14, based on the parameters given in /Rhén et al. 2008, cf. Section 10.5 therein/. The semi-correlated and correlated models follow similar trends and also intercept the uncorrelated model for fractures of about 10 m radius. This is to be expected since fractures around 10–100 m form the main body of the water-conducting network that gives the inflows in the simulations. There is less consistency between the transmissivity models below –650 m elevation as the distribution of inflows is poorly determined at these depths, there being so few data points to guide the calibration.

The similarity between the transmissivities for 10–100 m size fractures and the simulated inflow statistics for the different transmissivity relations (cf. /Rhén et al. 2008/) constitutes another illustration of the robustness of the hydrogeological DFN that comes from the model calibration steps, in this case the matching to inflow data. A further example of the stability of the flow characteristics predicted by the hydrogeological DFN is the consistency of upscaled hydraulic conductivities for 100 m blocks derived for each of the model variants considered (cf. /Rhén et al. 2008/).

Figure 6-15 shows an example of a realisation of the regional hydrogeological DFN model. The realisation is shown as two vertical cross-sections with only the connected open fractures and HCD displayed. The effect of the low connectivity below –650 m elevation is apparent, as is the higher fracture intensity associated with HRD_EW007 beneath KLX08 shown in the N-S section.

The definition of mass balance aperture e_t for single fractures is part of the hydrogeological DFN and uses the empirical function, $e_t = 0.705\ T^{0.404}$, cf. /Rhén et al. 2009, Hjerne et al. 2009/ for details. The kinematic porosity used in the ECPM models can be calculated within a grid cell by summing up the area of water conducting fractures multiplied by mass balance aperture and dividing by the volume of the grid element.

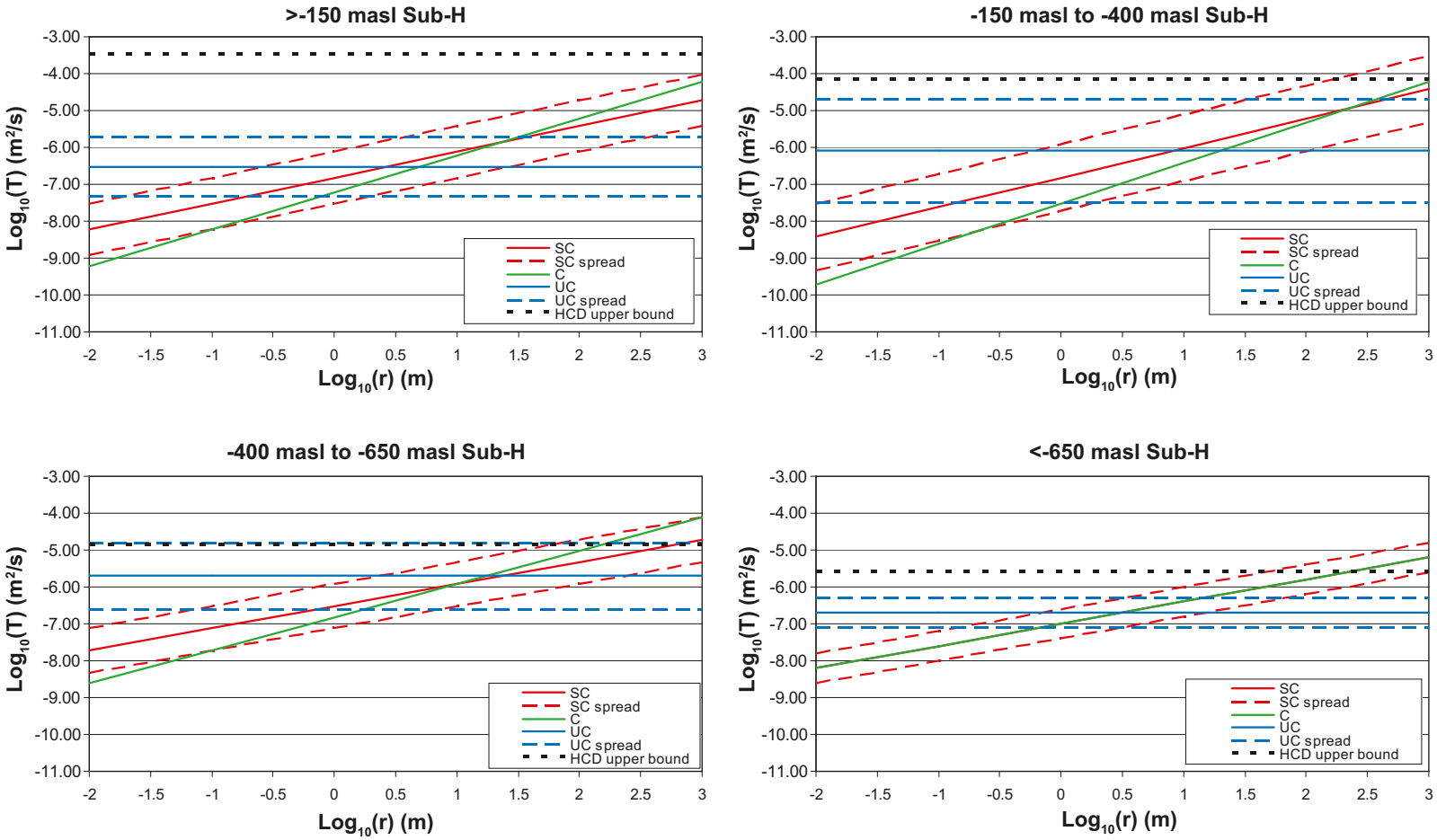

Figure 6-14. *Comparison of the relationships between fracture transmissivity and fracture size in each depth zone for HRD_C. The plots are for the calibrated model with r_0=0.038 m and open fracture intensity based on OPO fractures. The plots show the central trend for each relationship together with lines at one standard deviation above and below the central trend. The dashed black line indicates the maximum value measured in the deterministically interpreted deformation zones (HCD).*

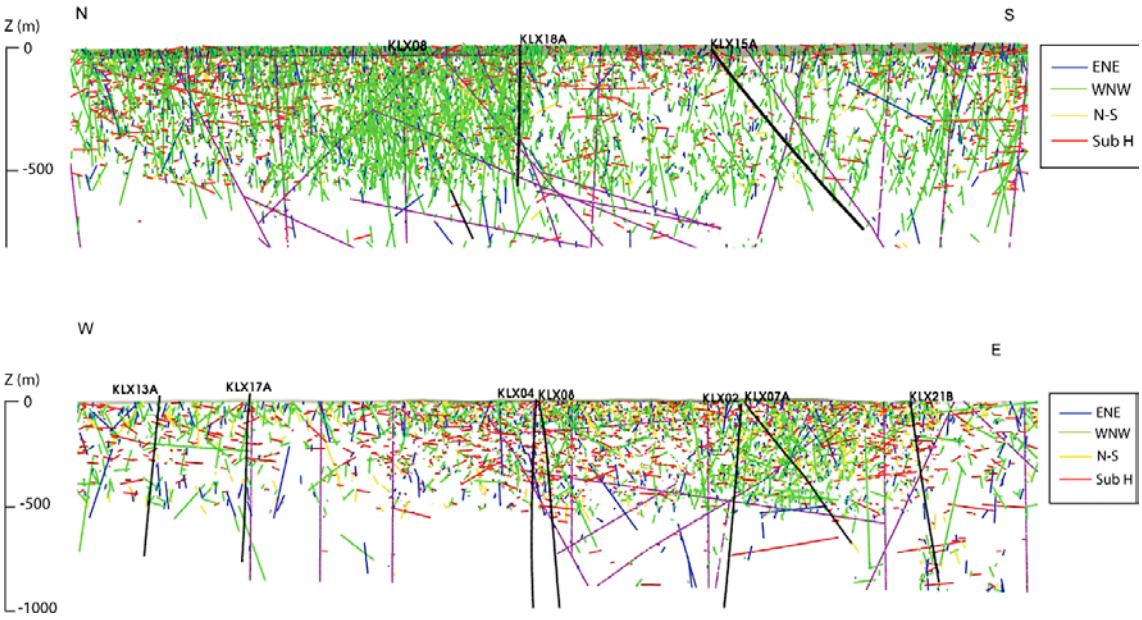

Figure 6-15. *Traces of connected OPO fractures in the N-S Section A and the WNW-ESE Section B (see Figure 8-50) through the base case hydrogeological DFN simulation. The fractures are coloured according to orientation set (ENE – blue, WNW – green, N-S – yellow, SubH – red). The HCD are shown in purple together with core drilled boreholes in the close proximity of the vertical section.*

6.3.1 Transport properties

The transport properties kinematic porosity (n_e), flow wetted surface area (a_r), matrix porosity and matrix diffusion length are also assigned to the HRD model. These two entities have been inferred as depth-dependent properties. Dispersion lengths and effective diffusion coefficients were assigned uniformly throughout the model.

The flow-wetted surface is the amount of open connected fracture surface area per unit volume of rock. The values are estimated from measured average (within a HRD and depth zone) Terzaghi corrected intensity, $P_{10,corr}$, of conductive fractures detected by the PFL-f method as, $2 \cdot P_{10,corr}(PFL)$. The kinematic porosity was calculated based on the integrated fracture volume within each grid cell, and can be approximated by $n_e = e_T \times P10,corr(PFL)$, where e_T is the mass-balance aperture (see above). The matrix diffusion length is the maximum penetration of the solute into the matrix, usually set to 1/flow-wetted surface, i.e. $1/\sigma$. For practical numerical reasons this was actually implemented as $\min(1/\sigma, 6\ m)$, with 6 m used as a maximum penetration depth since the time taken to diffuse 6 m into the matrix is larger than the 10,000 years duration simulated. The transport parameters in HRDs are discussed in/ Rhén et al. 2009/.

6.3.2 Comparison between hydrogeological DFN model and KLX27A data

KLX27A is a core-drilled borehole in the south-west corner of Laxemar, cf. Figure 3-2. It is approximately 645 m long, inclined northwards, starting in HRD_C, crossing the ZSMNW042A deformation zone, and ending in HRD_W. About 408 m of the borehole is in HRD_W (excluding major deformation zones) and only these latter data are used in the comparison study. Data from KLX27A were excluded from the data used to develop and calibrate the hydrogeological DFN model, and therefore it may be used to compare predictions of the Hydrogeological DFN model with the hydraulic properties observed in relevant parts of KLX27A. The comparison is presented in /Rhén et al. 2008/.

The comparison between the model and the borehole data from KLX27A, demonstrates that a number of the observed hydraulic characteristics fall within the predicted variability, but some properties such as the intensity of PFL-f features below –400 m are exceptionally high in KLX27A. Considering the large spatial variability of occurrence of PFL-f features and the use of only one borehole for the comparison, the conditions for a statistically significant comparison cannot be expected to be

fulfilled. It is therefore not possible to draw firm conclusions from the comparison, other than that the outcome of KLX27A confirms that HRD_W is characterised by a strong element of heterogeneity and it is also probably more difficult to predict than HRD_C.

6.3.3 Summary comparison of HRD hydraulic properties

Key hydraulic properties of the three HRD inside the focused volume are summarised by depth zone in Table 6-1 based on PFL flow measurements. The HRD are compared in terms of the Terzaghi corrected flowing fracture intensity; PFL $P_{10,corr}$, the geometric mean transmissivity, the sum of transmissivities divided by borehole length, and the corrected fracture intensity multiplied by geometric mean transmissivity. The last two columns are alternative estimates of the bulk hydraulic conductivities of the bedrock based on arithmetic and geometric averaging, respectively. HRD_EW007 has the highest intensity of flowing features and the least decrease with depth. HRD_W has the least intensity of flowing features and the most marked drop in intensity below –150 m**.** At repository depth, the intensity of flowing features in HRD_EW007 is about twice that in HRD_C, which is nearly twice that in HRD_W. Geometric mean transmissivities are similar in HRD_EW007 and HRD_W and about three times higher than HRD_C. The variability in transmissivity, apparent from the difference between arithmetic and geometric mean estimates of bulk hydraulic conductivity, is greatest in HRD_W. HRD_C and HRD_W are similar in terms of geometric mean hydraulic conductivities, and about 3–5 times lower than HRD_EW007. HRD_W has the least fracture intensity, but the most variability.

The palaeohydrogeological simulations suggested that the upscaled hydraulic conductivity of the HRD in the ECPM below –150 m should be slightly decreased, by multiplication factor of 1/3, cf. Section 7.4.1.

Table 6-1. Summary of statistics of flowing features detected by PFL for the borehole intervals outside of interpreted deterministic deformation zones. MDZ are included in these statistics, but the transmissivity of individual PFL fractures are summed within an MDZ such that each is treated as a single feature.

Hydraulic Rock Domain	Depth Zone (m)	PFL $P_{10,corr}$ (m^{-1})	Geometric mean T (m^2/s)	Sum T/ Length (m/s)	$P10_{,PFL,corr}$ × geometric mean T (m/s)
HRD_EW007	50 to –150	0.816	3.58E–08	3.1E–07	2.9E–08
	–150 to –400	0.550	3.0E–08	1.2E–07	1.7E–08
	–400 to –650	0.225	2.6E–08	1.2E–08	5.9E–09
	–650 to –1,000	N/A	N/A	N/A	N/A
HRD_W	50 to –150	0.499	4.39E–08	2.8E–07	2.2E–08
	–150 to –400	0.078	1.4E–08	2.9E–08	1.1E–09
	–400 to –650	0.060	2.9E–08	2.8E–08	1.7E–09
	–650 to –1,000	0.005	3.7E–09	1.4E–11	1.9E–11
HRD_C	50 to –150	0.564	3.33E–08	2.1E–07	1.9E–08
	–150 to –400	0.164	1.1E–08	2.4E–08	1.8E–09
	–400 to –650	0.107	8.5E–09	3.4E–09	9.1E–10
	–650 to –1,000	0.008	2.3E–08	5.5E–10	1.8E–10

6.4 Hydraulic soil domains (HSD)

The Quaternary deposits model consisting of 6 layers (Z1–Z6), cf. Section 4.3.2, was provided as a soil type indicator, horizon depth for the bottom of each layer, and the total Quaternary deposits thickness on a grid resolution for the data of 20×20 m. This detailed model was simplified in the regional groundwater flow modelling representing it by four element layers vertically, each of a constant 1 m thickness, with the horizontal extent of the hydrogeological grid element (40–120 m), to represent the HSD. The same hydraulic conductivity tensor was specified for each element in a vertical stack of 4 grid elements, but varied horizontally from element-to-element, and was anisotropic with regard to horizontal and vertical components in order to represent the effective hydraulic properties of the Quaternary deposit layers. The calibration indicated that it was considered appropriate to generally decrease the vertical hydraulic conductivities to 1/10 of the originally suggested values (isotropic), to enable reproduction of the head differences between the soil and the near-surface bedrock. To reproduce the drawdowns on mainland Laxemar-Simpevarp resulting from pumping in the Äspö HRL facility, it was necessary to use Gyttja clay soil type in the bays around Äspö HRL with a vertical hydraulic conductivity $5 \cdot 10^{-9}$ m/s. HSD properties are described in Table 6-2 and illustrated in Figure 6-16. See /Rhén et al. 2009/ for details of the implementation.

Table 6-2. Prescription for hydrogeological properties of soil property domains used in the hydrogeological modelling. The relation to the model and description of the Quaternary deposits /Nyman et al. 2008, Sohlenius and Hedenström 2008, Werner et al. 2008/ is given in the second column. The modifications relative to the initial HSD assignments are highlighted in bold font, with main change to introduce anisotropy. Porosity is derived from specific yield /Werner et al. 2008/.

Hydraulic soil property domain	QD type and layer applied to	*K* (m/s)	Porosity
Surface affected layer	Soil > 5 m thick: QD type: 1, 2, 5, 6, 7, 9, 13, 16, 17, 18, 20, 22, 24, 25, 26, 27 Layer Z1 Domain 2–24 Layer Z6	**$K_h = 8 \cdot 10^{-4}$** **K_h/K_v = 10:1** Original: $4 \cdot 10^{-4}$	0.15
Peat	QD type: 11, 12 Layer Z2	$K_h = 3 \cdot 10^{-6}$ **K_h/K_v = 10:1**	0.24
Glacial clay	QD type: 6, 8, 9, 10, 12 Layer Z3	$K_h = 1 \cdot 10^{-7}$ **K_h/K_v = 10:1**	0.03
Postglacial sand/gravel	QD type: 6, 7, 8, 9, 10, 12 13, 14, 15, 16, 20, 23, 24, 25, 26 Layer Z4	$K_h = 5 \cdot 10^{-3}$ **K_h/K_v = 10:1**	0.25
Glacial clay	QD type: 6, 8, 9, 10, 12, 13, 14, 15, 16, 17, 18, 19, 20, 21, 22, 23, 24 Layer Z5	$K_h = 1 \cdot 10^{-8}$ **K_h/K_v = 2:1**	0.03
Till	Soil < 5 m thick: QD type: 1, 2, 5, 6, 7, 9, 13, 16, 17, 18, 20, 22, 24, 25, 26, 27 Layer Z1 Domain 2–24 Layer Z6	$K_h = 4 \cdot 10^{-5}$ **K_h/K_v = 10:1**	0.05
Surface affected peat	QD type: 3.8, 21, 23 Layer Z1	$K_h = 3 \cdot 10^{-6}$ **K_h/K_v = 10:1**	0.24
Surface affected shingle	QD type: 4 Layer Z1	$K_h = 1 \cdot 10^{-2}$ **K_h/K_v = 10:1**	0.25
Surface affected sand	QD type: 10, 15 Layer Z1	$K_h = 1 \cdot 10^{-2}$ **K_h/K_v = 10:1**	0.25
Gyttja	QD type: 7 Layer Z3	$K_h = 1 \cdot 10^{-8}$ **K_h/K_v = 2:1**	0.03
Postglacial fine sand	QD type: 17 Layer Z4	$K_h = 5 \cdot 10^{-4}$ **K_h/K_v = 10:1**	0.25
Postglacial sand	Domain 18, 19 Layer Z4	$K_h = 1 \cdot 10^{-3}$ **K_{hh}/K_v = 10:1**	0.25
Postglacial gravel	QD type: 21, 22 Layer Z4	$K_h = 1 \cdot 10^{-2}$ **K_h/K_v = 10:1**	0.25
Artificial fill	QD type: 27 Layer Z4	$K_h = 4 \cdot 10^{-5}$ **K_h/K_v = 10:1**	0.05

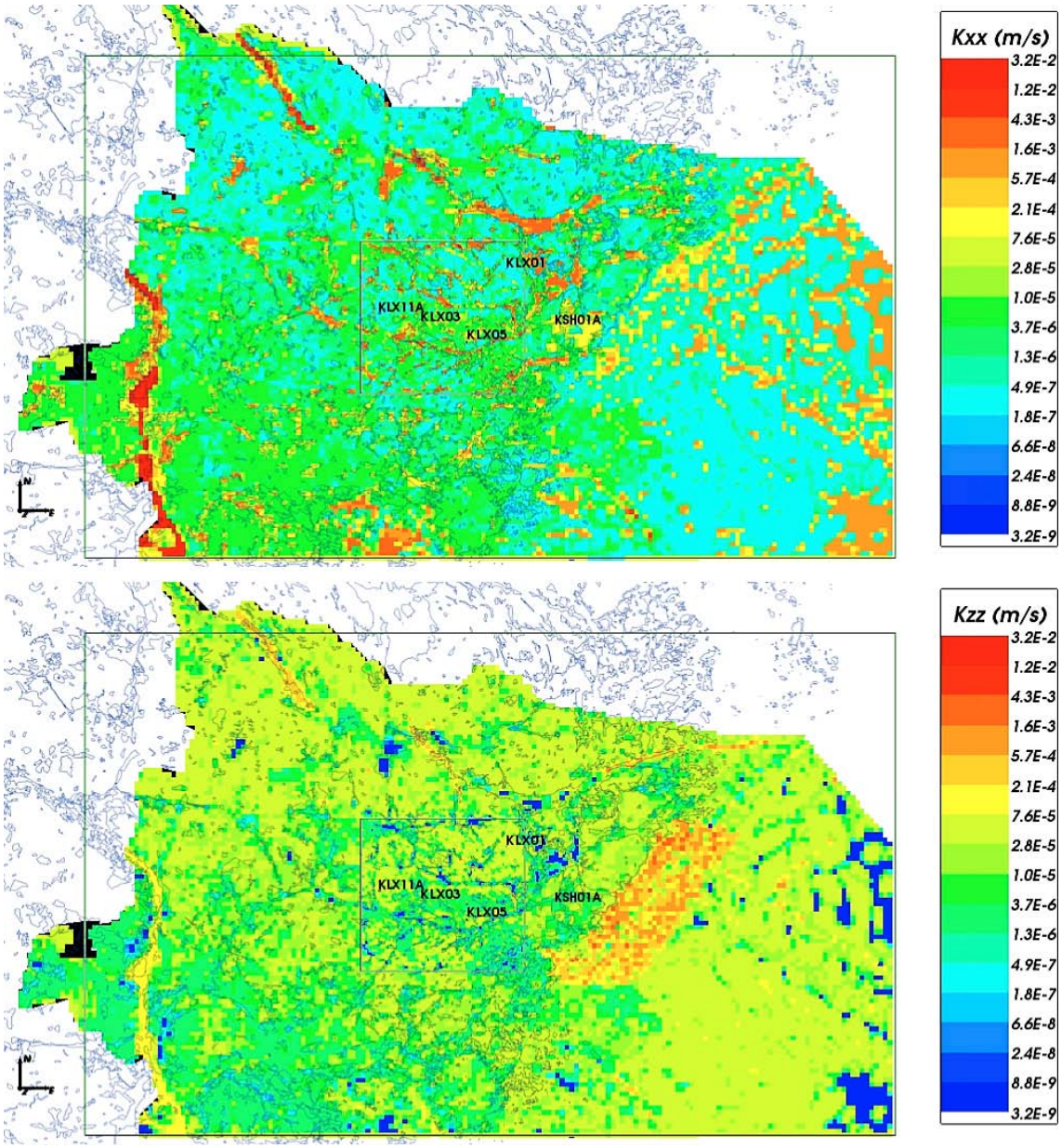

Figure 6-16. *Resulting effective hydraulic conductivity for HSD top layer based on layer thicknesses and hydraulic properties of the Quaternary deposits. Top: E-W horizontal component; Bottom: vertical component.*

6.5 Groundwater flow boundary conditions

For the area under the sea, it is most natural and convenient to use a specified head type boundary condition, where the head is equal to the depth of the sea multiplied by $(\rho_s-\rho_0)/\rho_0$, where ρ_s is density of the Baltic Sea and ρ_0 is fresh water density.

On land the recharge flux, R, into or out of the model is defined as a function of the current head, h, in the model, the topographic surface elevation, z, and the maximum potential groundwater recharge, R_p. The potential groundwater recharge to the saturated zone is equal to the precipitation (P) minus evapotranspiration (E) and overland flow and flow through the unsaturated zone (Q_s) ($R_p=P-E-Q_s$). It should be noted that in this model any groundwater that discharges through the top surface exits the model and does not enter a separate surface model that allows recharge further downstream.

When simulating the palaeohydrogeology over the last 10,000 years, transient variations in surface boundary conditions have to be considered both due to changes in shoreline displacement and salinity of the Littorina/Baltic sea. For an overview of assumed boundary conditions cf. Sections 2.3.8 and 5.2.1, and for details on the implementation of the boundary conditions cf. /Rhén et al. 2009/.

6.6 Palaeohydrogeology and hydrogeochemistry

The transient evolution of the chemical composition of surface waters infiltrating the bedrock over approximately the last 10,000 years offers a series of natural tracers that have entered the groundwater system and are mixed with the pre-existing groundwater. A conceptual model for the evolution of the chemistry of surface waters and groundwaters has been developed by the ChemNet group /Laaksoharju et al. 2009/ in terms of the chemical composition and mixing of different reference waters (see also Section 4.5.3). This is implemented in a 3D transient coupled groundwater flow and solute transport model to simulate the mixing of the different reference waters to give a prediction of the present-day distribution of groundwater chemistry for calibration against analysed groundwater samples from packed-off borehole sections.

6.6.1 Solute boundary conditions

The boundary conditions for solutes, here formulated in terms of mass fractions of reference waters, must represent the plausible evolution of groundwater composition on the upper surface of the model, which mainly vary as a consequence of changes in shoreline displacement due to post-glacial rebound and the variations in the salinity of the Baltic Sea, cf. Figure 6-17 and in /Rhén et al. 2009, cf. Section 7.8.2 therein/.

6.6.2 Initial conditions

The initial hydrochemical condition at 8000 BC is by its nature uncertain. Nevertheless in order to perform numerical modelling it is necessary to make an informed guess of appropriate initial hydrochemical conditions, and consider suitable variants to quantify the sensitivity to the speculation made, which is discussed in /Rhén et al. 2009, cf. Section 7.8.3 therein/.

Two alternative initial conditions were tested for the fracture water, cf. Figure 6-18. The profile of the initial condition in the matrix porewater varies both with depth and distance from the nearest conductive fracture, i.e. distance in to the matrix block, cf. /Rhén et al. 2009, cf. Section 7.8.3 therein/. The variation with distance in to the matrix block is calculated by assuming distinct initial compositions in the fracture water and in the pore water at a point furthest in to the matrix block, and then allowing a diffusive equilibration in the matrix over a suitable period, with 5,000 years being used in the base case.

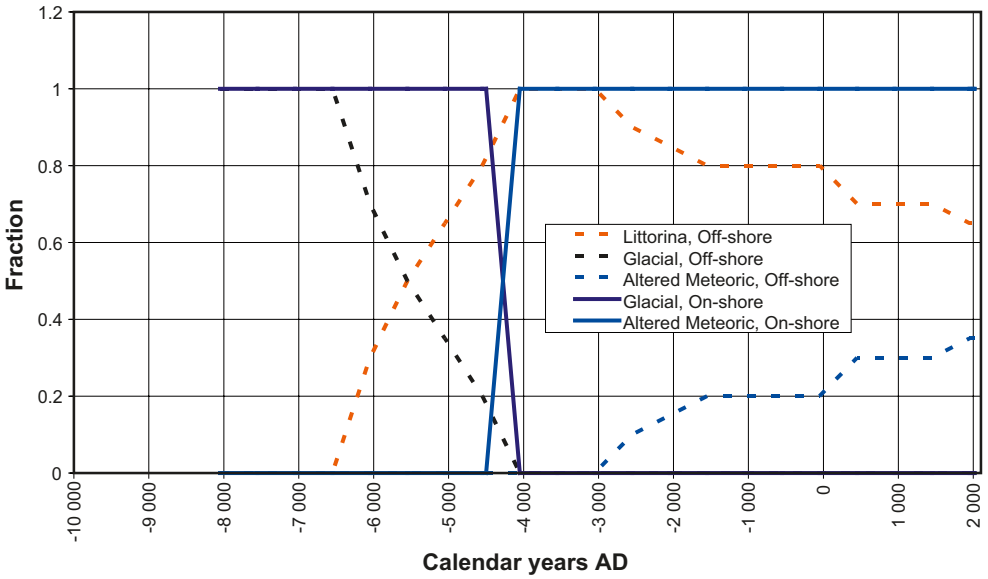

Figure 6-17. *A sketch of the assumed transient hydrogeochemical boundary conditions on the top surface of the hydrogeological model. For off-shore parts of the model, i.e. below the shoreline z < z0(t), the dashed curves show the mixture of Glacial Melt Water, Littorina Sea Water and Altered Meteoric Water. For the on-shore parts of the model, i.e. above the shoreline z > z0(t), the solid curves show the mixture of Glacial Melt Water and Altered Meteoric Water.*

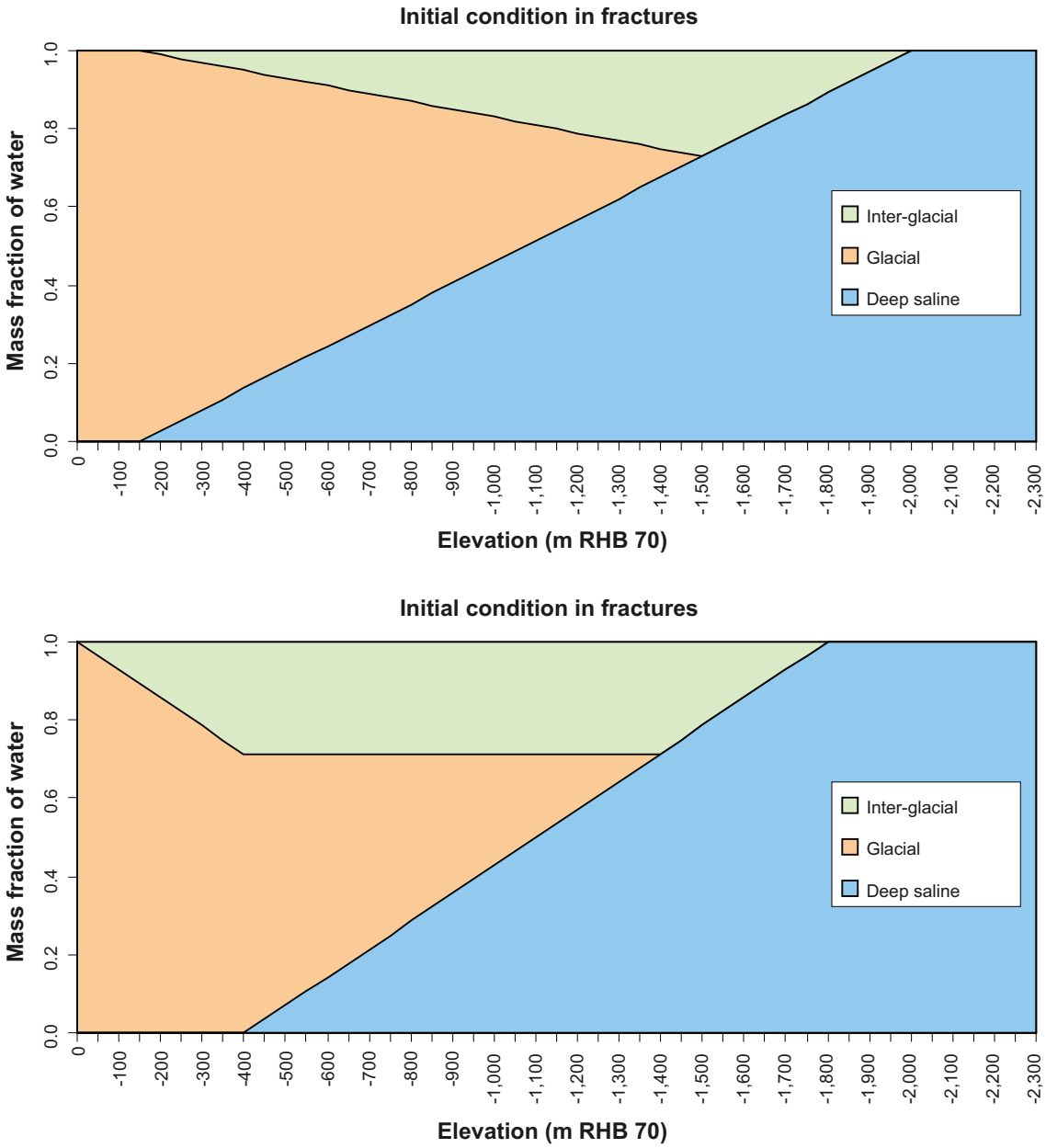

Figure 6-18. *The 2 alternative initial conditions at 8000 BC tested for the fracture water: Case 1 (top, used as base case), Case 2 (bottom).*

7 Regional scale flow model calibration

This chapter presents the results of confirmatory tests of the groundwater flow model against measurements of groundwater levels, pressures and drawdowns from a variety of different hydraulic tests as described in Chapter 4. The chapter also presents the results of confirmatory tests of the groundwater flow and solute transport model based on the concepts described in Chapters 5 and 6 against measurements of hydrogeochemistry data as described in Chapter 4. The comparisons made are based on the results of simulations performed using the calibrated *base case model* as specified in Chapter 6, cf. /Rhén et al. 2009/ for details.

7.1 Matching natural groundwater levels

Groundwater levels measured in open boreholes are available for the upper bedrock and Quaternary deposits to help confirm appropriate boundary conditions and hydraulic properties for the near-surface hydrogeology. In addition, groundwater levels in deep, core-drilled boreholes are also available for comparisons. Since salinity increases with depth, so does the groundwater density. The groundwater levels measured in deep boreholes are therefore conceived to represent point-water heads due to installation procedures, cf. /Rhén et al. 2009/. However, in order to understand vertical head gradients in a variable-density groundwater flow system, measured groundwater levels (point-water heads) must be transformed to environmental heads, i.e. the buoyancy term due to groundwater density variations is removed, so that vertical flows are linearly proportional to the environmental head gradient.

As discussed in Section 4.4.2, there are some uncertainties as to whether the correct density adjustments have been possible to estimate for the data transformation from point-water heads to environmental water heads, and hence the simulated point-water head is plotted in addition to the environmental head to quantify the likely maximum possible error in calculating the measured environmental heads. This uncertainty is mainly present below about –400 m, and becomes very significant below about –800 m, and therefore the comparisons are truncated at this lowermost depth. Details on the methodology and strategy for the employment of point-water heads and environmental water heads in the model calibration are provided by /Rhén et al. 2008/.

7.1.1 Calibration steps

Initial simulations used the parameterisation of HCDs and HRDs suggested in /Rhén et al. 2008/ although gradually adjusted toward the *base case* described in Chapter 6. Since the heads in the deep boreholes are dependent on the salinity distribution, the calibration on heads and palaeohydrogeology (see Section 7.4) were largely performed in parallel, although it was possible to make some scoping calculations of effects of the HSD without performing repetitive palaeohydrogeological simulations. The main changes made to the hydrogeological model guided by the head data were to:

1. Increase the transmissivity of HCD ZSMEW007A;
2. Introduce anisotropy 1:0.01 (longitudinal: transverse) in HCD ZSMEW002A;
3. Use anisotropy of 1:0.0001 (longitudinal:transverse) in the dolerite dykes associated with HCD ZSMNS001A–E, ZSMNS059A and KLX19DZ5–8;
4. Introduce anisotropy of 1:0.1 (horizontal: vertical) in the HSD (except Gyttja clay, which uses 1:0.5).

Change 1) was necessary to lower predicted heads in and around HCD ZSMEW007A. Change 2) was necessary to produce the large drop in head at around –300 m across HCD ZSMEW002A. Change 3) was made to sustain elevated heads in the south of HRD_W around HLX28. Change 4) was made to bring groundwater levels close to the topographic surface in the HSD as generally indicated by the data.

7.1.2 Resulting calibration

An example of the matching of the point water heads is shown here for HLX boreholes in Figure 7-1 and for SSM boreholes in Figure 7-2 for the *base case* model. Lines indicating the elevation of the topographic surface and the elevation of the soil/bedrock contact are shown for reference.

The simulations predict a distribution of heads for HLX boreholes that is in reasonable agreement with the distribution in the data, i.e. predicted heads are generally within the measured seasonal variations. The general pattern of behaviours is consistent.

For the *base case model*, the average head difference for HLX boreholes is 0.32 m within the Laxemar local scale model area, implying a slight overall over-prediction of the head, and the average absolute difference is 1.17 m. This should be compared with the average seasonal variation of 1.85 m (i.e. average max.–min. measured head) for the HLX measurements.

For the SSM groundwater monitoring wells, the predicted heads largely follow topography as for the measurements. For the *base case model*, the average head difference for SSM holes is 0.35 m within the Laxemar local scale model area, implying a slight overall over-prediction of the head, and the average absolute difference is 0.98 m. This should be compared with the average seasonal variations of 1.57 m (i.e. average max.–min. measured head) for the SSM measurements. It may be seen that the head exceeds the topographic height of the ground surface at some locations. This is an issue of grid resolution, 40 m is used.

Most of the core drilled boreholes in the Laxemar subarea display a gradual decrease in environmental head with depth, i.e. recharge conditions, as exemplified by the data and simulations of KLX10 and KLX12A in Figure 7-3 for the *base case*. A full set of KLX borehole comparisons is included in /Rhén et al. 2009/. These boreholes are situated in the Laxemar focused area, involving HRD_C and HRD_EW007. The measurements of lower environmental head in KLX10 illustrate the occasional sudden drop in measured environmental head at about –650 m associated with uncertainty in correcting the data for measured groundwater density. The magnitude of uncertainty is consistent with the difference between the simulated environmental and point-water heads. Figure 7-4 gives examples of the environmental heads in KLX11A and KLX21B, both within HRD_W. The gradual decrease in environmental head with depth is reproduced; although with a higher gradient around –100 m in KLX11A, probably associated with the transmissivity of the subhorizontal HLX28_DZ1 minor deformation zone, being slightly under-predicted by the model. The environmental head predicted in the upper 400 m of KLX21B seems acceptable, and the sudden drop in environmental head below –400 m may result from the density correction, as it is predicted by the point-water head deviation. The mean difference between modelled and measured environmental head over all borehole packer intervals is calculated at 0.41 m and a mean absolute difference of 2.04 m, compared with an average seasonal variation of 1.21 m (i.e. average max.–min. measured head).

The horizontal and vertical extent of flow cells can in part be interpreted from visualising contours of environmental water head on several vertical slices as shown in Figure 7-5. Several flow cells with variations in environmental water head of about 6–10 m, often delimited by HCD, can be seen within the Simpevarp subarea that typically extend about 1–2 km horizontally and about 600–1,000 m vertically, possibly getting deeper toward the west. This suggests the presence of several local flow cells within Simpevarp subarea rather than a single west to east regional flow cell.

Table 7-1 presents the arithmetic average discharge and recharge through a series of surfaces at different depths below the ground surface topography of the local model area extended to also cover the Simpevarp subarea, as extracted from the SDM-Site Laxemar base case model groundwater flow simulation. The Darcy velocity is also illustrated in a vertical section in Figure 7-17. The average recharge is based on the downward flow rate at 2000 AD divided by that part of the extended local model area (as defined above) for which flow is downward at each depth. Correspondingly, the average discharge is based on the upward flow rate divided by the area over which flow is upward at each depth. The Darcy velocities are based on the velocity components in each element, sorted on HCDs and HRDs. The bulk bedrock Darcy velocity in the near surface bedrock between deformation zones at a depth of 20 m is in the order of 60 mm/year where the corresponding velocity at repository depth is 0.16 mm/year, i.e. about a factor 380 lower. At repository depth (500 m) the Darcy velocity in HCD is about 0.6 mm/year, which is 4 times higher than in the HRD at the corresponding depth.

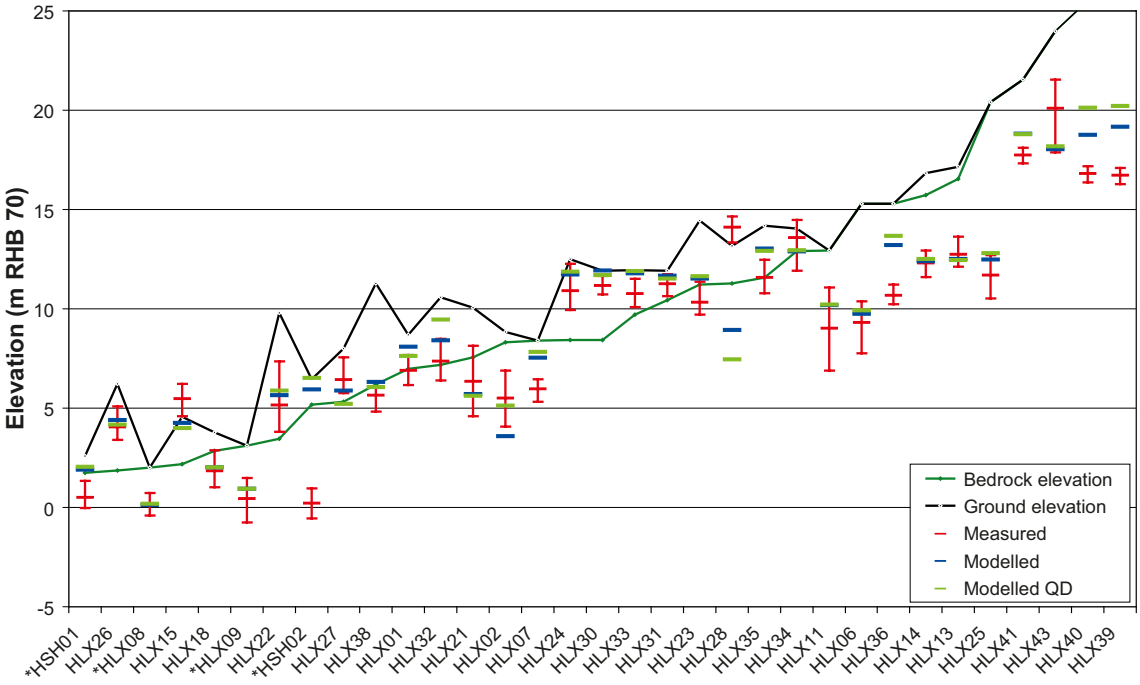

Figure 7-1. *Comparison of measured heads in percussion-drilled boreholes (HLX) with results of the base case model. For the model, values are given for the Quaternary deposits and at the mid elevation of the borehole section in the bedrock. The field data are plotted as mean point water heads in the bedrock with error bars to show the range of values at different measurement times. Boreholes marked by a * (bottom of figure) are outside the local model area.*

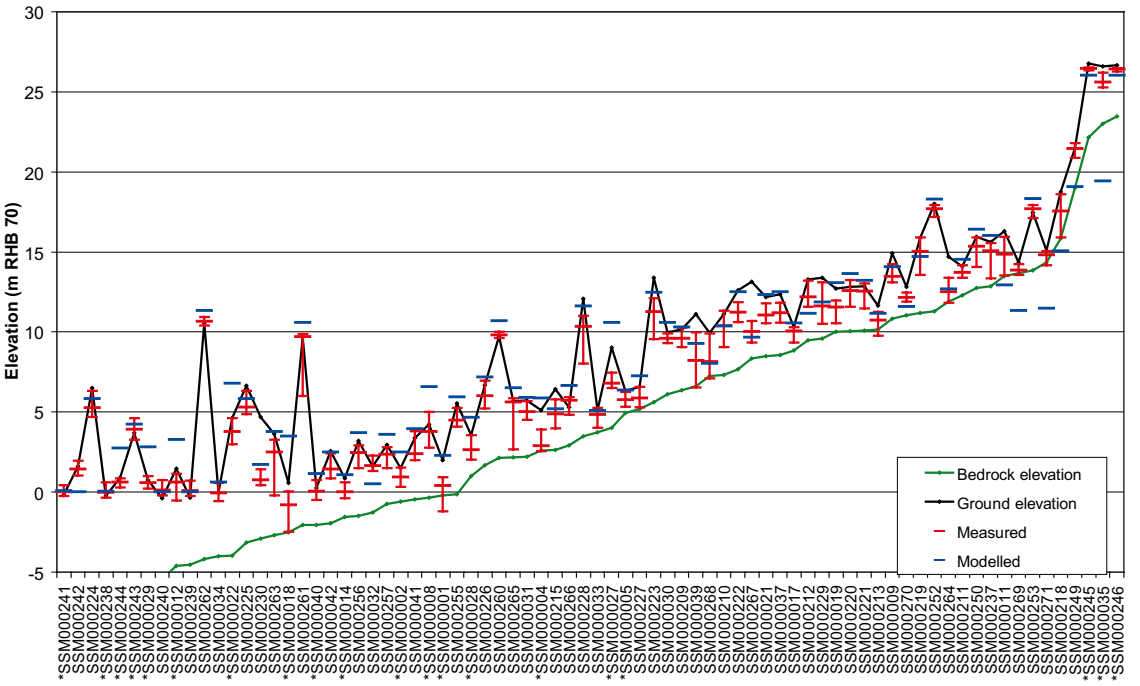

Figure 7-2. *Comparison of measured heads in groundwater monitoring wells (SSM) with the results of the base case model. For the model, values are given for the QD only. The field data are plotted as mean point water heads in the soil with error bars to show the range of values at different measurement times. Boreholes are ordered by bedrock elevation at the borehole collar. Boreholes marked by a * (bottom of figure) are outside the Laxemar local model area.*

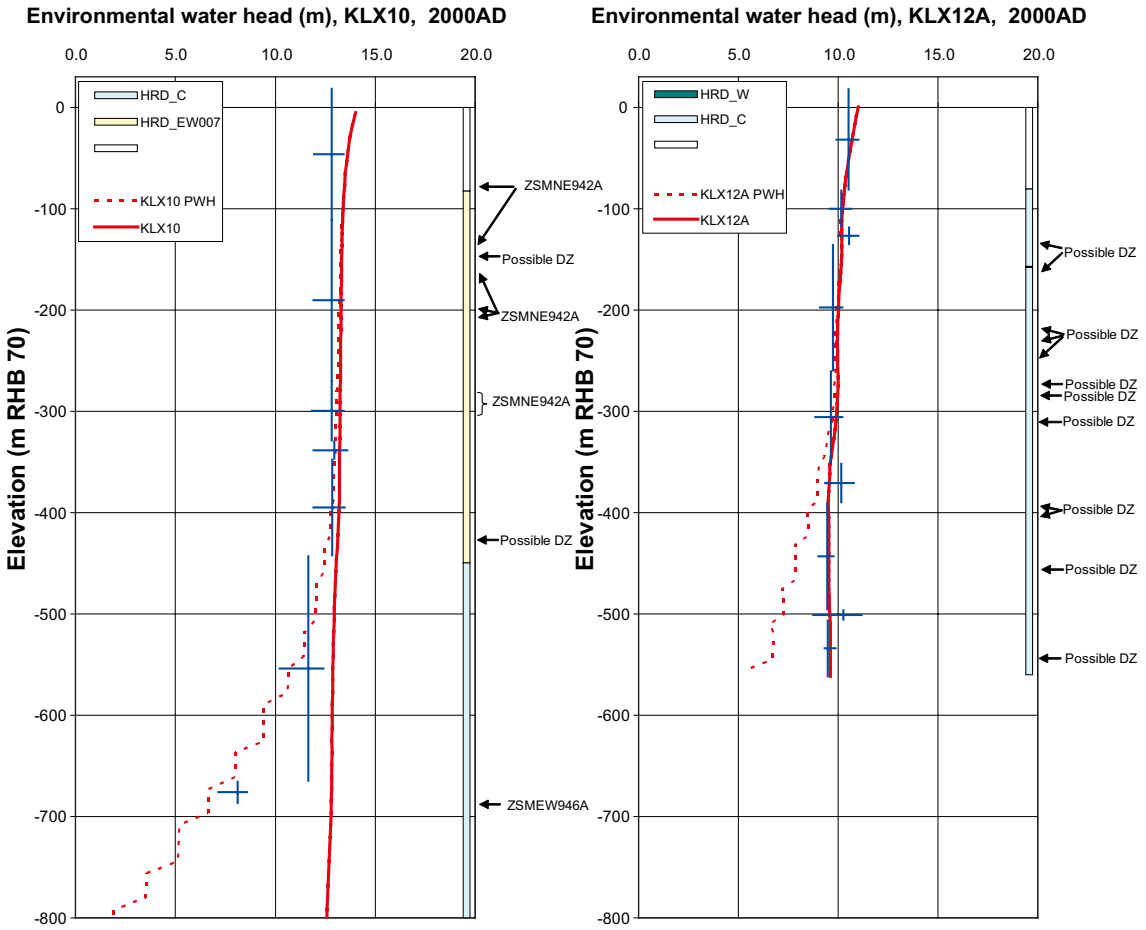

Figure 7-3. *Examples of modelled environmental-water head (solid red line) and point-water head (dotted red line) in KLX10 and KLX12A in HRD_C for the base case compared with environmental-water heads (blue crossed lines; centre showing midpoint of the section, vertical line showing the extent of the section and horizontal line showing the temporal variation of the measured head) calculated from measured point-water head data in sections along the borehole. At the right hand side, the hydraulic rock domains are shown as coloured bars along the borehole. Interpreted deformation zones are indicated at their intersection depth in the borehole.*

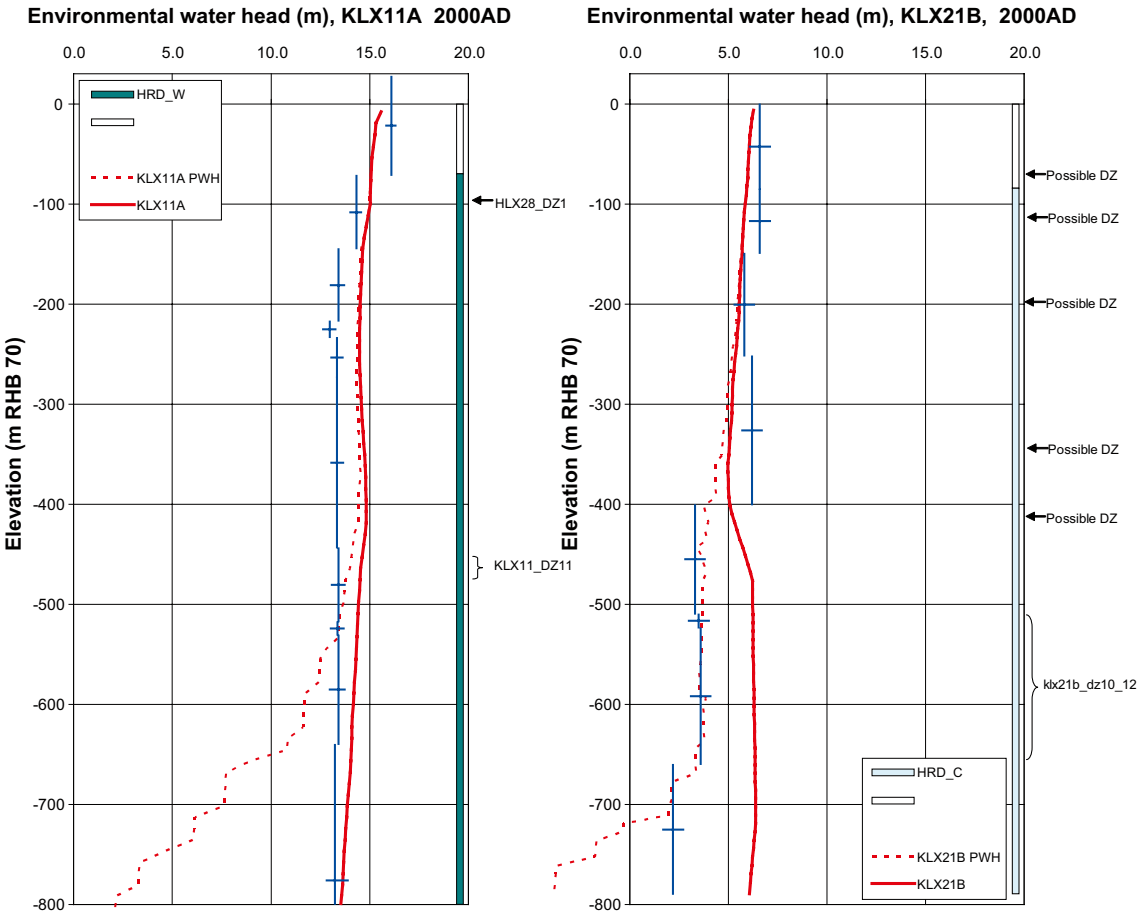

Figure 7-4. *Examples of modelled environmental-water head (solid red line) and point-water head (dotted red line) in KLX11A and KLX21B in HRD_W for the base case compared with environmental-water heads (blue crossed lines; centre showing midpoint of the section, vertical line showing the extent of the section and horizontal line showing the temporal variation of the measured head) calculated from measured point-water head data in sections along the borehole. At the right hand side, the prevailing hydraulic rock domains are shown as coloured bars along the borehole. Interpreted deformation zones are indicated at their intersection depth in the borehole.*

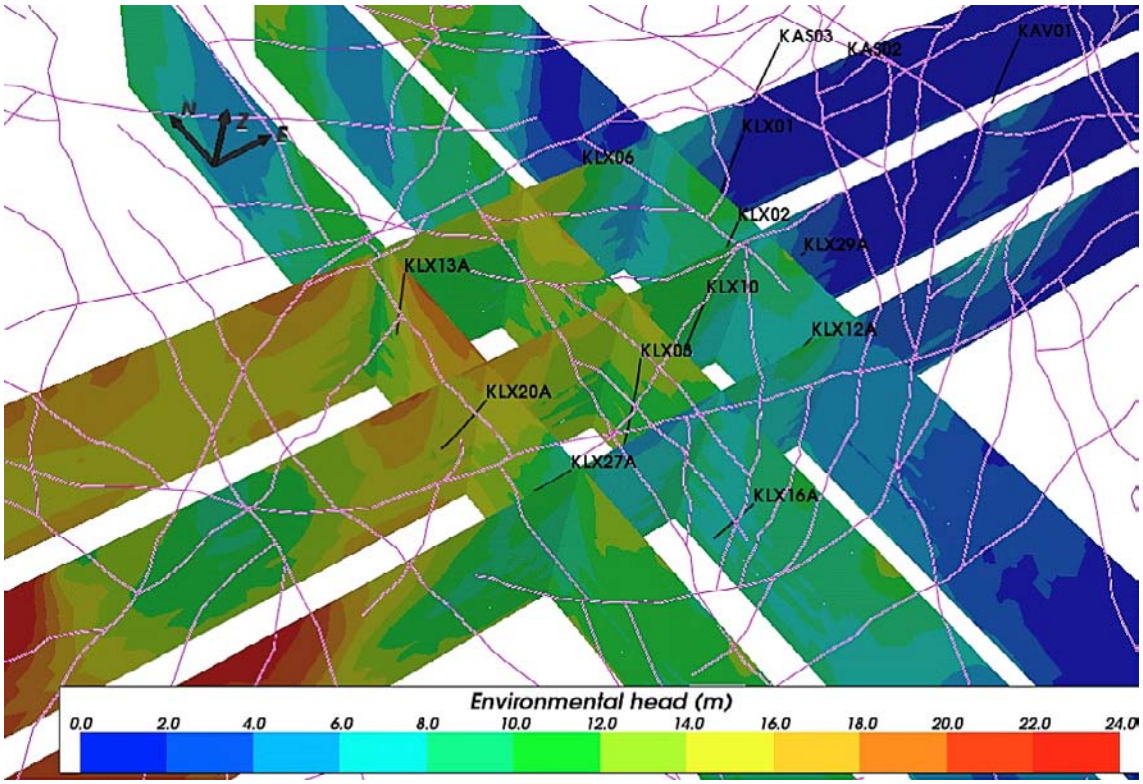

Figure 7-5. *Distribution of environmental water head on three E-W slices and three N-S slices (see Appendix 3 for locations of slices). The slices extend down to an elevation of –1,500 m. The position of the HCD on the top surface (purple) and selected cored boreholes are superimposed.*

Table 7-1. Summary of arithmetic average upward flow (discharge) and downward flow (recharge) at different depth below the ground surface in the Laxemar 1.2 local model area, cf. Figure 1-6, as extracted from the SDM-Site Laxemar *base case model* groundwater flow simulation. The geometric means of the magnitude of the Darcy velocity vector for points in each plane are given for the entire bedrock, outside of the deformation zones, and inside the deformation zones.

Vertical depth below ground surface [m]	Average upward flow in discharge areas [m/year]	Average downward flow in recharge areas [m/year]	Geometric mean Darcy velocity [m/year]	Geometric mean Darcy velocity outside deformation zones [m/year]	Geometric mean Darcy velocity in deformation zones [m/year]
–1	$4.96 \cdot 10^{-2}$	$1.86 \cdot 10^{-1}$	$1.3 \cdot 10^{0}$	$9.7 \cdot 10^{-1}$	N/A
–20	$4.38 \cdot 10^{-2}$	$4.57 \cdot 10^{-2}$	$6.6 \cdot 10^{-2}$	$5.8 \cdot 10^{-2}$	$8.8 \cdot 10^{-2}$
–100	$2.21 \cdot 10^{-2}$	$2.35 \cdot 10^{-2}$	$4.5 \cdot 10^{-2}$	$3.7 \cdot 10^{-2}$	$6.2 \cdot 10^{-2}$
–180	$6.93 \cdot 10^{-3}$	$6.52 \cdot 10^{-3}$	$6.1 \cdot 10^{-3}$	$4.2 \cdot 10^{-3}$	$1.2 \cdot 10^{-2}$
–340	$1.82 \cdot 10^{-3}$	$1.95 \cdot 10^{-3}$	$1.7 \cdot 10^{-3}$	$1.0 \cdot 10^{-3}$	$4.0 \cdot 10^{-3}$
–500	$3.21 \cdot 10^{-4}$	$3.15 \cdot 10^{-4}$	$2.9 \cdot 10^{-4}$	$1.6 \cdot 10^{-4}$	$6.4 \cdot 10^{-4}$
–660	$8.36 \cdot 10^{-5}$	$9.37 \cdot 10^{-5}$	$5.5 \cdot 10^{-5}$	$2.6 \cdot 10^{-5}$	$1.5 \cdot 10^{-4}$
–780	$4.10 \cdot 10^{-5}$	$4.02 \cdot 10^{-5}$	$1.4 \cdot 10^{-5}$	$8.5 \cdot 10^{-6}$	$2.8 \cdot 10^{-5}$

7.2 Matching the drawdown due to inflow to Äspö hard rock laboratory (HRL)

The calibration of the groundwater flow model, against the measured drawdowns in percussion-drilled monitoring boreholes surrounding the Äspö HRL and the measured inflows to the tunnels and shafts is largely a repetition of one of the pre-modelling exercises reported in /Hartley et al. 2007/. The inflow rates to Äspö HRL vary over time and the maximum measured inflow was 1,900 m^3/s in 1994. This time-dependent flow-rate was included in the calibration of the flow model. /Hartley et al. 2007 concluded that the measured drawdowns could be reproduced provided the Quaternary deposits in the bays around Äspö were of gyttja clay type so as to reduce recharge from the sea bed since this would otherwise restrict the zone of influence of pumping on the Laxemar-Simpevarp mainland. Another significant finding was that the operation of the Äspö HRL facility has had little effect on the natural hydrochemistry measured in the Laxemar subarea, and hence it was not necessary to include pumping at the Äspö HRL in the palaeohydrogeology simulations reported in Section 7.4.

The SDM-Site Laxemar model of the HSD has largely gyttja clay type sediments in the bays around Äspö, but there are a few gaps. It was found necessary to modify all the remaining HSD on the seabed to use gyttja clay type in the bays around the Äspö HRL to confine the upper bedrock for sea water infiltration. This was done in a square of side 2 km centred on the bay south of Äspö. Possibly this is just a consequence of using a coarser grid, 40 m, rather than the 20 m grid used to define the Quaternary deposits model. A vertical hydraulic conductivity of $5 \cdot 10^{-9}$ m/s for gyttja clay was chosen for the *base case model*. The comparison is broadly consistent in that small drawdowns are predicted in the boreholes where no response was seen in the measurements, and responses in the Laxemar local model area are predicted to occur at HLX08 and HLX09. The effect of the Äspö HRL on head and groundwater velocities at 2004 AD is demonstrated on horizontal slices at–450 m in Figure 7-6 through Figure 7-7. At depth the changes in Darcy velocity are highest in the HCD. At shallower depths effects on Darcy velocity only extend as far as HLX08 and HLX09 in the Laxemar local model area apart from the eastern end of HCD ZSMEW007A (see Figure 7-7).

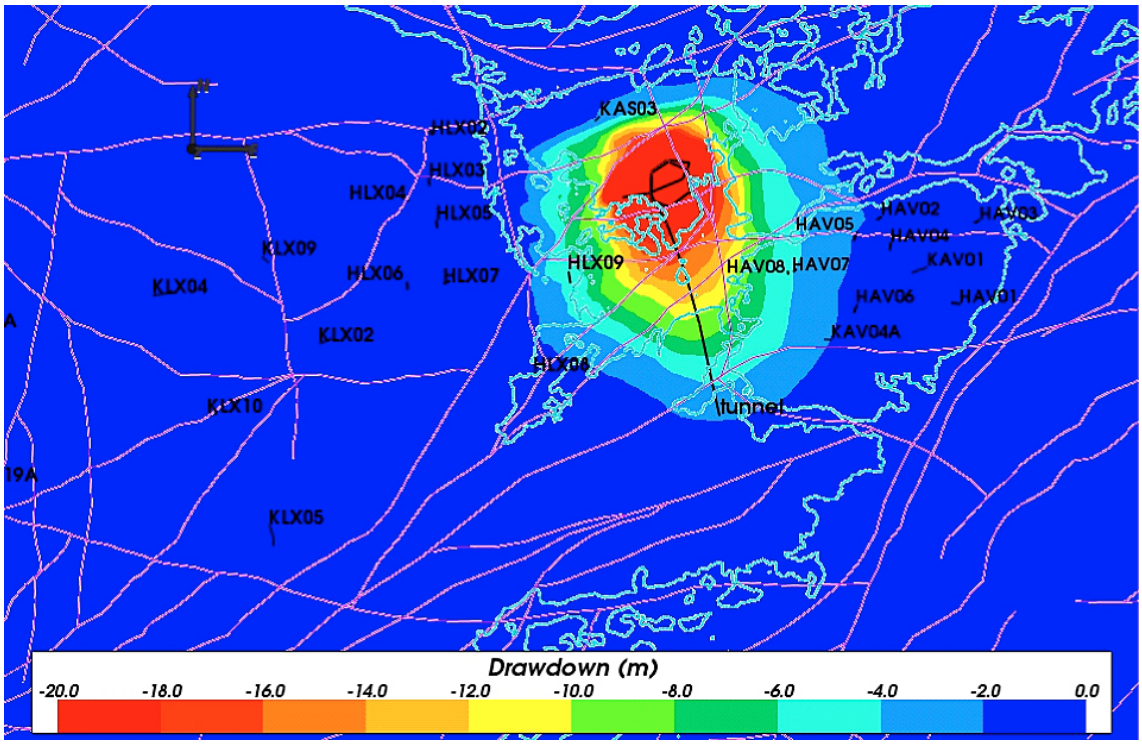

Figure 7-6. *The simulated drawdown resulting from groundwater extraction in the Äspö HRL for the base case model. The slice is shown for 2004 AD at –450 m elevation. The shoreline (cyan) and deformation zones (purple) on the top surface are superimposed.*

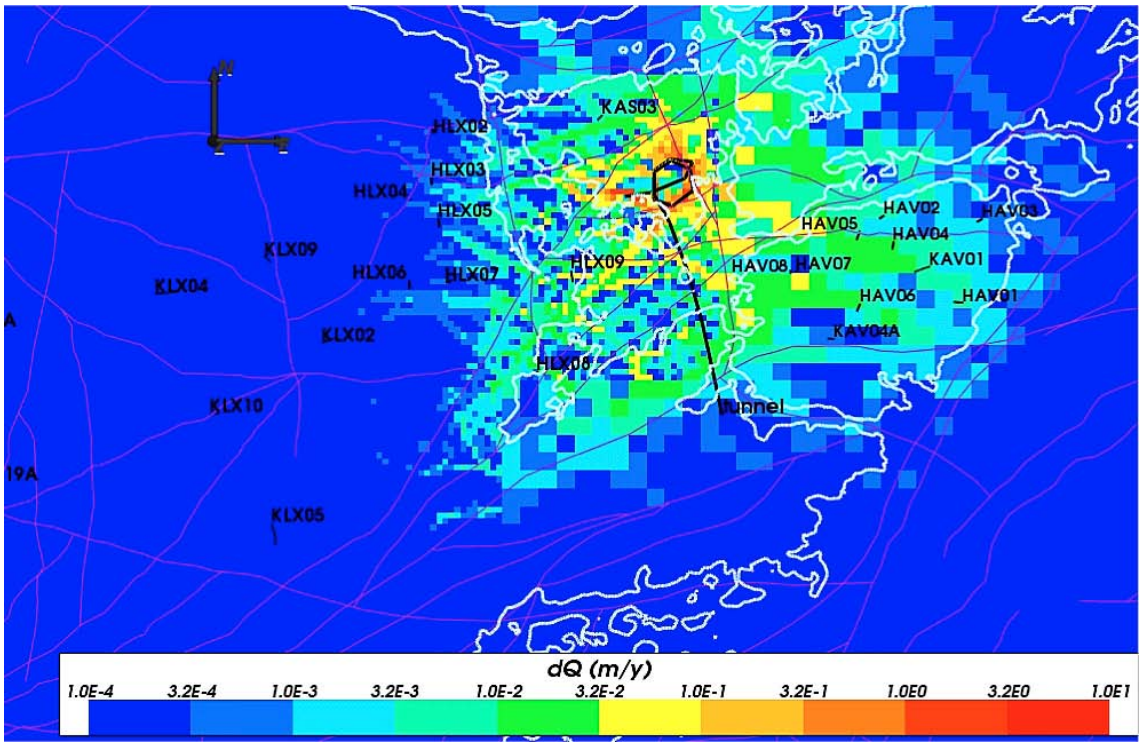

Figure 7-7. *The magnitude of difference in Darcy velocity between simulations with and without groundwater extraction in the Äspö HRL for the base case model. The slice is shown for 2004 AD at –450 m elevation. The shoreline (white) and deformation zones (purple) on the top surface are superimposed.*

In summary, the following conclusions can be drawn:

- A reasonable match to the observed drawdowns resulting from the Äspö HRL can be obtained by modifying the HSD on the seabed in the bays around Äspö to be of gyttja clay type with vertical hydraulic conductivity in the range 10^{-9} to 10^{-8} m/s, centred on $5 \cdot 10^{-9}$ m/s, and uncalibrated hydraulic conductivities for HRD_A2 (i.e. 3 times higher than the *base case model* between –150 m and –650 m elevation).
- The drawdowns in tunnels and shafts are mainly controlled by the hydraulic conductivities of HRD_A2. The drawdowns have a lesser but still significant dependence on HCD and HSD.
- The drawdowns in the percussion boreholes are mostly sensitive to the hydraulic conductivity of the HSD below the sea around Äspö.

The simulations of the drawdown resulting from the Äspö HRL suggest that measurements of point-water heads and hydrochemistry have not been significantly affected by the facility, apart from the far eastern part of Laxemar local model area.

7.3 Matching the interference tests in HLX33 and HLX28

7.3.1 HLX33

As described in Section 4.3.2, the interference test in HLX33 is dominated by responses in HCD ZSMNEW007A. The configuration is shown in Figure 4-6. It confirms the adjustments to the transmissivity of this zone for the *base case*, but introduces a strong constraint on the hydraulic properties of the HRD.

The drawdown responses to pumping in HLX33 are modest (up to a maximum of 1 m) and appear to vary quite predictably with distance from HLX33 since assignment of an appropriate value to the transmissivity of ZSMEW007A and assuming radial flow within this HCD seems sufficient to gain a

qualitative understanding of the hydraulic test. The main changes made in calibrating the *base case model* to match the HLX33 test were:

- An increase in the transmissivity of HCD ZSMEW007A in the top two depth zones by factors of 50 and 10 (see /Rhén et al. 2009, cf. Table 7-3 therein/), respectively, was required to obtain the right magnitude of drawdown in HLX33 and responses observed down to c. –300 m elevation in KLX04 and KLX02;
- Introduction of low specific storage coefficients of around 10^{-7} m^{-1} for the bedrock and 10^{-3} m^{-1} for the soil to obtain the correct timescales for transmitting the responses.

The storage coefficient above suggests a storativity of about 10^{-5} for ZSMEW007A, which is at the low end of values suggested by /Rhén et al. 2008, cf. Chapter 7 therein/, but within the range of values interpreted for HCD at Laxemar and Äspö.

The lowering of the hydraulic conductivity of HRD_EW007 by a factor 0.3 below –150 m used in the calibrated *base case* to match point-water heads resulted in a significantly increased drawdown which improved the calibration in boreholes KLX04 and KLX07A/B, while other increases were less beneficial at boreholes such as HLX25 and HLX30. Hence, the tightening of HRD_EW007 at depth suggested by point-water heads and palaeohydrogeology is only partially confirmed by the HLX33 interference test.

7.3.2 HLX28

The interference test in HLX28 is again dominated mainly by the HCD model. The configuration is shown in Figure 4-7. In this case, mainly the minor deformation zone HLX28_DZ1 is responsible for transmitting the response, while KLX19_DZ5–8 ZSMNS059A, ZSMNS001C and ZSMNW042A-west act to transmit the response longitudinally and inhibit it transversely. This confirms the barrier effect attributed to these zones. Some response in the HRD is seen in this test, but these are generally in the close vicinity of the HCD. That is, the HCD are responsible for the primary responses, and the background fractures distribute these responses slightly further. If the HRD were too hydraulically conductive, then the responses in the HCD would be reduced since the background rock would provide additional water flux to replenish that pumped. Preliminary tests suggest the hydraulic conductivity in the immediate vicinity of HLX28 is perhaps lower than interpreted in the hydrogeological DFN model for HRD_W.

Therefore, the underlying DFN model, without upscaling, was used directly to simulate the transient pumping in HLX28. It should be noted however that anisotropy of the dolerite dykes could not be implemented in the DFN model. As a result the model using the underlying DFN model directly tends to predict some responses propagating across ZSMNS001C and ZSMNS0059A via stochastic fractures crossing these two dolerite dykes. Still, by using a DFN model it was possible to simulate the correct levels of drawdown in the system even at large distance from HLX28. To achieve this it was necessary to modify the properties of 3 HCD from those used in the calibrated *base case* ECPM model as specified in Section 6.2 and /Rhén et al. 2009/. The changes were:

- A factor 4 increase in transmissivity of HCD HLX28_DZ1;
- A factor 3 increase in the transmissivity of HCD ZSMNW042A-west;
- A factor 3 increase in the transmissivity of HCD ZSMNS059A.

The storativity model used in these transient DFN calculations was based on a preliminary relationship $S=aT^b$, with a=0.001, and b=0.5. The relationship recommended in Chapter 7 of /Rhén et al. 2008/ has a=0.01 and b=0.71, which gives similar storativities for transmissivities around 10^{-5} m^2/s that are characteristic of the HCD in the superficial bedrock.

7.3.3 Comment in relation to outcome of LPT (HLX28)

A long-term pumping and tracer test (LPT) was started 20th January 2009 with borehole HLX28 as pumping borehole and HLX32:2, HLX37:1, HLX38:3, KLX11A:3, KLX20A:5, and KLX27:6 as tracer injection sections (KLXxx:Y, Y is the number of the packed-off observation sections), cf. Figure 4-7. The purpose of the test was to verify and shed light upon:

- HCD HLX28_DZ1 and its hydraulic contact with HCD ZSMNW042,
- ZSMNW042A and its hydraulic contact with ZSMNS001C and ZSMNS059A, respectively,
- The barrier effect coupled to the dolerite dykes ZSMNS001C and ZSMNS059A,
- The hydraulic contact between HRD and HLX28_DZ1 and ZSMNW042A.
- The approximate transport properties for HCD HLX28_DZ1 and ZSMNW042A and the indications for transport properties for the coupled system with ZSMNS001C and ZSMNS059A using tracer injections in packed-off borehole sections; HLX32:2, HLX37:1, HLX38:3, KLX11A:3, KLX20A:5 and KLX27:6, respectively.

The test was finished in May 2009 and only preliminary results are available for this report.

The pressure response was monitored in 257 borehole sections during the test within the Laxemar local model area. The responses in KLX20A and HLX37 after two months of pumping clearly demonstrated the barrier effect of ZSMNS001. Responses in KLX03 and KLX14A, although rather small in KLX03 and the two eastern-most sections in KLX14A, showed that ZSMNS059A is not a complete hydraulic barrier. The reason may be that, as the dyke is thin, it is locally permeable and/or that some deformation zones intersecting ZSMNS059A, e.g. ZSMNW042A, actually are not cross-cut by the dolerite dyke in such way that it prohibits pressure responses from being transmitted through the deformation zone. The responses south of ZSMNW042 in KLX27A are small, indicating that the suggested barrier effect attributed to fault gouge is a reasonable assessment. The response in KLX19A below the possible dolerite dyke, KLX19_DZ5–8 is small, as previously seen in other tests, and thus provides evidence for interpretation that this local zone acts as a barrier to flow across it.

7.4 Matching hydrochemical data in cored boreholes

The hydraulic parameters for the *base case* described in /Rhén et al. 2009, cf. Chapter 7 therein/ were arrived at based on the calibration on hydraulic tests as described in Sections 7.1 through 7.3. Hydrochemical data was then used as a series of natural tracer tests to check the consistency of the hydraulic parameters in the *base case model* and for examining the description of transport parameters and concepts for the palaeohydrogeological evolution. The calibration against hydrogeochemistry measurements involves the simulation of palaeohydrogeology in terms of the evolution of coupled solute transport and groundwater flow from 8000 BC to the present-day. The transport of solutes is modelled in terms of the infiltration and mixing of several different reference waters that are assumed to be transported conservatively, i.e. without reaction, but subject to advection, dispersion, and diffusive exchange between the fracture- and pore-waters (i.e. rock matrix diffusion). Groundwater flow is subject to buoyancy forces that arise due to variations in fluid density according to salinity, temperature, and total pressure. Variations in fluid viscosity with temperature, salinity and total pressure are also considered. The chemical compositions of the reference waters are fixed. Therefore, given the simulated mixture of references waters (defined by the mass fraction) at any point in space and time, the concentration of the major ions or environmental isotope ratios can be calculated. This is done by multiplying the reference water fraction by the concentration of the component in that reference water and then summing over the reference waters by which the predicted concentrations, or isotope ratios, can then be compared with data. The chemical composition is calculated both for the mobile water in the fractures and the immobile (no advection) porewater in the matrix. For simplicity, the simulated values for the porewater used for comparison purposes are essentially an average within the matrix blocks. The spatial variations of hydrochemistry within the porewater are likely to be large where the spacing between water conducting fractures becomes larger than about 10 m (i.e. when PFL-f intensity is below about 0.1 m^2/m^3) since the timescales for rock matrix diffusion into the matrix blocks are long, 10,000s years, compared to the timescales for changes in chemistry of infiltrating groundwater at the surface. In Laxemar this occurs in HRD_C below –400 m and in HRD_W below –150 m. Hence, it should be borne in mind that there may be trends within the porewater data according to where a sample was taken relative to water-bearing fracture locations that are as important as trends with respect to, for example, the absolute elevation of the sample. For further detailing of methodology and code-specific aspects, cf. /Rhén et al. 2009/.

7.4.1 Calibration steps

The calibration is assessed by comparing the predicted and measured profiles of major ions and environmental isotope ratios in the core-drilled boreholes grouped together according to HRD and general flow conditions (recharge or discharge areas), cf. /Rhén et al. 2009, cf. Section 5.6.1 therein/. Primarily, the predicted and measured profiles in the fracture system are compared, though comparisons are also made with the porewater data in the three boreholes (KLX03, KLX08 and KLX17A) where this information is available to better understand the role of rock matrix diffusion (RMD) on solute transport. The calibration process was based primarily on one single realisation of the HRD ECPM properties and deterministic properties for the HCD. Only once a satisfactory *base case* had been identified, the sensitivity of the calibration to the HRD realisation and spatial variability in the HCD were quantified. This sensitivity proves to be significant, as is demonstrated in Chapter 9, and so it is not appropriate to expect any single simulation to match all the data points. Instead, the ideal goal is to obtain a *base case* that approximates the data to within a margin that is consistent with variability between realisations of the HRD and HCD. Also, because of grid resolution the representation of hydraulic conditions near a borehole will be smeared out according to the grid size used, and so zones not seen in the actual borehole may affect the simulated borehole, and the effects of individual hydraulic features may be more discrete in reality than is possible to reproduce in the model. Therefore, it is important to look at the profiles of chemical constituents on vertical and horizontal sections as well as along borehole profiles to obtain an impression of the predicted groundwater chemistry in the neighbourhood of a calibration borehole in case the borehole just misses a simulated lens of glacial or brackish water, for example. Hence, the calibration process is a mixture of quantitative and qualitative comparisons.

The key calibration steps (to reach the parameterisation as defined by the *base case model*) in matching the hydrochemical data were:

- Reducing the transmissivity of each HCD by the factors specified in /Rhén et al. 2009, cf. Chapter 7 therein/;
- Increasing the kinematic porosity of HCD;
- Reducing the hydraulic conductivity of the HRD below –150 m by a multiplication factor 1/3;
- Increasing the kinematic porosity of the HRD by a multiplication factor 5 to compensate for the effects of truncating the fracture size distribution in the regional model;
- To use a physically based initial condition in the matrix porewater that varies according to distance from a flowing feature and allows for a difference in composition, mainly $\delta^{18}O$, in the porewater far from a flowing feature to that in fracture water.
- Use low values of the flow-wetted surface area per unit volume of rock, so as to maintain the difference in Cl and $\delta^{18}O$ between matrix and fracture water seen at some places in the bedrock. Modelling suggests values of $a_r < 0.2$ m^2/m^3 at depth, consistent with values suggested by the intensity of fractures detected by the PFL method, see /Rhén et al. 2009, cf. Chapter 7 therein/.

7.4.2 Resulting calibration

The quality of the calibration for the *base case model* is discussed in this subsection. It should be noted that the *base case* does not necessarily represent the best match to the hydrogeochemistry data that can be achieved. More it is a model that yields an acceptable match to data. Section 9.2 considers sensitivities of the palaeo-hydrogeological simulations and identifies changes that improve the match. However, it was considered that such changes would need further investigation and integration with other information before they could become definite modifications to the site-descriptive hydrogeological model.

Figure 7-8 and Figure 7-9 show the match between the simulated *base case* and measured salinity in the fracture system for eight groups of boreholes associated with different HRD and/or hydrological conditions. The agreement is reasonable with salinity (> 200 mg/l) starting to occur from –200 m to –400 m depending on borehole and gradually increasing with depth. The initial condition at 8000 BC is largely preserved below –600 m to –800 m, and hence the match could be improved simply by devising a more complex initial condition than the simple linear initial *Deep saline* distribution

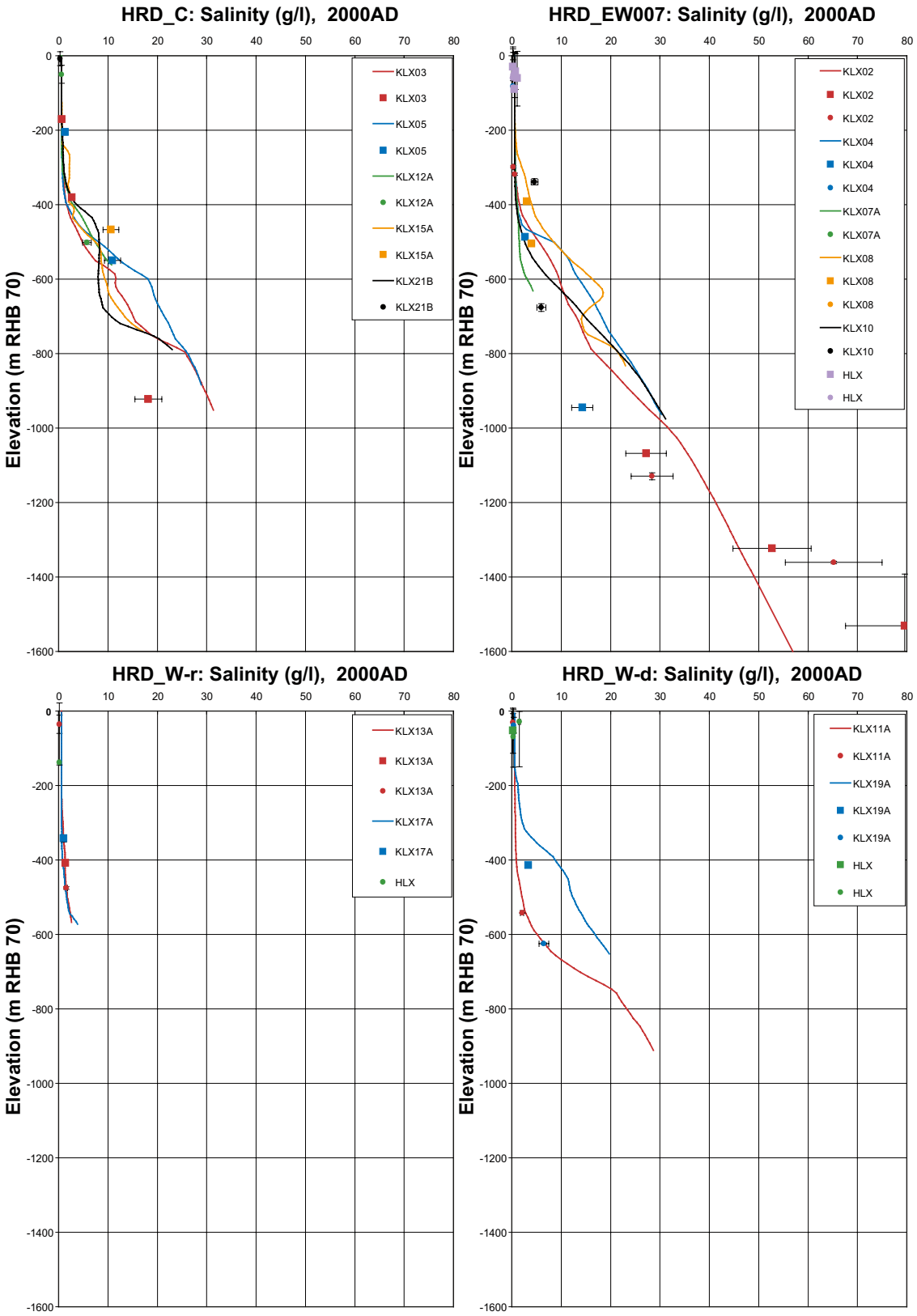

Figure 7-8. *Comparison of modelled and measured distributions of salinity (TDS) in fracture water for different groups of calibration boreholes. Square symbols are used for Category 1–3 data (Table 4-2), and small point symbols for the Category 4 data. The error bars on the data indicate the laboratory analytical error. The solid lines show the complete distribution in the borehole simulated in the fracture system.*

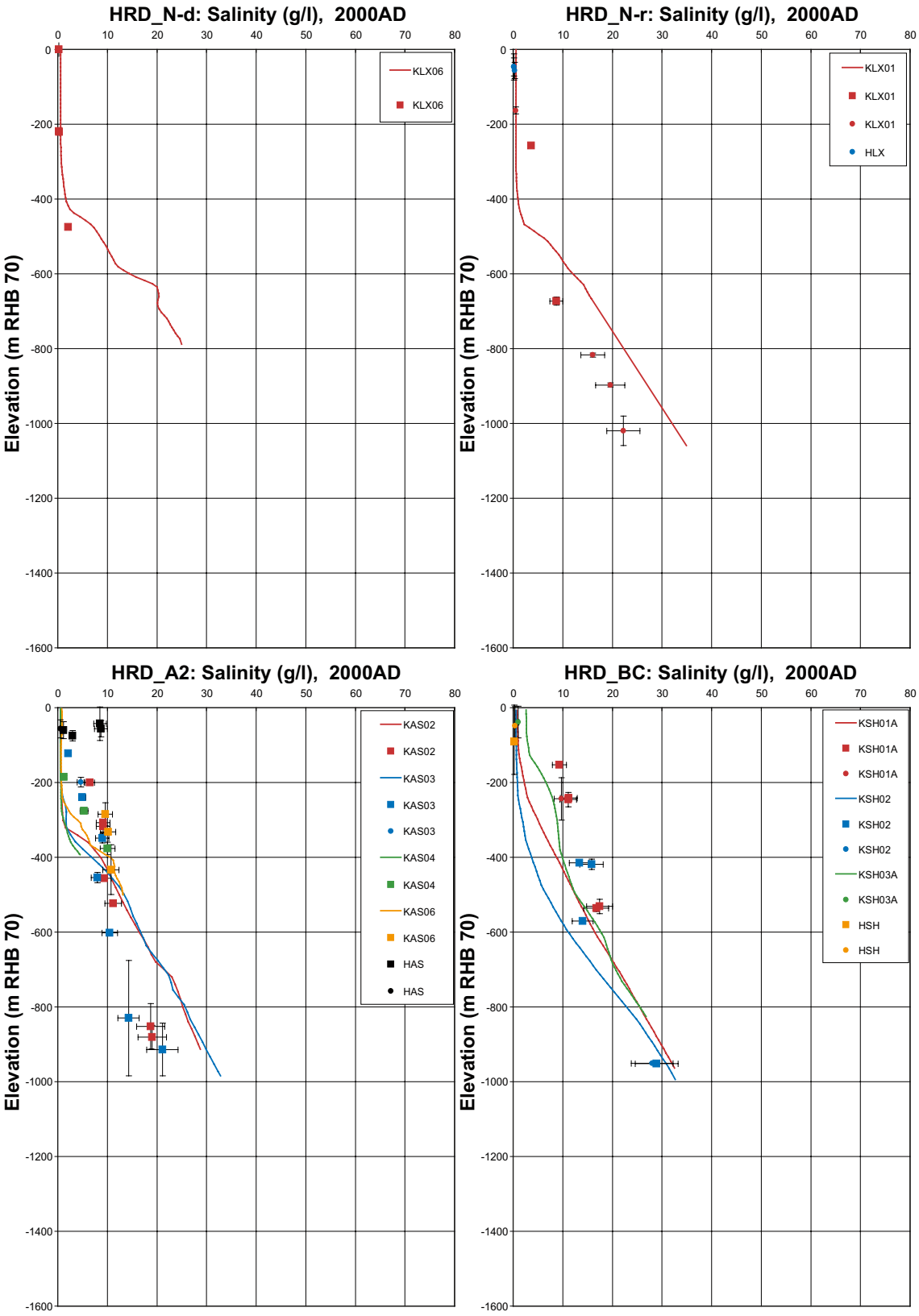

Figure 7-9. *Comparison of modelled and measured distributions of salinity (TDS) in fracture water for different groups of calibration boreholes. Square symbols are used for Category 1–3 data, and small point symbols for the Category 4 data. The error bars on the data indicate the laboratory analytical error. The solid lines show the complete distribution in the borehole simulated in the fracture system.*

described in Section 4.5.1. The salinity in most boreholes seems acceptable, although the measured salinity is lower in some boreholes than simulated, but again this is a direct result of using a simple initial condition that does not account for local heterogeneity.

Further, Figure 7-10 through Figure 7-13 show the comparison of the simulations with data for selected major ions and environmental isotopes for the core-drilled borehole grouped according to HRD and hydrogeological conditions. The chemical indicators used in these plots are pointed out in Section 4.5.3 together with additional details about the reference waters.

Figure 7-10 for Cl in the fracture water HRD_C shows reasonable results, and the inclusion of porewater data for KLX03 suggests less saline water in the matrix. This is not reproduced in the model since the model assumes an equality of *Deep saline* water in the initial fracture and matrix water. Better results could be obtained by simply reducing the proportion of *Deep saline water* in the initial condition for the matrix rock. The initial condition used in the *base case* assumes that *Deep saline water* is relatively shallow, starting from –150 m. Qualitatively this seems consistent with the Br/Cl ratios, although the sparsity of data means that probably any initial condition for *Deep saline water* starting between –150 m and –400 m would be judged consistent with the data. The penetration of post-glacial meteoric water suggested by HCO_3 is well predicted by the model, perhaps somewhat too deep in the simulations. The general absence of glacial water in HRD_C, apart from one measurement in KLX03 around –380 m, is reproduced by the model, which also matches the higher levels of $\delta^{18}O$ in the porewater below –650 m associated with *Inter-glacial Porewater*.

In the case of recharge areas of HRD_W, cf. Figure 7-11, the model predicts flushing of the fracture water by altered meteoric water to almost the bottom of these boreholes at about –600 m, whereas data suggests –500 m. The likely cause for this discrepancy is thought to be the model underestimating the effects of rock matrix diffusion (RMD) in KLX13A and KLX17A, which intersect many minor deformation zones between –200 m and –400 m that would result in a higher fracture surface area per unit and more retardation by RMD than what is present in the flow model. The model does, however, predict the retention of a *Deep saline water* in the porewater in these boreholes and a lower salinity in the fracture water as measured in the boreholes.

Figure 7-12, for the discharge areas of HRD_W, shows the brackish water below about –400 m is predicted by the *base case model* and that this has a high Br/Cl ratio, i.e. *Deep saline* water origin. Again, post-glacial meteoric flushing is well predicted based on HCO_3, including the prediction of some glacial water below –400 m which is consistent with data.

Figure 7-13 for HRD_EW007 suggests consistent predictions of Cl in the fracture system, although KLX08 data would again suggest less salinity in the matrix than is assumed in the initial condition. The transition from salinity of deep origin rather than marine at depths between –400 m to –500 m is consistent with available data. Post-glacial meteoric flushing is perhaps 50 m deeper in the model than suggested by measured data. Similarly, $\delta^{18}O$ would suggest slightly less flushing by recent surface water to preserve glacial lenses higher up. The transition to *Inter-glacial Porewater* in the porewater below –650 m is consistent between the model and data. /Rhén et al. 2009/ also present results for boreholes outside the Laxemar focused area.

Another way of representing the palaeohydrogeological conceptual model of the mixing of different reference waters is to plot the predicted mass fractions of reference waters as a function of elevation in boreholes, i.e. show the composition of groundwater relative to the five reference waters modelled. This is done for KLX03, KLX04, KLX05 and KLX08, all within the Laxemar focused area, in Figure 7-14. These are included to illustrate in a compact way the composition of the fracture water and average matrix porewater in terms of mixes of reference waters. Such plots provide useful insights into the mixing of reference waters and the influence of structures observed in the single-hole interpretations indicated on the right hand side of the graphs. They are not used as a calibration target in the same way as the major ions, but still comparisons are made to the fractions computed by the M3 method /Laaksoharju et al. 2009/ to aid conceptual discussions. It should be noted that the M3 analysis was based on four reference waters (*Inter-glacial Porewater* excluded), and hence the sum of the two simulated fractions for *Altered meteoric water* (orange line) and *Inter-glacial Porewater* (green line) should be compared with the M3-interpreted *Altered meteoric* results (orange squares). The mass fractions predicted for the fracture system are shown as solid lines, while those predicted for the matrix are plotted as dashed lines. *Deep saline water* follows a consistent profile and there is

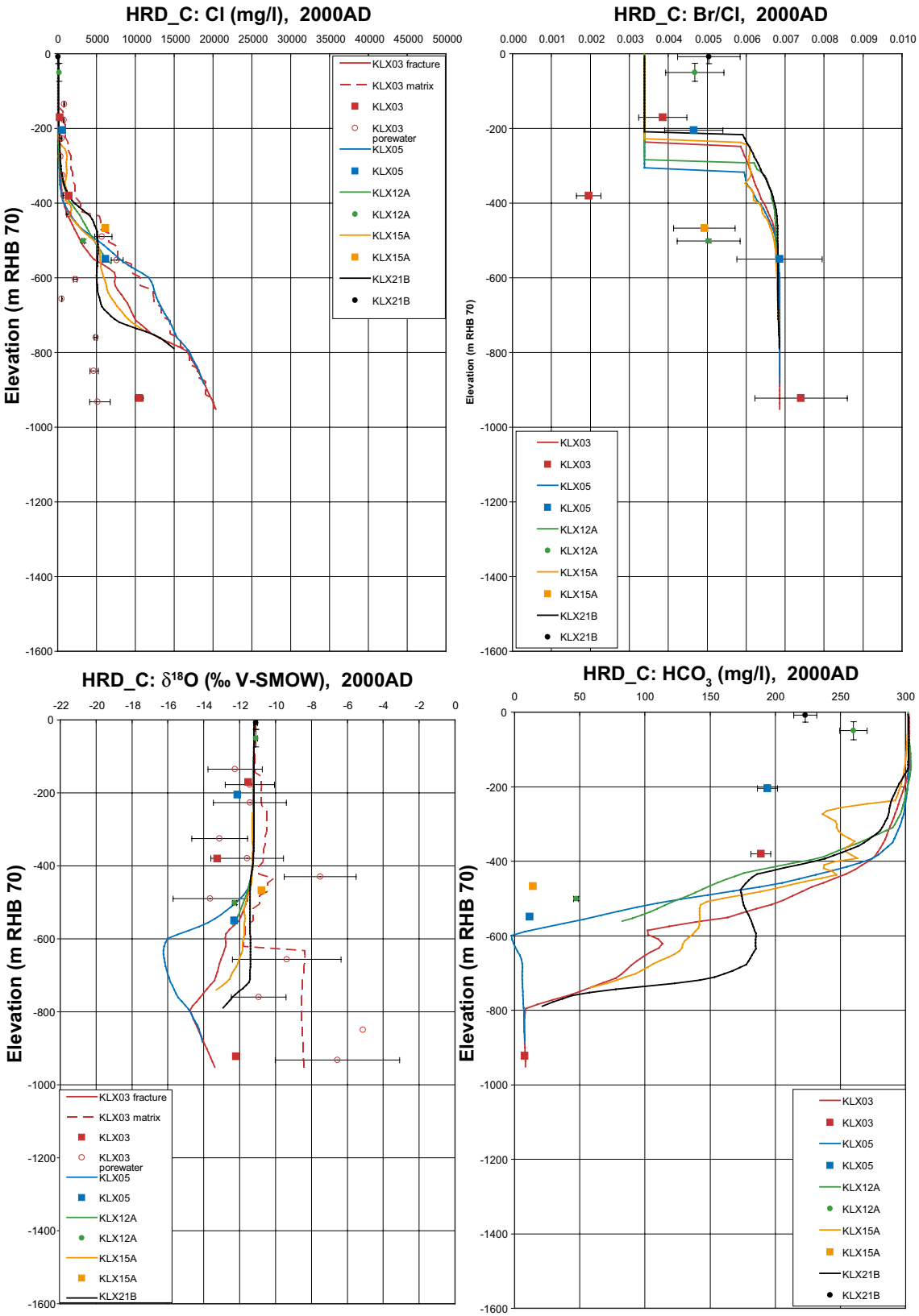

Figure 7-10. *Comparison of modelled and measured Cl, Br/Cl, $\delta^{18}O$ and HCO_3 in fracture water and porewater for boreholes in HRD_C. Square symbols are used for Category 1–3 data, circles are used for the porewater data, and small point symbols for the Category 4 data. The error bars on the data indicate the laboratory analytical error. The solid lines show the complete distribution in the borehole simulated in the fracture system, and the dashed lines are for the matrix.*

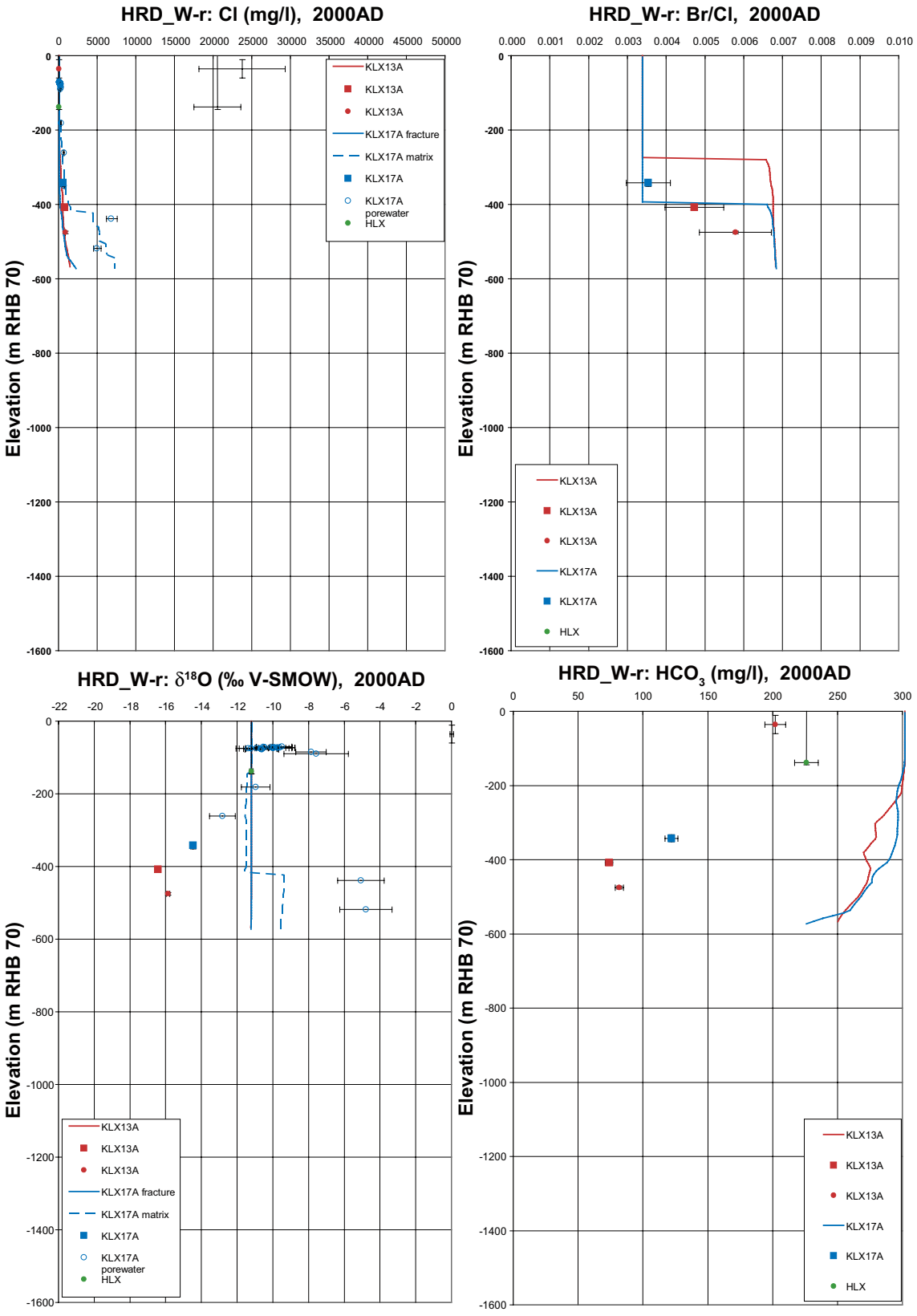

Figure 7-11. *Comparison of modelled and measured Cl, Br/Cl, $\delta^{18}O$ and HCO_3 in fracture water and porewater for boreholes in HRD_W-recharge. Square symbols are used for Category 1–3 data, circles are used for the porewater data, and small point symbols for the Category 4 data. The error bars on the data indicate the laboratory analytical error. The solid lines show the complete distribution in the borehole simulated in the fracture system, and the dashed lines are for the matrix.*

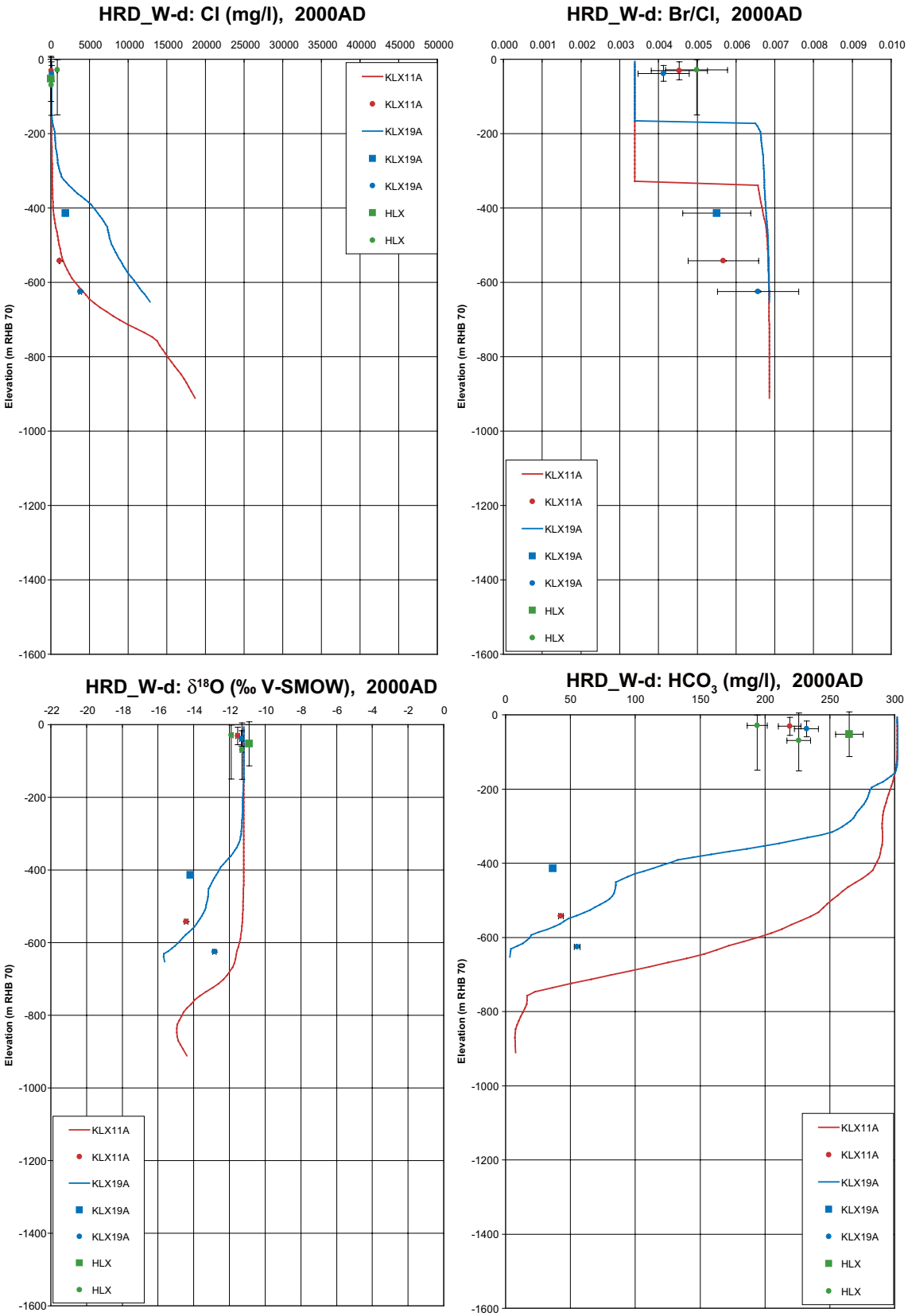

Figure 7-12. *Comparison of modelled and measured Cl, Br/Cl, $\delta^{18}O$ and HCO_3 in fracture water for boreholes in HRD_W-discharge. Square symbols are used for Category 1–3 data, and small point symbols for the Category 4 data. The error bars on the data indicate the laboratory analytical error. The solid lines show the complete distribution in the borehole simulated in the fracture system, and the dashed lines are for the matrix.*

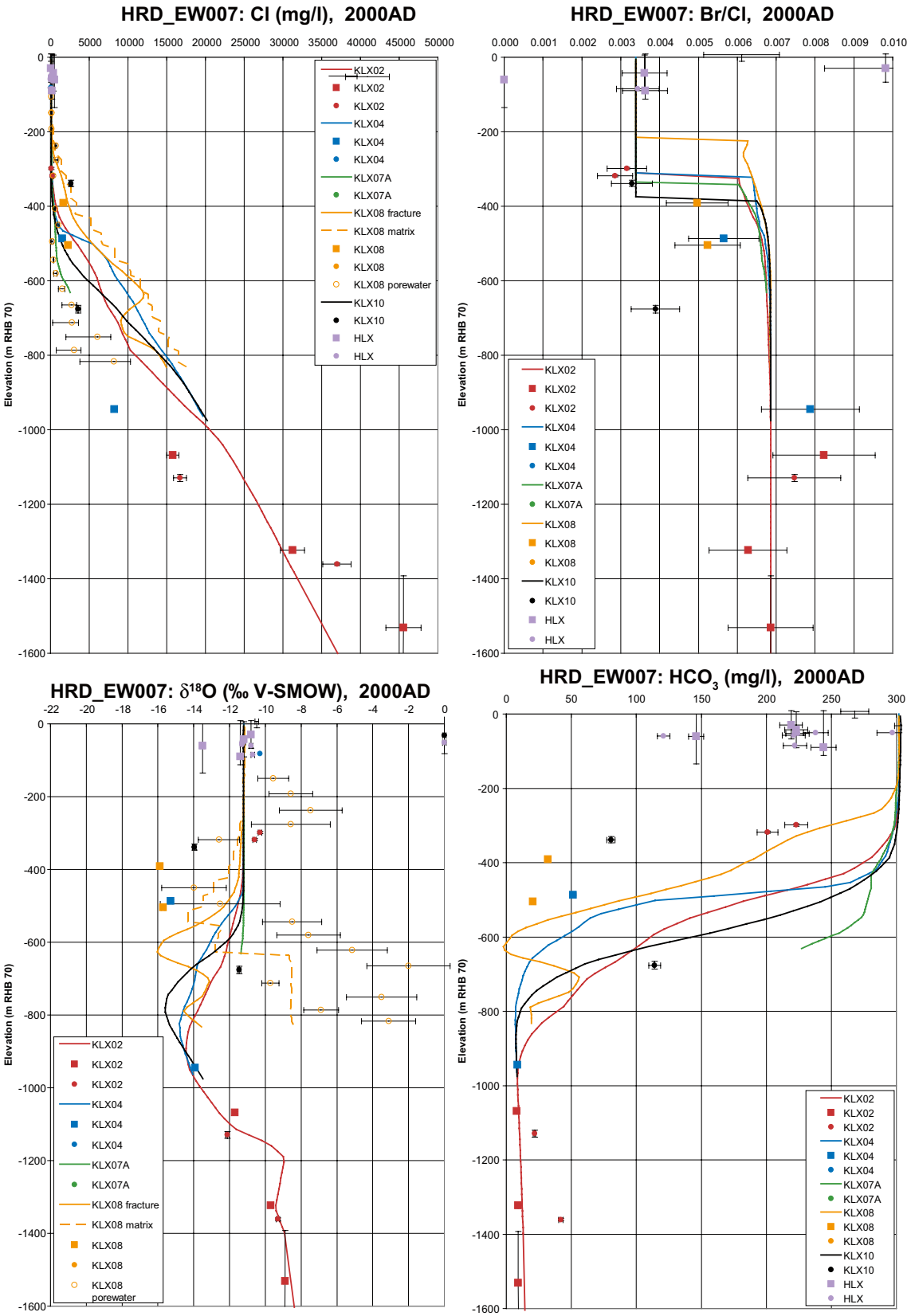

Figure 7-13. *Comparison of modelled and measured Cl, Br/Cl, $\delta^{18}O$ and HCO_3 in fracture water and porewater for boreholes in HRD_EW007. Square symbols are used for Category 1–3 data, circles are used for the porewater data, and small point symbols for the Category 4 data. The error bars on the data indicate the laboratory analytical error. The solid lines show the complete distribution in the borehole simulated in the fracture system, and the dashed lines are for the matrix.*

very little *Littorina sea water* (2–3%) in any borehole as interpreted by M3. *Altered meteoric water* circulates perhaps a little too deep in the model, considering *Glacial water* in KLX03 and KLX05, cf. Figure 7-14 and /Rhén et al. 2009, cf. Appendix 9 therein/. It is interesting to see that in these boreholes, the prediction for matrix water fractions is closer to the interpreted fractions (based on measurements), which would suggest that slightly enhanced RMD in the depth zone –150 m and –400 m would improve the simulation results. The comparison is better in KLX04 and KLX08. Plots of this type for other boreholes are included in /Rhén et al. 2009, cf. Appendix 9 therein/, where it is seen than the Littorina content increases to 10–20% in the east, as seen in the data.

Examples of the palaeohydrogeological cross-section information (Figure 7-14) used qualitatively in the calibration are shown in Figure 7-16 for Cl and $\delta^{18}O$ on horizontal section at –500 m (–300 m is also shown in Rhén et al. 2009/) at time 2000 AD. It can be seen that continuous lenses of Cl exist along the low-lying E-W valleys associated with the Laxemarån river valley in the south, the Mederhult zone to the north, and ZSMEW007A in the centre of the Laxemar local model area. There are more localised lenses of brackish-glacial water within HRD_C associated with regions of lower hydraulic conductivity. At repository depth, –500 m, brackish water is much more common with large lenses of brackish-glacial water beneath low lying areas and also beneath HCD ZSMEW007A that dips towards north. There are also smaller localised lenses of glacial-brackish water throughout the focused area that are the result of spatial variability, and hence may vary in position and magnitude according to the particular realisation of HRD and HCD hydraulic properties. The model predicts that KLX01, KLX02, KLX03, KLX04, KLX05, KLX08 all either intersect, or are very close to, lenses of brackish water at this depth. There are areas of non-saline water predicted in the centre of HRD_C and HRD_W which are not intersected by any boreholes with chemical sampling. At –300 m, cf. /Rhén et al. 2009/, it can be seen that KLX05, KLX08 and KLX15A (of the boreholes with chemical data) are predicted to intersect brackish water at this quite shallow depth, which is consistent with data. KLX05, KLX08 and KLX15A are also predicted to be close to lenses of *Glacial water*, although it is not actually seen at the borehole in either the simulations, or in data.

As an example of simulated hydrochemistry on a vertical slice, Figure 7-17 shows Cl, TDS, $\delta^{18}O$ and Darcy velocity on a WNW-ESE section at time 2000 AD, cf. Figure 7-15 for location of section. The large scale modelling of eastern Småland, cf. /Ericsson et al. 2006, figure 6-64 therein/ show similar distribution of TDS.

As an example of simulated hydrochemistry on a vertical section, Figure 7-18 shows the composition of fracture groundwater in terms of mass fractions of *Littorina Sea* Water, *Glacial Melt* Water, *Altered Meteoric Water* and *Deep Saline Water* on the WNW-ESE Section B (see Figure 7-15). This shows that *Littorina Sea Water* is generally below 10% throughout the Laxemar subarea, persisting at the level of just a few percent at the present-day. It does enter the fracture system in the lower lying areas (below about 15 m for the present-day topography) during the Littorina maximum, but gets displaced by post-glacial meteoric infiltration once the land has risen above sea level. This contrasts with the clear *Littorina Sea Water* signature seen at Forsmark /Follin et al. 2007c/, which persists mainly due to the lower topography and lower hydraulic gradients. *Altered Meteoric Water* generally penetrates to –200 m to –400 m in the Laxemar subarea, a little deeper in HRD_W. Continuous lenses of remnant *Glacial Mel*t *Water* in HRD_EW007 exist beneath the northwardly gently dipping zone ZSMEW007A and further east beneath lower lying areas, centred on repository depth, –500 m. Highly saline (> 600 mg/l of Cl) non-marine water associated with Deep Saline Water starts at about –500 m.

Additional confirmatory tests were made of the palaeohydrogeological model by simulating the migration of tritium over the last 120 years using the derived calibrated *base case model* and selected variants. These calculations are presented in /Rhén et al. 2009, cf. Appendix 10 therein/ where it is concluded that the developed palaeohydrogeological models are consistent with the interpretation of /Laaksoharju et al. 2009, cf. Section 7.2.2 therein/ that modern meteoric recharge from the last 50–60 years has penetrated the groundwater system to a depth of approximately 150 to 200 m.

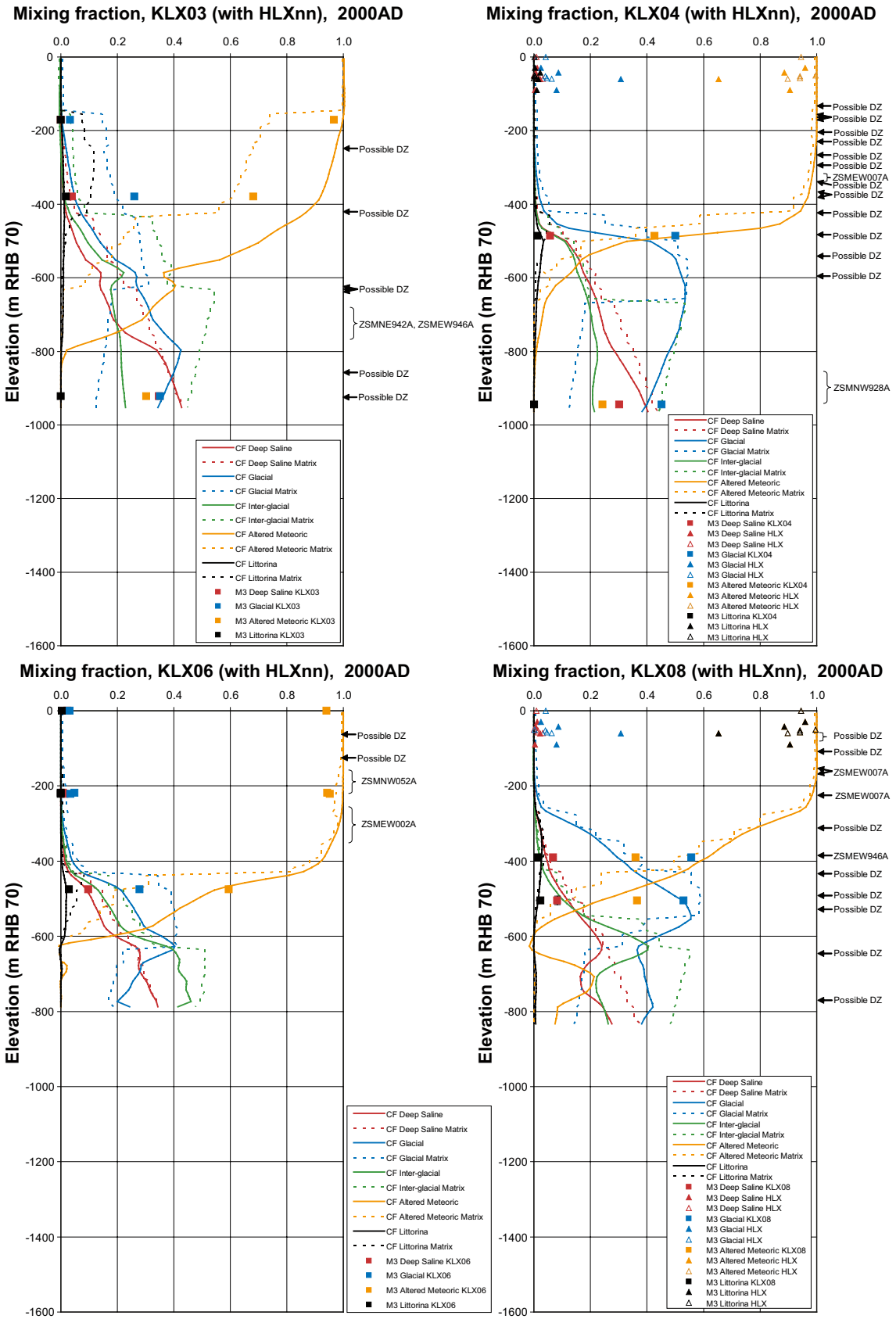

Figure 7-14. *Illustration of simulated mixtures of reference water mass fractions in boreholes KLX03, KLX04, KLX05 and KLX08. Solid lines show simulated reference water mass fractions for Deep Saline, Littorina, Altered Meteoric, Glacial and Inter-glacial porewater in the fracture system; dashed correspond to the reference water mass fractions in the matrix. The points show the mixture of four reference waters (Deep Saline, Littorina, Altered Meteoric, Glacial and Inter-glacial porewater) interpreted from groundwater samples by the M3 method.*

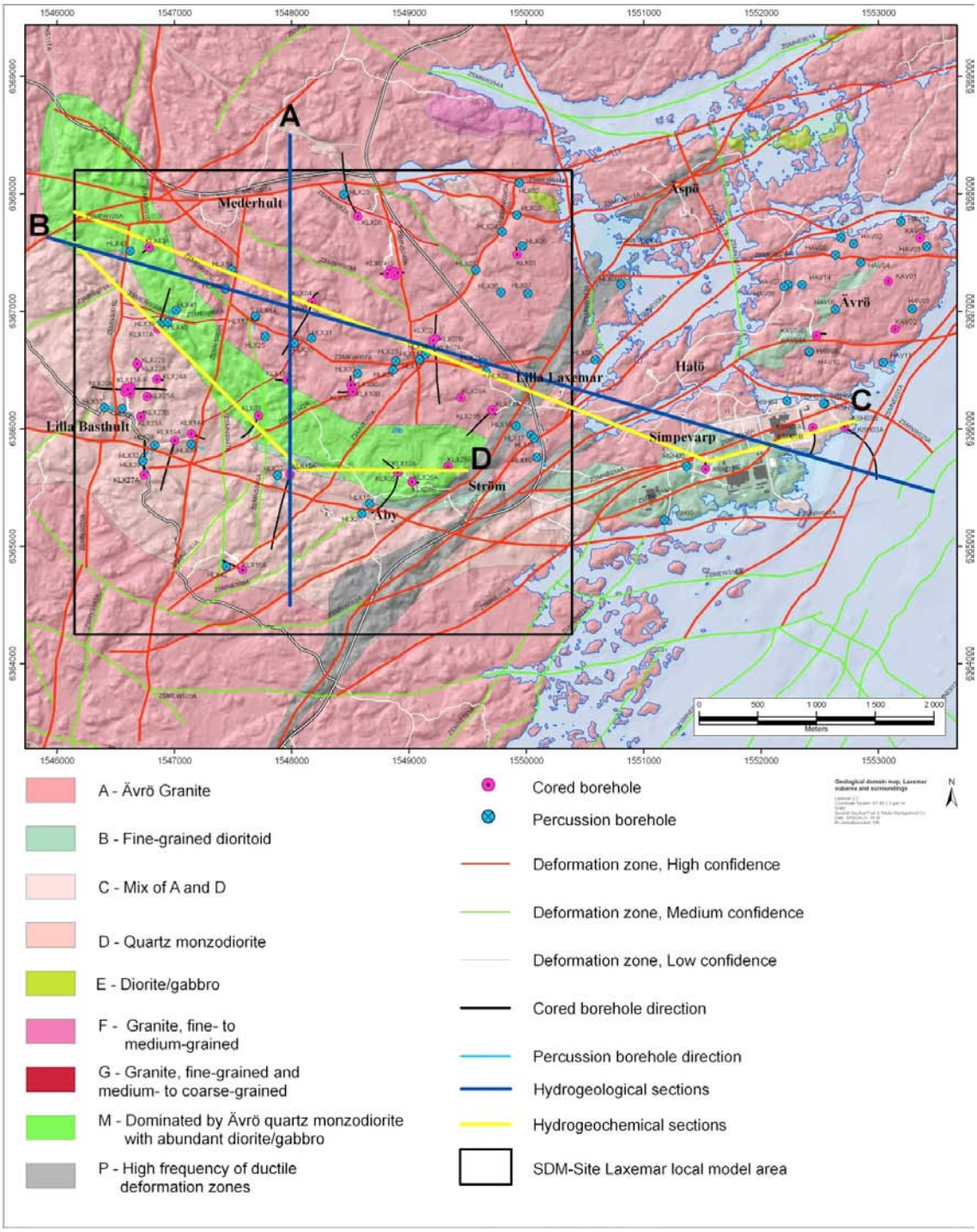

Figure 7-15. *Sections A and B (blue lines) correspond to hydrogeological sections 5 and 7, respectively, in /Rhén et al. 2009/. Sections c and D (yellow lines) correspond to hydrochemical sections 3 and 5, respectively, in /Laaksoharju et al. 2009/.*

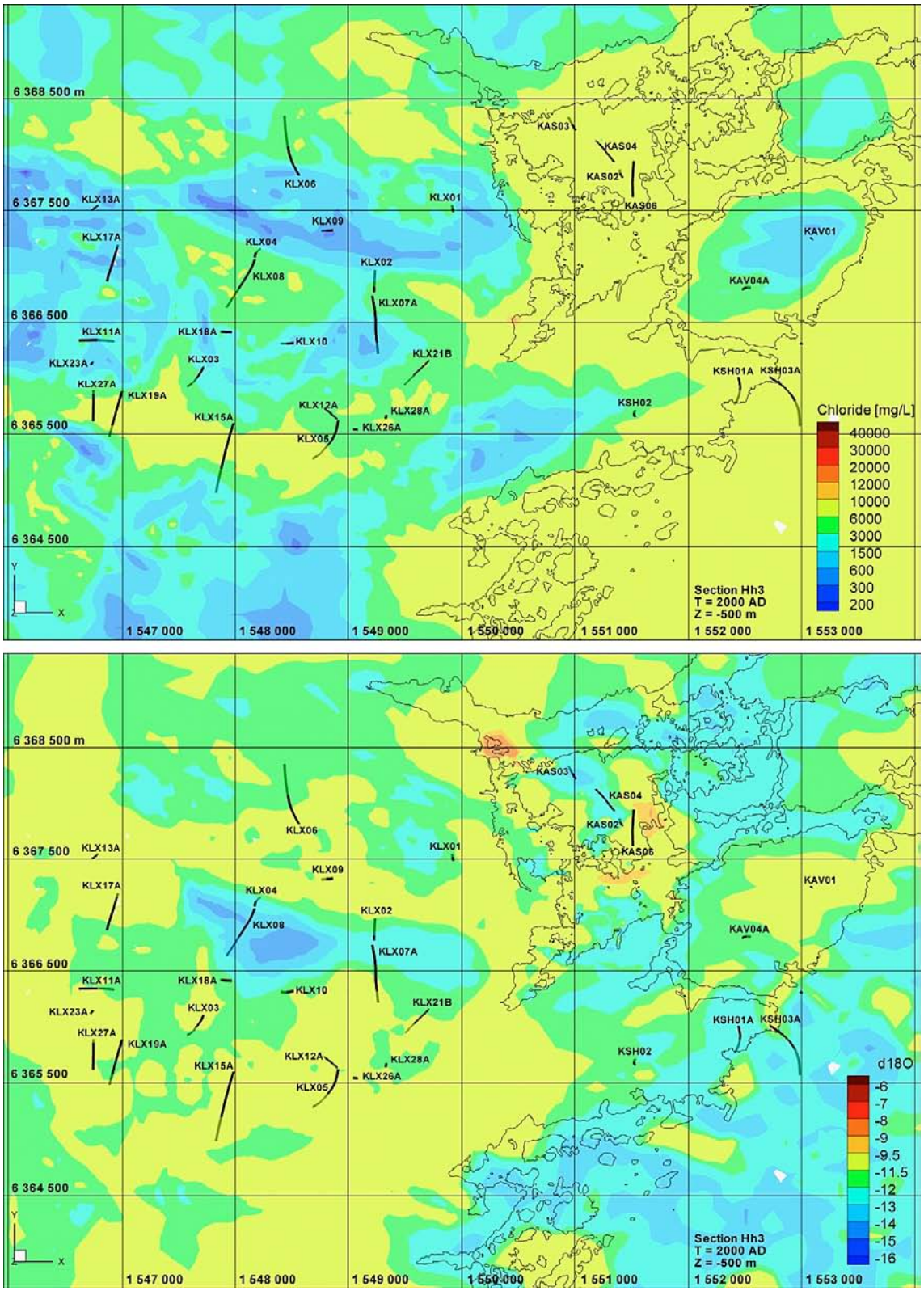

Figure 7-16. *Distribution of Cl (top) and $\delta^{18}O$ (bottom) predicted on a horizontal slice at –500 m covering the Laxemar-Simpevarp area through the base case model.*

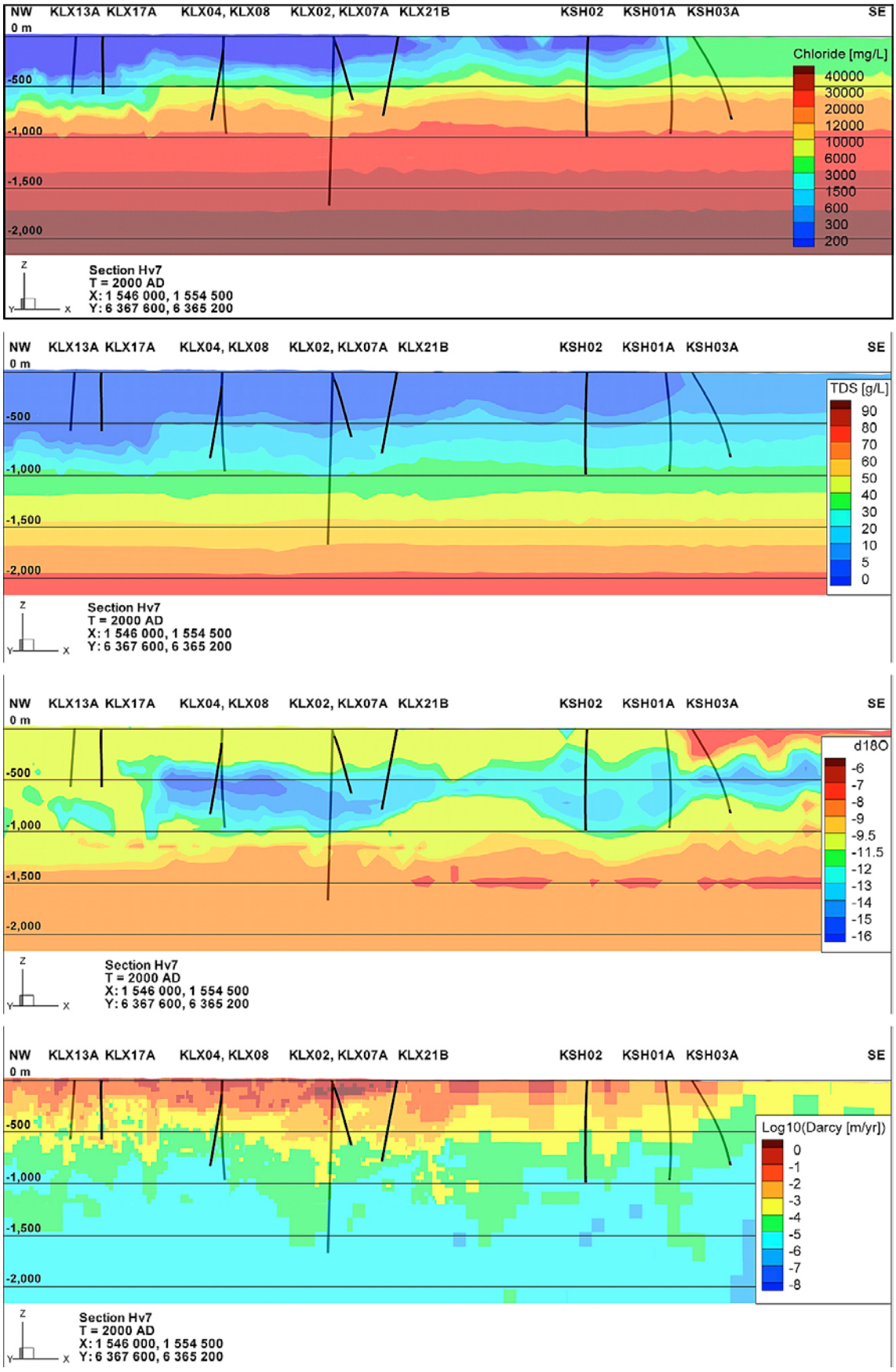

Figure 7-17. *Distribution of Cl , TDS , $\delta^{18}O$ and Darcy velocity (top to bottom) predicted by the base case model on vertical WNW-ESE Section B through the Laxemar-Simpevarp area (See /Rhén et al. 2009, cf Appendix 9 therein/ for details).*

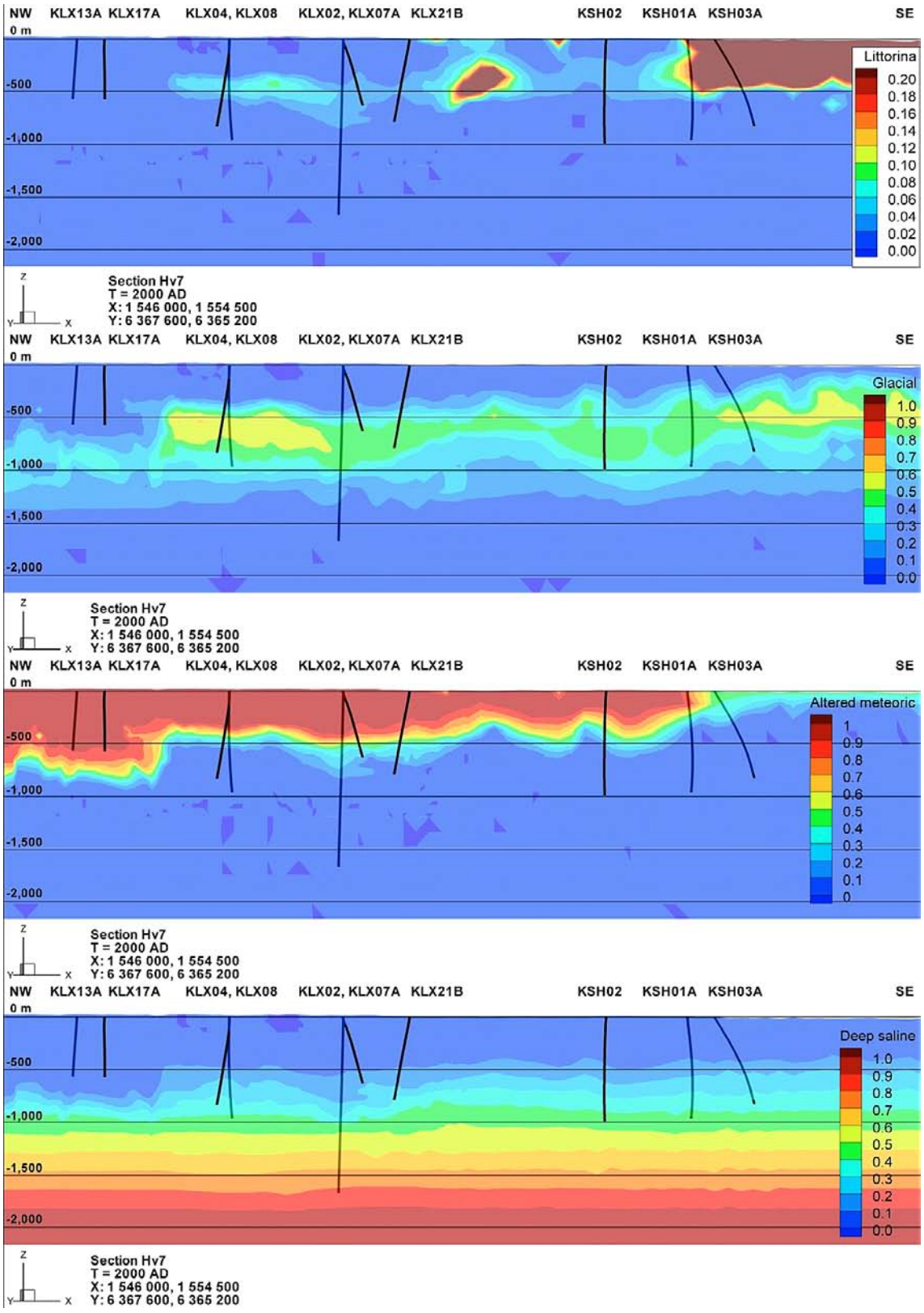

Figure 7-18. *Distribution of mass fractions reference waters: Littorina Sea Water (on a scale 0–0.2), Glacial Melt Water, Altered Meteoric Water, and Deep Saline Water (top to bottom) predicted by the deterministic base model simulation on vertical WNW-ESE Section B through the Laxemar-Simpevarp area.*

8 Exploration simulations

8.1 Flow-paths from a tentative repository layout

Following the calibration exercises, flow-paths from a tentative repository layout have been simulated for the *base case* and a limited number of key variants. The pathlines calculations were performed in the groundwater flow-field simulated for year 2000 AD (i.e. based on a snapshot in time, and not considering the successive future evolution of groundwater flow as the particles move in that flow). The flow-paths are simulated by releasing particles in relevant parts of HRD_C, HRD_EW007 and HRD_W with the approximate repository footprint positioned at –500 m. Initially, particle starting positions were considered within the Laxemar focused area on a 40 m by 40 m mesh, but those starting positions within the same element as a HCD were removed, leaving a total of 2,142 particles traced. This is illustrated in Figure 8-1.

Figure 8-2 through Figure 8-3 show particle exit locations on the top surface of the model (black points) for pathlines released in the *base case*. Exit locations for a release from HRD_W are mostly localised to zones ZSMNW042A-west and ZSMNS059A; for HRD_C, their destinations are grouped around HCDs ZSMNW042A-east or ZSMNE005A; for HRD_EW007A, the exit locations are associated with ZSMNE006A or ZSMNE012A.

Apart from considering the discharge points it is interesting to consider the sub-surface paths taken by particles. Hence, the pathlines followed by each particle are plotted, sorted according to the HRD that they start in, and identifying which HCD transport the most particles. Figure 8-2 and Figure 8-3 show the paths followed by particles starting in HRD_C, HRD_W and HRD_EW007, respectively. The pathlines are necessarily 3D, but are here shown in map view. In HRD_C the particles generally head south toward ZSMNW042A or east toward ZSMNE005A and ZSMNE006A where they reach

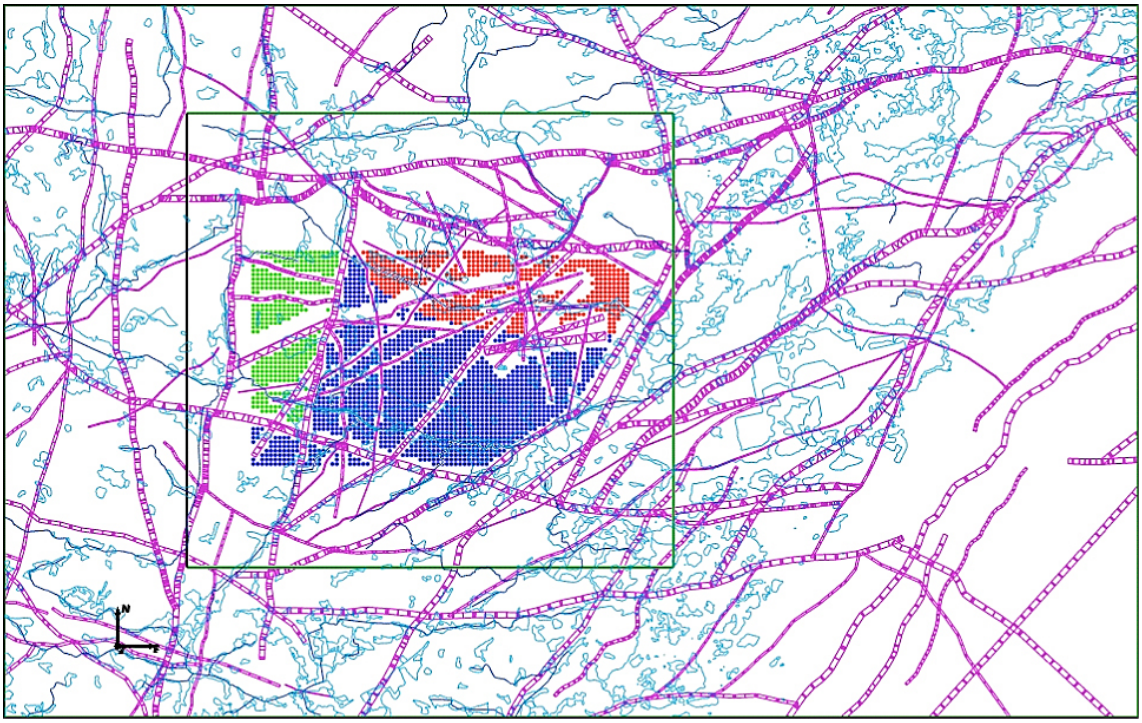

Figure 8-1. *Particle starting positions representing a tentative repository area in map view of a slice centred at –500 m. The green particles are starting in HRD_W, the red particles are starting in HRD_EW007 and the blue particles are starting in HRD_C. The particles are initially located in a 40 m by 40 m mesh at –500 m, but positions within HCD are omitted. HCDs are sliced at –500 m (purple), surface water bodies (cyan), streams (blue), and the Laxemar local model area (green box) are indicated.*

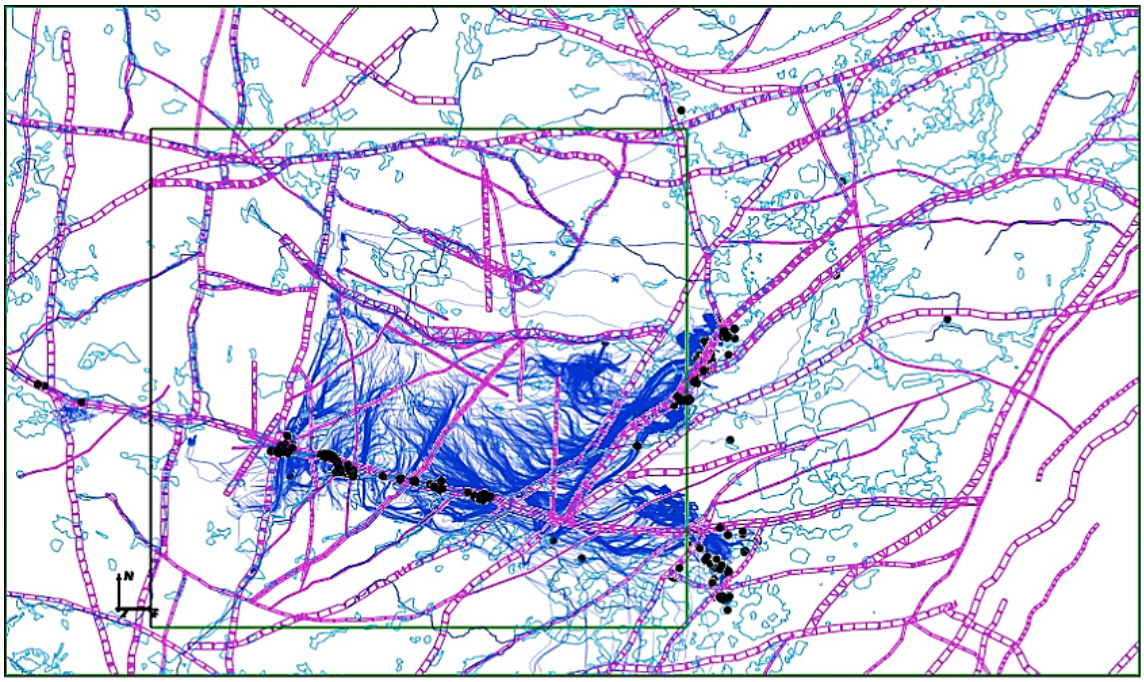

Figure 8-2. *Pathlines for the base case model. Pathlines starting in HRD_C are shown in blue with the exit locations (discharge) in black. HCDs at 0 m (purple), surface water bodies (cyan), streams (blue), and the Laxemar local model area (green box) are superimposed. The start positions for these pathlines are the blue ones shown in Figure 8-1.*

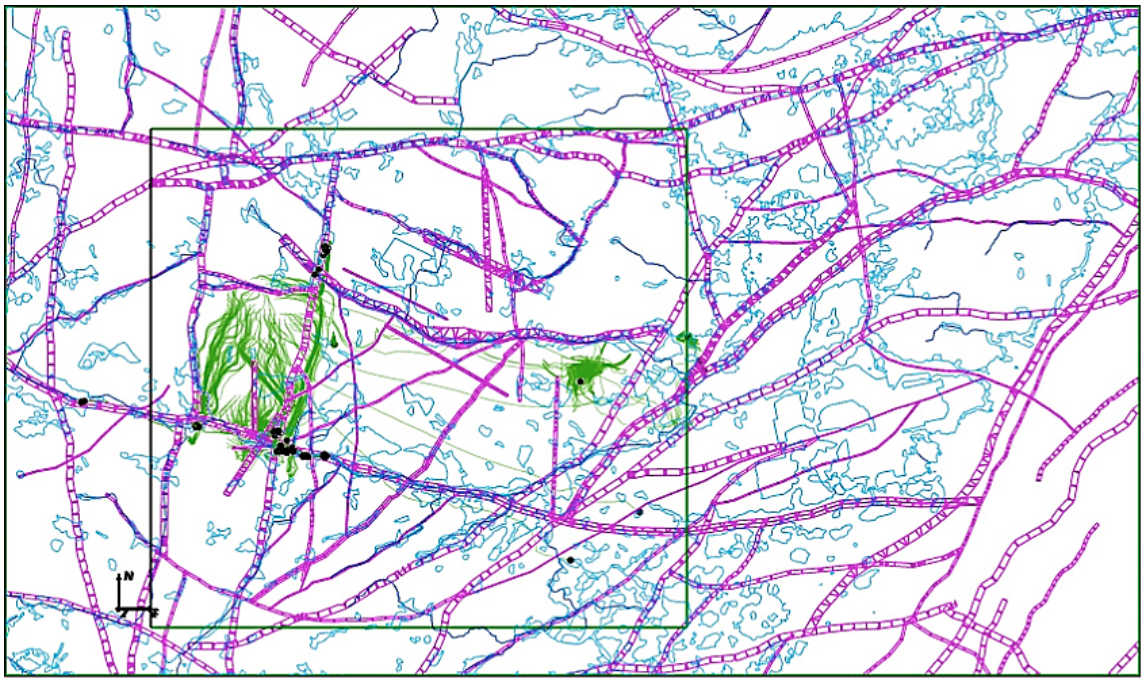

Figure 8-3. *Pathlines for the base case model. Pathlines starting in HRD_W are shown in green with the exit locations (discharge) in black. HCDs at 0 m (purple), surface water bodies (cyan), streams (blue), and the Laxemar local model area (green box) are superimposed. The start positions for these pathlines are the green ones shown in Figure 8-1.*

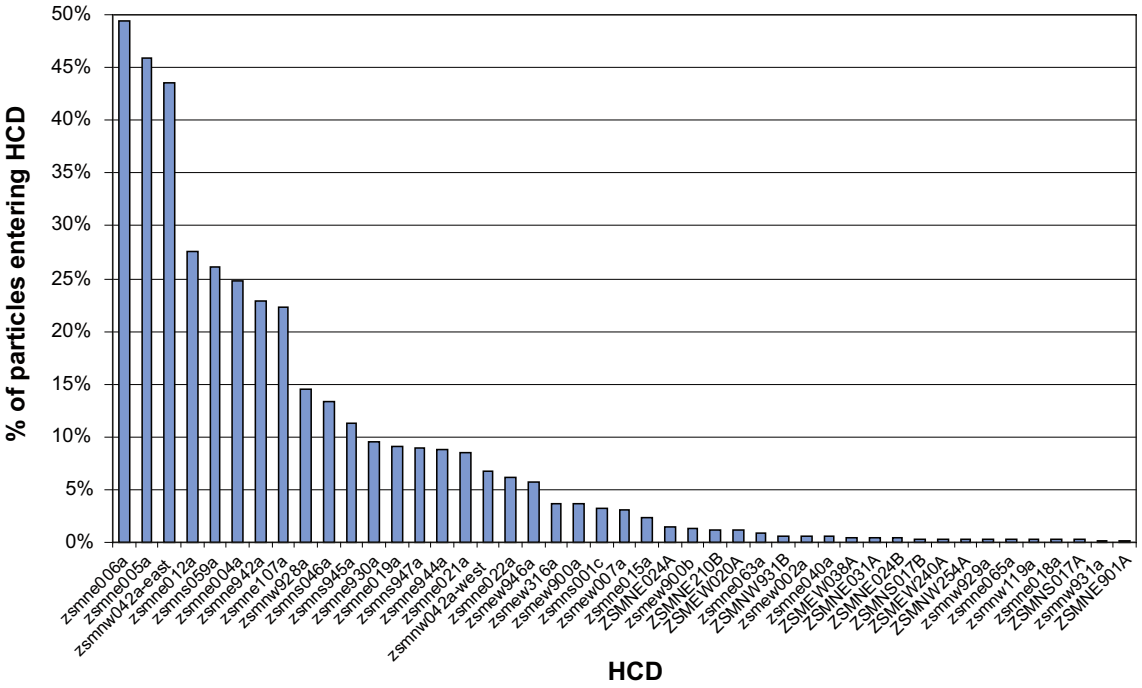

Figure 8-4. *Histogram showing the percentage of particles that enter each HCD along pathlines started at the 2,142 locations shown in Figure 8-1 for the base case. The HCD are ordered accordingly. Thus, almost 50% of the particles enter ZSMNE006A. A particle may enter several HCD, and so the percentages add to > 100%.*

the bay near Äspö, with some particles continuing further south-east to the Baltic, south of the Simpevarp peninsula. For HRD_W, the flow-paths are controlled by the dolerite dykes associated with ZSMNS001C and ZSMNS059A, and hence most discharge to the south in ZSMNW042A. For HRD_EW007 (not shown), most particles follow ZSMEW007A eastward to discharge either in ZSMNE005A or in ZSMNE006A, where they reach the bay near Äspö.

In order to identify which HCD are most important for transport, the number of particles that enter each HCD is recorded, and then the HCD are ranked according to how many particles that pass through them. This shows that ZSMNE005A, ZSMNW04A-east and ZSMNE006A form the down-stream path for 40–50% of particles. ZSMNE012A, ZSMNE004A, ZSMNE107A, ZSMNS059A and ZSMNE942A all encounter about 20–30% of the particles.

8.2 Flow-paths indicating present-day recharge areas relevant to the repository volume

In addition to following flow-paths downstream with the advective velocity from the repository, it is also informative to track particles upstream, reversing the Darcy velocity vector to trace back flow-paths from the repository to where the surface recharge comes from, and hence locate the origin of surface water that reaches the focused volume at repository depth. The particles are tracked upstream until they reach the top surface based on the flow-field calculated at 2000 AD. This approach is deterministic since it identifies the unique flow-path that links a point in the focused volume to a point on the surface. It does not consider the divergence or convergence of flow near to this path, or how groundwater flow may have changed during the time it takes for a particle released at the surface to reach repository depth (backward pathlines suggest timescales of 10,000s years).

The backward pathlines for the *base case* are illustrated for HRD_C and HRD_W in Figure 8-5 and Figure 8-6, respectively. The main recharge area for HRD_C is the low hills south of HRD_EW007 within the HRD_C area. South of ZSMNW042A, the recharge areas are some low hills further south, again very localised. For HRD_W, the recharge area is also within the HRD lying toward the north,

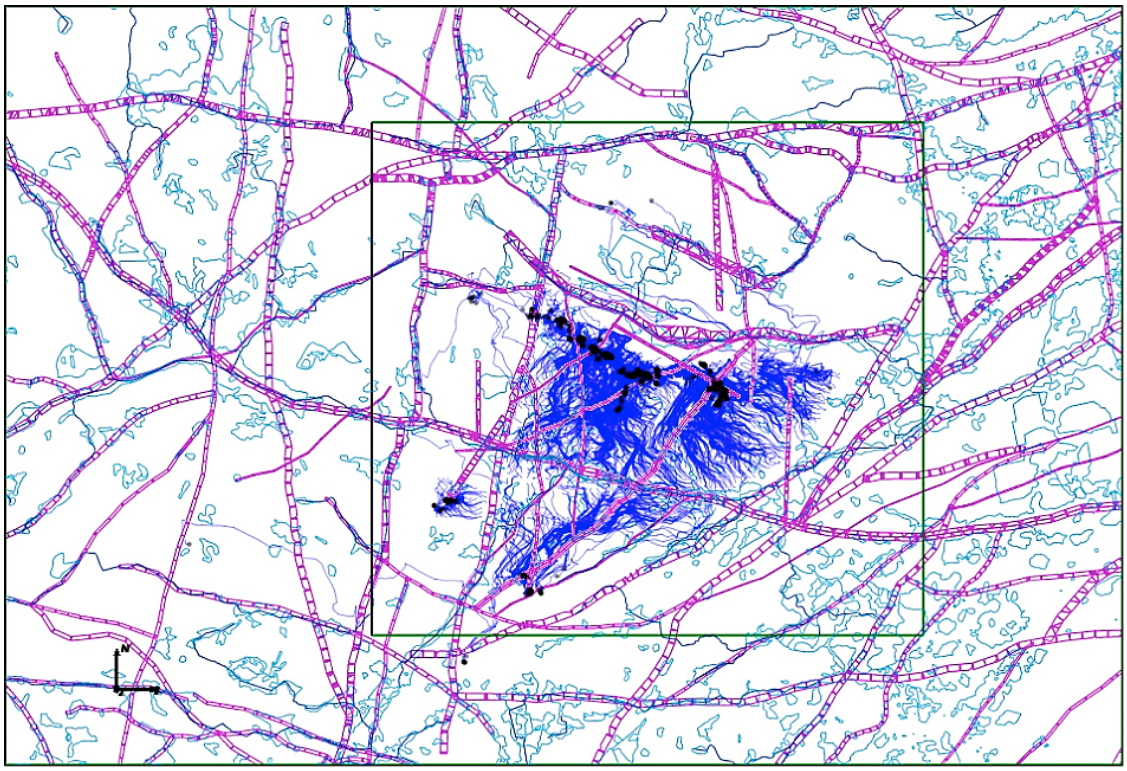

Figure 8-5. *Backward pathlines for the base case model. Pathlines starting in HRD_C are shown in blue with the exit locations (recharge) in black. HCDs on a slice at 0 m (purple), surface water bodies (cyan), streams (blue), and the Laxemar local model area (green box) are shown. The start points for the paths are the blue points in Figure 8-1.*

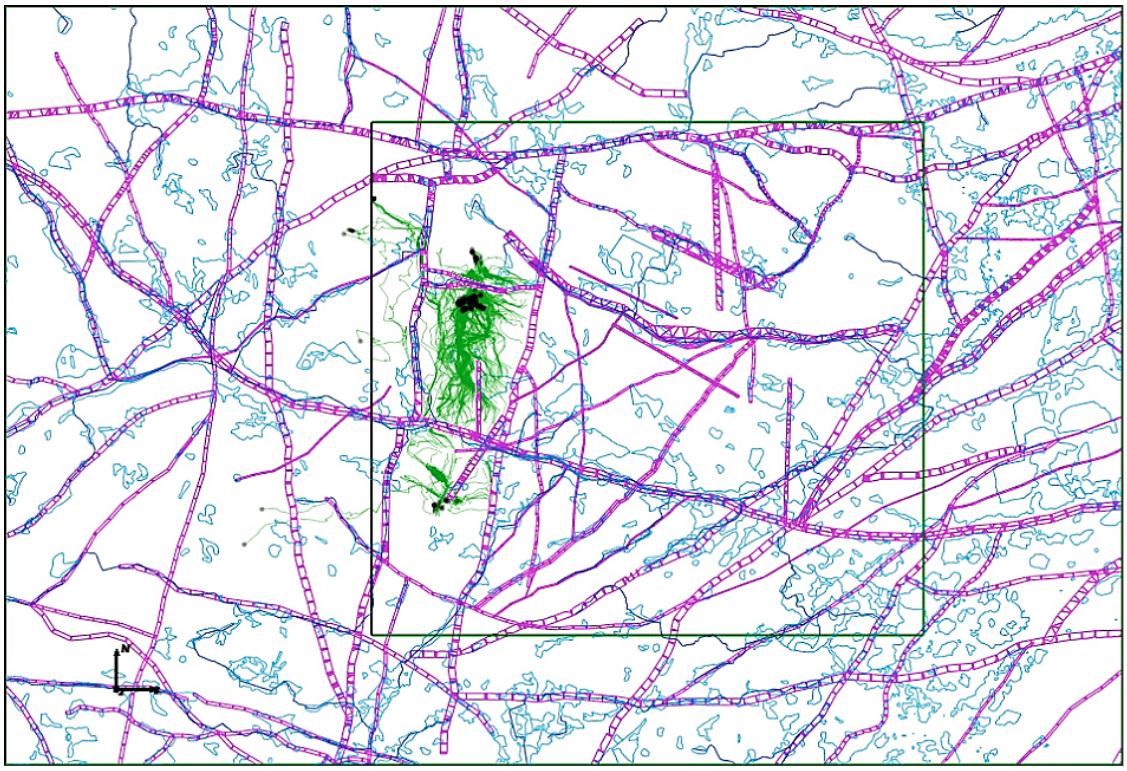

Figure 8-6. *Backward pathlines for the base case model. Pathlines starting in HRD_W are shown in green with the exit locations (recharge) in black. HCDs on a slice at 0 m (purple), surface water bodies (cyan), streams (blue), and the Laxemar local model area (green box) are superimposed. The start locations for these paths are the green points shown in Figure 8-1.*

near high topography around ZSMEW900A. HRD_EW007 (not shown) receives recharge from the same low hills near the northern part of the HRD_C south of ZSMEW007A, and from some hills slightly to the north. In summary, all recharge areas affecting the focused volume at 2000 AD are localised, predominantly within the Laxemar local model area. Hence, flow and chemistry boundary conditions far west of the Laxemar local model area have limited influence on hydrogeological conditions in the focused volume, although this depends on whether the ZSMNS001 acts as a barrier along its length within the Laxemar local model area.

A summary plot of all forward (discharge) and backward (recharge) pathlines is presented in Figure 8-7 with pathlines drawn so that lines are drawn weighted by the number of particles following each pathway. This reveals that there is generally a relatively diffuse horizontal initial forward path from each start point until paths converge on HCD and discharge in several concentrated areas. Recharge also starts in relatively concentrated areas mostly associated with topographic highs within each rock block and then move down and often in a generally eastwards direction toward repository depth (considered to be –500 m here).

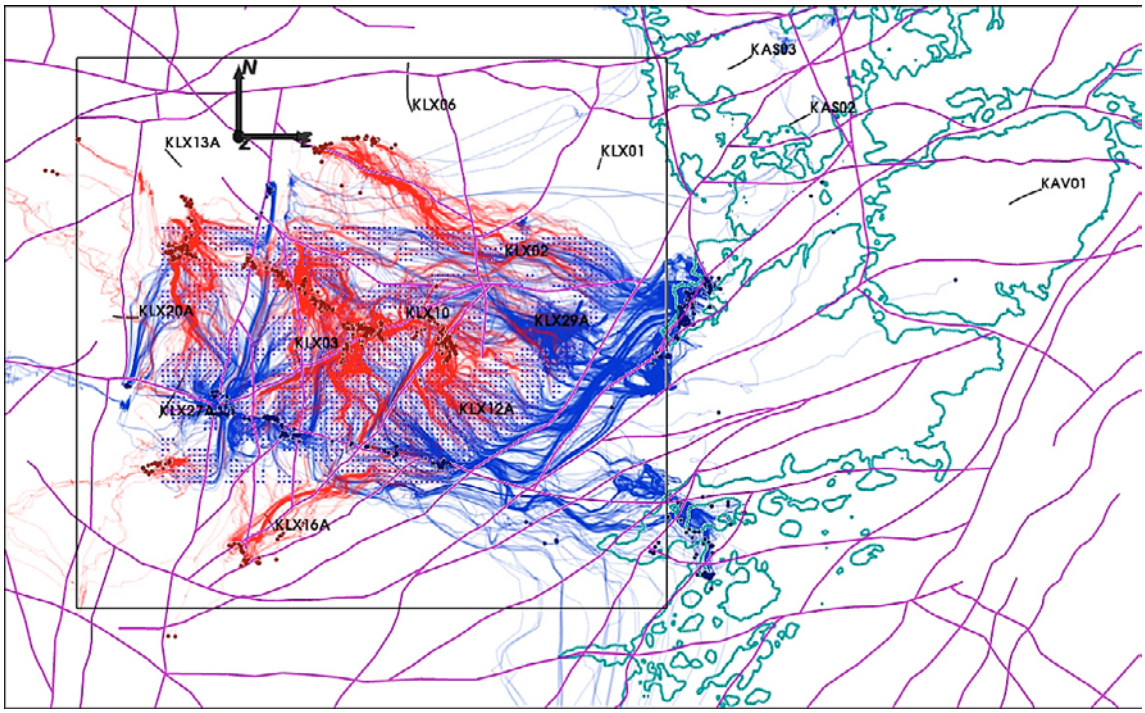

Figure 8-7. *Summary plot of forward pathlines (blue) and associated discharge points (dark blue) and backward paths (red) and associated recharge points (brown) for release points in HRD_C, HRD_W and HRD_EW007. The weight of the lines reflects the number of particles that follow the same path. HCDs on a slice at 0 m (purple), shoreline (turquoise), and the Laxemar local model area (black square) along with selected core drilled boreholes are superimposed.*

9 Conceptual and parameter uncertainty analysis

In this chapter a series of variants, based on the base model, are used to illustrate some of the steps to quantify the sensitivity to some remaining uncertainties. A more detailed account is found in /Rhén et al. 2009/.

9.1 Illustration of sensitivities considered during calibration of natural groundwater levels

The derived hydraulic properties of both HCD and HRD show significant spatial variability. Therefore, one important factor to be quantified in the simulations is how sensitive is the calibration to the effects of spatial variability, which can be estimated by generating several realisations of the hydrogeological model including lateral heterogeneity in the property assignment to HCD. For the HRD, 10 realisations of the hydrogeological DFN model were generated and each upscaled to give an ECPM model. Each of these was combined with one of 10 stochastic realisations of the HCD hydraulic property model with transmissivity sampled on a 200 m triangulated grid of each HCD (with local conditioning to measured transmissivities), see Section 6.2. A standard deviation of Log10(transmissivity) equal to 1.4 was used in the HCD, based on data (see Section 5.1.2). Since this gives variability over nearly 6 orders of magnitude within the same deformation zone and depth zone, 10 realisations with standard deviation 0.7 were also run to give a comparison. The same set of realisations was used to predict both environmental heads and palaeohydrogeology, as presented in Chapter 7.

Figure 9-1 illustrates the variability in predicted point-water heads for the percussion drilled boreholes by plotting the minimum, mean, and maximum modelled point-water head for the variant with a standard deviation of 1.4 in Log(T) in HCD. (A similar figure for groundwater monitoring wells is shown in /Rhén et al. 2009/.) This indicates which borehole measurements are most subject to spatial variability, e.g. percussion boreholes HLX06 and HLX36. The span of simulated point-water heads and measured variations overlap for many of the boreholes. Some that do not overlap, such as HLX02

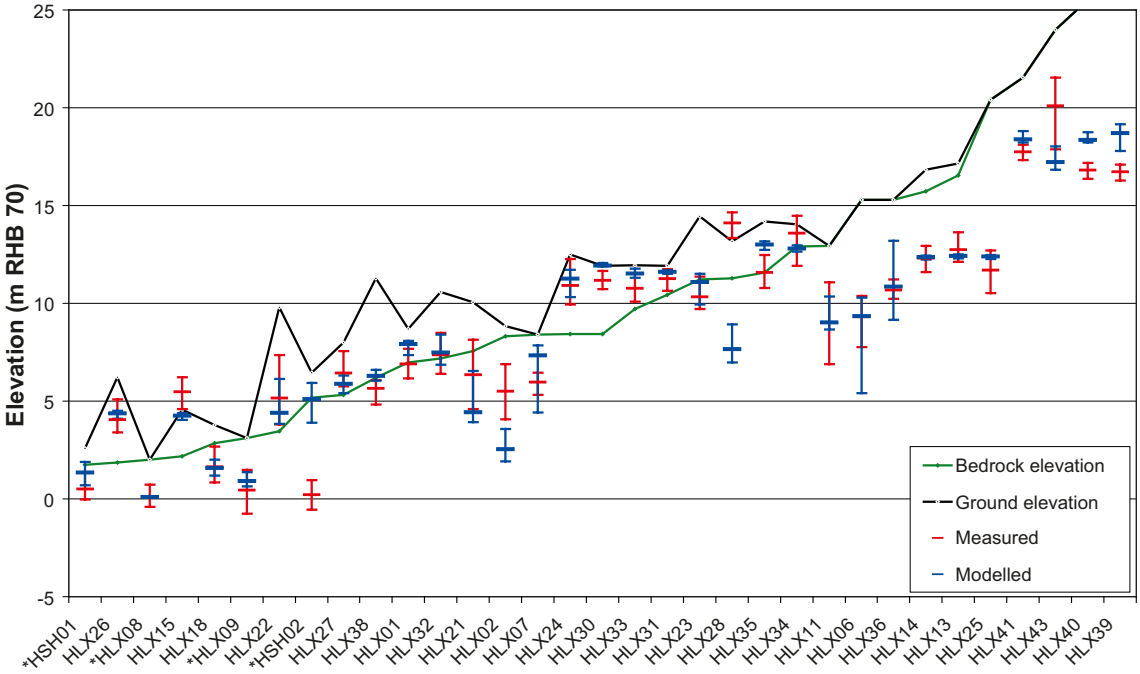

Figure 9-1. *Comparison of measured heads in percussion drilled boreholes (HLX) for 10 stochastic realisations of HCD and HRD. For the model, the minimum, maximum and median value in the bedrock is shown in blue. The field data are plotted as mean point water heads in the bedrock with error bars to show the range of values at different measurement times. Boreholes marked by a * (bottom of figure) are outside the local model area.*

and HSH02 are indications that these boreholes are affected by pumping at Äspö HRL (HLX02 on Laxemar) and possibly Clab (the interim storage facility for spent nuclear fuel) as well as drainage from shafts around the nuclear power plants (cf. Section 4.2) (HSH02 on the Simpevarp peninsula). The variability in the near-surface point-water heads in SSM holes appears to be small, cf. /Rhén et al. 2009/. SSM holes are biased towards lower elevations, i.e. discharge areas, while HLX boreholes are typically in more elevated areas. Point-water heads in recharge areas are generally more sensitive to variations in recharge and hydraulic properties; whereas point-water heads in discharge areas tend to follow topography, and hence a lower sensitivity in SSM holes is to be expected.

Figure 9-2 and Figure 9-3 show examples of the variability in the profiles of environmental head in core drilled boreholes due to spatial variability. The variations are generally 1–2 m on either side of the mean value and span nearly all measured data, indicating that the deviations of the measurements from the *base case model* predictions can be explained by the combined effects of spatial variability in the HCD and HRD. As mentioned in Section 7.1.2, a limited number of adjustments of model parameters were made in order to obtain a reasonable match to the head data. Two variants are used here to illustrate why such changes were considered necessary. The first is based on the original prescription for HCD transmissivities defined in /Rhén et al. 2008/. This generally over-predicted heads in the boreholes, cf. /Rhén et al. 2009/.

The second important ingredient in the HCD property description was strong anisotropy in the dolerite dykes (associated with ZSMNS001C and ZSMNS059A, KLX19DZ5–8) as well as ZSMEW002A and ZSMNW042A-west that are thought to have some fault gouge in the core of the

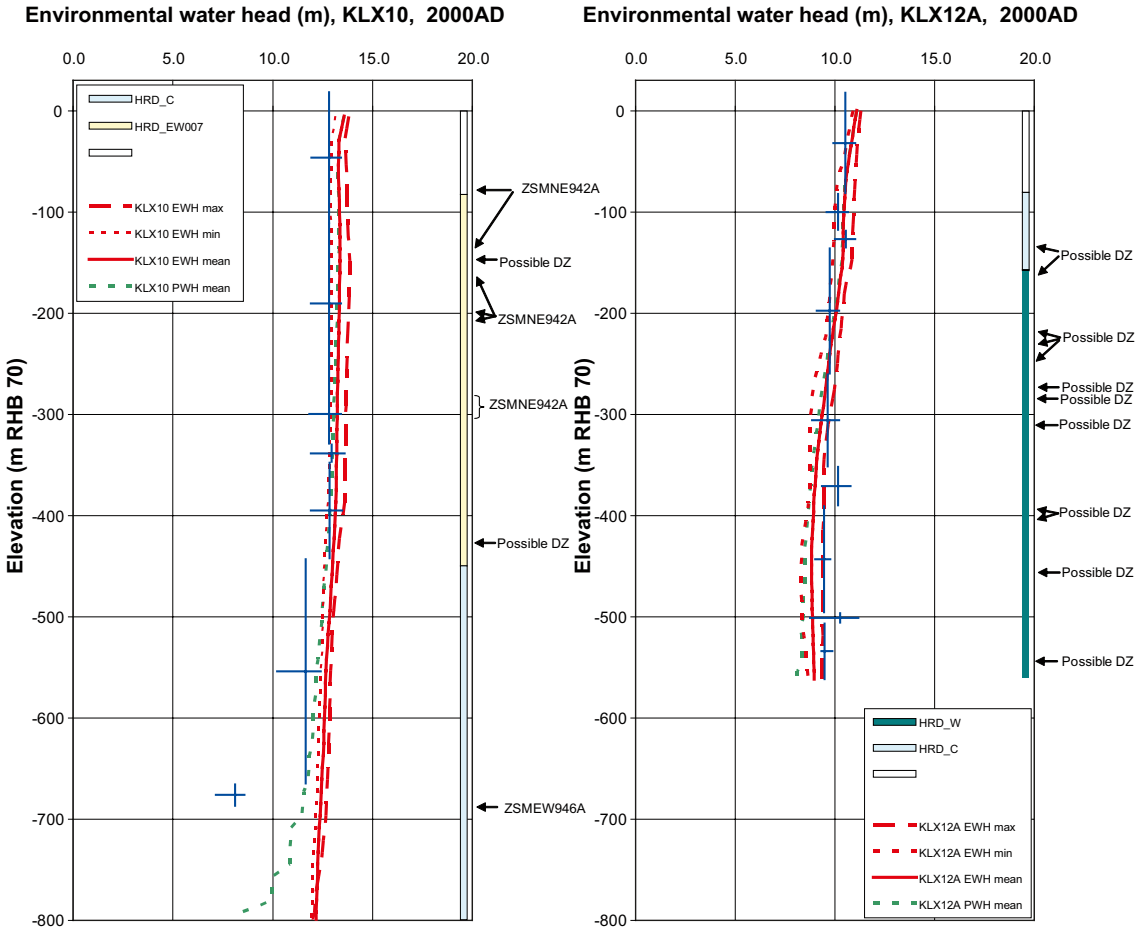

Figure 9-2. *Examples of stochastic variability of modelled environmental water head for 10 realisations of HCD and HRD (mean: solid red line; min:dotted red line; max: dashed red line) and point-water head (mean: dotted green line) in KLX10 and KLX12A in HRD_C compared with environmental-water heads (blue crossed lines; centre showing midpoint of the section, vertical line showing the extent of the section and horizontal line showing the temporal variation of the measured head). Environmental water heads calculated from measured point-water head data in sections along the borehole. At the right hand side, the prevailing hydraulic rock domains are shown as coloured bars along the borehole. Interpreted deformation zones are indicated at the intersection depth in the borehole.*

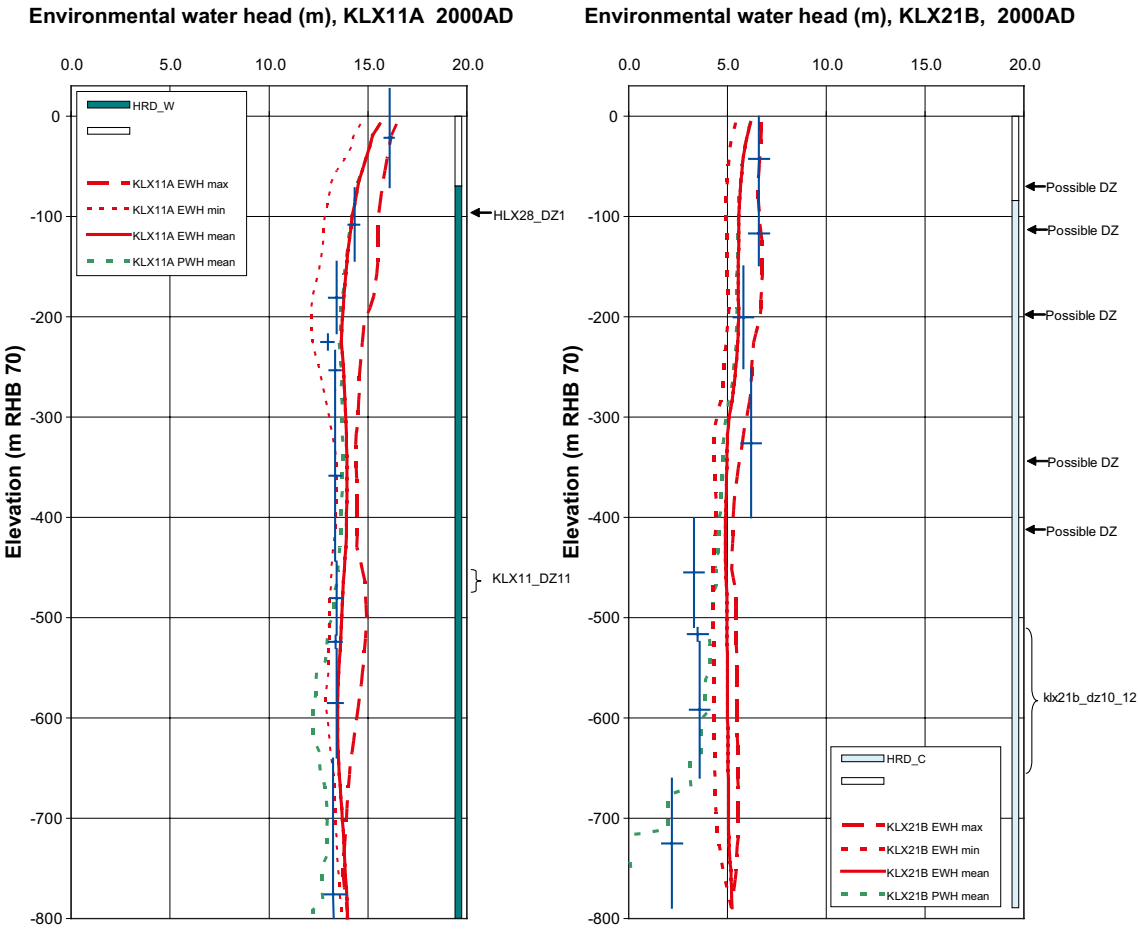

Figure 9-3. *Examples of stochastic variability of modelled environmental water head for 10 realisations of HCD and HRD (mean: solid red line; min:dotted red line; max: dashed red line) and point-water head (mean: dotted green line) in KLX11A in HRD_W and KLX21B in HRD_C compared with environmental-water heads (blue crossed lines; centre showing midpoint of the section, vertical line showing the extent of the section and horizontal line showing the temporal variation of the measured head). Environmental water heads calculated from measured point-water head data in sections along the borehole. At the right hand side, the prevailing hydraulic rock domains are shown as coloured bars along the borehole. Interpreted deformation zones are indicated at the intersection depth in the borehole.*

zone (see Section 5.1.2) creating a hydraulic barrier effect. Hence, as a second illustration, these HCD were made isotropic. The result is that the simulated sharp drop in head near ZSMEW002A shown in KLX06 disappears, and environmental head increases in the lower part of KLX19A rather than having a sharp drop across the dolerite dyke in DZ5–8. The effects of the dolerite dykes ZSMNS001A–C and ZSMNS059A, KLX19DZ5–8 in HRD_W can be seen on point-water head contours and Darcy velocity, cf. /Rhén et al. 2009/. Head contours tend to run mainly perpendicular to the dolerite dykes and flow is forced to run parallel to these HCD within and on either side of them. It results in large gradients in point-water heads toward the Laxemarån river valley in the south, which is confirmed by data in HLX28 and KLX19A, cf. /Rhén et al. 2009/ for details.

As discussed in Section 5.1.2, a number of the HCDs that are modelled as discs, have an uncertain size. However, no model variants were made with different sizes of these discs. Other main calibration variants and the resulting objective functions for comparing simulated and measured heads in the three different types of boreholes are summarised in /Rhén et al. 2009/. In summary, the sensitivity analysis confirms that using a general increase of a factor of around 3 of the hydraulic conductivity in the top 150 m of bedrock is about optimal for improving the head match. The sensitivities to the other variants were low apart from the changes made in calibrating the HCD. The changes made to the HRD properties, reducing hydraulic conductivity by a factor 1/3 below –150 m, made very little difference to environmental and point-water heads, as did the changes to the HSD in calibrating on the drawdown due to the Äspö HRL. The only other significant sensitivity of the environmental and point-water heads was to the calibration of the HCD properties.

9.2 Illustration of sensitivities considered during calibration of hydrochemical data

Around 30 variant simulations were performed to quantify the sensitivity of the palaeo-hydrogeology calibration to the hydraulic properties of the HRD and HCD, as well as initial and boundary conditions. Detailed illustrations of the results for these sensitivity variants can be found in /Rhén et al. 2009/ and below a few cases are discussed.

The effects of spatial variability in the HCD and HRD are illustrated in more detail in Figure 9-4 through Figure 9-5 for the case with std(Log10(T))=1.4 in the HCD. The plots compare the minimum, mean and maximum of chosen chemical constituents across 10 realisations for KLX03 and KLX08 with the *base case*.

Several variants were made to illustrate why changes were made in the calibration by using uncalibrated HCD, or uncalibrated HRD, or both, or a variant without anisotropy in the HCD. All demonstrate a significant deterioration in the match to hydrogeochemistry data. A case with both uncalibrated HCD and HRD was based directly on the transmissivities and hydrogeological DFN specified in /Rhén et al. 2008/, which gave a very poor match to the hydrogeochemistry data since it predicted virtually no *Glacial Water* remaining, for example. Changes to HSD made little difference.

A variant based on a change to the hydrochemical boundary conditions to assume the freshwater specified on the top surface to be *Altered Meteoric Water* prior to 4500 BC rather than *Glacial Melt Water* made little difference to the simulated present-day hydrogeochemistry.

Three variants on the initial condition were considered. The first had an alternative initial mixture of reference waters in the fractures and porewater corresponding to Case 2 in Section 6.6.2. This case predicted saline groundwater to be slightly deeper, and to have a *Littorina Water* component about 2–3 times higher than the *base case*. The second variant allowed more time for diffusive exchange (i.e. longer equilibration time of 10,000 years) between the initial condition in the fracture and matrix porewater (see Section 6.6.2) and /Rhén et al. 2009, Section 7.8.3 therein/, which only affects the levels of $\delta^{18}O$ in the fractures and matrix, resulting in less *Glacial Melt Water* in the fracture water. Shorter equilibration times tend to improve the match for the fracture water, but degrade the match to the porewater for $\delta^{18}O$. The third variant used the composition of *Inter-glacial Water* endorsed by the ChemNet Group (the Site Investigation group responsible for the hydrogeochemical data evaluation) referred to as 'Case 2' in Table 4-3 (Note: the initial amount of *Deep Saline* water in the matrix was reduced for this variant since *Inter-glacial porewater* is brackish in this case). This gave very similar results apart from predicting slightly lower salinity in the porewater below –500 m which is more consistent with the data.

Two further variants were considered as possible ways of improving the palaeohydrogeological calibration beyond that achieved for the *base case*. The first was to increase fracture surface area per unit volume in the HCD, σ, which governs the magnitude of rock matrix diffusion of solutes in the HCD, with the increase based on the values suggested in /Rhén et al. 2009/. ConnectFlow treats σ as a property of the hydrogeological rock units (HRD, HCD) rather than as a function associated with each finite-element, and hence modifying σ for the finite-elements intersected by each HCD required modifications to ConnectFlow. This case set the flow wetted surface area parameter used for solute transport, σ, in HCD consistent with that used for estimating flow-related transport resistance, a_r, generally resulting in an increase in σ. Such code changes were not available in time to be included for the *base case* simulations. This variant gave the best results overall, especially for boreholes intersecting major HCD, since the increased fracture surface area, σ, in the HCD resulted in a retardation of the mixing where advection was greatest. The change implemented in the model reflects the observation seen in the hydraulic data (see Table 5-2, for example) that effective hydraulic conductivity correlates strongly with PFL intensity whether it be in HRD or HCD. In more general terms, it suggests the numerical modelling would be more representative if the surface area per unit volume, σ, were correlated to hydraulic conductivity (in HRD and HCD) in ECPM models, since both correlate strongly to the underlying connected open fracture intensity. The second variant considered a higher hydraulic conductivity in the top 150 m of bedrock. This resulted in moderate improvements to the match of hydrochemistry data in many boreholes (more boreholes were affected by this variant than the first). Overall though the first variant gave the most significant improvements in improving the calibration.

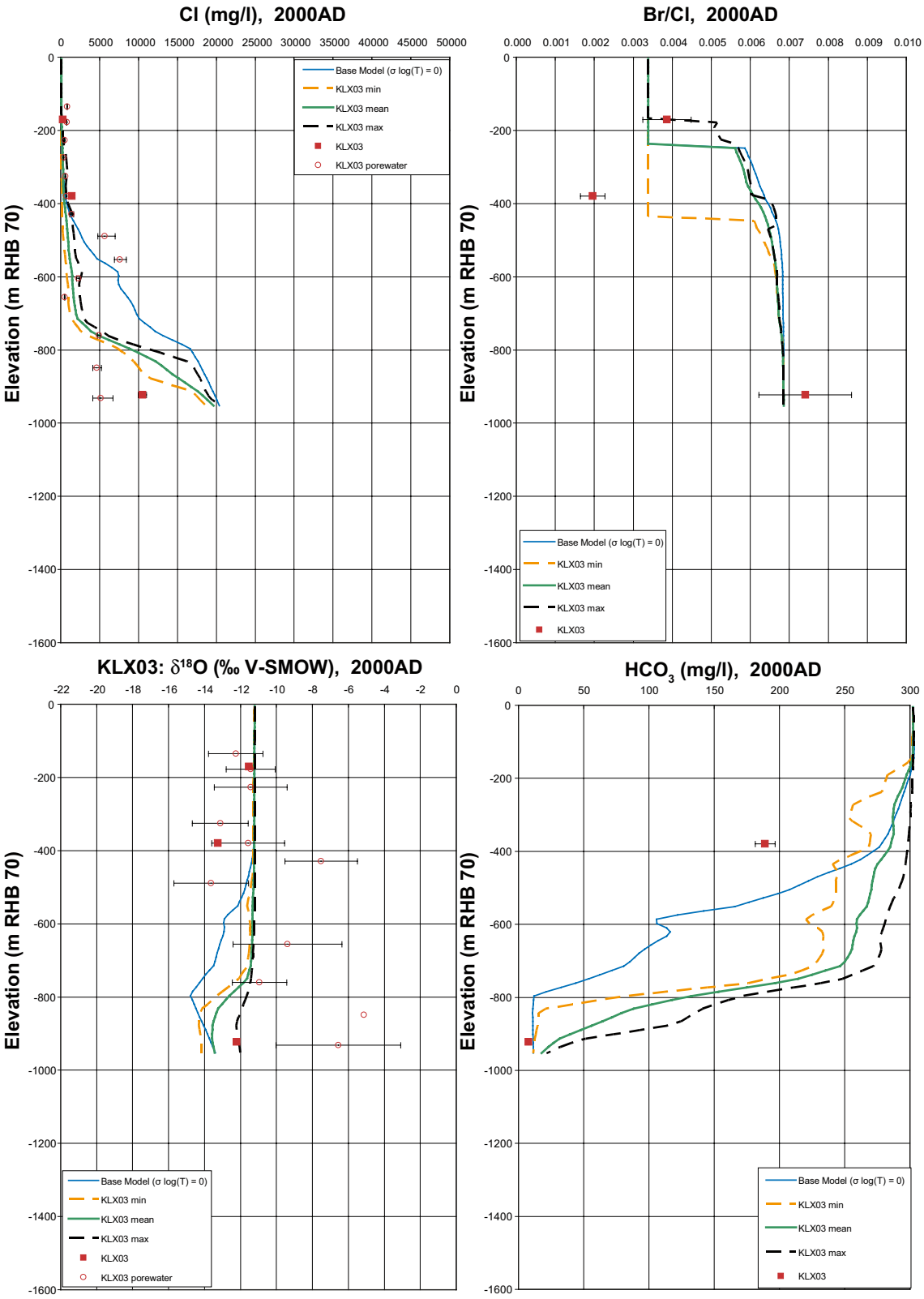

Figure 9-4. *Examples of stochastic variability of Cl, Br/Cl, $\delta^{18}O$ and HCO_3 in fracture water and porewater for 10 realisations of HCD and HRD (mean: solid green line; min: dashed orange; max: dashed black; base case: solid blue) compared to data in KLX03. Square symbols are used for Category 1–3 data, circles are used for the porewater data, and small point symbols for the Category 4 data. The error bars on the data indicate the laboratory analytical error.*

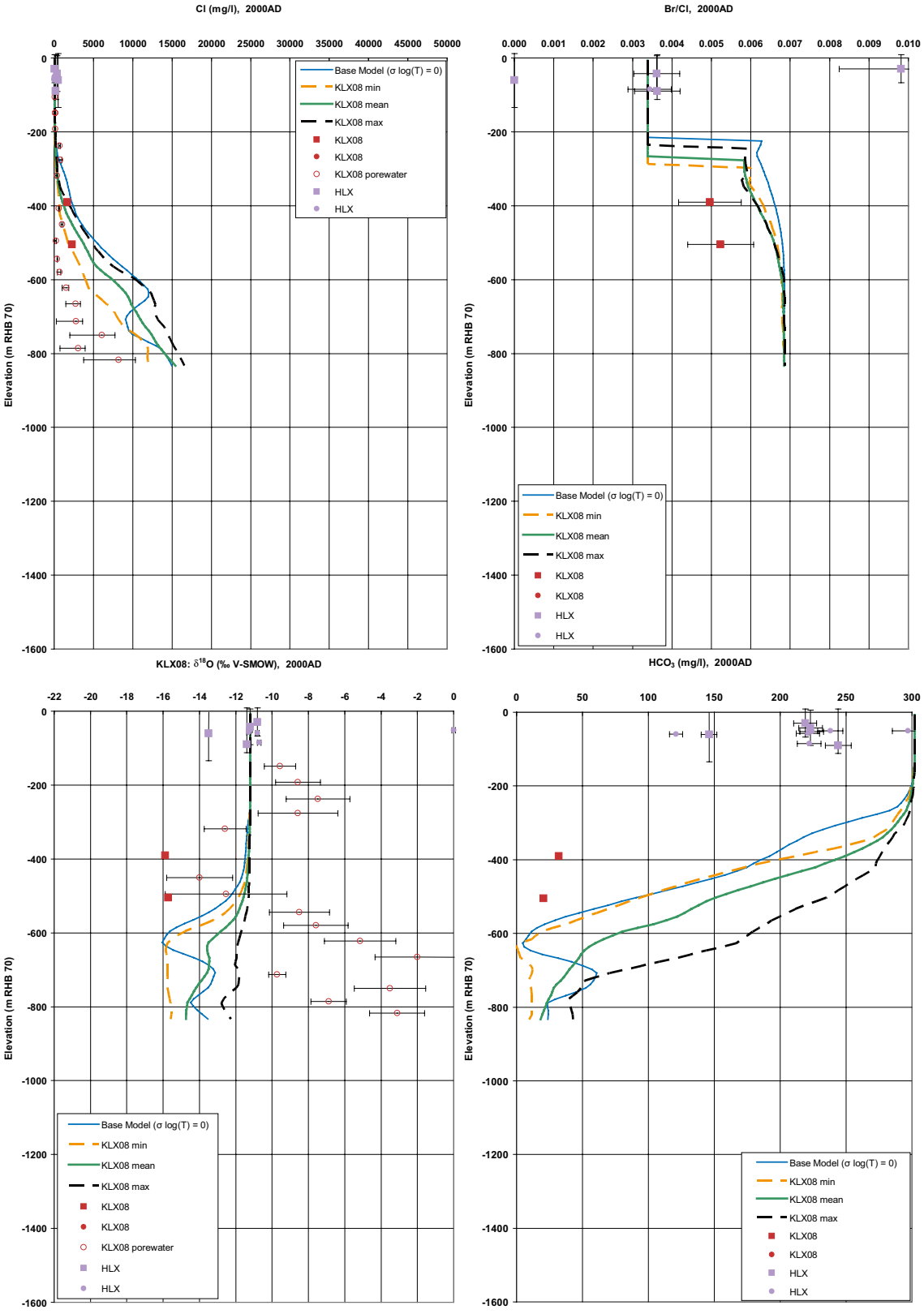

Figure 9-5. *Examples of stochastic variability of Cl, Br/Cl, $\delta^{18}O$ and HCO_3 in fracture water and porewater for 10 realisations of HCD and HRD (mean: solid green line; min: dashed orange; max: dashed black; base case: solid blue) compared to data in KLX08. Square symbols are used for Category 1–3 data, circles are used for the porewater data, and small point symbols for the Category 4 data. The error bars on the data indicate the laboratory analytical error.*

9.3 Illustration of flow-path sensitivities

The two most important sensitivities considered relevant to flow-paths are those relating to spatial variability and the influence of hydraulic anisotropy, especially that seen in the dolerite dykes ZSMNS059A and ZSMNS001. To quantify the effects of anisotropy, exit locations were calculated for the variant without any anisotropy in the HCD as shown in Figure 9-6. The main difference is that particles starting in HRD_W generally exit further to the east. Backward pathlines for this case as shown in /Rhén et al. 2009/ and one can see that more of the recharge to the HRD_C comes from west of ZSMNS059A, and more of the recharge to HRD_W comes from west of ZSMNS001C. Some particles reaching HRD_C and HRD_W originate from a considerable distance to the west southwest of the site. The *base case* also has anisotropy included in ZSMEW002A and the part of ZSMNW042A between ZSMNS059A and ZSMNS001. ZSMEW002A is too far north to have an effect. The changes in exit locations for HRD_W are attributed to the isotropy in ZSMNS059A rather than ZSMNW042A-west. These results demonstrate the strong influence of the dolerite dykes on HRD_W for the *base case*.

The variability of exit locations for the 10 realisations of HCD/HRD were considered with a standard deviation in Log10(T) of 1.4 in the HCD. The results are presented in Figure 9-7 and indicate the same key areas of discharge, but there are also quite a lot of additional minor discharge areas that occur when spatial variability is considered. Discharge associated with ZSMNS001D, ZSMEW002A, ZSMNW254A, ZSMNE021A all appear as being possible discharge areas when a stochastic representation of HCD/HRD is used. Hence, it is recommended that multiple realisations should be considered in future modelling work.

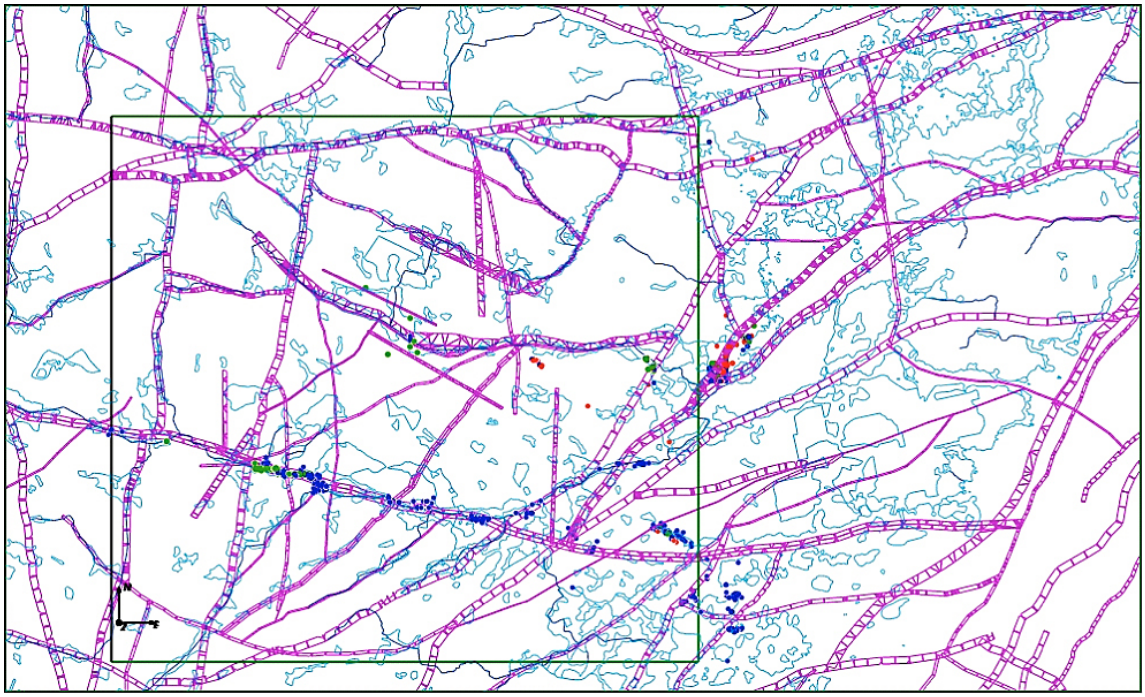

Figure 9-6. *Particle exit locations of pathlines released in HRD_C (blue), HRD_EW007 (red) and HRD_W (green) for the variant without anisotropy in HCD. HCDs on a slice at 0 m (purple), surface water bodies (cyan), streams (blue), and the Laxemar local model area (green box) are indicated.*

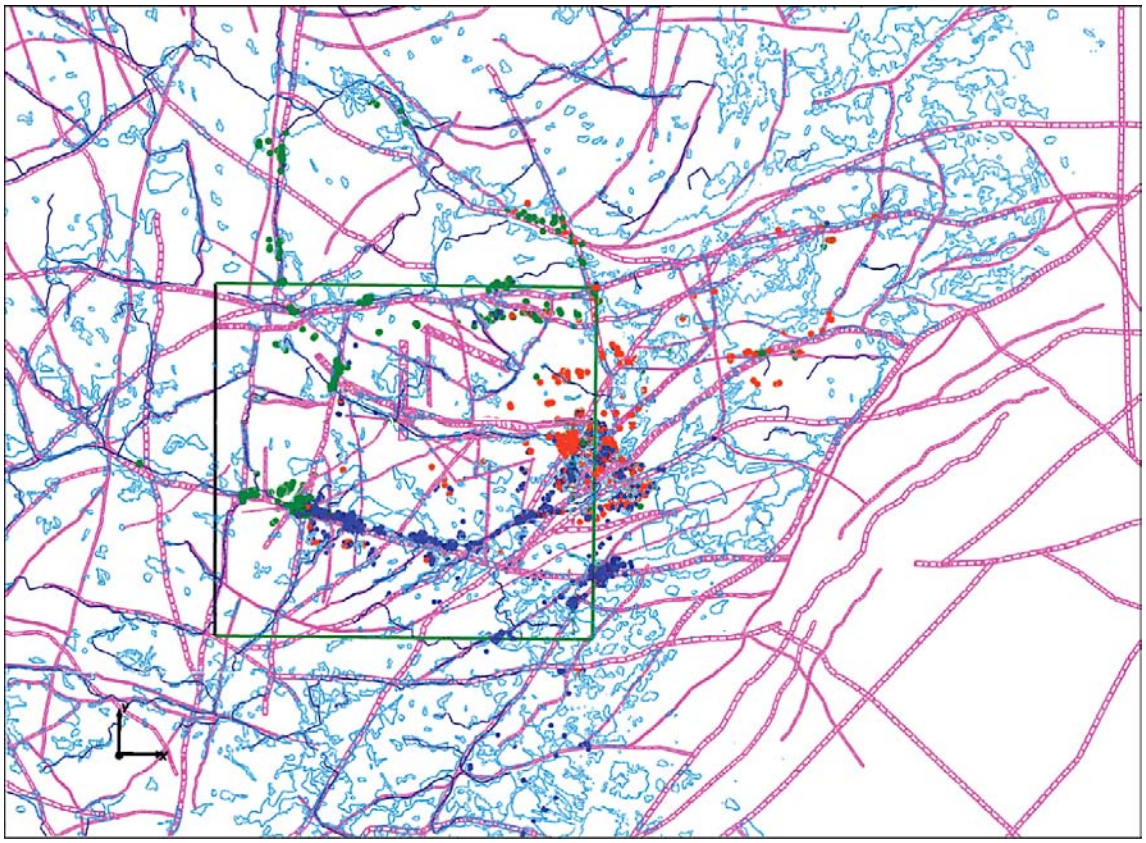

Figure 9-7. *Particle exit locations of pathlines released in HRD_C (blue), HRD_EW007 (red) and HRD_W (green) for 10 realisations of the HRD and HCD. HCDs on a slice at 0 m (purple), surface water bodies (cyan), streams (blue), and the Laxemar local scale model area (green box) are superimposed.*

10 Discussion and conclusions

10.1 Summary of the bedrock hydrogeological model

The overall hydrogeological characteristics of the investigated area are featured by close proximity to the coast, a fairly flat topography (regional topographic gradient in the order of 4%) but with relatively distinct valleys. The investigation area is located within a crystalline basement, mostly covered by a rather thin till in the elevated areas and with glaciofluvial sediments in the larger valleys. The average annual precipitation and specific discharge at the site are estimated to be approximately 600 mm and 160–170 mm, respectively.

The groundwater recharge takes place in the elevated areas and groundwater discharge is located in the valleys and near the coast. A large part of the infiltrated groundwater is only flowing through the Quaternary deposits and the upper most part of the bedrock to its discharge points. Deeper down in the bedrock large deformation zones are important for how the groundwater flow field develops.

The site models, e.g. the bedrock hydrogeological model, have been developed in several steps with modelling reports describing investigations, data and modelling after each step. With the successively data evaluation and reporting, investigations in the following step were focused on issues that were not sufficiently described and it also provided means for the important integration between the disciplines involved; surface systems, bedrock geology, bedrock thermal properties, rock mechanics, bedrock hydrogeology, bedrock hydrogeochemistry and bedrock transport properties.

The bedrock hydrogeology within the SDM-Site Laxemar regional model area, with main part of the investigations within the focused area (cf. Figure 1-6), has been investigated with several hydrogeological investigation methods; e.g. single-hole tests (pumping tests (PSS and HTHB), constant injection tests (PSS), difference flow logging (PFL)) and interference (or cross-hole) tests to characterise the hydraulic properties of the large deterministic deformation zones and the rock between these zones. In the hydrogeological model, the large deformation zones that are modelled deterministically are denoted as hydraulic conductor domains (HCD) and the rock between the HCDs is named hydraulic rock domains (HRD). Main findings are that there is a significant depth trend in the hydraulic properties and also a large spatial variability of the hydraulic properties making the rock mass highly heterogeneous. The parameterisation of the base case model is detailed in /Rhén et al. 2009/.

10.1.1 Hydraulic characteristics of the hydraulic conductor domains (HCD)

The key interpreted characteristics are:

- A clear trend of decreasing transmissivity with depth.
- A positive correlation between interpreted deformation zone “size” and transmissivity. Size here corresponds to interpreted trace length on the surface.
- Indications that the transmissivity of HCDs is dependent on the orientation of deformation zones. E-W zones appear more conductive than zones of other orientations.
- Significant lateral variability with an estimated standard deviation of Log10(T) of 1.4. The standard deviation of Log10(T) of the entire sample of HCD transmissivities is 1.4 and standard deviation of Log10(T) of transmissivities within individual zones is in the range 0.5 to 2. Sample sizes within individual zones were between 2 to 14.

10.1.2 Hydraulic characteristics of the hydraulic rock domains (HRD)

The key interpreted characteristics are:

- The flowing features (fractures and minor deformation zones) can be grouped in four orientation sets; steep ENE, WNW, N-S and a subhorizontal set.
- The intensity of flowing features is generally highest for the WNW set (aligned with the principal horizontal stress) with the subhorizontal set also being important in the upper bedrock.
- A clear decreasing intensity of flowing features with depth but generally with a similar transmissivity distribution of the flowing features for the specific depth interval studied (as measured by difference flow logging; PFL-f).
- As a consequence – a resulting clear trend of decreasing hydraulic conductivity with depth, (injection tests, test scale 100 m) may be observed.
- The hydraulic conductivity is c. 10 times lower in HRDs than that of the HCDs (injection tests, test scale 100 m).

The orientations of the principal sets of flowing features roughly correspond to the main orientation groupings of the deterministic deformation zones, see /Wahlgren et al. 2008, cf. Chapter 5 therein/.

10.1.3 Hydraulic characteristics of the focused volume

Combining the interpretation of hydraulic characteristics of the bedrock from /Rhén et al. 2008/ with the understanding gained from simulating the palaeohydrogeological evolution, the hydrogeological situation for groundwater flow and solute transport /Rhén et al. 2009/ is summarised in Figure 10-1 which is a schematic representation of Table 10-1.

Table 10-1. Schematic summary of groundwater flow and solute transport characteristics under the current temperate climate conditions.

Depth zone	General characteristics
dZ1: > –150 m	Near-surface rock, characterised by a high intensity of conductive fractures. Subhorizontal and steeply dipping fractures striking WNW dominate.
	Advection dominated – high groundwater flow rates with subhorizontal fracturing giving $K_h > K_v$ in many areas. Flushed by post-glacial meteoric water. High fracture intensity implies matrix blocks 1–2 m in size, which gives equilibrium between fracture and matrix on timescales of ~1,000 years.
dZ2: –150 m to –400 m	Intermediate-depth rock, characterised by an intermediate intensity of conductive fractures. Steeply dipping fractures striking WNW dominate except for in HRD_W where no set is clearly dominant and in HRD_N and HRD_C the subhorizontal set is also important beside the WNW set.
	Some advection, but rock matrix diffusion (RMD) retards post-glacial meteoric penetration. Fracture intensity is generally much lower, reducing groundwater flux and increasing matrix blocks to typically ~5 m in size, such that porewater chemistry lags behind that of the fracture water by 1,000s of years. Fracture intensity is generally much lower, reducing groundwater flux and increasing matrix blocks to typically ~5 m in size, such that porewater chemistry lags behind that of the fracture water by 1,000s of years.
dZ3: –400 m to –650 m	Rock at repository level, characterised by a low intensity of conductive fractures. Steeply dipping fractures striking WNW dominate except for HRD_W where no set is clearly dominant.
	Low advection. RMD important because advective flow rates are small. Fracture intensity lower still, with typical matrix blocks ~10 m in size, such that porewater chemistry lags behind that of fracture water ~10,000 years. Expect some difference between fracture and porewater chemistries.
dZ4: < –650 m	Deep rock, characterised by a sparse network of conductive fractures. Steeply dipping fractures striking WNW dominate except for HRD_W where no set is clearly dominant (however rather few data occur within dZ4).
	Very low advection. RMD dominates Fracture intensity very low, with typical matrix blocks ~100 m in size, such that porewater chemistry lags behind that of fracture water ~100,000 years. Differences between fracture and porewater chemistries are to be expected.

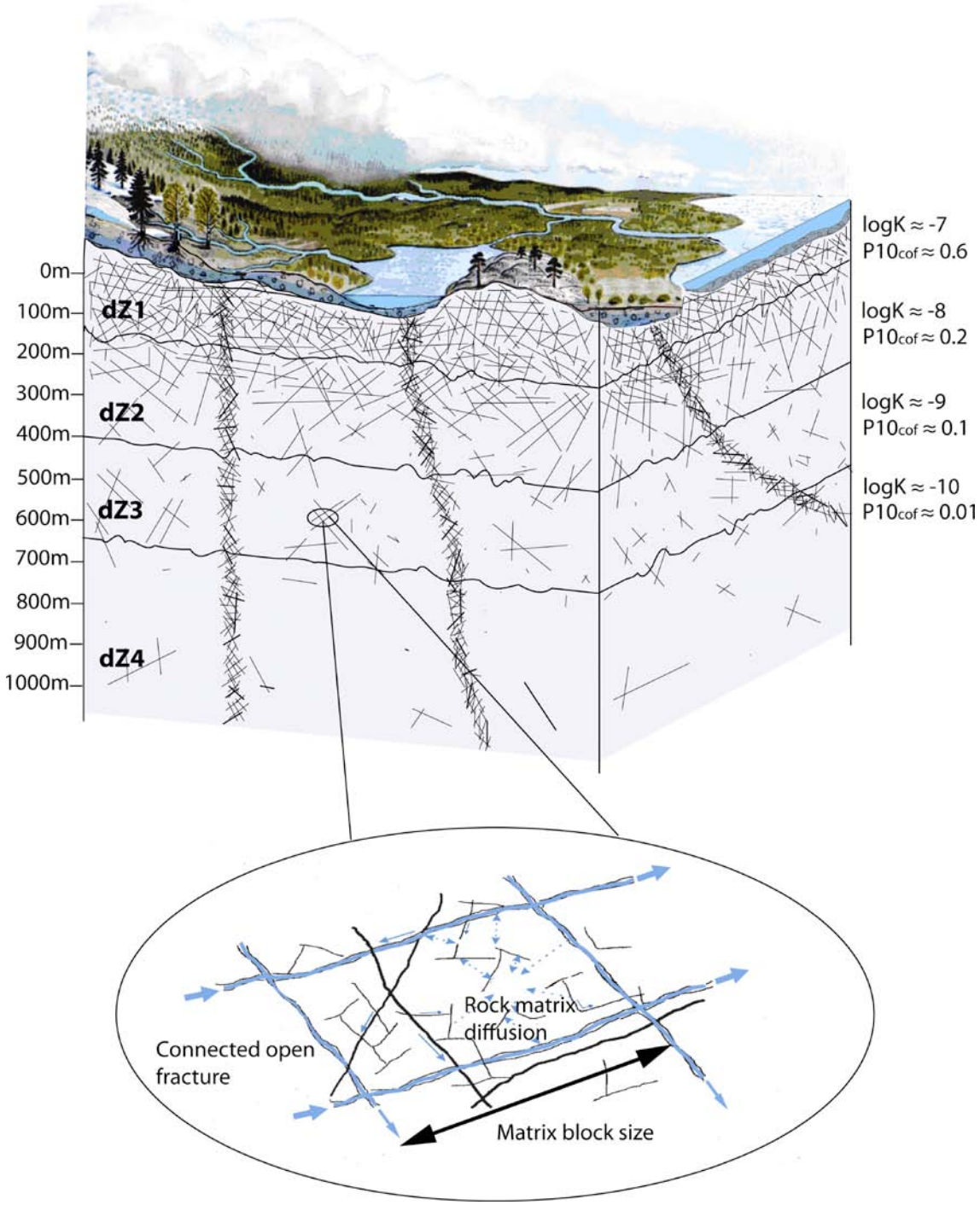

Figure 10-1. *Schematic 3D cross-section summarising the hydrogeological conceptual model of the bedrock within the focused volume in Laxemar. Flow in the uppermost depth zone dZ1 is dominated by subhorizontal and WNW fracturing. Solute transport is dominated by advection with matrix block sizes of about 2 m, and about 1,000 years for hydrochemical equilibrium between fractures and matrix. WNW fractures dominate flow in dZ2–dZ4. In dZ2, solute transport is retarded significantly by RMD with matrix block sizes of about 5 m and chemical signatures in the matrix lagging 1,000s of years behind the evolution in the fractures. RMD dominates solute transport in dZ3 with a few sparse areas of significant advection. Matrix block sizes are around 10 m, and matrix hydrochemistry lags 10,000s of years behind the evolution in the fractures. There is very little advection in dZ4 with matrix block sizes of about 100 m and 100,000s of years lag between matrix and fracture hydrochemistry. (K: hydraulic conductivity (m/s), approximate values in scale c 100 m. P_{10cof}: Intensity (P_{32}) of connected open fractures with a transmissivity > c. 10^{-9} m^2/s.)*

10.2 Conceptual modelling

The hydrogeological conceptual modelling has focused on:

- the geometries and properties of large hydraulically conductive fracture zones that should be described deterministically in space (the HCDs),
- the geometries and properties of the rock volumes between the HCDs (the HRDs), and
- the boundary and initial conditions suitable for groundwater flow modelling.

The basis for the hydrogeological analyses of hydraulic test results has been the geological models of the deformation zones, the rock domains and the fracture domains. Monitoring of water levels in borehole observation sections and water samples from boreholes were important for assessing boundary and initial conditions.

Hydraulic injection tests and difference flow logging gave an early indication of a depth trend of the hydraulic properties and of a difference between HCDs and HRDs in terms of permeability, which were successively better established during the investigations.

The role of N-S dolerite dykes associated with ZSMNS001A–C and ZSMNS059A (along with some other dolerite-affected minor HCD) as flow barriers appears to be confirmed by differences in measurements in natural heads and the results of interference tests across/along these zones. A similar effect arising from clayey fracture infills or fault gouge in ZSMEW002A and ZSMNW042A-west also appears to be confirmed by natural head data.

Hydraulic head is estimated from borehole measurements; water levels in short boreholes or measurements of the point water head in packed-off borehole sections. The water level in the uppermost borehole section provides an estimate of the groundwater level and the deeper sections of the head variation towards depth. The natural (undisturbed) groundwater levels generally follow the topography. In the Quaternary deposits, the depth to the groundwater table is expected to be within a few metres from the ground surface, with maximum depth at topographic highs and minimum depth in the valleys, as shown by measurements. The natural (undisturbed) point water head in the upper bedrock behaves similarly, but there is a noticeable downward gradient in the upper 200 m of bedrock for around half the core drilled boreholes (generally drilled from smaller hills), the rest showing low vertical hydraulic gradients.

The major ions considered important in the groundwater flow model calibration are Br, Ca, Cl, HCO_3, Mg, Na, K and SO_4. The two stable isotopes of interest to hydrogeology are δ^2H and $\delta^{18}O$. Chemical constituents, such as Cl, Br and $\delta^{18}O$, are transported conservatively within the transport times considered. Other chemical constituents are likely to be non-conservative, such as HCO_3 and SO_4, which can be affected by chemical and microbial processes. However, more rapid reactions that take place in the soil and upper bedrock are treated implicitly by defining '*Altered Meteoric Water*' based on groundwater samples in the upper bedrock and using this for the composition of water infiltrating the groundwater system on the top model boundary. Mg is not a conservative tracer either, but it is a useful indicator to help differentiate between Deep Saline Water at depth and shallower Littorina Sea Water near the top surface of the model domain. Along with the hydrochemical interpretation of the water sample data, cf. /Laaksoharju et al. 2009/, and the interpretation of the palaeohydrogeological development, cf. /Söderbäck 2008/, the spatial distribution of the present chemical components indicate how the groundwater flow system has evolved over time. To a large extent the traces of the *Littorina Sea Water* has been flushed out in Laxemar but remains to some extent near the coast. Within the depth interval –250 to –600 m the Laxemar groundwaters are characterised mainly by brackish glacial types with some examples of brackish non-marine and transition types. The depth interval –600 to –1,200 m marks the transition from brackish non-marine to a saline groundwater type, characterised by a steady increase in chloride to about 16,000 mg/L /Laaksoharju et al. 2009/.

10.3 Numerical modelling and confirmatory testing

Regional scale groundwater flow and solute transport simulation tests of palaeohydrogeological evolution, natural head measurements and hydraulic interference test data have confirmed that hydrogeological properties, as given by the hydrogeological DFN model *base case* /Rhén et al. 2008/ (based on all open and partly open fractures and semi-correlated transmissivity model), together with the HCD parameterisation provide an appropriate description of the hydrogeological situation in the bedrock. Only relatively minor modifications were considered necessary to obtain an acceptable match between the regional groundwater flow model results and field data.

10.3.1 Numerical model domain size

A much larger model size than the size of the *base case* was tested by /Holmén 2008/ who demonstrated that the weakly developed surface water divide employed for delimiting the western regional model boundary in the *base case model* is in fact not a groundwater divide for groundwater flow at greater depth. Furthermore, it was shown that a model with model size as the *base case model* may underestimate groundwater flow at repository depth, and overestimate both lengths of flow paths as well as the breakthrough times of flow paths from the repository area within a factor 1.5, which is considered a small difference. As the *base case model*, unlike the model used by /Holmén 2008/, also includes N-S striking dolerite dykes that probably act, at least in part, as flow barriers, the factor 1.5 is possibly overestimated.

10.3.2 Natural groundwater levels

The confirmatory testing with the regional groundwater flow model has shown that in general the initially assessed transmissivity models for the HCD (based on the hydraulic test results) complies with the resulting confirmatory model, however with a general slightly lower transmissivity (Multiplication factors of 1.0, 0.3 and 0.1 of original values were employed between ground surface down to –150 m, between –150 to –650 m and below –650 m, respectively.) included in the SDM-Site *base case.*

Simulations of the natural heads demonstrate the need for anisotropy in the hydraulic properties of the ZSMEW002A, the origin of which is attributed to the effects of fault gouge.

10.3.3 Drawdown due to inflow to Äspö hard rock laboratory (HRL)

By modifying the HSD on the sea floor in the bays around Äspö to be of gyttja clay type with a vertical hydraulic conductivity in the range 10^{-9} to 10^{-8} m/s, centred on $5 \cdot 10^{-9}$ m/s, the responses in eastern part of Laxemar and north-western part of Ävrö could be reproduced.

The modelling of the drawdown around the Äspö HRL indicated that HRD_A2 (located east of the focused area) should be based on initial values for hydraulic conductivity rather than the reduction by a multiplication factor 1/3 of the hydraulic conductivity below –150 m found relevant for the entire regional model area based on the palaeohydrogeological calibration. (This has not been implemented in the *base case model*.)

The simulations of the drawdown resulting from the Äspö HRL suggest that measurements of point-water heads and hydrochemistry within the Laxemar local model area have not been significantly affected by the Äspö HRL facility, apart from the far eastern part of Laxemar local model area.

10.3.4 Interference tests in HLX33 and HLX28

Simulations of the natural heads and HLX28 interference tests demonstrate the need for anisotropy in the hydraulic properties of the dolerite dykes ZSMNS001C, ZSMNS0059A and in HCD ZSMNW042A-west.

The hydraulic interference test in HLX28 also suggests a possible increase by a factor 3–4 of the transmissivity (in plane) than in the *base case* for the upper sections of HCD HLX28_DZ1, HCD ZSMNW042A-west and ZSMNS059A. (This has not been implemented in the *base case model*.)

Modelling of the HLX33 interference test confirms the dip to the north of HCD ZSMEW007 but also that the upper part of this HCD should be attributed a transmissivity than initially suggested based on single-hole test results.

10.3.5 Hydrochemical data in cored boreholes

The *base case model* gave a reasonable reproduction of the measured groundwater chemistry in the site boreholes and predicted a 3D distribution of groundwater chemistry broadly consistent with the interpretation made by Hydrochemistry on vertical slices across the focused volume.

The key step for the calibration of the palaeohydrogeological simulations was a slight reduction (1/3 of initial assessed values) in hydraulic conductivity (horizontal and vertical) below –150 m elevation for both the HCD and HRD.

Other transport related parameters that were important for the palaeohydrogeological calibration were kinematic porosity and flow wetted surface area, and of HCD in particular. For kinematic porosity, it was found appropriate to account for all fracture void area associated with all connected open fractures and compensate for any voidage lost through fracture size truncation. It was found important to represent the relatively high flow wetted surface in the HCD by estimating this from PFL feature intensity within HCDs in order to include the locally enhanced RMD.

Simulated hydrochemical conditions in individual boreholes were found to be sensitive to spatial variability in HCD and HRD. The results indicate that the depth to which post-glacial meteoric flushing of the fracture groundwater takes place (typically –400 to –500 m in the Laxemar local model area) varies by about 50 to 100 m between realisations (here incorporating the combined effect of the variation generated by the stochastic variation of HCDs and HRDs). Considering this variation between the realisations, the modelling results compare well with measured data.

Simulations of tritium migration have confirmed that the developed palaeohydrogeological models are generally consistent with the interpretation of hydrogeochemistry /Laaksoharju et al. 2009, cf. Section 7.2.2 therein/, in that modern meteoric recharge from the last 50–60 years to the groundwater system is restricted to a depth of approximately 150 to 200 m.

A series of what were considered credible ranges of initial and boundary conditions for past hydrochemical conditions were considered in the modelling. Sensitivities to these choices are small compared to changes in hydraulic or transport properties. Hence, it is concluded that although these initial and boundary conditions are quite uncertain, those considered have been defined based on careful conceptual considerations, and simulation made confirm their credibility. Further, they demonstrate that palaeohydrogeological modelling results are not overshadowed by the inherent uncertainty in initial and boundary conditions.

Likewise, the hydrogeochemical composition of the porewater at depth is uncertain, but plausible alternatives can be accommodated within the conceptual model without large implications for the results.

10.3.6 Flow-paths from a tentative repository layout

The HCDs that are considered strongly anisotropic, i.e. large contrast between longitudinal (in plane) hydraulic conductivity and transverse hydraulic conductivity, were introduced in the groundwater flow modelling. Particle tracking has shown that this anisotropy has significant impact on groundwater flow patterns, in at least, the western part of Laxemar local model area.

10.4 Confidence and remaining uncertainties

The parameter assessments of the hydrogeological model based on single-hole tests were tested using several types of data; drawdown caused by Äspö HRL, interference tests, natural point-water head measurements and hydrochemical data. These tests with the regional groundwater flow model resulted in a few suggested changes of the parameterisation (e.g. a general decrease by factors around 1/3 for some transmissivities or hydraulic conductivities of HCD and HRD, respectively, assessed by single-hole tests) but in general the initial parameterisation was found satisfactory. The transport parameters used for the hydrogeological modelling are considered uncertain but provides reasonable matches to the data available. The uncertainties involved in the transport of solutes are discussed further by /Crawford and Sidborn 2009/. There are however also other remaining uncertainties that are discussed below.

10.4.1 Groundwater levels in the bedrock aquifer

The calculated environmental heads in the deeper part of the bedrock, based on the point-water heads under natural (undisturbed) conditions, are uncertain due to difficulties to collect representative water density of the formation water. Due to this it was judged that adjustments of hydraulic properties below c. –800 m elevation should not be made based solely on data representing natural head conditions. It is judged that this lack of high quality data has not had any severe consequences for the calibration but contributes to the uncertainty of assessed properties below c. –800 m elevation.

10.4.2 Structural model (HCD)

Within the focused volume several of the deformation zones (HCD) are intersected by one or more boreholes. It was observed that there is a large variability of hydraulic properties within some of the deformation zones, indicating that heterogeneity is likely to be high within the HCD. As a consequence most assessments of hydraulic properties for an individual HCD in the present model must be considered highly uncertain, although the general depth trends of mean transmissivity seem well justified by the tests made with the regional groundwater flow model. The assessed variability of the transmissivity used in the modelling (as a large-scale variation) is supported by data but must still be considered uncertain.

One should also observe that within the Laxemar local model volume the numbers of borehole intercepts with deformation zones are more limited below –150 m elevation compared with above, and the total number of intercepts is smaller compared with the regional data set. Therefore, the assessment of trend functions of the transmissivity with depth for the HCD is uncertain (but the uncertainty is quantified in terms of confidence limits of geometric mean, cf. /Rhén et al. 2008/).

Outside the local model area there are only hydraulic tests available east of the local model area, providing data for estimating properties of HCD. As there are no data for larger parts of the regional model volume, the assessed properties outside the Laxemar local model volume are obviously highly uncertain.

The existence of dolerite dykes and their possible function as hydraulic barriers have been substantiated by cross-hole test results. However, it is not known if the most obvious example, ZSMNS001, acts as a barrier along its entire extent. The other substantiated dolerite dykes seem to be possible local hydraulic barriers but it is considered very uncertain if they constitute barriers over longer distances. The thicknesses observed in boreholes are limited and may indicate that one should not expect a barrier effect of similar character to ZSMNS001 seen in south-western part of the focused area. The geological description also indicates that possibly other dolerite dykes than those observed in boreholes may exist, but they are expected to be relatively thin and may only act as highly localised hydraulic barriers, and are regarded to be of low significance for the overall groundwater flow pattern.

Some HCD, lacking surface outcrop (lineament) and being intercepted only by one borehole, are modelled with an assumed radius of 564 m. The size and character of these HCD is considered highly uncertain. These HCDs also are of similar size as the largest minor deformation zones modelled stochastically, see next section.

10.4.3 Hydraulic rock domain (HRD) model

The investigations have been extensive but also covered a large area (volume) including both the Laxemar local model area and the Simpevarp subarea, cf. Chapter 1. As a consequence there are fairly large distances between boreholes even within the focused area and there are limited amounts of data to assess spatial distributions of hydraulic properties to define subvolumes (HRD) with different properties, as well as depth dependencies. One should therefore expect that there can be a considerable variation in the properties within the hydraulic rock domains defined in the focused volume. Especially below elevation –650 m, data on the conductive fractures are sparse and the hydrogeological DFN models below that elevation should be considered uncertain.

Hydrogeological DFN models with three different types of transmissivity distributions have been developed but only the transmissivity model that is considered to be the conceptually most reasonable based on all open fractures has been tested in the regional groundwater flow modelling. It remains to test the other hydrogeological DFN models developed on a regional scale to assess how they behave relative to the hydraulic tests available for testing out the groundwater flow model.

The developed hydrogeological DFN models exhibit anisotropic conditions that vary mainly by depth (horizontal and WNW conductive fractures dominate near surface and by depth the intensity of the horizontal set decreases). The magnitude of the ratio between maximum and minimum permeability estimated from block modelling of the hydrogeological DFN models is considerably less than that observed in the nearby Äspö HRL, possibly suggesting that the anisotropy within the Laxemar local model volume is underestimated. Still, the directions for maximum and minimum permeability in the horizontal plane are consistent, and provide the right indications of how the anisotropy changes with depth.

The hydrogeological DFN includes conductive features from decimetre scale to features with radius of 564 m, where the largest can be assumed to be minor deformation zones (MDZ). The hydraulic character of these MDZ is uncertain. The intensity of MDZs (P_{32}) was estimated to be in the range c. 0.02 to 0.06 m^{-1} for different fracture domains, leading to that the minimum radius of MDZ is estimated to be in the range of 50–200 m based on the geological DFN models. However, only for 60% of all the MDZ-intercepts of boreholes can be expected to have a conductive feature with a transmissivity $T > 10^{-9}$ m^2/s, and the intensity of these hydraulically conductive MDZs decrease with depth. Data have shown that the geologically mapped MDZ are likely to be hydraulically heterogeneous, but so far all hydrogeological DFN features are modelled homogenous. Modelling the largest hydrogeological DFN features as heterogeneous features may thus appear as conceptually more appropriate, but has not been tested yet.

Outside the local model volume there are only a few hydraulic tests east of the Laxemar local model area relevant for calibrating the hydrogeological DFN models. The assessed hydrogeological DFN properties within the regional volume outside the Laxemar local model volumes are obviously highly uncertain.

10.4.4 Compartmentalised fracture networks at repository depth

The calibration of the hydrogeological DFN model considers the connected conductive fractures on a large scale, since it is based on the results of PFL logging established during long-term pumping. The comparison of the PFL test results with results of transient PSS tests, with fairly short-term pumping/injection, in the corresponding boreholes indicate that there probably exist local, fairly low-transmissive (generally less than c. 10^{-8} m^2/s), fracture networks (compartmentalised networks) that are not, or at least poorly, connected to the "global hydraulically connected fracture system" tested by the PFL logging /Rhén et al. 2008/. The role of compartmentalised networks, if existent, needs to be addressed in future modelling.

10.4.5 Summary of remaining uncertainties

The remaining uncertainties can be summarised as below:

- Given that a large volume of rock has been investigated with a limited number of boreholes, and given that the spatial variation of hydraulic properties is large within the HCDs and the HRDs, the uncertainties associated with the hydraulic properties of an individual HCD and the spatial variation of hydraulic properties within individual HRDs are high.
- Below a depth of 650 m the rock is considered low-conductive. However, data are sparse and the assessment of properties is inherently uncertain.
- Some of the HCDs are associated with dolerite dykes that act as hydraulic barriers, as evidenced by *in situ* measurements, but it is unclear if these dykes act as barriers along their entire HCD extents.
- Some HCD, lacking surface outcrop (lineament), being only intercepted by one borehole, are modelled deterministically with an assumed radius of 564 m. The size and character of these

HCD are considered highly uncertain. These HCDs are of similar size as the largest MDZ modelled stochastically.

- It is also recognised that the minor deformation zones (MDZ) are likely to be hydraulically heterogeneous. Of the geologically defined MDZs, c. 60% have a conductive feature (with transmissivity larger than c. 10^{-9} m^2/s). However, so far these MDZs are included as homogenous features in the hydrogeological DFN model.
- The developed hydrogeological DFN has been calibrated using different transmissivity models, but only the conceptually most reasonable model, the semi-correlated transmissivity-size model, has been tested in the context of regional scale flow modelling. The hydraulic anisotropy evidenced by the developed hydrogeological DFN model is also considered uncertain; it may in fact be larger than what the current model shows, as presently observed at the Äspö Hard Rock Laboratory immediately east of the focused area.

10.5 Concluding remarks

The general conditions of the groundwater flow situation in the Laxemar model area is well established after several stages of investigations followed by updated hydrogeological models. The aspects of the spatial variation of the hydraulic properties within the Laxemar focused area are well understood, with a clear depth dependency and the deterministic deformation zones (HCD) in general being c. one order of magnitude more conductive than the average rock. Numerical groundwater flow modelling has been used both to test the parameterisation of the hydraulic domains as well as for furnishing confirmatory tests of the understanding and interpretations developed. In particular, hydrogeological DFN models of the HRD and parameterisations of the HCD have been defined for end-users such as Repository Design and Safety Assessment. A demonstration of the consistency between these model parameterisations and hydraulic tests and head measurements performed at the site has been made. Further, the integrated understanding of the evolution of the hydrogeological and hydrochemical conditions in the Laxemar-Simpevarp area has been demonstrated by simulation of the palaeohydrogeological evolution during the Holocene period.

11 References

SKB's (Svensk Kärnbränslehantering AB) publications can be found at www.skb.se/publications.

Andersson J, Ström A, Almén K-E, Ericsson LO, 2000. Vilka krav ställer djupförvaret på berget? Geovetenskapliga lämplighetsindikationer och kriterier för lokalisering och platsutvärdering. SKB R-00-15, Svensk Kärnbränslehantering AB.

Andersson J, Berglund J, Follin S, Hakami E, Halvarson J, Hermanson J, Laaksoharju M, Rhén I, Wahlgren C-H, 2002. Testing the methodology for site descriptive modelling. Application for the Laxemar area, SKB TR-02-19, Svensk Kärnbränslehantering AB.

Ask H, 2003. Installation of four monitoring wells, SSM000001, SSM000002, SSM000004 and SSM000005 in the Simpevarp subarea. Oskarshamn site investigation. SKB P-03-80, Svensk Kärnbränslehantering AB.

Ask H, Samuelsson L, 2003. Drilling of three flushing water wells, HSH01, HSH02 and HSH03. Oskarshamn site investigation. SKB P-03-114, Svensk Kärnbränslehantering AB.

Ask H, Morosini M, Samuelsson L, Stridsman H, 2003. Drilling of cored borehole KSH01. Oskarshamn site investigation. SKB P-03-113, Svensk Kärnbränslehantering AB.

Ask H, 2004. Drilling and installation of two monitoring wells, SSM 000006 and SSM 000007 in the Simpevarp subarea. Oskarshamn site investigation. SKB P-04-46, Svensk Kärnbränslehantering AB.

Ask H, Samuelsson L, 2004a. Drilling of two flushing water wells, HAV09 and HAV10. Oskarshamn site investigation. SKB P-04-150, Svensk Kärnbränslehantering AB.

Ask H, Samuelsson L, 2004b. Drilling of two percussion boreholes, HLX13 and HLX14. Oskarshamn site investigation. SKB P-04-234, Svensk Kärnbränslehantering AB.

Ask H, Samuelsson L, 2004c. Percussion drilling of borehole HLX20 for investigation of lineament EW002. Oskarshamn site investigation. SKB P-04-236, Svensk Kärnbränslehantering AB.

Ask H, Morosini M, Samuelsson L, Ekström L, 2004a. Drilling of cored borehole KSH02. Oskarshamn site investigation. SKB P-04-151, Svensk Kärnbränslehantering AB.

Ask H, Morosini M, Samuelsson L, Ekström L, Håkansson N, 2004b. Drilling of cored borehole KSH03. Oskarshamn site investigation. SKB P-04-233, Svensk Kärnbränslehantering AB.

Ask H, Samuelsson L, Zetterlund M, 2004c. Percussion drilling of boreholes HLX15, HLX26, HLX27, HLX28, HLX29 and HLX32 for investigation of lineament NW042. Oskarshamn site investigation. SKB P-04-235, Svensk Kärnbränslehantering AB.

Ask H, 2005. Percussion drilling of boreholes HLX36 and HLX37 for investigation of lineament NS001. Oskarshamn site investigation. SKB P-05-275, Svensk Kärnbränslehantering AB.

Ask H, Zetterlund M, 2005. Percussion drilling of boreholes HLX16, HLX17, HLX18 and HLX19. Oskarshamn site investigation. SKB P-05-190, Svensk Kärnbränslehantering AB.

Ask H, Morosini M, Samuelsson L, Ekström L, Håkansson N, 2005a. Drilling of cored borehole KAV04. Oskarshamn site investigation. SKB P-05-25, Svensk Kärnbränslehantering AB.

Ask H, Samuelsson L, Zetterlund M, 2005b. Percussion drilling of boreholes HLX21, HLX22, HLX23, HLX24, HLX25, HLX30, HLX31 and HLX33 for investigation of lineament EW007. Oskarshamn site investigation. SKB P-05-55, Svensk Kärnbränslehantering AB.

Ask H, Morosini M, Samuelsson L, Ekström L, Håkanson N, 2005c. Drilling of cored borehole KLX04. Oskarshamn site investigation. SKB P-05-111, Svensk Kärnbränslehantering AB.

Ask H, Morosini M, Samuelsson L, Ekström L, Håkanson N, 2005d. Drilling of cored borehole KLX03. Oskarshamn site investigation. SKB P-05-167, Svensk Kärnbränslehantering AB.

Ask H, Morosini M, Samuelsson L, Ekström L, Håkanson N, 2005e. Drilling of cored borehole KLX05. Oskarshamn site investigation. SKB P-05-233, Svensk Kärnbränslehantering AB.

Ask H, Morosini M, Samuelsson L, Ekström L, Håkanson N, 2005f. Drilling of cored borehole KLX06. Oskarshamn site investigation. SKB P-05-234, Svensk Kärnbränslehantering AB.

Ask H, 2006a. Core drilling of short boreholes KLX09B, KLX09C, KLX09D, KLX09E and KLX09F for discrete fracture network investigation (DFN). Oskarshamn site investigation. SKB P-06-265, Svensk Kärnbränslehantering AB.

Ask H, 2006b. Core drilling of short boreholes KLX11B, KLX11C, KLX11D, KLX11E and KLX11F for discrete fracture network investigation (DFN). Oskarshamn site investigation. SKB P-06-283, Svensk Kärnbränslehantering AB.

Ask H, 2006c. Percussion drilling of boreholes HLX38, HLX39, HLX40, HLX41, HLX42 and HLX43 for lineament investigation. Oskarshamn site investigation. SKB P-06-291, Svensk Kärnbränslehantering AB.

Ask H, Morosini M, Samuelsson L, Ekström L, Håkanson N, 2006a. Drilling of cored boreholes KLX07A and KLX07B. Oskarshamn site investigation. SKB P-06-14, Svensk Kärnbränslehantering AB.

Ask H, Morosini M, Samuelsson L, Ekström L, Håkanson N, 2006b. Drilling of cored borehole KLX10. Oskarshamn site investigation. SKB P-06-116, Svensk Kärnbränslehantering AB.

Ask H, Morosini M, Samuelsson L, Ekström L, Håkanson N, 2006c. Drilling of cored borehole KLX08. Oskarshamn site investigation. SKB P-06-222, Svensk Kärnbränslehantering AB.

Ask H, Morosini M, Samuelsson L, Ekström L, Håkanson N, 2006d. Drilling of cored borehole KLX12A. Oskarshamn site investigation. SKB P-06-305, Svensk Kärnbränslehantering AB.

Ask H, Morosini M, Samuelsson L, Ekström L, Håkanson N, 2006e. Drilling of cored borehole KLX11A. Oskarshamn site investigation. SKB P-06-306, Svensk Kärnbränslehantering AB.

Ask H, Morosini M, Samuelsson L, Ekström L, Håkanson N, 2007a. Drilling of cored borehole KLX18A. Oskarshamn site investigation. SKB P-07-98, Svensk Kärnbränslehantering AB.

Ask H, Morosini M, Samuelsson L, Ekström L, Håkanson N, 2007b. Drilling of cored borehole KLX20A. Oskarshamn site investigation. SKB P-07-134, Svensk Kärnbränslehantering AB.

Ask H, Morosini M, Samuelsson L, Tiberg L, 2007c. Drilling of cored borehole KLX13A. Oskarshamn site investigation. SKB P-07-195, Svensk Kärnbränslehantering AB.

Ask H, Morosini M, Samuelsson L, Tiberg L, 2007d. Drilling of cored borehole KLX19A. Oskarshamn site investigation. SKB P-07-202, Svensk Kärnbränslehantering AB.

Björck S, 1995. A review of the history of the Baltic Sea 13-8 ka. Quaternary International 27, 19–40.

Bosson E, 2006. Near-surface hydrogeological model of Laxemar, Open repository – Laxemar 1.2, SKB R-06-66, Svensk Kärnbränslehantering AB.

Bosson E, Sassner M, Gustafsson L-G, 2008. Numerical modelling of hydrology and near-surface hydrogeology at Laxemar-Simpevarp. Site descriptive modelling, SDM-Site Laxemar. SKB R-08-72, Svensk Kärnbränslehantering AB.

Caine J S, Evans J P, Forster c. B, 1996. Fault zone architecture and permeability structure. Geology 24 (11), 1025–1028.

Crawford J, Sidborn M (eds.) 2009. Bedrock transport properties Laxemar. Site descriptive modelling. SDM Site Laxemar. SKB R-08-94, Svensk Kärnbränslehantering AB.

Ekman L, 2001. Project deep drilling KLX02 – Phase 2, Methods, scope of activities and results. Summary report. SKB TR-01-11, Svensk Kärnbränslehantering AB.

Enachescu C, Böhner J, Rohs S, 2006a. Hydraulic interference tests, pumping borehole KLX07A Subarea Laxemar. Oskarshamn site investigation. SKB P-06-145, Svensk Kärnbränslehantering AB.

Enachescu C, Rohs S, Wolf P, 2006b. Hydraulic injection tests in borehole KLX11A Subarea Laxemar. Oskarshamn site investigation. SKB P-06-201, Svensk Kärnbränslehantering AB.

Enachescu C, Rohs S, van der Wall R, 2006c. Hydraulic injection tests in borehole KLX18A Subarea Laxemar. Oskarshamn site investigation. SKB P-06-225, Svensk Kärnbränslehantering AB.

Enachescu C, Rahm N, 2007. Method evaluation of single-hole hydraulic injection tests at site investigations Oskarshamn. Oskarshamn site investigation. SKB P-07-79, Svensk Kärnbränslehantering AB.

Enachescu C, Rohs S, 2007a. Hydraulic injection tests in borehole KLX20A, 2006 Subarea Laxemar. Oskarshamn site investigation. SKB P-07-49, Svensk Kärnbränslehantering AB.

Enachescu C, Rohs S, 2007b. Hydraulic injection tests in borehole KLX13A Subarea Laxemar. Oskarshamn site investigation. SKB P-07-99, Svensk Kärnbränslehantering AB.

Enachescu C, Rohs S, Wolf P, 2007a. Hydraulic injection tests in borehole KLX08, 2006 Subarea Laxemar. Oskarshamn site investigation. SKB P-07-48, Svensk Kärnbränslehantering AB.

Enachescu C, Böhner J, Wolf P, 2007b. Pumping tests and hydraulic injection tests in borehole KLX19A, 2007 Subarea Laxemar. Oskarshamn site investigation. SKB P-07-90, Svensk Kärnbränslehantering AB.

Enachescu C, Böhner J, van der Wall R, 2007c. Hydraulic injection tests in borehole KLX21B Subarea Laxemar. Oskarshamn site investigation. SKB P-07-94, Svensk Kärnbränslehantering AB.

Enachescu C, Rohs S, Wolf P, 2007d. Hydraulic injection tests in borehole KLX16A, 2007 Subarea Laxemar. Oskarshamn site investigation. SKB P-07-120, Svensk Kärnbränslehantering AB.

Enaschescu C, Rohs S, van der Wall R, Wolf P, 2007e. Hydraulic injection tests in borehole KLX15A, 2007 Subarea Laxemar. Oskarshamn site investigation. SKB P-07-192, Svensk Kärnbränslehantering AB.

Enachescu C, van der Wall R, Wolf P, 2007f. Hydraulic Injection Tests in Borehole KLX17A, 2007 Subarea Laxemar. Oskarshamn site investigation. SKB P-07-193, Svensk Kärnbränslehantering AB.

Enachescu C, Roh S, Wolf P, 2007g. Hydraulic interference tests, pumping borehole KLX20A Subarea Laxemar. Oskarshamn site investigation. SKB P-07-39, Svensk Kärnbränslehantering AB.

Enachescu C, Wolf P, Rohs S, van der Wall R, 2007h. Hydraulic interference tests, pumping borehole KLX08 Subarea Laxemar. Oskarshamn site investigation. SKB P-07-18, Svensk Kärnbränslehantering AB.

Enachescu C, Rohs S, van der Wall R, 2008a. Evaluation of hydraulic interference tests, pumping borehole KLX19A Subarea Laxemar. Oskarshamn site investigation. SKB P-08-15, Svensk Kärnbränslehantering AB.

Enachescu C, Rohs S, van der Wall R, Wolf P, Morosini M, 2008b. Evaluation of hydraulic interference tests, pumping borehole KLX27A Subarea Laxemar. Oskarshamn site investigation. SKB P-08-16, Svensk Kärnbränslehantering AB.

Enachescu C, Wolf P, Rohs S, van der Wall R, 2008c. Hydraulic injection tests in borehole KLX27A, 2008 Subarea Laxemar. Oskarshamn site investigation. SKB P-08-27, Svensk Kärnbränslehantering AB.

Enachescu C, Lenné S, Rohs S, van der Wall R, 2008d. Transient evaluation of PFL pumping tests. Subarea Laxemar and Simpevarp. Oskarshamn site investigation, SKB P-08-57, Svensk Kärnbränslehantering AB.

Ericsson L, Holmén J, Rhén I, Blomquist N, 2006. Storregional grundvattenmodellering - fördjupad analys av flödesförhållanden i östra Småland. Jämförelse av olika konceptuella beskrivningar, SKB R-06-64, Svensk Kärmbränslehantering AB

Follin S, Stigsson M, Berglund S, Svensson U, 2004. Variable-density groundwater flow simulations and particle tracking – numerical modelling using DarcyTools. Preliminary site description of the Simpevarp area – version 1.1. SKB R-04-65, Svensk Kärnbränslehantering AB.

Follin S, Stigsson M, Svensson U, 2005. Variable-density groundwater flow simulations and particle tracking – Numerical modelling using DarcyTools. Preliminary site description Simpevarp subarea – version 1.2. SKB R-05-11, Svensk Kärnbränslehantering AB.

Follin S, Stigsson M, Svensson U, 2006. Hydrogeological DFN modelling using structural and hydraulic data from KLX04, Preliminary site description, Laxemar subarea – version 1.2. SKB R-06-24, Svensk Kärnbränslehantering AB.

Follin S, Johansson P-O, Levén J, Hartley L, Holton D, McCarthy R, Roberts D, 2007a. Updated strategy and test of new concepts for groundwater flow modelling in Forsmark in preparation of site descriptive modelling stage 2.2. SKB R-07-20, Svensk Kärnbränslehantering AB.

Follin S, Levén J, Hartley L, Jackson P, Joyce S, Roberts D, Swift B, 2007b. Hydrogeological characterisation and modelling of deformation zones and fracture domains, Forsmark modelling stage 2.2. SKB R-07-48, Svensk Kärnbränslehantering AB.

Follin S, Johansson P-O, Hartley L, Jackson P, Roberts D, Marsic N, 2007c. Hydrogeological conceptual model development and numerical modelling using CONNECTFLOW. Forsmark modelling stage 2.2. SKB R-07-49, Svensk Kärnbränslehantering AB.

Follin S, 2008. Bedrock hydrogeology Forsmark, Site descriptive modelling, SDM-Site Forsmark. SKB R-08-95, Svensk Kärnbränslehantering AB.

Forsmark T, Wikström M, Forssman I, Rhén I, 2008. Oskarshamn site investigation. Correlation of Posiva Flow Log anomalies to core mapped features in KLX17A, KLX18A, KLX19A, KLX20A, KLX21B. SKB P-07-215, Svensk Kärnbränslehantering AB.

Forssman I, Zetterlund M, Forsmark T, Rhén I, 2005a. Oskarshamn site investigation. Correlation of Posiva Flow Log anomalies to core mapped features in KSH01A, KSH02A and KAV01. SKB P-05-65, Svensk Kärnbränslehantering AB.

Forssman I, Zetterlund M, Forsmark T, Rhén I, 2005b. Oskarshamn site investigation. Correlation of Posiva Flow Log anomalies to core mapped features in KLX02, KLX03, KLX04, KAV04A and KAV04b. SKB P-05-241, Svensk Kärnbränslehantering AB.

Fredén c. (ed.), **2002.** Berg och jord. Sveriges nationalatlas. Tredje upplagan.

Gimeno M J, Auqué L F, Gómez J, Acero P, 2009. Water-rock interaction modelling and uncertainties of mixing modelling./ SDM-Site Laxemar. SKB R-08-110, Svensk Kärnbränslehantering AB.

Gokall-Norman K, Ludvigson J, 2007. Hydraulic pumping- and interference tests in soil monitoring wells on Laxemar, spring of 2007. Oskarshamn site investigation, SKB P-07-173, Svensk Kärnbränslehantering AB.

Gustafsson E, Ludvigson J, 2005. Combined interference test and tracer test between KLX02 and HLX10. Oskarshamn site investigation, SKB P-05-20, Svensk Kärnbränslehantering AB.

Hakami E, Fredriksson A, Lanaro F, 2008. Rock mechanics Laxemar, Site descriptive modelling SDM-Site Laxemar, SKB R-08-57, Svensk Kärnbränslehantering AB.

Harrström J, Ludvigson J, Hjerne C, 2006a. Hydraulic injection tests in borehole KLX12A Subarea Laxemar. Oskarshamn site investigation. SKB P-06-148, Svensk Kärnbränslehantering AB.

Harrström J, Ludvigson J, Hjerne C, 2006b. Single-hole injection tests in borehole KLX10. Oskarshamn site investigation. SKB P-06-182, Svensk Kärnbränslehantering AB.

Harrström J, Walger E, Ludvigson J, Morosini M, 2007. Hydraulic interference tests HLX27, HLX28 and HLX32 , Subarea Laxemar. Oskarshamn site investigation. SKB P-07-186, Svensk Kärnbränslehantering AB.

Hartley L, Worth D, Gylling B, Marsic N, Holmén J, 2004. Preliminary site description: Groundwater flow simulations. Simpevarp area (version 1.1) modelled with CONNECTFLOW. SKB R-04-63, Svensk Kärnbränslehantering AB.

Hartley L, Hoch A, Hunter F, Jackson P, Marsic N, 2005. Regional hydrogeological Simulations – Numerical modelling using CONNECTFLOW. Preliminary site description. Simpevarp subarea – version 1.2. SKB R-05-12, Svensk Kärnbränslehantering AB.

Hartley L, Hunter F, Jackson P, McCarthy R, Gylling B, Marsic N, 2006. Regional hydrogeological simulations using CONNECTFLOW. Preliminary site description Laxemar subarea – version 1.2, SKB R-06-23, Svensk Kärnbränslehantering AB.

Hartley L, Jackson P, Joyce S, Roberts D, Shevelan J, Swift B, Gylling B, Marsic N, Hermanson J, Öhman J, 2007. Hydrogeological Pre-Modelling Exercises: Assessment of impact of the Äspö Hard Rock Laboratory; Sensitivities of Palaeo-Hydrogeology; Development of a Local Near-Surface Hydro-DFN for KLX09B-F. Site descriptive modelling SDM-Site Laxemar SKB R-07-57, Svensk Kärnbränslehantering AB.

Hermanson J, Fox A, Öhman J, Rhén I, 2008. Compilation of data used for the analysis of the geological and hydrogeological DFN models. Site Descriptive Modelling. SDM-Site Laxemar. SKB R-08-56. Svensk Kärnbränslehantering AB.

Hjerne C, Nordqvist R, Harrström J, 2009 (in prep). Compilation and analyses of results from cross-hole tracer tests with conservative tracers, SKB R-09-28. Svensk Kärnbränslehantering AB.

Holmén J G, 2008. Premodelling of the importance of the location of the upstream hydraulic boundary of a regional flow model of the Laxemar-Simpevarp area. Site descriptive modelling, SDM-Site Laxemar, SKB R-08-60, Svensk Kärnbränslehantering AB.

Johansson T, Adestam L, 2004. Drilling and sampling in soil. Installation of groundwater monitoring wells in the Laxemar area. Oskarshamn site investigation. SKB P-04-317, Svensk Kärnbränslehantering AB.

Kristiansson S, 2006. Oskarshamn site investigation. Difference flow logging of borehole KLX20A. Subarea Laxemar. SKB P-06-183, Svensk Kärnbränslehantering AB.

Kristiansson S, Pöllänen J, Väisäsvaara J, Kyllönen H, 2006. Oskarshamn site investigation. Difference flow logging of borehole , KLX22A–B, KLX23A–B, KLX24A, KLX25A, Subarea Laxemar. SKB P-06-246, Svensk Kärnbränslehantering AB.

Kyllönen H, Leppänen H, 2007. Oskarshamn site investigation. Difference flow logging of borehole KLX19A. Subarea Laxemar. SKB P-07-20, Svensk Kärnbränslehantering AB.

La Pointe P, Fox A, Hermanson J, Öhman J, 2008. Geological discrete fracture network model for the Laxemar site, Site Descriptive Modelling, SDM-Site Laxemar, SKB R-08-55, Svensk Kärnbränslehantering AB.

Laaksoharju M, Skårman C, Skårman E, 1999. Multivariate Mixing and Mass-balance (M3) calculations, a new tool for decoding hydrogeochemical information. Applied Geochemistry Vol. 14, #7, 1999, Elsevier Science Ltd., pp 861–871.

Laaksoharju M, Smellie J, Tullborg E-L, Wallin B, Drake H, Gimeno M, Hallbeck L, Molinero J, Waber N, 2009. Bedrock hydrogeochemistry Laxemar, Site descriptive modelling SDM-Site Laxemar, SKB R-08-93, Svensk Kärnbränslehantering AB.

Larsson-McCann S, Karlsson A, Nord M, Sjögren J, Johansson L, Ivarsson M, Kindell S, 2002. Meteorological, hydrological and oceanographical data for the site investigation program in the community of Oskarshamn. SKB TR-02-03, Svensk Kärnbränslehantering AB.

Ludvigson J-E, Hansson K, 2002. Methodology study of Posiva difference flow meter in borehole KLX02 at Laxemar. SKB R-01-52, Svensk Kärnbränslehantering AB.

Ludvigson J, Levén J, Jönsson S, 2003. Hydraulic tests and flow logging in borehole HSH03. Oskarshamn site investigation. SKB P-03-56, Svensk Kärnbränslehantering AB.

Ludvigson J, Levén J, Källgården J, Jönsson S, 2004. Single-hole injection tests in borehole KSH02. Oskarshamn site investigation. SKB P-04-247, Svensk Kärnbränslehantering AB.

Ludvigson J-E, Hansson K, Hjerne C, 2007. Method evaluation of single-hole hydraulic injection tests at site investigations in Forsmark, Forsmark site investigation. SKB P-07-80, Svensk Kärnbränslehantering AB.

Molinero J, Salas J, Arcos D, Duro L, 2009. Integrated hydrogeological and geochemical modelling of the Laxemar-Simpevarp area during the recent Holocene (last 8000 years). In: Kalinowski, B. (ed.), /Background complementary hydrogeochemical studies/. SKB R-08-111, Svensk Kärnbränslehantering AB.

Morén L, Påsse T, 2001. Climate and shoreline in Sweden during Weichsel and the next 150,000 years. SKB TR-01-19, Svensk Kärnbränslehantering AB.

Morosini M, Wass E, 2006. Hydraulic interference and tracer testing of a rock-soil aquifer system between HLX35 and HLX34, SSM000037, SSM000222 and SSM000223. Subarea Laxemar. Oskarshamn site investigation, SKB P-06-151, Svensk Kärnbränslehantering AB.

Morosini M, Jönsson S, 2007. Pump- and interference testing of percussion drilled section of cored boreholes KLX09, KLX11A, KLX12A, KLX13A, KLX18A, KLX19A and KLX39 Subarea Laxemar. Oskarshamn site investigation, SKB P-07-182, Svensk Kärnbränslehantering AB.

Morosini M, Ludvigson J-E, Walger E, 2009. Hydraulic characterisation of deformation zone EW007, Subarea Laxemar. Oskarshamn site investigation, SKB P-05-193, Svensk Kärnbränslehantering AB.

Nilsson A-C, 2009. Quality of hydrochemical analyses in data freeze Laxemar 2.3. In: B. Kalinowski (ed.) 2009. Background complementary hydrogeochemical studies Model, Site descriptive modelling, SDM-Site Laxemar. SKB R-08-111, Svensk Kärnbränslehantering AB.

Nyberg G, Wass E, 2005. Oskarshamn site investigation. Groundwater monitoring program. Report for November 2004–June 2005. SKB P-05-282, Svensk Kärnbränslehantering AB.

Nyberg G, Wass E, Askling P, 2005. Oskarshamn site investigation. Groundwater monitoring program. Report for December 2002–October 2004. SKB P-05-205, Svensk Kärnbränslehantering AB.

Nyberg G, Wass E, 2007a. Oskarshamn site investigation. Groundwater monitoring program. Report for July 2005–December 2006. SKB P-07-219, Svensk Kärnbränslehantering AB.

Nyberg G, Wass E, 2007b. Oskarshamn site investigation. Groundwater monitoring program. Report for January-August 2007. SKB P-08-28, Svensk Kärnbränslehantering AB.

Nyberg G, Wass E, 2008. Oskarshamn site investigation. Groundwater monitoring program. Report for September 2007 – September 2008. SKB P-08-88, Svensk Kärnbränslehantering AB.

Nyman H, Sohlenius G, Strömgren M, Brydsten L, 2008. Depth and stratigraphy of regolith. Site descriptive modelling SDM-Site Laxemar, SKB R-08-06, Svensk Kärnbränslehantering AB.

Olsson T, Stanfors R, Sigurdsson O, Erlström M, 2006. Oskarshamn site investigation, Identification and characterisation of minor deformation zones based on lineament interpretation. SKB P-06-282, Svensk Kärnbränslehantering AB.

Påsse T, 1996. A mathematical model of the shore level displacement in Fennoscandia. SKB TR 96-24, Svensk Kärnbränslehantering AB.

Påsse T, 1997. A mathematical model of past, present and future shore level displacement in Fennoscandia. SKB TR-97-28, Svensk Kärnbränslehantering AB.

Påsse T, 2001. An empirical model of glacio-isostatic movements and shore-level displacement in Fennoscandia. SKB R-01-41, Svensk Kärnbränslehantering AB.

Pöllänen J, Sokolnicki M, 2004. Oskarshamn site investigation – Difference flow measurements in borehole KAV04A and KAV04B. SKB P-04-216, Svensk Kärnbränslehantering AB.

Pöllänen J, 2007a. Oskarshamn site investigation. Difference flow logging of borehole, KLX28 and KLX29A, Subarea Laxemar. SKB P-07-17, Svensk Kärnbränslehantering AB.

Pöllänen J, 2007b. Oskarshamn site investigation. Difference flow logging of borehole KLX17A. Subarea Laxemar. SKB P-07-34

Pöllänen J, 2007c. Oskarshamn site investigation. Difference flow logging of borehole, KLX26A and KLX26B, Subarea Laxemar. SKB P-07-72, Svensk Kärnbränslehantering AB.

Pöllänen J, Sokolnicki M, Väisäsvaara J, 2007. Oskarshamn site investigation. Difference flow logging of borehole KLX15A. Subarea Laxemar. SKB P-07-176, Svensk Kärnbränslehantering AB.

Pöllänen J, Pekkanen J, Väisäsvaara J, 2008. Oskarshamn site investigation. Difference flow logging of borehole, KLX27A, Subarea Laxemar. SKB P-08-22, Svensk Kärnbränslehantering AB.

Rahm N, Enachescu C, 2004a. Oskarshamn site investigation, Hydraulic testing of percussion drilled lineament boreholes on Ävrö and Simpevarp, 2004 Sub-area Simpevarp, SKB P-04-287, Svensk Kärnbränslehantering AB.

Rahm N, Enachescu C, 2004b. Hydraulic injection tests in borehole KLX02, 2003. Subarea Laxemar. Oskarshamn site investigation. SKB P-04-288, Svensk Kärnbränslehantering AB.

Rahm N, Enachescu C, 2004c. Hydraulic injection tests in borehole KSH01A, 2003/2004. Subarea Simpevarp. Oskarshamn site investigation. SKB P-04-289, Svensk Kärnbränslehantering AB.

Rahm N, Enachescu C, 2004d. Hydraulic injection tests in borehole KSH03A, 2004. Subarea Simpevarp. Oskarshamn site investigation. SKB P-04-290, Svensk Kärnbränslehantering AB.

Rahm N, Enachescu C, 2004e. Hydraulic injection tests in borehole KAV04A, 2004. Subarea Simpevarp. Oskarshamn site investigation. SKB P-04-291, Svensk Kärnbränslehantering AB.

Rahm N, Enachescu C, 2004f. Hydraulic injection tests in borehole KLX04, 2004. Subarea Laxemar. Oskarshamn site investigation. SKB P-04-292, Svensk Kärnbränslehantering AB.

Rahm N, Enachescu C, 2005a. Pumping tests and hydraulic injection tests in borehole KLX06, 2005. Subarea Laxemar. Oskarshamn site investigation. SKB P-05-184, Svensk Kärnbränslehantering AB.

Rahm N, Enachescu C, 2005b. Hydraulic injection tests in borehole KLX03, 2005. Subarea Laxemar. Oskarshamn site investigation. SKB P-05-192, Svensk Kärnbränslehantering AB.

Rahm N, Enachescu C, 2005c. Hydraulic injection tests in borehole KLX05, 2005. Subarea Laxemar. Oskarshamn site investigation. SKB P-05-222, Svensk Kärnbränslehantering AB.

Rahm N, Enachescu C, 2005d. Hydraulic injection tests in borehole KLX07A, 2005 Laxemar. Oskarshamn site investigation. SKB P-05-273, Svensk Kärnbränslehantering AB.

Rahm N, Enachescu C, 2005e. Pumping tests and water sampling in borehole KLX04, 2004. Subarea Laxemar. Oskarshamn site investigation. SKB P-05-16, Svensk Kärnbränslehantering AB.

Rhén I (ed.), Gustafson G, Stanfors R, Wikberg P, 1997. Äspö HRL – Geoscientific evaluation 1997/5. Models based on site characterization 1986-1995. SKB TR 97-06, Svensk Kärnbränslehantering AB.

Rhén I, Forsmark T, 2001. Äspö Hard Rock Laboratory, Prototype repository, Hydrogeology, Summary report of investigations before the operation phase. SKB IPR-01-65, Svensk Kärnbränslehantering AB.

Rhén I, Smellie J, 2003. Task force on modelling of groundwater flow and transport of solutes, Task 5 Summary report, SKB TR-03-01, Svensk Kärnbränslehantering AB**.**

Rhén I, Follin S, Hermanson J, 2003. Hydrological Site Descriptive Model – a strategy for its development during Site Investigations, SKB R-03-08, Svensk Kärnbränslehantering AB.

Rhén I, Forsmark T, Forsman I, Zetterlund M, 2006a. Hydrogeological single-hole interpretation of KSH01, KSH02, KSH03, KAV01 and HSH01–03, Preliminary site description, Simpevarp subarea – version 1.2, SKB R-06-20, Svensk Kärnbränslehantering AB.

Rhén I, Forsmark T, Forsman I, Zetterlund M, 2006b. Hydrogeological single-hole interpretation of KLX02, KLX03, KLX04, KAV04A and KAV04b, Preliminary site description, Laxemar subarea – version 1.2, SKB R-06-21, Svensk Kärnbränslehantering AB.

Rhén I, Forsmark T, Forsman I, Zetterlund M, 2006c. Evaluation of hydrogeological properties for Hydraulic Conductor Domains (HCD) and Hydraulic Rock Domains (HRD), Laxemar subarea – version 1.2, SKB R-06-22, Svensk Kärnbränslehantering AB.

Rhén I, Forsmark T, Hartley L, Jackson c. P, Roberts D, Swan D, Gylling B, 2008. Hydrogeological conceptualisation and parameterisation, Site descriptive modelling. SDM-Site Laxemar. SKB R-08-78, Svensk Kärnbränslehantering AB.

Rhén I, Forsmark T, Hartley L, Joyce S, Roberts D, Gylling B, Marsic N, 2009. Bedrock Hydrogeology: model testing and synthesis, Site descriptive modelling, SDM-Site Laxemar. SKB R-08-91, Svensk Kärnbränslehantering AB.

Rohs S, 2006. Flow logging in boreholes HLX21, HLX35 and HLX38 Subarea Laxemar. Oskarshamn site investigation. SKB P-06-147, Svensk Kärnbränslehantering AB.

Rohs S, van der Wall R, Wolf P, 2006. Flow logging in boreholes HLX14, HLX20, HLX27, HLX28, HLX32, HLX33, HLX37, HLX39 and HLX43 Subarea Laxemar. Oskarshamn site investigation. SKB P-06-319, Svensk Kärnbränslehantering AB.

Rouhiainen P, 2000. Äspö Hard Rock Laboratory – Difference flow measurements in borehole KLX02 at Laxemar. SKB IPR-01-06, Svensk Kärnbränslehantering AB.

Rouhiainen P, Pöllänen J, 2003a. Oskarshamn site investigation – Difference flow measurements in borehole KSH01A at Simpevarp. SKB P-03-70, Svensk Kärnbränslehantering AB.

Rouhiainen P, Pöllänen J, 2003b. Oskarshamn site investigation – Difference flow measurements in borehole KSH02 at Simpevarp. SKB P-03-110, Svensk Kärnbränslehantering AB.

Rouhiainen P, Pöllänen J, 2004. Oskarshamn site investigation – Difference flow measurements in borehole KAV01 at Ävrö. SKB P-04-213, Svensk Kärnbränslehantering AB.

Rouhiainen P, Sokolnicki M, 2005. Oskarshamn site investigation. Difference flow logging of bore-hole KLX04. Subarea Laxemar. SKB P-05-68, Svensk Kärnbränslehantering AB.

Rouhiainen P, Pöllänen J, Sokolnicki M, 2005. Oskarshamn site investigation. Difference flow logging of borehole KLX03. Subarea Laxemar. SKB P-05-67, Svensk Kärnbränslehantering AB.

Sigurdsson O, Ekström L, 2005. Percussion drilling of boreholes HSH04, HSH05, HSH06, HAV11, HAV12, HAV13 and HAV14. Oskarshamn site investigation. SKB P-05-194, Svensk Kärnbränslehantering AB.

Sigurdsson O, Ask H, Zetterlund M, 2005. Percussion drilling of boreholes HLX34 and HLX35. Oskarshamn site investigation. SKB P-05-237, Svensk Kärnbränslehantering AB.

SKB, 2000. Förstudie Oskarshamn – Slutrapport. Svensk Kärnbränslehantering AB (in Swedish).

SKB, 2002. Simpevarp – site descriptive model version 0. SKB R-02-35, Svensk Kärnbränslehantering AB.

SKB, 2004. Preliminary site description Simpevarp area – version 1.1. SKB R-04-25, Svensk Kärnbränslehantering AB.

SKB, 2005. Preliminary site description. Simpevarp subarea – version 1.2. SKB R-05-08, Svensk Kärnbränslehantering AB.

SKB, 2006a. Preliminary site description. Laxemar subarea – version 1.2. SKB R-06-10, Svensk Kärnbränslehantering AB.

SKB, 2006b. Preliminary site description Laxemar stage 2.1. Feedback for completion of the site investigation including input from safety assessment and repository engineering. SKB R-06-110, Svensk Kärnbränslehantering AB.

SKB, 2009a. Site description of Laxemar at completion of the site investigation phase. SDM-Site Laxemar. SKB TR-09-01, Svensk Kärnbränslehantering AB.

SKB, 2009b. Confidence Assessment. Ste descriptive modelling. SDM-Site Laxemar. SKB R-08-101, Svensk Kärnbränslehantering AB.

Sohlenius G, Hedenström A, 2008. Description of regolith at Laxemar-Simpevarp. Site descriptive modelling SDM-Site Laxemar, SKB R-08-05, Svensk Kärnbränslehantering AB.

Sokolnicki M, Pöllänen J, 2005. Oskarshamn site investigation. Difference flow logging of borehole KLX08. Subarea Laxemar. SKB P-05-267, Svensk Kärnbränslehantering AB.

Sokolnicki M, Rouhianien P, 2005a. Oskarshamn site investigation. Difference flow logging of borehole KLX06. Subarea Laxemar. SKB P-05-74, Svensk Kärnbränslehantering AB.

Sokolnicki M, Rouhianien P, 2005b. Oskarshamn site investigation. Difference flow logging of borehole KLX05. Subarea Laxemar. SKB P-05-160, Svensk Kärnbränslehantering AB.

Sokolnicki M, Rouhianien P, 2005c. Oskarshamn site investigation. Difference flow logging of borehole KLX07A and KLX07B. Subarea Laxemar. SKB P-05-225, Svensk Kärnbränslehantering AB.

Sokolnicki M, 2006. Oskarshamn site investigation. Difference flow logging of borehole KLX10. Subarea Laxemar. SKB P-06-58, Svensk Kärnbränslehantering AB.

Sokolnicki M, Kristiansson S, 2006. Oskarshamn site investigation. Difference flow logging of borehole KLX18A. Subarea Laxemar. SKB P-06-184, Svensk Kärnbränslehantering AB.

Sokolnicki M, Väisäsvaara J, 2006. Oskarshamn site investigation. Difference flow logging of bore-hole KLX09B-F. Subarea Laxemar. SKB P-06-199, Svensk Kärnbränslehantering AB.

Sokolnicki M, Kristiansson S, 2007. Oskarshamn site investigation. Difference flow logging of borehole KLX11B-F. Subarea Laxemar. SKB P-07-64, Svensk Kärnbränslehantering AB.

Sokolnicki M, Pöllänen J, 2007. Oskarshamn site investigation. Difference flow logging of borehole KLX21B. Subarea Laxemar. SKB P-07-116, Svensk Kärnbränslehantering AB.

Stigsson M, 2008. Analysis of uncertainty in orientation of fractures coupled to PFL anomalies, Site descriptive modelling, SDM-Site Laxemar. SKB P-08-104, Svensk Kärnbränslehantering AB.

Sundberg J, Wrafter J, Back P-E, Rosén L, 2008. Thermal properties Laxemar Site descriptive modelling, SDM-Site Laxemar. SKB R-08-61, Svensk Kärnbränslehantering AB.

Svensson T, 2004. Pumping tests and flow logging in boreholes KSH03A and HSH02. Oskarshamn site investigation. SKB P-04-212, Svensk Kärnbränslehantering AB.

Svensson T, Ludvigsson J-E, Walger E, Thur P, Gokall-Norman K, Wass Morosini M, 2007. Combined interference- and tracer test in HLX33, SSM000228, and SSM000229, Subarea Laxemar. Oskarshamn site investigation, SKB P-07-187, Svensk Kärnbränslehantering AB

Söderbäck B (ed.), 2008. Geological evolution, palaeoclimate and historic development of the Forsmark and Laxemar-Simpevarp areas. Site descriptive modelling SDM-Site. SKB R-08-19, Svensk Kärnbränslehantering AB.

Söderbäck B, Lindborg T (eds.), 2009. Surface system Laxemar-Simpevarp. Site descriptive modelling, SDM-Site Laxemar. SKB R-09-01, Svensk Kärnbränslehantering AB

Terzhagi R D, 1965. Sources of error in joint surveys, Geotechnique, Vol. 15, pp. 287–304.

Teurneau B, Forsmark T, Forssman I, Rhén I, 2008. Oskarshamn site investigation. Correlation of Posiva Flow Log anomalies to core mapped features in KLX05, KLX06, KLX07A-B and KLX08. SKB P-07-212, Svensk Kärnbränslehantering AB.

Thur P, Walger E, Ludvigson J-E, 2007. Hydraulic interference in HLX34, HLX27, and HLX42 in the Laxemar subarea. Oskarshamn site investigation, SKB P-07-185, Svensk Kärnbränslehantering AB.

Tröjbom M, Söderbäck B, Kalinowski B, 2008. Hydrochemistry of surface water and shallow groundwater. Site descriptive modelling SDM-Site Laxemar, SKB R-08-46, Svensk Kärnbränslehantering AB.

Vidstrand P, 2003. Äspö Hard Rock Laboratory, Update of the Hydrogeological model 2002, SKB IPR-03-35, Svensk Kärnbränslehantering AB.

Väisäsvaara J, 2006. Oskarshamn site investigation. Difference flow logging of borehole KLX14A. Subarea Laxemar. SKB P-06-318, Svensk Kärnbränslehantering AB.

Väisäsvaara J, Pekkanen J, 2006. Oskarshamn site investigation. Difference flow logging of borehole KLX13A. Subarea Laxemar. SKB P-06-245, Svensk Kärnbränslehantering AB.

Väisäsvaara J, Heikkinen P, Kristiansson S, Pöllänen J, 2006a. Oskarshamn site investigation. Difference flow logging of borehole KLX09. Subarea Laxemar. SKB P-06-164, Svensk Kärnbränslehantering AB.

Väisäsvaara J, Heikkinen P, Kristiansson S, Pöllänen J, 2006b. Oskarshamn site investigation. Difference flow logging of borehole KLX12A. Subarea Laxemar. SKB P-06-185, Svensk Kärnbränslehantering AB.

Väisäsvaara J, Leppänen H, Kristiansson S, Pöllänen J, 2006c. Oskarshamn site investigation. Difference flow logging of borehole KLX09G, KLX10B and KLX10C. Subarea Laxemar. SKB P-06-229, Svensk Kärnbränslehantering AB.

Väisäsvaara J, 2007. Oskarshamn site investigation. Difference flow logging of borehole KLX16A. Subarea Laxemar. SKB P-07-87, Svensk Kärnbränslehantering AB.

Väisäsvaara J, Kristiansson S, Sokolnicki M, 2007. Oskarshamn site investigation. Difference flow logging of borehole KLX11A. Subarea Laxemar. SKB P-07-24, Svensk Kärnbränslehantering AB.

Waber H N, Smellie J A T, 2008. Characterisation of porewater in crystalline rocks. Applied Geochemistry 23, 1834–1861.

Waber H N, Gimmi T, deHaller A, Smellie J A T, 2009. Pore water in the rock matrix, Site descriptive modelling, SDM-Site Laxemar, SKB R-08-112, Svensk Kärnbränslehantering AB.

Wahlgren C-H, Hermanson J, Curtis P, Forssberg O, Triumf C-A, Drake H, Tullborg E-L, 2005. Geological description of rock domains and deformation zones in the Simpevarp and Laxemar subareas. Preliminary site description, Laxemar subarea, version 1.2. SKB P-05-69, Svensk Kärnbränslehantering AB.

Wahlgren C-H, Curtis P, Hermanson J, Forssberg O, Öhman J, Fox A, La Pointe P, Drake H, Triumf C-A, Mattsson H, Thunehed H, Juhlin C, 2008. Geology Laxemar. Site descriptive modelling. SDM-Site Laxemar. SKB-R-08-54, Svensk Kärnbränslehantering AB.

Walger E, Ludvigson J-E, Svensson T, Thur P, Harrström J, 2007. Hydraulic interference in KLX06, KLX14A, KLX15A, KLX16A, KLX17A, KLX18A, KLX19A, KLX21B, KLX22A, KLX22B, KLX23A, KLX23B, KLX26A and KLX26B, Laxemar subarea. Oskarshamn site investigation, SKB P-07-183, Svensk Kärnbränslehantering AB.

Werner K, 2008. Description of surface hydrology and near-surface hydrogeology at Laxemar-Simpevarp. Site descriptive modelling, SDM-Site Laxemar. SKB R-08-71, Svensk Kärnbränslehantering AB.

Werner K, Öhman J, Holgersson B, Rönnback K, Marelius F, 2008. Meteorological, hydrological and hydrogeological monitoring data and near-surface hydrogeological properties data from Laxemar-Simpevarp. Site descriptive modelling, SDM-Site Laxemar. SKB R-08-73, Svensk Kärnbränslehantering AB.

Westman P, Wastegård S, Schoning K, Gustafsson B, Omstedt A, 1999. Salinity change in the Baltic Sea during the last 8,500 years: evidence, causes and models. SKB TR-99-38, Svensk Kärnbränslehantering AB.

Wijnbladh E, Aquilonius K, Floderus S, 2008. The marine ecosystems at Forsmark and Laxemar-Simpevarp. Site descriptive modelling SDM-Site, SKB R-08-03, Svensk Kärnbränslehantering AB.

Wikström M, Forsmark T, Teurneau B, Forssman I, Rhén I, 2008a. Oskarshamn site investigation. Correlation of Posiva Flow Log anomalies to core mapped features in KLX09, KLX09B–G. KLX10, KLX10B–C and KLX11A–F. SKB P-07-213, Svensk Kärnbränslehantering AB.

Wikström M, Forsmark T, Zetterlund M, Forssman I, Rhén I, 2008b. Oskarshamn site investigation. Correlation of Posiva Flow Log anomalies to core mapped features in KLX12A, KLX13A, KLX14A, KLX15A and KLX16A. SKB P-07-214, Svensk Kärnbränslehantering AB.

Wikström M, Forsmark T, Forssman I, Rhén I, 2008c. Oskarshamn site investigation. Correlation of Posiva Flow Log anomalies to core mapped features in KLX22A–B, KLX23A–B, KLX24A, KLX25A, KLX26A–B, KLX27A, KLX28A and KLX29A. SKB P-07-216, Svensk Kärnbränslehantering AB.

Wilson W E, Moore J E, 1998. Glossary of hydrology. American Geological Institute, Alexandra, Virginia, USA.

Appendix 1

A1.1 Borehole investigations

The investigations made within the Laxemar-Simpevarp regional model area, cf. Chapter 1, cover the Laxemar local model area, the Simpevarp peninsula and the Ävrö Island. Figure A1-1 and Figure A1-2 show the Laxemar local model area and the eastern part of the regional model area with the boreholes available for interpretation of the bedrock properties and conditions in the area. Figure A1-3 and Figure A1-4 illustrate the drilled groundwater monitoring wells that in part have helped to define the bedrock surface, but mainly provide input to the model of the Quaternary deposits (HSD) within the regional model area and groundwater head data in the Quaternary deposits. The drilling and hydraulic tests in conjunction with the drilling are reported in the drilling reports. All drilling reports for percussion and core holes as well as monitoring wells in overburden are: /Ask 2003, 2004, 2005, 2006a, b, c, Ask and Samuelsson 2003, 2004a, b, c, Ask and Zetterlund 2005, Ask et al. 2003, 2004a, b, c, 2005a, b, c, d, e, f, 2006a, b, c, d, e, 2007a, b, c, d, Johansson and Adestam 2004, Sigurdsson and Ekström 2005, Sigurdsson et al. 2005/.

During the site investigations in Laxemar, boreholes have mainly been drilled within the Laxemar local model area (HLX10–43, KLX03–29A), cf. Figure A1-1. Boreholes have previously also been drilled on the Simpevarp peninsula (HSH01–06, KSH01–KSH03B) and on the Ävrö island (HLX09–14, KAV04A, B) as part of investigations of the Simpevarp subarea, cf. Figure A1-2. The additional boreholes shown, eg. KLX01 and KLX02 (cf. Figure A1-1) were drilled during projects preceding the site investigations in the Laxemar-Simpvarp area. The boreholes from projects preceding the site investigations generally provide less geological and hydrogeological data and are sometimes based on methodologies other than those employed in the current site investigations. Data from cored borehole KLX27A, cf. Figure A1-1, drilled late in complete site investigations, have not been used for the geological DFN and hydrogeological DFN models, as the corresponding data became available late in the project. However, the hydrogeological DFN model of HRD_W was used to predict the fracturing and inflow in this borehole and subsequently compared with measured data, see /Rhen et al. 2008, cf. Appendix 10 therein/.

Table A1-1 lists the boreholes available within the regional model area. The logging and test methods as well as the core mapping procedures applied to the drill cores employed by SKB have developed significantly over the years and consequently the borehole data from the current site investigation period (2002–2007) are more comprehensive and also based on new methodologies. These data therefore constitute the corner stone of the results reported in this report. Some of the older data have been used for assessing properties of deformation zones (in some instances denoted DZ) and for assessing probable ranges of hydraulic properties for some rock domains (Götemar granite), properties of deformation zones, and in some cases properties of rock between deformation zones (using the 100 m test scale). Table A1-2 lists the cored boreholes investigated with the Posiva Flow Log (PFL) method and the Pipe String System (PSS) method, respectively. PFL is used to measure 5 m sections (PFL-s) and fracture/feature specific transmissivities (PFL-f), see Section 4.1 for details. In the older boreholes, equipment similar to the PSS was used, but in some cases only steady-state tests (not transient tests) were performed.

Tests with PSS have been performed using 3 different test scales: 5, 20 and 100 m. The individual PSS single-hole tests are reported in /Enachescu and Rohs 2007a, b, Enachescu et al. 2006b, c, 2007a, b, c, d, e, f, Harrström et al. 2006a, b, Ludvigson et al. 2004, Rahm and Enachescu 2004a, b, c, d, e, f, 2005a, b, c, d/. The evaluation methods used are discussed in /Rhén et al. 2008/ and in more detail in /Enachescu and Rahm 2007, Ludvigson et al. 2007/. Test results from KLX27A and transient evaluation of the PFL-pumping tests /Enachescu et al. 2008c, d/ were not available for the evaluation for the SDM.

A large number of boreholes have been tested with the PFL method. The PFL-s provides an estimate of the transmissivivity within a certain test section length, in the Laxemar case 5 m, that is moved stepwise 0.5 m. PFL-s (s stands for section) also provides the undisturbed flow rate distribution with indicated flow direction (in or out of the borehole) along the borehole. The PFL-f (f stands for fracture or feature) method is a geophysical logging device developed to detect continuously flowing fractures in sparsely fractured crystalline bedrock by means of difference flow logging, using a 1 m test section that is moved stepwise 0.1 m. Cf /Rhén et al. 2008/ for more details. The PFL-measurements are reported in /Ludvigson and Hansson 2002, Kristiansson 2006, Kristiansson et al. 2006, Kyllönen and Leppänen 2007, Pöllänen 2007a, b, c, Pöllänen and Sokolnicki 2004, Pöllänen et al. 2007, 2008, Rouhiainen 2000, Rouhiainen and Pöllänen 2003a, b, 2004, Rouhiainen and Sokolnicki 2005, Rouhiainen et al. 2005, Sokolnicki 2006, Sokolnicki and Kristiansson 2006, 2007, Sokolnicki and Pöllänen 2005, 2007, Sokolnicki and Rouhianien 2005a, b, c, Sokolnicki and Väisäsvaara 2006, Väisäsvaara 2006, 2007, Väisäsvaara and Pekkanen 2006, Väisäsvaara et al. 2006a, b, c, Väisäsvaara et al. 2007/.

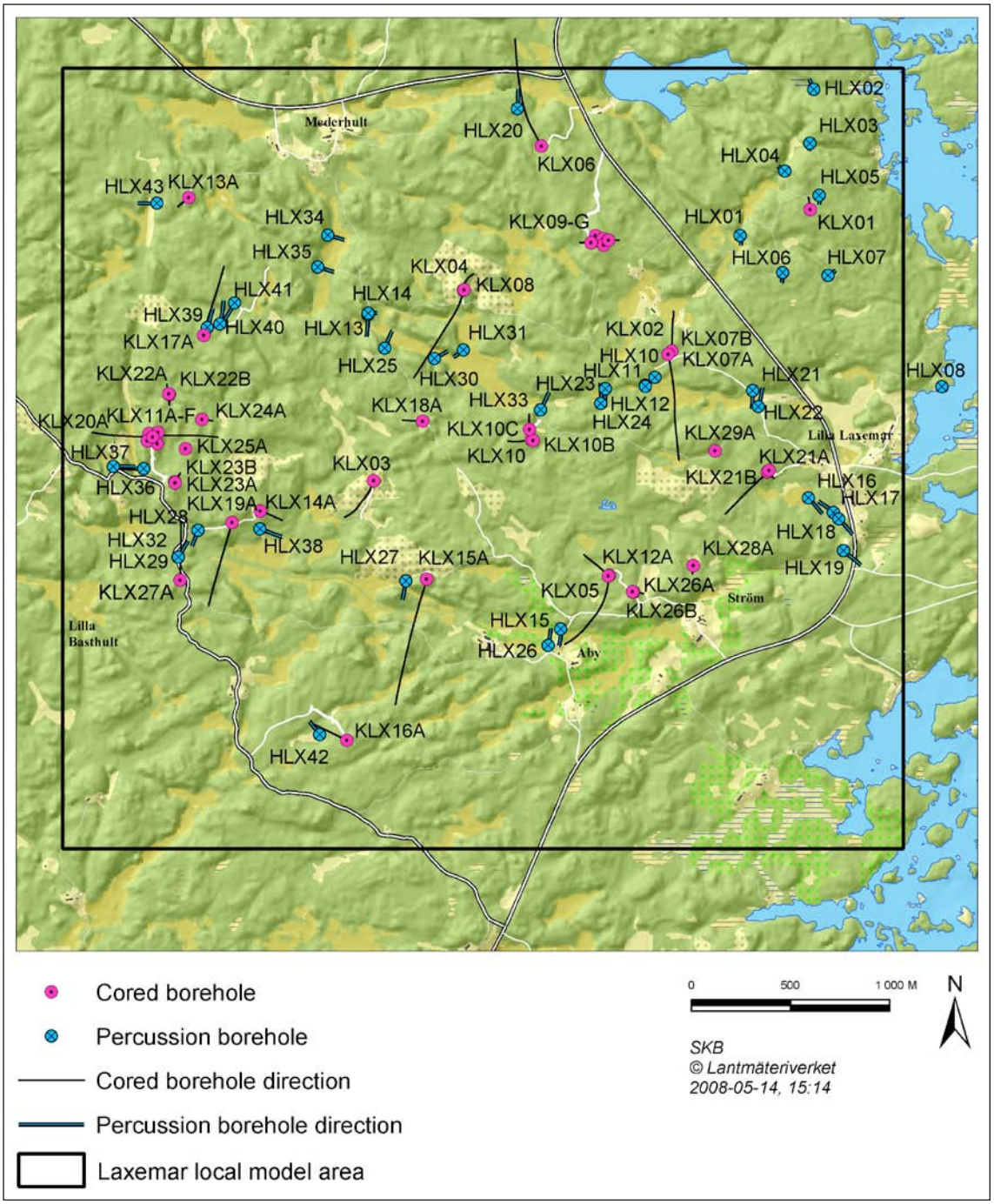

Figure A1-1. *Cored and percussion-drilled boreholes within and close to the Laxemar local model area. Borehole KLX27A has not been used for primary data analysis and for hydrogeological DFN model as the data was available late in the project. Cf also Figure A1-2.*

Pumping tests, and on a few occasions flow logging, have been performed with the Hydraulic Test System for Percussion Boreholes (HTHB) (Swedish abbreviation for *Hydro Testutrustning i Hammar-Borrhål)*, and are reported in /Ludvigson et al. 2003, Rahm and Enachescu 2004a, 2005e, Rohs 2006, Rohs et al. 2006, Svensson 2004/.

Interference tests during the site investigations in the Laxemar-Simpevarp area have been performed in a number of boreholes and are reported in Enachescu et al. 2006a, 2007g, h, Enachescu et al. 2008a, Gokall-Norman and Ludvigson 2007, Gustafsson and Ludvigson 2005, Harrström et al. 2007,

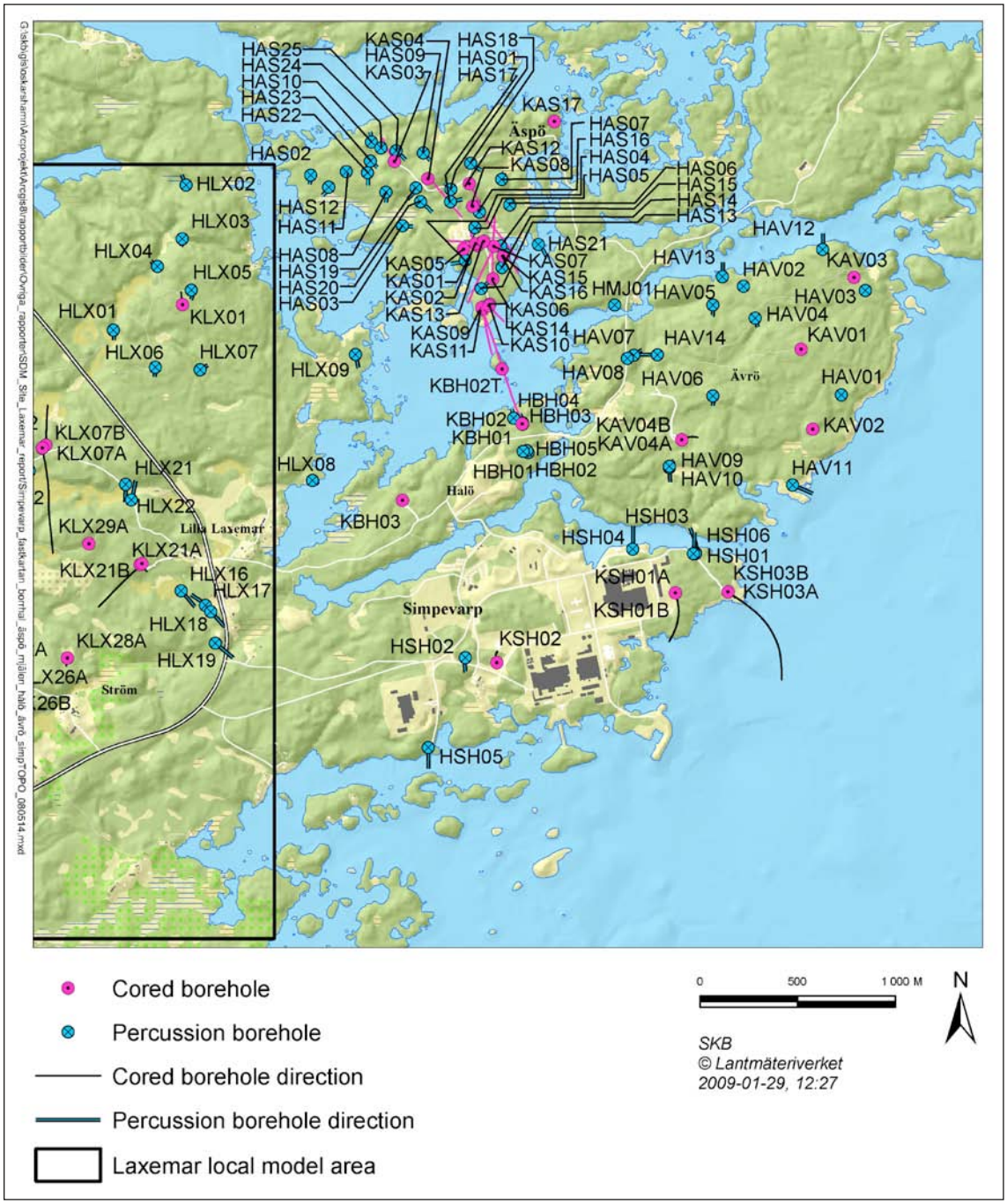

Figure A1-2. *Cored and percussion boreholes within the regional model area covering Äspö, Hålö, Ävrö, Mjälen and Simpevatp peninsula (ie. parts of the Simpevarp subarea). Cf also Figure A1-1.*

Morosini and Jönsson 2007, Morosini et al. 2009, Morosini and Wass 2006, Rahm and Enachescu 2004a, Svensson et al. 2007, Thur et al. 2007, Walger et al. 2007/. Interference test data involving observations in KLX27A /Enachescu et al. 2008b/ were not available for the SDM. Cf /Rhén et al. 2009/ for details on the interference tests.

The monitoring of the surface system (Surface discharge measurements, sampling points for surface water chemistry etc can be found in /Söderbäck and Lindborg 2009/.)

The monitoring data are stored in the Sicada data base and are reported regularly in progress reports, see e.g /Nyberg and Wass, 2005, 2007a, b, 2008, Nyberg et al. 2005/.

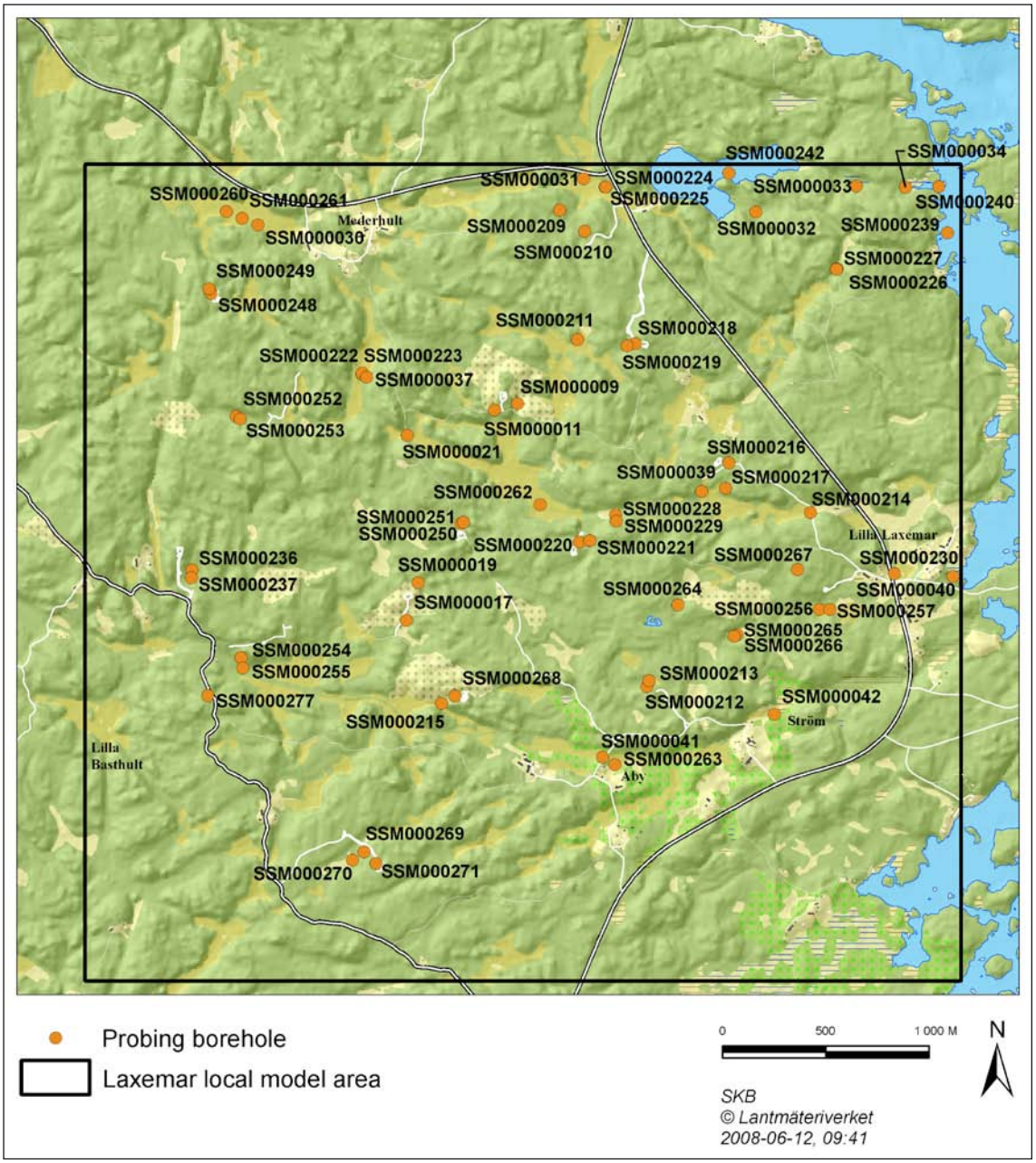

Figure A1-3. *Groundwater monitoring wells within and close to the Laxemar local model area. Cf Figure A1-4.*

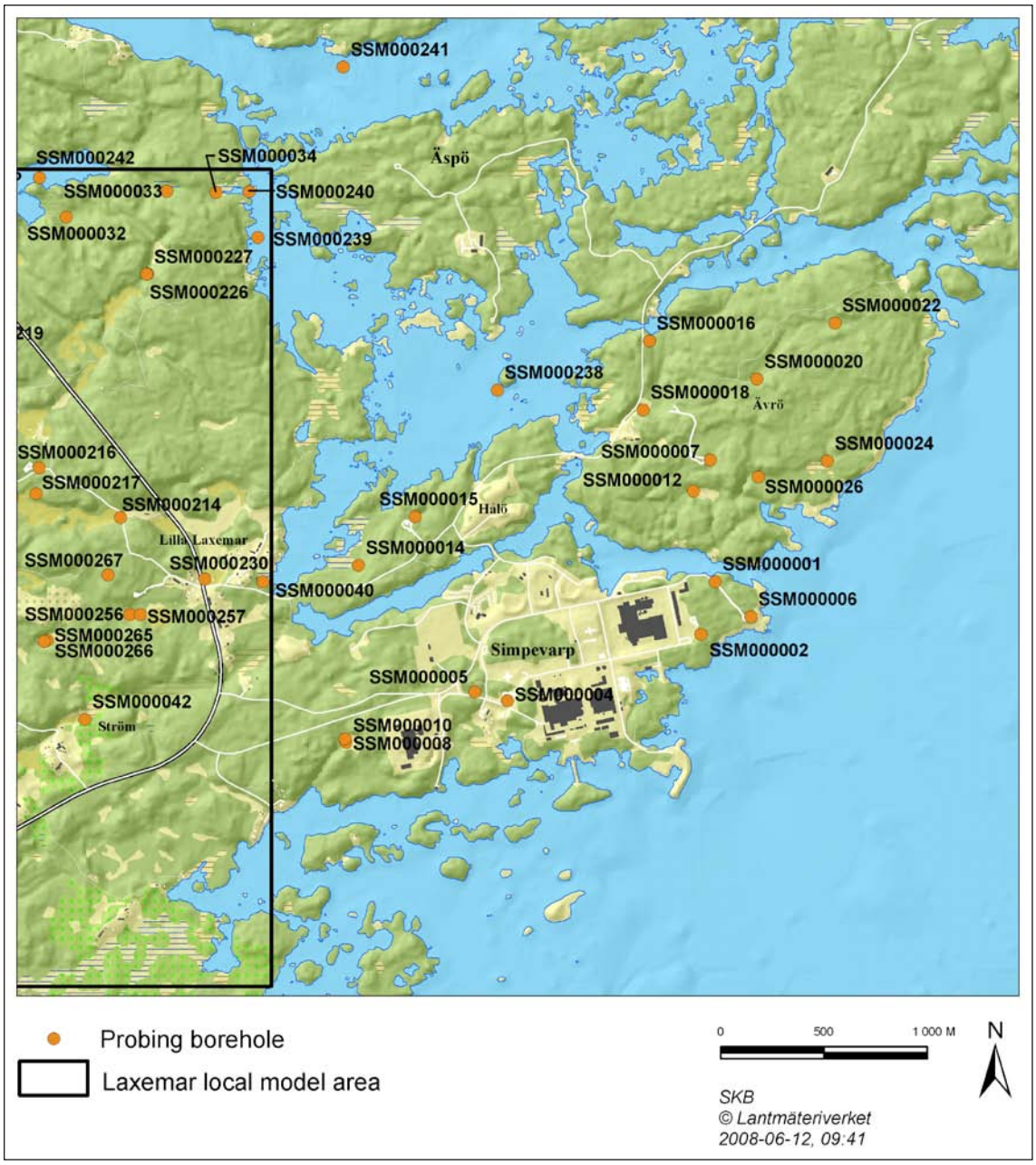

Figure A1-4. *Groundwater monitoring wells within the regional model area covering Äspö, Hålö, Ävrö, Mjälen and Simpevatp peninsula (ie. parts of the Simpevarp subarea). Cf Figure A1-3.*

Table A1-1. List of cored and percussion-drilled boreholes drilled from ground surface relative to different geographical locations within the Laxemar-Simpevarp area. Boreholes drilled during the site investigations are indicated "new" and those completed before the site investigations (before year 2002) are indicated "old". No. of core drilled boreholes: All boreholes (long boreholes/short boreholes). Long core holes: > 300 m, Short core holes : < 300 m. NB. KLX27A included in the table.

Area	No. of core drilled boreholes	Kzzxxx	No. of percussion drilled boreholes	Hzzxx
Laxemar-new	44 (19/25)	KLX03–KLX29A	34	HLX10–43
Laxemar-old	2 (2/0)	KLX01–02	9	HLX01–09
Simpevarp-new (1)	5 (3/2)	KSH01A–KSH03	6	HSH01–06
Ävrö, new	2 (1/1)	KAV04A, B	6	HAV09–14
Ävrö-old	3 (1/2)	KAV01–03	8	HAV01–08
Äspö-old	17 (13/4)	KAS01–17	25	HAS01–25
Hålö, Mjälen -old	2 (1/1)	KBH01–02	6	HBH01–05, HMJ01
Götemar granite-old	3 (3/0)	KKR01–03	0	

(1): There are a few boreholes also near the CLAB facility (called HSI and KSI) on the Simpevarp peninsula, but they are all fairly short.

Table A1-2. List of PFL and PSS tests in the Laxemar-Simpevarp area made in boreholes from ground-surface. PSS: Test scale 100 m, 20 m and 5 m. (KLX27A included in the table.) The model version Laxemar 1.2 was mainly based on the KAV, KSH and KLX01–04 boreholes. KLX05–KLX29A were drilled and investigated after data freeze for model version Laxemar 1.2.

Area	No. of PFL tested borholes. PFL: All (PFL–s/ PFL–f).	PFL–s. Test scale (m)	PFL tested boreholes Kzzxxx (9)	No. of PSS (and similar tests) tested boreholes (1)	PSS (and similar tests). Test scales (m) (2) (9)	PSS (and similar tests) tested boreholes Kzzxxx (3) (9)
Laxemar-new	44 (42/44)	5 m	KLX03–KLX29A	43	**5** (KLX02, 04, 10, 11A, 12A, 15A, 17A, 18A, 19A, 21B, 27A), **20** (KLX02–07A, 08, 10, 11A–13A, 15A–21B, 27A), **100** (KLX02–10B, 11A–13A, 15A–24A, 26A, 27A, 28A)	KLX02–KLX29A
Laxemar-old	1 (1/0)	3	KLX02 (8)	2	**3** (KLX01), **30** KLX01), ca **200–500** (KLX02)	KLX01–02 (4)
Simpevarp-new	2 (2/2)	5	KSH01A–KSH02	3	**5** (KSH01A, 02), **20** (KSH01A, 02), **100**	KSH01A–KSH03
Ävrö, new	3 (2/3)	5	KAV01, KAV04A, B	1	**20**, **100**	KAV04A
Ävrö-old	0			3	**2** (KAV02), **10** (KAV01,03)	KAV01–03 (6)
Äspö-old	0			15	**3** (7 bh), **30**(2 bh), **100** (13 bh)	KAS01–17 (4)
Hålö, Mjälen -old	0			2	Ca **100**	KBH01–02 (7)
Götemar granite-old	0			3	**2**, **3**, **20**(KKR01)	KKR01–03 (6)

(1): Tests in boreholes, with any test scale.

(2): If no comments with brackets, all bh were tested with the test scale shown.

(3): If no note is made, then PSS was used.

(4): Airlift test, short pumping test or injection tests similar equipment as PSS.

(5): 20 and 100 m test scale made systematically in borehole. 5 m tests limited to depth interval –300 to –700 m.

(6): Injection test with similar equipment as PSS.

(7): Airlift test or short pumping test.

(8): Flowing features between 200 to 1,000 m bh-length has been assessed based on Boremap data, BIPS and PFL-s data.

(9): If several boreholes have been drilled from the same drill site they are named with A, B etc (e.g. KLX11A, KLX11B. KLX11C etc). In some cases one short borehole B have been drilled near a longer borehole but near KLX10, KLX09A and KLX11A 2/6/5 short boreholes, respectively, were drilled.Appendix 2.

Appendix 2

Table of SKB reports that describe the primary data archived in Sicada and used for parameterisation of hydraulic domains

Table A2-1. Available data on hydrogeology and their handling in the SDM-Site Laxemar hydrogeological modelling.

Available data Data specification	Ref	Usage in SDM-Site Analysis/Modelling
Geometrical and topographical data		
Digital Elevation Model (DEM)	P-04-03 P-04-254 P-05-38 R-05-35	Basic input to flow and mass transport models, descriptions and modelling of the marine ecosystem.
Geological data		
Map and model of Quaternary deposits in the terrestrial part and sea bottom of the Simpevarp regional model area	R-08-05 R-08-06	
Rock types	R-08-54	
Bedrock model, geometry	P-06-282 P-07-223 R-08-54 R-09-01	
Cored borehole data		
Wireline tests coreholes, drilling information)	P-03-113 P-04-151 P-04-233 P-05-25 P-05-111 P-05-167 P-05-233 P-05-234 P-06-14 P-06-116 P-06-222 P-06-265 P-06-283 P-06-305 P-06-306 P-07-98 P-07-134 P-07-195 P-07-202	Borehole data and (prel) transmissivity distribution in large scale.

Available data Data specification	Ref	Usage in SDM-Site Analysis/Modelling
Difference flow logging	P-03-70 P-03-110 P-04-213 P-04-216 P-05-67 P-05-68 P-05-74 P-05-160 P-05-225 P-05-267 P-06-58 P-06-164 P-06-183 P-06-184 P-06-185 P-06-199 P-06-229 P-06-245 P-06-246 P-06-318 P-07-17 P-07-20 P-07-24 P-07-34 P-07-64 P-07-72 P-07-87 P-07-116 P-07-176 P-08-22 IPR-01-06 R-01-52	Conductive parts of the borehole, Statistics of conductive fractures.
Correlation Difference flow logging and core mapping	P-05-65 P-05-241 P-07-212 P-07-213 P-07-214 P-07-215 P-07-216	Conductive parts of the borehole, Base for orientation of conductive fractures for usage in the hydrogeological DFN.
Hydraulic injection tests, pumping tests (single hole)	P-04-247 P-04-288 P-04-289 P-04-290 P-04-291 P-04-292 P-05-16 P-05-184 P-05-192 P-05-222 P-05-273 P-06-148 P-06-182 P-06-201 P-06-225 P-07-48 P-07-49 P-07-79 P-07-80 P-07-90 P-07-94 P-07-99 P-07-120 P-07-192 P-07-193 P-08-27 P-08-57	Transmissivity distribution along the borehole in different scales.

Available data Data specification	Ref	Usage in SDM-Site Analysis/Modelling
Percussion hole data		
Drilling and hydraulic tests	P-03-114 P-04-150 P-04-234 P-04-235 P-04-236 P-05-55 P-05-190 P-05-194 P-05-237 P-05-275 P-06-291	
Hydraulic tests	P-03-56 P-04-212 P-04-287 P-06-147 P-06-319	Hydraulic test data for the bedrock.
Standpipes in QD deposits data		
Drilling	P-03-80 P-04-22 P-04-46 P-04-121 P-04-317 P-05-49 P-06-121 P-06-248 P-07-91	Standpipes geometri used in the flowmodelling. Description of stratigraphical distribution and total depth of overburden in the terrestrial parts of the Simpevarp and Laxemar subareas.
Interference tests		
Interference tests using percussion and core holes	P-04-287 P-05-20 P-05-193 P-06-145 P-06-151 P-07-18 P-07-39 P-07-173 P-07-182 P-07-183 P-07-185 P-07-186 P-07-187 P-08-15 P-08-16 TR-01-11	Infer connectivity between deformation zones and estimate transmissivity and (if possible) storage coefficient for deformation zones.
Other borehole, construction, tunnel data and models		
Hydraulic tests in areas Äspö, Ävrö, Hålö, Simpevarp, Mjälen and Laxemar areas	TR-97-02 TR-97-03 TR-97-05 TR-97-06 TR-02-19 R-98-55 IPR-00-28 IPR-01-44 IPR-01-52 IPR-01-65 IPR-03-13 SICADA database	Previous made evaluations compared to new data and for assessment of properties not known or with few data from SI.
Other hydraulic data	R-04-09 TR-98-05	Previous made evaluations compared to new data and for assessment of properties not known or with few data from SI.
Meteorological and hydrological data		
Regional data		
Meteorological and hydrological data from surrounding stations prior to and during the site investigations	TR-02-03 R-99-70 R-08-73	General description of hydrology, comparison with site investigation data.

Table A2-2. Reports in the SKB P, IPR, ICR, R, and TR-series referenced in Tables 1 through 8.

P-03-56	**Ludvigson J-E, Levén J, Jönsson S.** Oskarshamn site investigation. Hydraulic tests and flow logging in borehole HSH03.
P-03-70	**Rouhiainen P, Pöllänen J.** Oskarshamn site investigation. Difference flow measurements in borehole KSH01A at Simpevarp.
P-03-80	**Ask H.** Installation of four monitoring wells, SSM000001, SSM000002, SSM000004 and SSM000005 in the Simpevarp subarea.
P-03-110	**Rouhiainen P, Pöllänen J.** Oskarshamn site investigation – Difference flow measurements in borehole KSH02 at Simpevarp.
P-03-113	**Ask H, Morosini M, Samuelsson L-E, Stridsman H.** Oskarshamn site investigation – Drilling of cored borehole KSH01.
P-03-114	**Ask H, Samuelsson L-E.** Oskarshamn site investigation – Drilling of three flushing water wells, HSH01, HSH02 and HSH03.
P-04-03	**Brydsten L.** A method for construction of digital elevation models for site investigation program at Forsmark and Simpevarp.
P-04-22	**Rudmark L.** Investigation of Quaternary deposits at Simpevarp peninsula and the islands of Ävrö and Hålö. Oskarshamn site investigation.
P-04-46	**Ask H.** Drilling and installation of two monitoring wells, SSM 000006 and SSM 000007 in the Simpevarp subarea.
P-04-121	**Johansson T, Adestam L.** Drilling and sampling in soil. Installation of groundwater monitoring wells.
P-04-150	**Ask H, Samuelsson L-E.** Drilling of two flushing water wells, HAV09 and HAV10.
P-04-151	**Ask H, Morosini M, Samuelsson L-E, Stridsman H.** Oskarshamn site investigation – Drilling of cored borehole KSH02.
P-04-212	**Svensson T.** Oskarshamn site investigation. Pumping tests and flow logging in boreholes KSH03 and HSH02.
P-04-213	**Rouhiainen P, Pöllänen J.** Oskarshamn site investigation – Difference flow measurements in borehole KAV01 at Ävrö.
P-04-216	**Pölännen J, Sokolnicki M.** Difference flow measurements in borehole KAV04A and KAV04B.
P-04-233	**Ask H, Morosini M, Samuelsson L-E, Ekström L, Håkansson N.** Drilling of cored borehole KSH03.
P-04-234	**Ask H, Samuelsson L-E.** Drilling of two percussion boreholes, HLX13 and HLX14.
P-04-235	**Ask H, Samuelsson L-E, Zetterlund M.** Percussion drilling of boreholes HLX15, HLX26, HLX27, HLX28, HLX29 and HLX32 for investigation of lineament NW042.
P-04-236	**Ask H, Samuelsson L-E.** Percussion drilling of borehole HLX20 for investigation of lineament EW002.
P-04-247	**Ludvigson J, Levén J, Källgården J, Jönsson S.** Single-hole injection tests in borehole KSH02. Oskarshamn site investigation,
P-04-254	**Ingvarson N, Palmeby A, Svensson O, Nilsson O, Ekfeldt T.** Oskarshamn site investigation, Marine survey in shallow coastal waters Bathymetric and geophysical investigation 2004.
P-04-287	**Rahm N, Enachescu C.** Hydraulic testing of percussion drilled lineament boreholes on Ävrö and Simpevarp, 2004.
P-04-288	**Rahm N, Enachescu C.** Hydraulic injection tests in borehole KLX02, 2003. Sub-area Laxemar.
P-04-289	**Rahm N, Enachescu C.** Hydraulic injection tests in borehole KSH01A, 2003/2004. Sub-area Simpevarp.
P-04-290	**Rahm N, Enachescu C.** Hydraulic injection tests in borehole KSH03, 2004, Sub-area Simpevarp.
P-04-291	**Rahm N, Enachescu C.** Hydraulic injection tests in borehole KAV04A, 2004. Sub-area Simpevarp.
P-04-292	**Rahm N, Enachescu C.** Hydraulic injection tests in borehole KLX04, 2004. Sub-area Laxemar.
P-04-317	**Johansson T, Adestam L.** Drilling and sampling in soil. Installation of groundwater monitoring wells in the Laxemar area.
P-05-16	**Rahm N, Enachescu C.** Pumping tests and water sampling in borehole KLX04, 2004. Sub-area Laxemar.
P-05-20	**Gustafsson E, Ludvigson J-E.** Combined interference test and tracer test between KLX02 and HLX10.
P-05-25	**Ask H, Morosini M, Samuelsson L-E, Ekström L, Håkansson N.** Drilling of cored borehole KAV04.
P-05-35	**Elhammer A, Sandkvist Å.** Detailed marine geological survey of the sea bottom outside Simpevarp.
P-05-49	**Rudmark L, Malmberg-Persson K, Mikko H.** Investigation of Quaternary deposits 2003-2004.
P-05-55	**Ask H, Samuelsson L-E, Zetterlund M.** Percussion drilling of boreholes HLX21, HLX22, HLX23, HLX24, HLX25, HLX30, HLX31 and HLX33 for investigation of lineament EW007.
P-05-65	**Forssman I, Zetterlund M, Forsmark T, Rhén I.** Oskarshamn site investigation. Correlation of Posiva Flow Log anomalies to core mapped features in KSH01A, KSH02A and KAV01.
P-05-67	**Rouhiainen P, Pöllänen J, Sokolnicki M.** Difference flow logging of borehole KLX 03. Subarea Laxemar.
P-05-68	**Rouhiainen P, Sokolnicki M.** Difference flow logging of borehole KLX04.
P-05-74	**Sokolnicki M, Rouhianien P.** Oskarshamn site investigation. Difference flow logging of borehole KLX06. Sub-area Laxemar.
P-05-111	**Ask H, Morosini M, Samuelsson L-E, Ekström L, Håkanson N.** Drilling of cored borehole KLX04.

P-05-160 **Sokolnicki M, Rouhiainen P.** Difference flow logging of borehole KLX05. Subarea Laxemar. Oskarshamn site investigation.

P-05-167 **Ask H, Morosini M, Samuelsson L-E, Ekström L, Håkanson N.** Drilling of cored borehole KLX03.

P-05-184 **Rahmn N, Enachescu C.** Pumping tests and hydraulic injection tests in borehole KLX06.

P-05-190 **Ask H, Zetterlund M.** Percussion drilling of boreholes HLX16, HLX17, HLX18 and HLX19.

P-05-192 **Rahm N, Enachescu C.** Hydraulic injection tests in borehole KLX03, 2005. Subarea Laxemar.

P-05-193 **Morosini M, Ludvigson J-E.** Hydraulic characterisation of deformation zone EW007, Subarea Laxemar.

P-05-194 **Sigurdsson O, Ekström L.** Percussion drilling of boreholes HSH04, HSH05, HSH06, HAV11, HAV12, HAV13 and HAV14.

P-05-222 **Rahm N, Enachescu C.** Hydraulic injection tests in borehole KLX05, 2005. Subarea Laxemar.

P-05-225 **Sokolnicki M, Rouhianien P.** Oskarshamn site investigation. Difference flow logging of borehole KLX07A and KLX07B. Sub-area Laxemar.

P-05-233 **Ask H, Morosini M, Samuelsson L-E, Ekström L, Håkansson N.** Oskarshamn site investigation. Drilling of cored borehole KLX05.

P-05-234 **Ask H, Morosini M, Samuelsson L-E, Ekström L, Håkansson N.** Oskarshamn site investigation. Drilling of cored borehole KLX06.

P-05-237 **Sigurdsson O, Ask H, Zetterlund M.** Percussion drilling of boreholes HLX34 and HLX35.

P-05-241 **Forssman I, Zetterlund M, Forsmark T, Rhén I.** Correlation of Posiva Flow Log anomalies to core mapped features in KLX02, KLX03, KLX04, KAV04A and KAV04B.

P-05-267 **Sokolnicki M, Pöllänen J.** Difference flow logging of borehole KLX08. Subarea Laxemar. Oskarshamn site investigation.

P-05-273 **Rahm N, Enachescu C.** Hydraulic injection tests in borehole KLX07A, 2005 Laxemar.

P-05-275 **Ask H.** Percussion drilling of boreholes HLX36 and HLX37 for investigation of lineament NS001.

P-06-14 **Ask H, Morosini M, Samuelsson L-E, Ekström L, Håkansson N.** Oskarshamn site investigation. Drilling of cored boreholes KLX07A and KLX07B.

P-06-58 **Sokolnicki M.** Oskarshamn site investigation. Difference flow logging of borehole KLX10. Sub-area Laxemar.

P-06-116 **Ask H, Morosini M, Samuelsson L-E, Ekström L, Håkansson N.** Oskarshamn site investigation. Drilling of cored borehole KLX10.

P-06-121 **Sohlenius G, Bergman T, Snäll S, Lundin L, Lode E, Stendahl J, Riise A, Nilsson J, Johansson T, Göransson M.** Oskarshamn site investigation. Soils, Quaternary deposits and bedrock in topographic lineaments situated in the Laxemar subarea.

P-06-145 **Enachescu C, Böhner J, Rohs S.** Hydraulic interference tests, pumping borehole KLX07A Subarea Laxemar.

P-06-147 **Rohs S.** Flow logging in boreholes HLX21, HLX35 and HLX38 Subarea Laxemar.

P-06-148 **Harrström J, Ludvigson J, Hjerne C.** Hydraulic injection tests in borehole KLX12A Subarea Laxemar.

P-06-151 **Morosini M, Wass E.** Oskarshamn site investigation. Hydraulic interference and tracer testing of a rock-soil aquifer system between HLX35 and HLX34, SSM000037, SSM000222 and SSM000223 – Subarea Laxemar.

P-06-164 **Väisäsvaara J, Heikkinen P, Kristiansson S, Pöllänen J**. Oskarshamn site investigation. Difference flow logging of borehole KLX09. Sub-area Laxemar.

P-06-182 **Harrström J, Ludvigson J, Hjerne C.** Single-hole injection tests in borehole KLX10.

P-06-183 **Kristiansson S.** Oskarshamn site investigation. Difference flow logging of borehole KLX20A. Sub-area Laxemar.

P-06-184 **Sokolnicki M, Kristiansson S.** Difference flow logging of borehole KLX18A Subarea Laxemar. Oskarshamn site investigation.

P-06-185 **Väisäsvaara J, Heikkinen P, Kristiansson S, Pöllänen J.** Oskarshamn site investigation. Difference flow logging of borehole KLX12A. Sub-area Laxemar.

P-06-199 **Sokolnicki M, Väisäsvaara J.** Oskarshamn site investigation. Difference flow logging of borehole KLX09B–F. Sub-area Laxemar.

P-06-201 **Enachescu C, Rohs S, Wolf P.** Hydraulic injection tests in borehole KLX11A Subarea Laxemar.

P-06-222 **Ask H, Morosini M, Samuelsson L-E, Ekström L, Håkansson N.** Oskarshamn site investigation. Drilling of cored borehole KLX08.

P-06-225 **Enachescu C, Rohs S, van der Wall R.** Hydraulic injection tests in borehole KLX18A Subarea Laxemar.

P-06-229 **Väisäsvaara J, Leppänen H, Kristiansson S, Pöllänen J.** Oskarshamn site investigation. Difference flow logging of borehole KLX09G, KLX10B and KLX10C. Sub-area Laxemar.

P-06-245 **Väisäsvaara J, Pekkanen J.** Oskarshamn site investigation. Difference flow logging of borehole KLX13A. Sub-area Laxemar.

P-06-246 **Kristiansson S, Pöllänen J, Väisäsvaara J, Kyllönen H.** Oskarshamn site investigation. Difference flow logging of borehole, KLX22A–B, KLX23A–B, KLX24A, KLX25A, Sub-area Laxemar.

P-06-248 **Johansson T, Göransson M, Zetterlund M, Jenkins K, Rönnback K.** Oskarshamn site investigation. Hydrogeological characterization in bogs, lakes and sea bays.

P-06-265 **Ask H.** Oskarshamn site investigation. Core drilling of short boreholes KLX09B, KLX09C, KLX09D, KLX09E and KLX09F for discrete fracture network investigation (DFN).

P-06-282 **Olsson T, Stanfors R, Sigurdsson O, Erlström M.** Oskarshamn site investigation. Identification and characterization of minor deformation zones based on lineament interpretation.

P-06-283 **Ask H.** Oskarshamn site investigation. Core drilling of short boreholes KLX11B, KLX11C, KLX11D, KLX11E and KLX11F for discrete fracture network investigation (DFN).

P-06-291 **Ask H.** Percussion drilling of boreholes HLX38, HLX39, HLX40, HLX41, HLX42 and HLX43 for lineament investigation.

P-06-305 **Ask H, Morosini M, Samuelsson L-E, Ekström L, Håkansson N.** Oskarshamn site investigation. Drilling of cored borehole KLX12A.

P-06-306 **Ask H, Morosini M, Samuelsson L-E, Ekström L, Håkansson N.** Oskarshamn site investigation. Drilling of cored borehole KLX11A.

P-06-318 **Väisäsvaara J.** Oskarshamn site investigation. Difference flow logging of borehole KLX14A. Sub-area Laxemar.

P-06-319 **Rohs S, van der Wall R, Wolf P.** Flow logging in boreholes HLX14, HLX20, HLX27, HLX28, HLX32, HLX33, HLX37, HLX39 and HLX43 Subarea Laxemar.

P-07-17 **Pöllänen J.** Oskarshamn site investigation. Difference flow logging of borehole, KLX28 and KLX29A, Sub-area Laxemar.

P-07-18 **Enachescu C, Wolf P, Rohs S, van der Wall R.** Hydraulic interference tests, pumping borehole KLX08 Subarea Laxemar.

P-07-20 **Kyllönen H, Leppänen H.** Oskarshamn site investigation. Difference flow logging of borehole KLX19A. Sub-area Laxemar.

P-07-24 **Väisäsvaara J, Kristiansson S, Sokolnicki M.** Oskarshamn site investigation. Difference flow logging of borehole KLX11A. Sub-area Laxemar.

P-07-34 **Pöllänen J.** Oskarshamn site investigation. Difference flow logging of borehole KLX17A. Sub-area Laxemar.

P-07-39 **Enachescu C, Rohs S, Wolf P.** Hydraulic interference tests, pumping borehole KLX20A Subarea Laxemar.

P-07-48 **Enachescu C, Rohs S, Wolf P.** Hydraulic injection tests in borehole KLX08, 2006 Subarea Laxemar.

P-07-49 **Enachescu C, Rohs S**. Hydraulic injection tests in borehole KLX20A, 2006 Subarea Laxemar.

P-07-64 **Sokolnicki M, Kristiansson S.** Oskarshamn site investigation. Difference flow logging of borehole KLX11B-F. Sub-area Laxemar.

P-07-72 **Pöllänen J.** Oskarshamn site investigation. Difference flow logging of borehole, KLX26A and KLX26B, Sub-area Laxemar.

P-07-79 **Enachescu C, Rahm N.** Method evaluation of single hole hydraulic injection tests at site investigations Oskarshamn.

P-07-80 **Ludvigson J-E, Hansson K, Hjerne C.** Method evaluation of single-hole hydraulic injection tests at site investigations in Forsmark.

P-07-87 **Väisäsvaara J.** Oskarshamn site investigation. Difference flow logging of borehole KLX16A. Sub-area Laxemar.

P-07-90 **Enachescu C, Böhner J, Wolf P.** Pumping tests and hydraulic injection tests in borehole KLX19A, 2007 Subarea Laxemar.

P-07-91 **Morosini M, Jenkins C, Simson S, Albrecht J, Zetterlund M.** Oskarshamn site investigation. Hydrogeological characterization of deepest valley soil aquifers and soil-rock transition zone at Laxemar, 2006 – Subarea Laxemar.

P-07-98 **Ask H, Morosini M, Samuelsson L-E, Ekström L, Håkansson N.** Oskarshamn site investigation. Drilling of cored borehole KLX18A.

P-07-99 **Enachescu C, Rohs S.** Hydraulic injection tests in borehole KLX13A Subarea Laxemar.

P-07-116 **Sokolnicki M, Pöllänen J.** Oskarshamn site investigation. Difference flow logging of borehole KLX21B. Sub-area Laxemar.

P-07-120 **Enachescu C, Rohs S, Wolf P.** Hydraulic injection tests in borehole KLX16A, 2007 Subarea Laxemar.

P-07-134 **Ask H, Morosini M, Samuelsson L-E, Ekström L, Håkansson N.** Oskarshamn site investigation. Drilling of cored borehole KLX20A.

P-07-173 **Gokall-Norman K, Ludvigson J-E.** Oskarshamn site investigation. Hydraulic pumping- and interference tests in soil monitoring wells on Laxemar, spring of 2007.

P-07-176 **Pöllänen J, Sokolnicki M, Väisäsvaara J.** Oskarshamn site investigation. Difference flow logging of borehole KLX15A. Sub-area Laxemar.

P-07-182 **Morosini M, Jönsson S.** Pump- and interference testing of percussion drilled section of cored boreholes KLX09, KLX11A, KLX12A, KLX13A, KLX18A, KLX19A and KLX39 Subarea Laxemar.

P-07-183 **Walger E, Ludvigson J-E, Svensson T, Thur P, Harrström J.** Hydraulic interference in KLX06, KLX14A, KLX15A, KLX16A, KLX17A, KLX18A, KLX19A, KLX21B, KLX22A, KLX22B, KLX23A, KLX23B, KLX26A and KLX26B, Laxemar subarea.

P-07-185 **Thur P, Walger E, Ludvigson J-E.** Hydraulic interference in HLX34, HLX27, and HLX42 in the Laxemar subarea.

P-07-186 **Harrström J, Walger E, Ludvigson J, Morosini M.** Hydraulic interference tests HLX27, HLX28 and HLX32, Subarea Laxemar.

P-07-187 **Svensson T, Ludvisgsson J-E, Walger E, Thur P, Gokall-Norman K, Wass E, Morosini M.** Combined interference- and tracer test in HLX33, SSM000228, and SSM000229, Subarea Laxemar.

P-07-193 **Enachescu C, van der Wall R, Wolf P.** Hydraulic Injection Tests in Borehole KLX17A, 2007 Subarea Laxemar.

P-07-195 **Ask H, Morosini M, Samuelsson L-E, Tiberg L.** Oskarshamn site investigation. Drilling of cored borehole KLX13A.

P-07-202 **Ask H, Morosini M, Samuelsson L-E, Tiberg L.** Oskarshamn site investigation. Drilling of cored borehole KLX19A.

P-07-212 **Teurneau B, Forsmark T, Forssman I, Rhén I**. Oskarshamn site investigation. Correlation of Posiva Flow Log anomalies to core mapped features in KLX05, KLX06, KLX07A-B and KLX08.

P-07-213 **Wikström M, Forsmark T, Teurneau B, Forssman I, Rhén I.** Oskarshamn site investigation. Correlation of Posiva Flow Log anomalies to core mapped features in KLX09, KLX09B–G. KLX10, KLX10B–C and KLX11A–F.

P-07-214 **Wikström M, Forsmark T, Zetterlund M, Forssman I, Rhén I**. Oskarshamn site investigation. Correlation of Posiva Flow Log anomalies to core mapped features in KLX12A, KLX13A, KLX14A, KLX15A and KLX16A.

P-07-215 **Forsmark T, Wikström M, Forssman I, Rhén I**. Oskarshamn site investigation. Correlation of Posiva Flow Log anomalies to core mapped features in KLX17A, KLX18A, KLX19A, KLX20A, KLX21B.

P-07-216 **Wikström M, Forsmark T, Forssman I, Rhén I.** Oskarshamn site investigation. Correlation of Posiva Flow Log anomalies to core mapped features in KLX22A–B, KLX23A–B, KLX24A, KLX25A, KLX26A–B, KLX27A, KLX28A and KLX29A.

P-07-223 **Triumf C-A.** Oskarshamn site investigation. Assessment of possible dolerite dykes in the Laxemar subarea from magnetic total field data and digital elevation models.

P-08-15 **Enachescu C, Rohs S, van der Wall R.** Evaluation of hydraulic interference tests, pumping borehole KLX19A Subarea Laxemar.

P-08-16 **Enachescu C, Rohs S, van der Wall R, Wolf P, Morosini M.** Evaluation of hydraulic interference tests, pumping borehole KLX27A Subarea Laxemar.

P-08-22 **Pöllänen J, Pekkanen J, Väisäsvaara J.** Oskarshamn site investigation. Difference flow logging of borehole, KLX27A, Sub-area Laxemar.

P-08-27 **Enachescu C, Wolf P, Rohs S, van der Wall R.** Hydraulic injection tests in borehole KLX27A, 2008 Subarea Laxemar.

P-08-57 **Enachescu C, Lenné S, Rohs S, van der Wall R.** Transient evaluation of PFL pumping tests. Sub-area Laxemar and Simpevarp.

IPR-00-28 **Andersson P, Ludvigson J-E, Wass E, Holmqvist M.** TRUE Block Scale. Tracer Test Stage. Interference tests, dilution tests and tracer tests, phase A.

IPR-01-06 **Rouhiainen P.** Difference flow measurements in borehole KLX02 at Laxemar.

IPR-01-44 **Andersson P, Ludvigsson J-E, Wass E.** TRUE Block Scale project. Preliminary characterisation stage. Combined interference tests and tracer tests. Performance and delivery evaluation.

IPR-01-52 **Andersson P, Ludvigsson J-E, Wass E, Holmqvist M.** True Block Scale, Detailed characterisation stage, Interference tests and tracer tests PT-1 PT-4.

IPR-01-65 **Forsmark T, Rhén I.** Summary report of investigations before the operation phase. Prototype Repository (D27).

IPR-03-13 **Dershowitz W, Winberg A, Hermanson J, Byegård J, Tullborg, E-L, Andersson P, Mazurek M.** Äspö Hard Rock Laboratory. Äspö Task Force on modelling of groundwater flow and transport of solutes. Task 6c. A semi-synthetic model of block scale conductive strctures at the Äspö HRL.

R-98-55 **Follin S, Årebäck M, Axelsson C-L, Stigsson M, Jacks G.** Förstudie Oskarshamn. Grundvattnets rörelse, kemi och långsiktiga förändringar (in Swedish).

R-99-70 **Lindell S, Ambjörn C, Juhlin B, Larsson-McCann S, Lindquist K.** Available climatological and oceanographical data for site investigation program.

R-01-52 **Ludvigson J-E, Hansson K, Rouhiainen P.** Methodology study of Posiva difference flow meter in borehole KLX02 at Laxemar.

R-04-09 **Smellie J.** Recent geoscientific information relating to deep crustal studies.

R-05-38 **Brydsten L, Strömgren M.** Digital elevation models for site investigation programme in Oskarshamn. Site description version 1.2.

R-08-05 **Solenius G, Hedenström A.** Description of regolith at Laxemar-Simpevarp. Site descriptive modelling, SDM-Site.

R-08-06 **Nyman H, Sohlenius G, Strömgren M, Brydsten L.** Oskarshamn site investigation – Depth and stratigraphy of regolith.

R-08-54 **Wahlgren C-H, Curtis P, Hermanson J, Forssberg O, Öhman J, Fox A, La Pointe P, Drake H, Triumf C-A, Mattsson H, Thunehed H, Juhlin C. G**eology Laxemar. Site descriptive modelling. SDM-Site Laxemar. SKB-R-08-54, Svensk Kärnbränslehantering AB.

R-08-73 **Werner K, Öhman J, Holgersson B, Rönnback K, Marelius F.** Meteorological, hydrological and hydrogeological monitoring data and near-surface hydrogeological properties data from Laxemar-Simpevarp. Site descriptive modelling, SDM-Site Laxemar.

R-09-01 **Söderbäck B, Lindborg T.** Surface system Laxemar-Simpevarp. Site descriptive modelling, SDM-Site Laxemar. SKB R-09-01, Svensk Kärnbränslehantering AB

TR-97-02 **Stanfors R, Erlström M, Markström I.** Äspö HRL – Geoscientific evaluation 1997/2. Overview of site chacterisation 1986–1995.

TR-97-03 **Rhén I (ed), Bäckblom G (ed), Gustafson G, Stanfors R, Wikberg P.** Äspö HRL – Geoscientific evaluation 1997/1. Results from pre-investigations and detailed site characterization.Summary report

TR-97-05 **Rhén I, Gustafson G, Wikberg P.** Äspö HRL – Geoscientific evaluation 1997/4. Results from pre-investigations and detailed site characterization. Comparison of predictions and observations. Hydrogeology, groundwater chemistry and transport of solutes.

TR-97-06 **Rhén I (ed), Gustafson G, Stanfors R, Wikberg P.** Äspö HRL – Geoscientific evaluation 1997/5. Models based on site characterization 1986–1995.

TR-98-05 **Juhlin C, Wallroth T, Smellie J, Eliasson T, Ljunggren C, Leijon B, Beswick J.** The Very Deep Hole Concept: Geoscientific appraisal of conditions at great depth.

TR-01-11 **Ekman L.** Project Deep Drilling KLX02 – Phase 2. Methods, scope of activities and results. Summary.

TR-02-03 **Larsson-McCann S, Karlsson A, Nord M, Sjögren J, Johansson L, Ivarsson M, Kindell S.** Meteorological, hydrological and oceanographical information and data for the site investigation program in the community of Oskarshamn.

TR-02-19 **Andersson J, Berglund J, Follin S, Hakami E, Halvarson J, Hermanson J, Laaksoharju M, Rhén I, Wahlgren C-H.** Testing the methodology for site descriptive modelling. Application for the Laxemar area.

Appendix 3

A3 Environmental water head for base case

Figure A3-1 shows the positions of the vertical sections used to visualise the distribution of environmental water head for the *base case*, cf. Figure 7-5. The distribution of environmental water head, TDS and $\delta^{18}O$ for the base case is also shown on a number of horizontal sections, cf. Figure A3-2 through Figure A3-13.

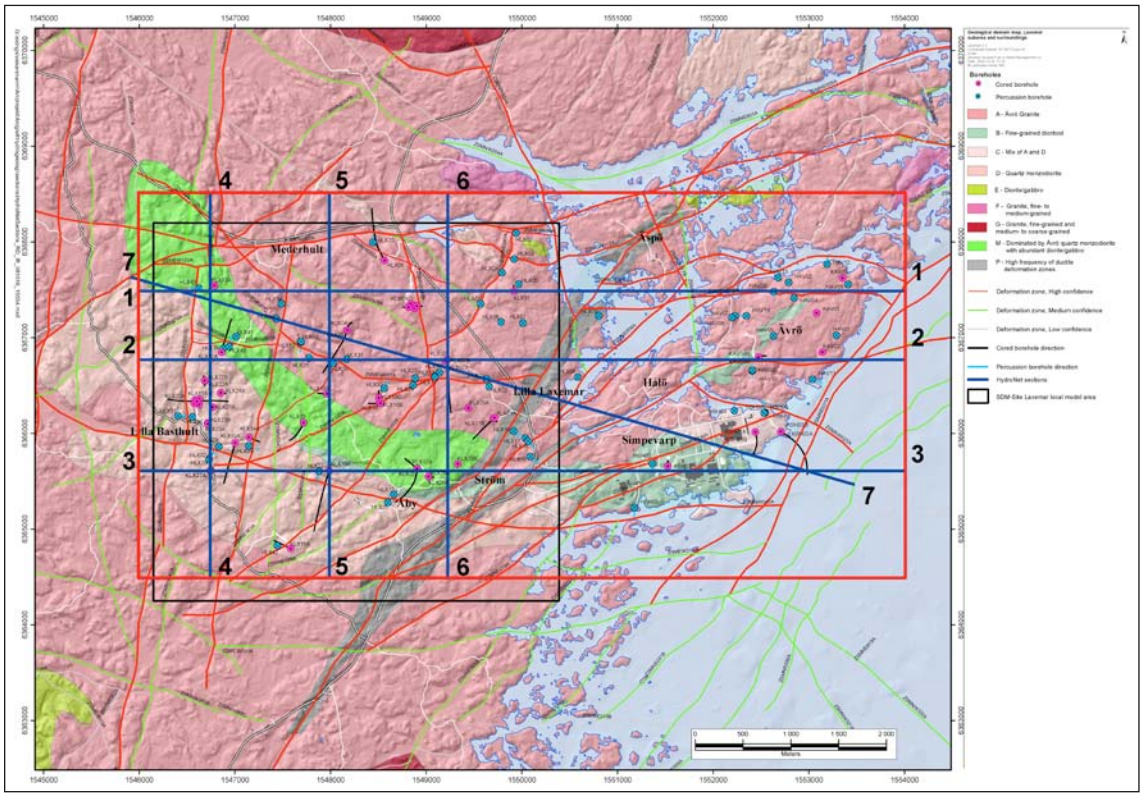

Figure A3-1. *Positions of vertical slices Hv1–6 used in the palaeo-hydrogeology plots shown in Figure 7-5. Hv7 is the same section as section B in Figure 7-15.*

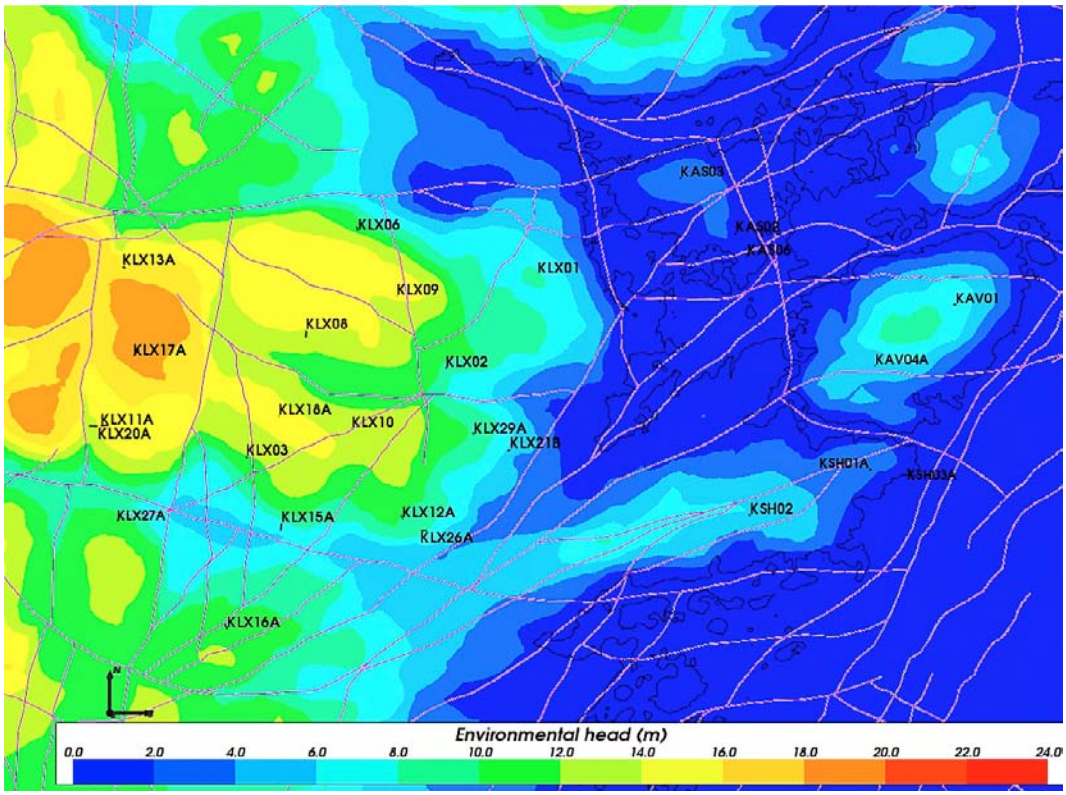

Figure A3-2. *Distribution of environmental water head predicted on a horizontal slice at –100 m covering the Laxemar-Simpevarp area through the base case model. HCDs at elevation 0 m and at time 2000 AD.*

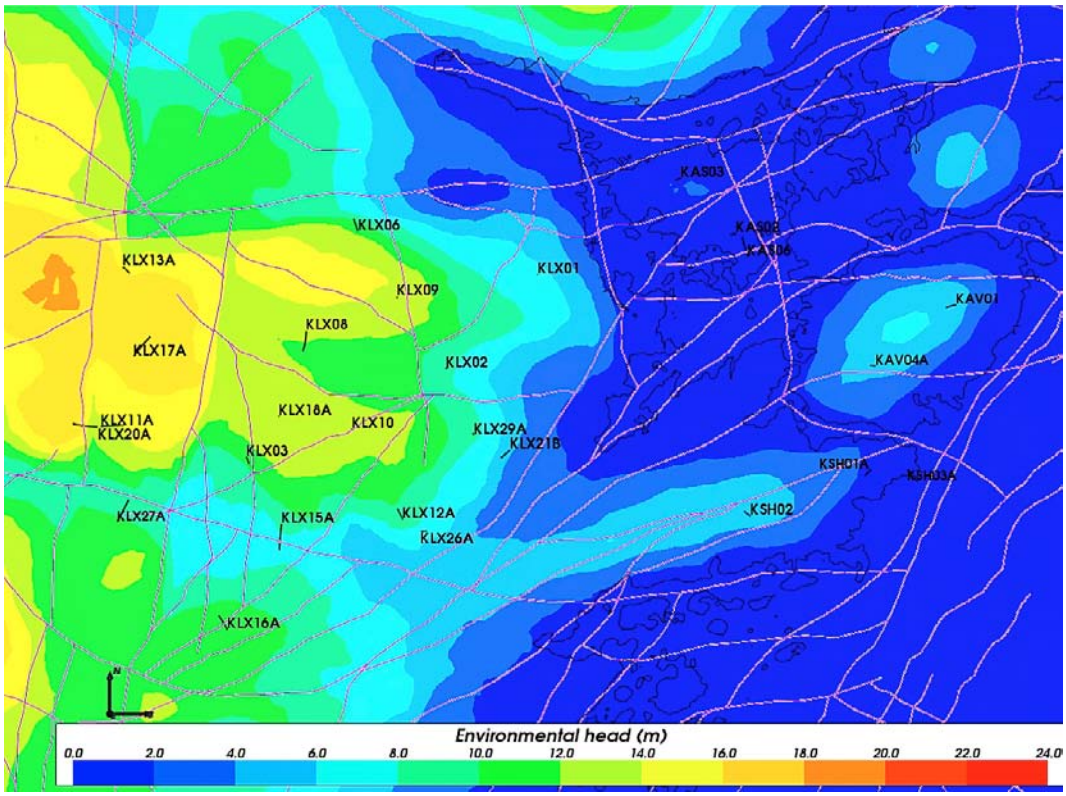

Figure A3-3. *Distribution of environmental water head predicted on a horizontal slice at –300 m covering the Laxemar-Simpevarp area through the base case model. HCDs at elevation 0 m and at time 2000 AD.*

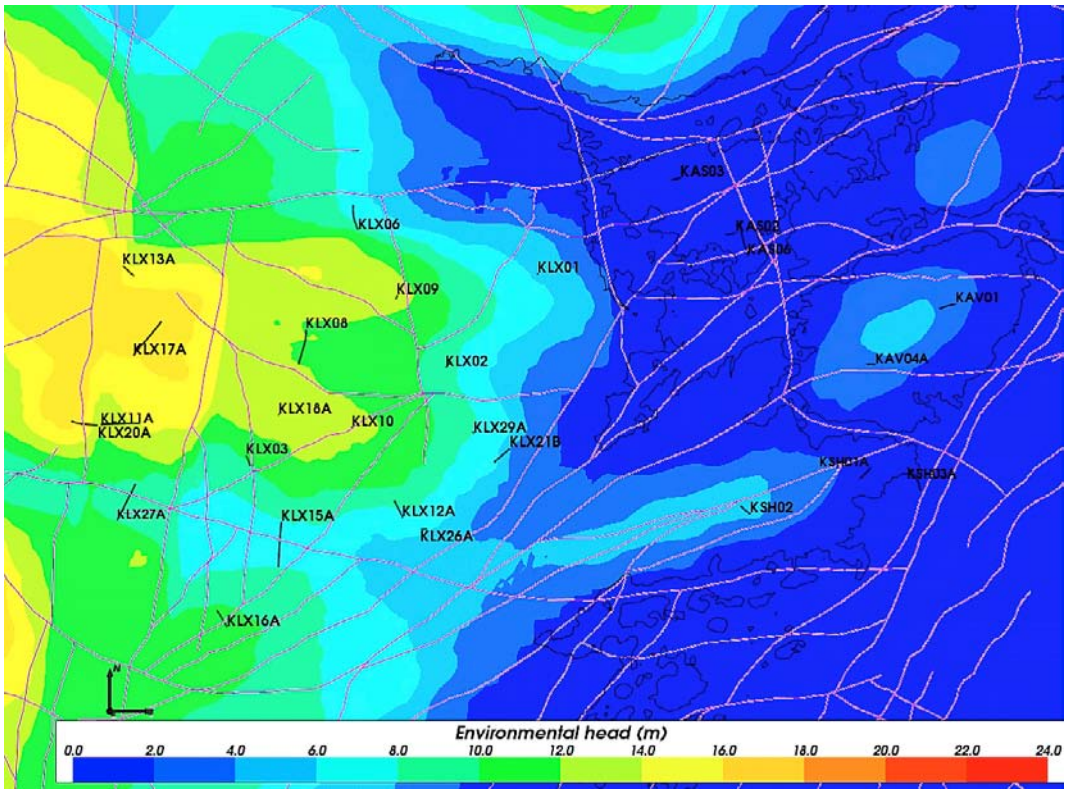

Figure A3-4. *Distribution of environmental water head predicted on a horizontal slice at –500 m covering the Laxemar-Simpevarp area through the base case model. HCDs at elevation 0 m and at time 2000 AD.*

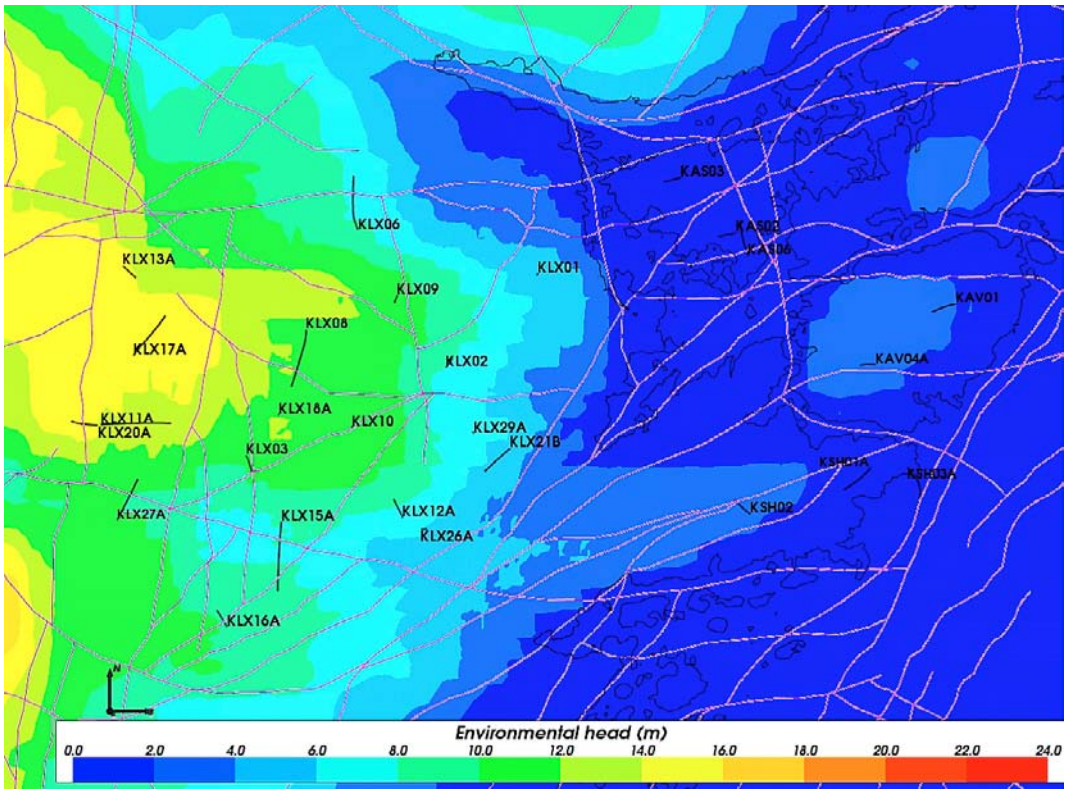

Figure A3-5. *Distribution of environmental water head predicted on a horizontal slice at –900 m covering the Laxemar-Simpevarp area through the base case model. HCDs at elevation 0 m and at time 2000 AD.*

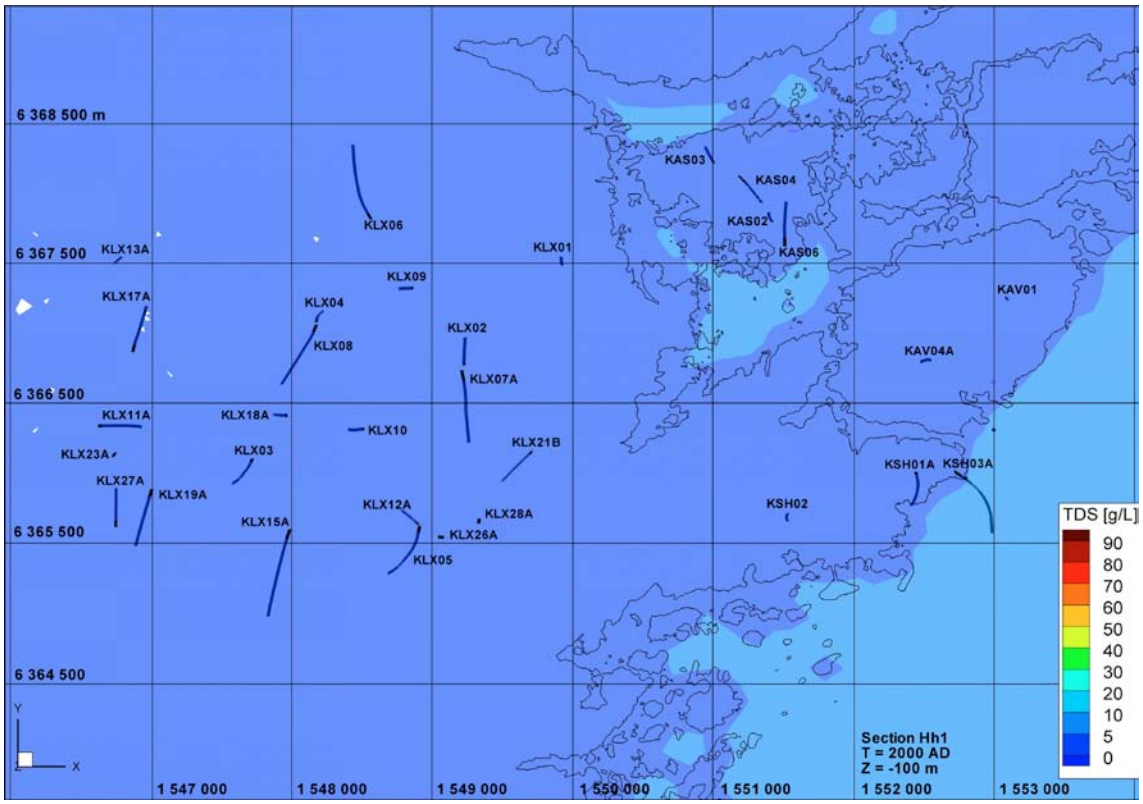

Figure A3-6. *Distribution TDS predicted on a horizontal slice at –100 m covering the Laxemar-Simpevarp area through the base case model.*

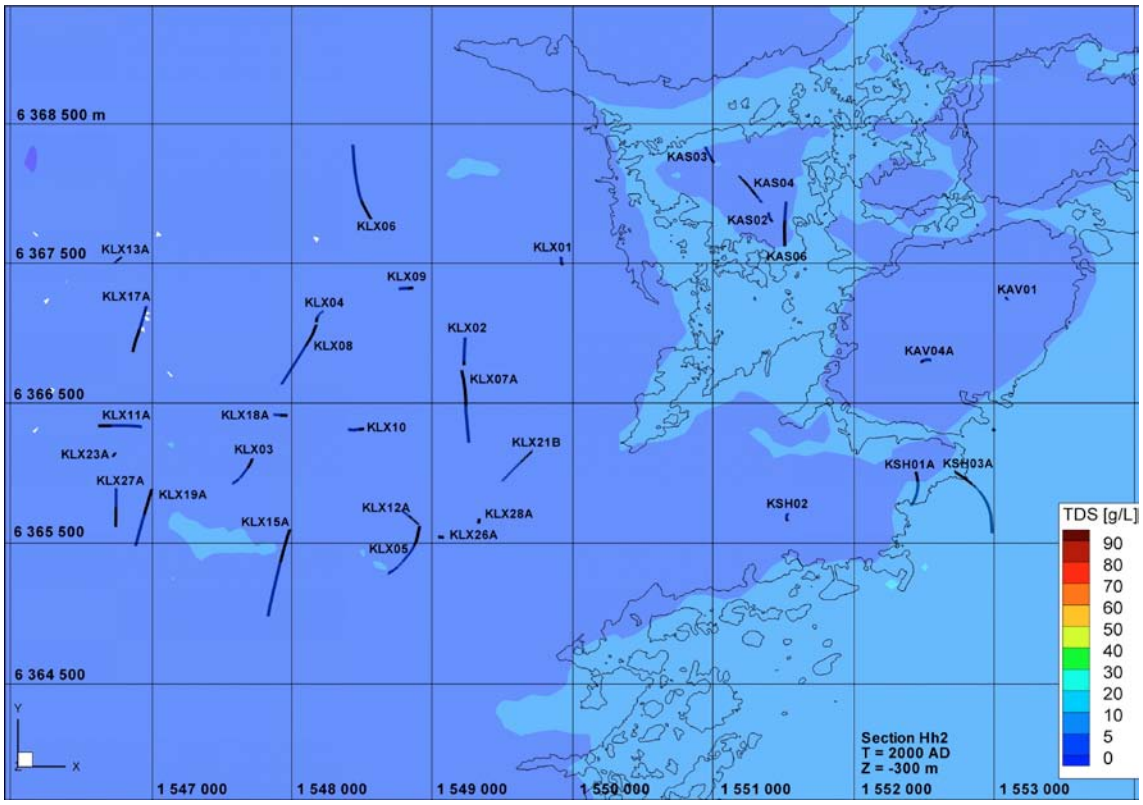

Figure A3-7. *Distribution TDS predicted on a horizontal slice at –300 m covering the Laxemar-Simpevarp area through the base case model.*

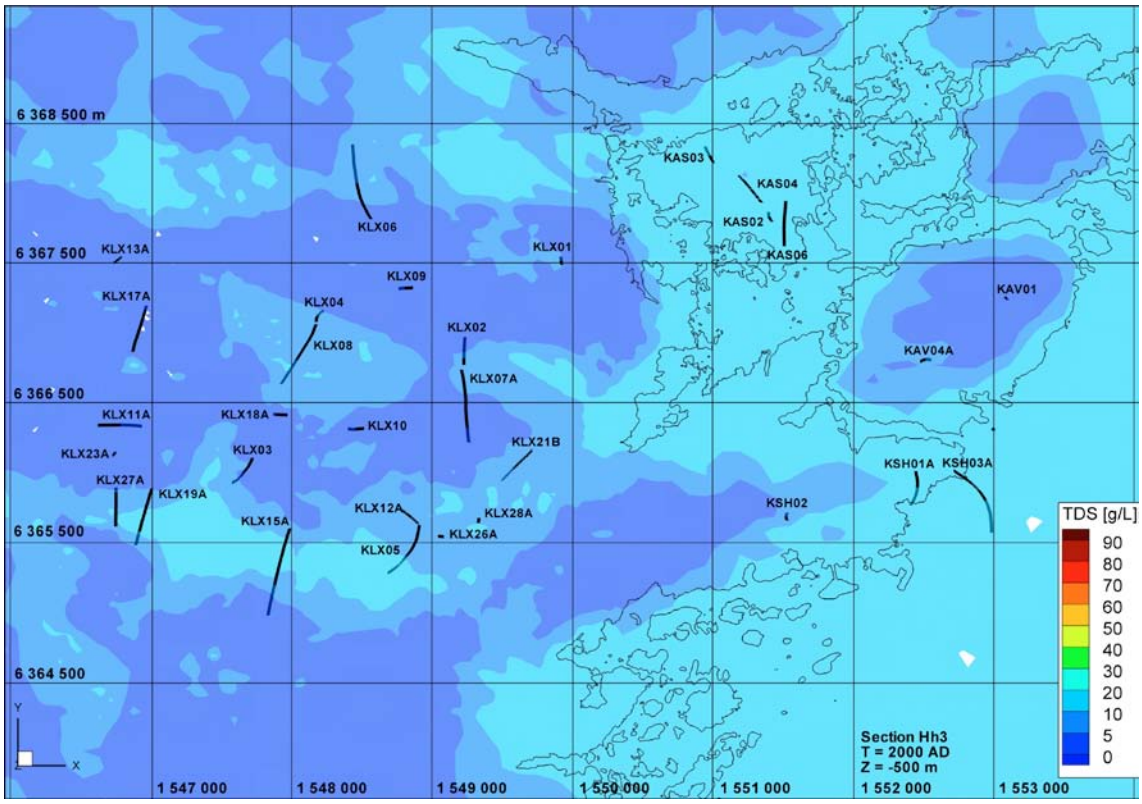

Figure A3-8. *Distribution TDS predicted on a horizontal slice at –500 m covering the Laxemar-Simpevarp area through the base case model.*

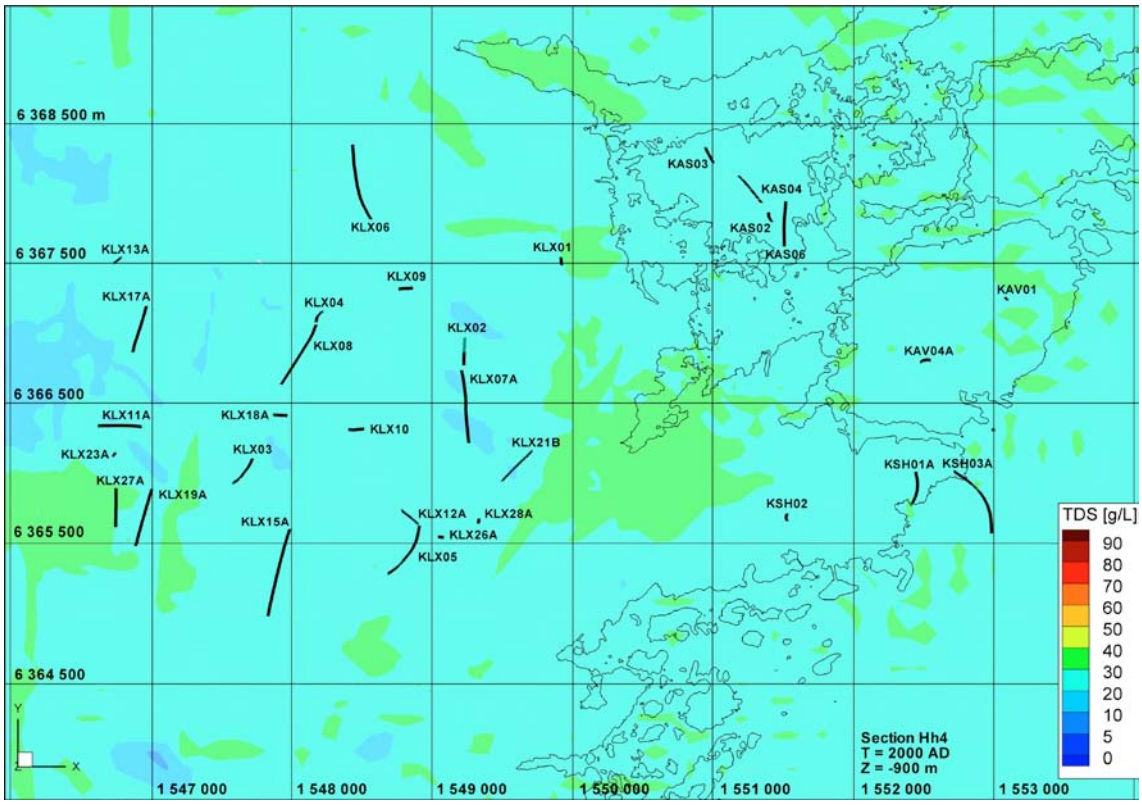

Figure A3-9. *Distribution TDS predicted on a horizontal slice at –900 m covering the Laxemar-Simpevarp area through the base case model.*

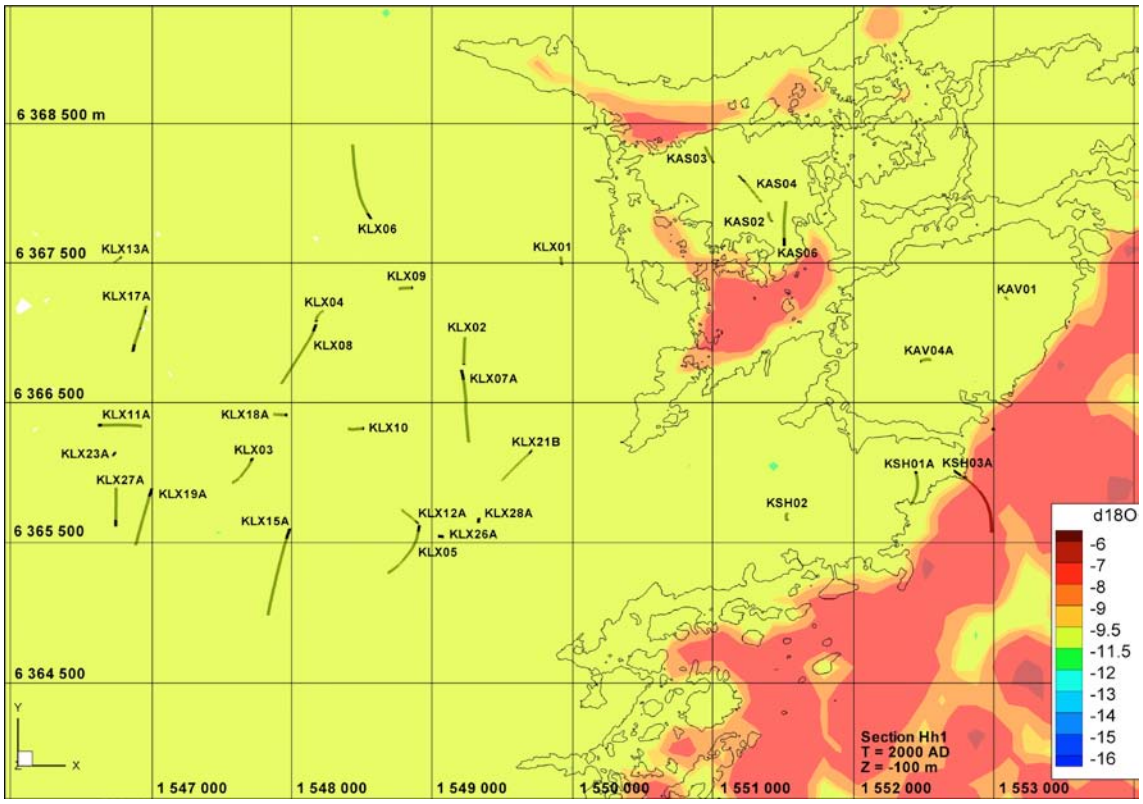

Figure A3-10. *Distribution of $\delta^{18}O$ predicted on a horizontal slice at –100 m covering the Laxemar-Simpevarp area through the base case model.*

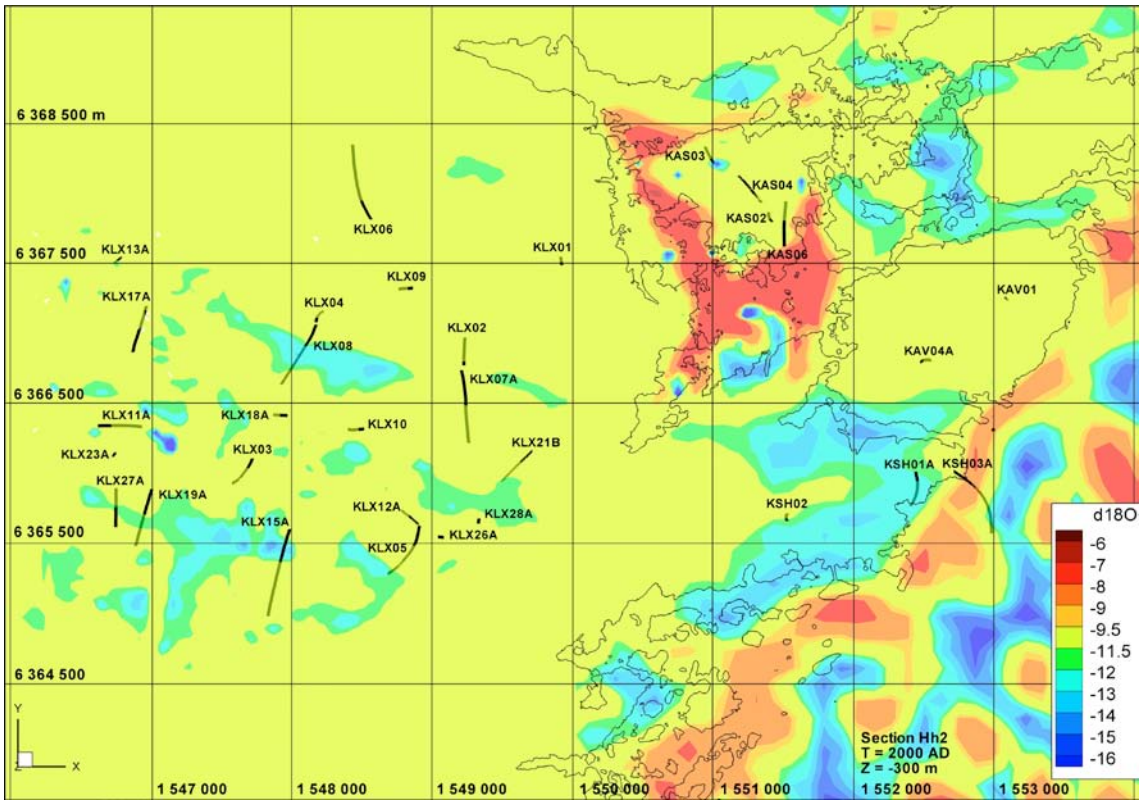

Figure A3-11. *Distribution of $\delta^{18}O$ predicted on a horizontal slice at –300 m covering the Laxemar-Simpevarp area through the base case model.*

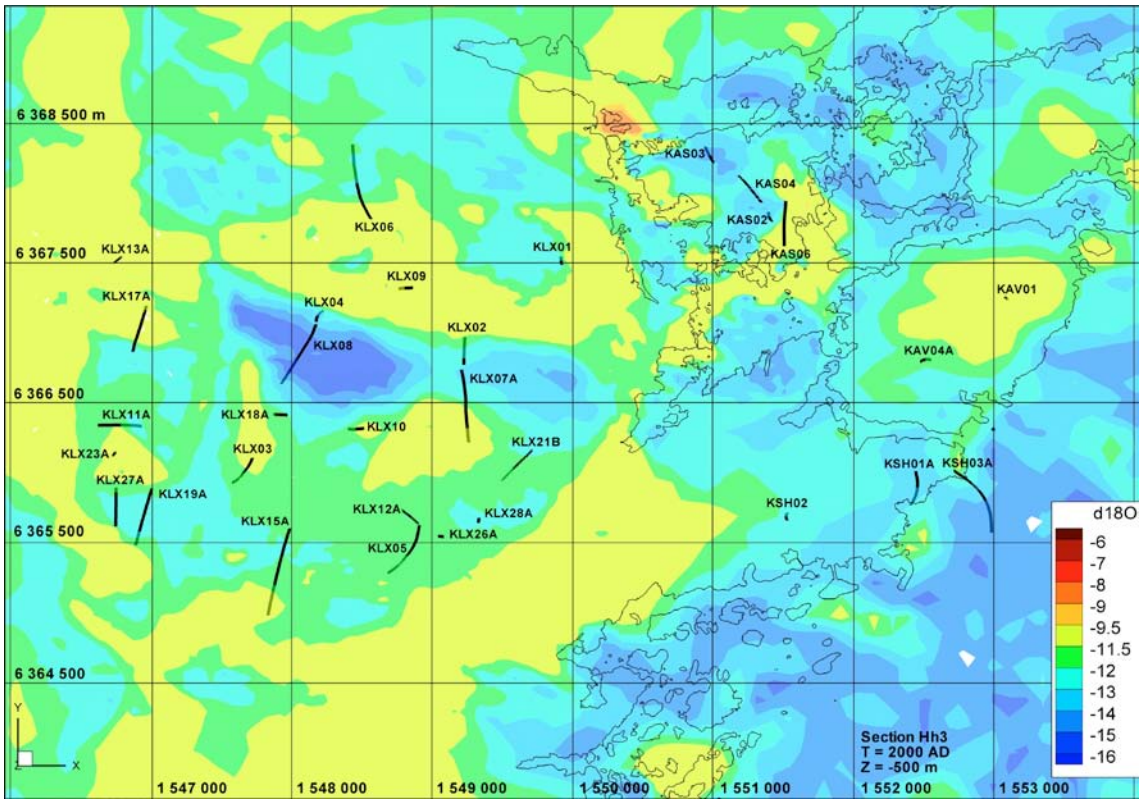

Figure A3-12. *Distribution of $\delta^{18}O$ predicted on a horizontal slice at –500 m covering the Laxemar-Simpevarp area through the base case model.*

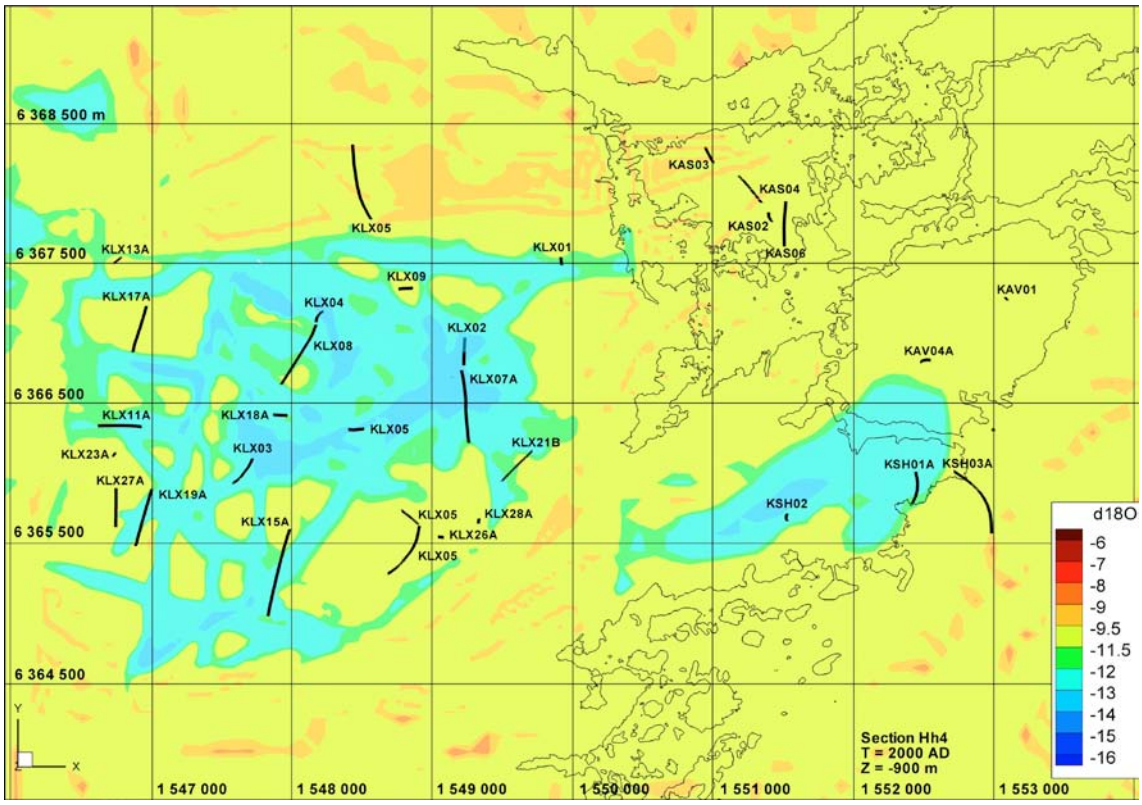

Figure A3-13. *Distribution of $\delta^{18}O$ predicted on a horizontal slice at –900 m covering the Laxemar-Simpevarp area through the base case model.*